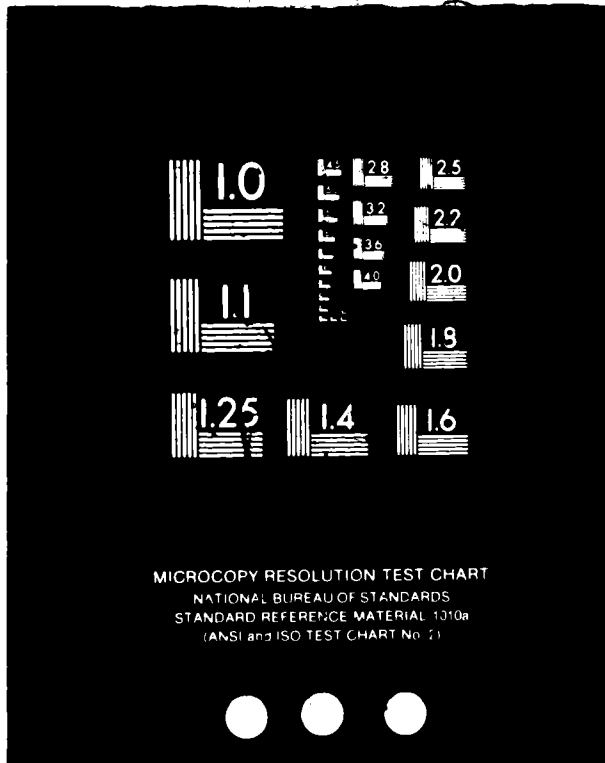


1 OF 3

N83-34329

UNCLAS



SRS

SPECTRA RESEARCH SYSTEMS

SOUTHEASTERN OPERATIONS
555 SPARKMAN SUITE 1406 HUNTSVILLE, ALABAMA 35805 (205) 830-0375

(NASA-CR-170856) BEARING TESTER DATA
COMPILATION, ANALYSIS, AND REPORTING AND
BEARING MATH MODELING Annual Report, Jul.
1982 - Jul. 1983 (Spectra Research Systems,
Inc.) 210 p HC A10/MF A01

N83-34329

CSSL 131 G3/37

Unclas
41993



BEARING TESTER DATA COMPILATION,
ANALYSIS, AND REPORTING AND
BEARING MATH MODELING
ANNUAL REPORT

AUGUST 10, 1983

PREPARED BY:
SPECTRA RESEARCH SYSTEMS
SOUTHEASTERN OPERATIONS
555 SPARKMAN DRIVE, SUITE 1406
HUNTSVILLE, AL 35805

UNDER CONTRACT NAS8-34586

FOR THE

GEORGE C. MARSHALL SPACE FLIGHT CENTER
NATIONAL AERONAUTICS AND SPACE ADMINISTRATION

FOREWORD

This report was prepared by Spectra Research Systems under Contract No. NAS8-34686 entitled "Bearing Tester Data Compilation, Analysis, and Reporting and Bearing Math Modeling" for the George C. Marshall Space Flight Center of the National Aeronautics and Space Administration. The work was administered under the technical direction of the Materials and Processes Laboratory, Engineering Physics Division of the George C. Marshall Space Flight Center with Mr. Fred J. Dolan acting as project manager.

This report describes the work performed by Spectra Research Systems Southeastern Operations during the July 1982 - July 1983 period. Mr. Rodney Bradford was the Spectra Research Systems Project Manager. The project technical staff was directed by Mr. Joseph C. Cody who was the Project Engineer. A listing of the key project staff members is shown below:

Dr. D. David Marshall
Mr. Edward E. Montgomery
Ms. Linda S. New
Mr. M. Anthony Stone
Mr. Bruce K. Tiller.

TABLE OF CONTENTS

| SECTION | PAGE |
|---|------|
| FOREWORD | ii |
| LIST OF FIGURES | vi |
| LIST OF TABLES | x |
| 1.0 INTRODUCTION | 1-1 |
| 2.0 SUMMARY | |
| 3.0 LISTING OF TASKS ACCOMPLISHED | 3-1 |
| 4.0 SYNOPSIS OF RESULTS | 4-1 |
| 5.0 DETAILED TASK DESCRIPTIONS AND RESULTS | 5-1 |
| 5.1 JULY, 1982 | 5-1 |
| 5.1.1 Wear Track and Ball Pass Count Analysis | 5-1 |
| 5.1.2 LOX Test Incident Analysis | 5-1 |
| 5.1.3 Energy and Flow Balance Estimates for the Bearing and Materials Tester | 5-10 |
| 5.2 AUGUST, 1982 | 5-17 |
| 5.2.1 Investigation of Bearing Temperature Gradients on Operational Characteristics | 5-17 |
| 5.2.2 Modeling the Effects of Ball Drag on Bearing Operating Characteristics | 5-17 |
| 5.2.3 Equivalent Thermal Conductance Between Rolling Elements and Races of High Speed Bearings | 5-22 |
| 5.2.4 Status of Bearing Thermal Model Development | 5-26 |
| 5.2.5 Graphics Capability Development for Data Reduction and Display | 5-26 |
| 5.3 SEPTEMBER, 1982 | 5-26 |
| 5.3.1 Continued Investigation of Bearing Temperature Gradient Effects on Operational Characteristics | 5-26 |
| 5.3.2 Estimates of Ball Drag Forces, Torques, and Heat Generation | 5-35 |
| 5.3.3 Correlation of Tester Internal Power Dissipation with Bearing Temperature Differences | 5-40 |
| 5.3.4 Bearing Thermal Model Development | 5-44 |
| 5.4 OCTOBER, 1982 | 5-50 |
| 5.4.1 Effects of Bearing Preload on Cage Slip and Frictional Heat Generation | 5-50 |

TABLE OF CONTENTS

| SECTION | PAGE |
|---|-------|
| 5.4.2 Recommended Coolant Temperature Limits for 57 mm | 5-50 |
| Bearing Operating in LN ₂ | |
| 5.4.3 Bearing Thermal Model Development | 5-58 |
| 5.5 NOVEMBER, 1982 | 5-58 |
| 5.5.1 Bearing Life Prediction Analysis | 5-58 |
| 5.5.2 Stiffness Characteristics of the Turbine End | 5-67 |
| LOX Pump Bearing | |
| 5.5.3 Heat Transfer Coefficients for Bearing Thermal | 5-67 |
| Model | |
| 5.5.4 Preliminary Results of Bearing Thermal Model | 5-74 |
| 5.6 DECEMBER, 1982 | 5-76 |
| 5.6.1 Bearing Operating Preloads | 5-76 |
| 5.6.2 Bearing Axial Reactions Resulting from Carrier | 5-81 |
| Loads | |
| 5.6.3 Interference Fit Between the Inner Race and | 5-86 |
| Shaft | |
| 5.6.4 Status of Bearing Thermal Model Development | 5-87 |
| 5.7 JANUARY, 1983 | 5-108 |
| 5.7.1 Potential Effects of Outer Race Misalignment | 5-108 |
| on Shaft Assembly Balancing | |
| 5.7.2 Status of Bearing Radial Stiffness Analysis | 5-111 |
| 5.7.3 Estimation of Heat Loads for the BMT Thermal Model | 5-111 |
| 5.7.4 Status and Results of Bearing Thermal Model | 5-114 |
| 5.8 FEBRUARY, 1983 | 5-117 |
| 5.8.1 Film Thickness Estimates for 57 mm Bearing | 5-117 |
| Operating in LN ₂ | |
| 5.8.2 Evaluating Radial Stiffness of 57 mm Bearing as | 5-125 |
| a Function of Ball Wear | |
| 5.8.3 Status and Results of Bearing Thermal Model | 5-128 |
| 5.8.4 Investigation of Outer Race Misalignment Effects | 5-131 |
| 5.9 MARCH, 1983 | 5-131 |
| 5.9.1 Effect of Friction on Rolling Element Contact | 5-131 |
| and Subsurface Stresses | |
| 5.9.2 Bearing Thermal Model and Analysis | 5-135 |
| 5.9.3 Estimation of Film Thickness for 57 mm Bearing | 5-135 |
| Operating on O ₂ | |
| 5.10 APRIL, 1983 | 5-135 |
| 5.10.1 Evaluation of Bearing Carrier to Housing Clearance | 5-135 |
| and the Effect on Bearing Operating Characteristics | |

TABLE OF CONTENTS

| SECTION | PAGE |
|---|-------|
| 5.10.2 Bearing Thermal Analysis | 5-144 |
| 5.10.3 Investigation of the Radial Stiffness of the BMT 57 mm Bearings | 5-144 |
| 5.10.4 Cumulative Load Assessment for BMT Bearing Life | 5-146 |
| 5.11 MAY, 1983 | 5-150 |
| 5.11.1 Radial Stiffness of the BMT 57 mm Bearings at 10,000 RPM | 5-150 |
| 5.11.2 Status and Results of Bearing Thermal Analysis | 5-150 |
| 5.11.3 Application of the Double Linear Damage Rule to Bearing Life Predictions | 5-156 |
| 5.12 JUNE, 1983 | 5-156 |
| 5.12.1 Update of Bearing Thermal Model Surface-to-Fluid Heat Transfer Coefficients | 5-156 |
| 5.12.2 Sensitivity of Bearing Component Temperatures to Transition to Film Boiling | 5-160 |
| 5.12.3 Bearing Life Modeling | 5-163 |
| 5.13 JULY, 1983 | 5-163 |
| 5.13.1 Fluid Film Thickness Estimates for Materials Fatigue Tester | 5-163 |
| 5.13.2 Fluid Heat Transfer Regimes and Film Coefficients for LOX Coolant | 5-179 |
| 5.13.3 Status of Thermal Model | 5-182 |
| 5.13.4 Planned Efforts for August 1983 Reporting Period | 5-182 |
| 6.0 REFERENCES | 6-1 |

LIST OF FIGURES

| NUMBER | TITLE | PAGE |
|--------|---|------|
| 5.1.1 | Comparison of Calculated and Measured Wear Tracks | 5-2 |
| 5.1.2 | Comparison of Estimated and Test Results | 5-3 |
| 5.1.3 | Simplified Pressure/Flow Network | 5-4 |
| 5.1.4 | Influence of Vapor Generation on Pressure | 5-5 |
| 5.1.5 | Boiling Curve for Oxygen | 5-7 |
| 5.1.6 | LOX Inlet Cavity Pressure (Load Side) | 5-8 |
| 5.1.7 | LOX Inlet Cavity Pressure (Drive Side) | 5-9 |
| 5.1.8 | LOX Test Conditions (Time-10 Sec) | 5-11 |
| 5.1.9 | LN ₂ Test Conditions (Time-0) | 5-12 |
| 5.1.10 | LOX Test Conditions (Time-140 Sec) | 5-13 |
| 5.1.11 | LN ₂ Test Conditions (Time-160 Sec) | 5-14 |
| 5.1.12 | Energy Balance Summary | 5-16 |
| 5.2.1 | Contact Angle and Stresses vs Bearing Temperature Difference | 5-18 |
| 5.2.2 | Bearing Operating Clearances vs Temperature Difference | 5-19 |
| 5.2.3 | Normal Forces vs Bearing Temperature Difference | 5-20 |
| 5.2.4 | Increase in Heat Generation vs Bearing Temperature Difference | 5-25 |
| 5.3.1 | Contact Angle and Stresses vs Bearing Temperature Difference | 5-28 |
| 5.3.2 | Bearing Operating Clearances vs Temperature Difference | 5-29 |
| 5.3.3 | Normal Forces vs Temperature Difference | 5-30 |
| 5.3.4 | Increase in Heat Generated vs Bearing Temperature Difference | 5-31 |
| 5.3.5 | Ball Spin Vector Diagram | 5-33 |
| 5.3.6 | Ball Spin/Roll Ratio vs Bearing ΔT | 5-34 |
| 5.3.7 | Heating and Ball Drag vs % Fluid in Cavity | 5-36 |
| 5.3.8 | Cage/Shaft Speed Ratio vs Axial Load, % LOX in Bearing Cavity and Friction Coefficient | 5-37 |
| 5.3.9 | Heat Generated vs Axial Load 50% Fluid in Cavity | 5-38 |
| 5.3.10 | Heat Generated vs Axial Load 100% Fluid in Cavity | 5-39 |
| 5.3.11 | Power Generation vs Temperature Difference Across Bearing | 5-41 |
| 5.3.12 | Energy Balance Summary | 5-42 |
| 5.3.13 | Energy vs Bearing ΔT | 5-43 |
| 5.3.14 | Status of Bearing Thermal Model | 5-45 |
| 5.3.15 | Schematic of Bearing Set | 5-46 |
| 5.3.16 | Cross Sectional View of Shaft, Bearing, Carrier, and Housing | 5-47 |
| 5.3.17 | Finite Element Description of Rolling Element | 5-48 |
| 5.3.18 | Center Section 1 | 5-49 |
| 5.4.1 | Heat Generation vs Axial Reaction | 5-51 |
| 5.4.2 | Cage-to-Shaft Speed Ratio | 5-52 |
| 5.4.3 | Contact Angle and Stresses vs Bearing Temperature Difference | 5-54 |
| 5.4.4 | Limiting Temperature Across Bearing and Materials Tester | 5-55 |

LIST OF FIGURES (CONTINUED)

| NUMBER | TITLE | PAGE |
|--------|---|-------|
| 5.4.5 | Run No. 2 Inlet and Outlet Temperature vs Time | 5-56 |
| 5.4.6 | Limited Temperature Difference Across Single Bearing Pair | 5-57 |
| 5.4.7 | BMT Bearing Set | 5-59 |
| 5.4.8 | Sinda Output | 5-60 |
| 5.4.9 | Bearing 1; Outer Race, Rolling Element, and Inner Race . . . Temperatures for 2500 lb Axial Load | 5-61 |
| 5.4.10 | Bearing 1 Detail of Inner and Outer Race Track Temperatures | 5-62 |
| 5.4.11 | Bearing 1 Detailed Temperature Gradient of Ball Track . . . | 5-63 |
| 5.5.1 | Lubrication Life Adjustment Factors | 5-66 |
| 5.5.2 | Radial Load vs Radial Deflection | 5-68 |
| 5.5.3 | Radial Stiffness vs Axial Reaction | 5-69 |
| 5.5.4 | Radial Load vs Radial Deflection | 5-70 |
| 5.5.5 | Bearing Radial Stiffness vs Shaft Speed | 5-71 |
| 5.5.6 | Comparison of Single Phase Flow Heat Transfer Correlations | 5-73 |
| 5.5.7 | Example Heat Rate Analysis Output from Sinda | 5-75 |
| 5.5.8 | Thermal Model Steady State Temperature | 5-77 |
| 5.5.9 | Bearing Node Locations and Temperatures | 5-78 |
| 5.5.10 | Comparison of Model Results with Test Data | 5-79 |
| 5.5.11 | Recommended Thermocouple Locations | 5-80 |
| 5.6.1 | Bearing Deflection vs Axial Reaction | 5-83 |
| 5.6.2 | Spring Deflection vs Load | 5-84 |
| 5.6.3 | Bearing Reaction vs Carrier Axial Load | 5-85 |
| 5.6.4 | Mass Flow Rate vs Inner Race Ball Track Temperature for Axial Reaction of 2500 Pounds | 5-89 |
| 5.6.5 | Mass Flow Rate vs Temperature Across Outer Race for FOV Axial Reaction of 2500 Pounds | 5-90 |
| 5.6.6 | Mass Flow Rate vs Temperature of Node 403 for an Axial . . . Reaction of 2500 Pounds | 5-91 |
| 5.6.7 | Comparison of Test Data and Thermal Model Results (Bgr 1, . Mass Flow = 3.2 lbs/sec, Inlet Temp = -305°F) | 5-92 |
| 5.6.8 | Comparison of Test Data and Thermal Model Results (Bgr 2, . Mass Flow = 3.2 lbs/sec, Inlet Temp = -305°F) | 5-93 |
| 5.6.9 | Comparison of Test Data and Thermal Model Results (Bgr 3, . Mass Flow = 3.2 lbs/sec, Inlet Temp = -305°F) | 5-94 |
| 5.6.10 | Comparison of Test Data and Thermal Model Results (Bgr 4, . Mass Flow = 3.2 lbs/sec, Inlet Temp = -305°F) | 5-95 |
| 5.6.11 | Comparison of Test Data and Thermal Model Results (Bgr 1, . Mass Flow = 6.3 lbs/sec, Inlet Temp = -305°F) | 5-96 |
| 5.6.12 | Comparison of Test Data and Thermal Model Results (Bgr 2, . Mass Flow = 6.3 lbs/sec, Inlet Temp = -305°F) | 5-97 |
| 5.6.13 | Comparison of Test Data with Thermal Model Results (Bgr 3, Mass Flow = 6.3 lbs/sec, Inlet Temp = -305°F) | 5-98 |
| 5.6.14 | Comparison of Test Data with Thermal Model Results (Bgr 4, Mass Flow = 6.3 lbs/sec, Inlet Temp = -305°F) | 5-99 |
| 5.6.15 | Comparison of Test Data with Thermal Model Results (Bgr 1, Mass Flow = 9.6 lbs/sec, Inlet Temp = -305°F) | 5-100 |

LIST OF FIGURES (CONTINUED)

| NUMBER | TITLE | PAGE |
|--------|---|-------|
| 5.4.5 | Run No. 2 Inlet and Outlet Temperature vs Time | 5-56 |
| 5.4.6 | Limited Temperature Difference Across Single Bearing Pair | 5-57 |
| 5.4.7 | BMT Bearing Set | 5-59 |
| 5.4.8 | Sinda Output | 5-60 |
| 5.4.9 | Bearing 1; Outer Race, Rolling Element, and Inner Race . . . Temperatures for 2500 lb Axial Load | 5-61 |
| 5.4.10 | Bearing 1 Detail of Inner and Outer Race Track Temperatures | 5-62 |
| 5.4.11 | Bearing 1 Detailed Temperature Gradient of Ball Track . . . | 5-63 |
| 5.5.1 | Lubrication Life Adjustment Factors | 5-66 |
| 5.5.2 | Radial Load vs Radial Deflection | 5-68 |
| 5.5.3 | Radial Stiffness vs Axial Reaction | 5-69 |
| 5.5.4 | Radial Load vs Radial Deflection | 5-70 |
| 5.5.5 | Bearing Radial Stiffness vs Shaft Speed | 5-71 |
| 5.5.6 | Comparison of Single Phase Flow Heat Transfer Correlations | 5-73 |
| 5.5.7 | Example Heat Rate Analysis Output from Sinda | 5-75 |
| 5.5.8 | Thermal Model Steady State Temperature | 5-77 |
| 5.5.9 | Bearing Node Locations and Temperatures | 5-78 |
| 5.5.10 | Comparison of Model Results with Test Data | 5-79 |
| 5.5.11 | Recommended Thermocouple Locations | 5-80 |
| 5.6.1 | Bearing Deflection vs Axial Reaction | 5-83 |
| 5.6.2 | Spring Deflection vs Load | 5-84 |
| 5.6.3 | Bearing Reaction vs Carrier Axial Load | 5-85 |
| 5.6.4 | Mass Flow Rate vs Inner Race Ball Track Temperature for Axial Reaction of 2500 Pounds | 5-89 |
| 5.6.5 | Mass Flow Rate vs Temperature Across Outer Race for FOV Axial Reaction of 2500 Pounds | 5-90 |
| 5.6.6 | Mass Flow Rate vs Temperature of Node 403 for an Axial . . . Reaction of 2500 Pounds | 5-91 |
| 5.6.7 | Comparison of Test Data and Thermal Model Results (Bgr 1, . Mass Flow = 3.2 lbs/sec, Inlet Temp = -305°F) | 5-92 |
| 5.6.8 | Comparison of Test Data and Thermal Model Results (Bgr 2, . Mass Flow = 3.2 lbs/sec, Inlet Temp = -305°F) | 5-93 |
| 5.6.9 | Comparison of Test Data and Thermal Model Results (Bgr 3, . Mass Flow = 3.2 lbs/sec, Inlet Temp = -305°F) | 5-94 |
| 5.6.10 | Comparison of Test Data and Thermal Model Results (Bgr 4, . Mass Flow = 3.2 lbs/sec, Inlet Temp = -305°F) | 5-95 |
| 5.6.11 | Comparison of Test Data and Thermal Model Results (Bgr 1, . Mass Flow = 6.3 lbs/sec, Inlet Temp = -305°F) | 5-96 |
| 5.6.12 | Comparison of Test Data and Thermal Model Results (Bgr 2, . Mass Flow = 6.3 lbs/sec, Inlet Temp = -305°F) | 5-97 |
| 5.6.13 | Comparison of Test Data with Thermal Model Results (Bgr 3, Mass Flow = 6.3 lbs/sec, Inlet Temp = -305°F) | 5-98 |
| 5.6.14 | Comparison of Test Data with Thermal Model Results (Bgr 4, Mass Flow = 6.3 lbs/sec, Inlet Temp = -305°F) | 5-99 |
| 5.6.15 | Comparison of Test Data with Thermal Model Results (Bgr 1, Mass Flow = 9.6 lbs/sec, Inlet Temp = -305°F) | 5-100 |

LIST OF FIGURES (CONTINUED)

| NUMBER | TITLE | PAGE |
|--------|--|-------|
| 5.6.16 | Comparison of Test Data with Thermal Model Results (Bgr 2, Mass Flow = 9.6 lbs/sec, Inlet Temp = -305°F) | 5-101 |
| 5.6.17 | Comparison of Test Data with Thermal Model Results (Bgr 3, Mass Flow = 9.6 lbs/sec, Inlet Temp = -305°F) | 5-102 |
| 5.6.18 | Comparison of Test Data with Thermal Model Results (Bgr 4, Mass Flow = 9.6 lbs/sec, Inlet Temp = -305°F) | 5-103 |
| 5.6.19 | Comparison of Test Data with Thermal Model Results (Bgr 1, Mass Flow = 12.8 lbs/sec Inlet Temp = -305°F) | 5-104 |
| 5.6.20 | Comparison of Test Data with Thermal Model Results (Bgr 2, Mass Flow = 12.8 lbs/sec, Inlet Temp = -305°F) | 5-105 |
| 5.6.21 | Comparison of Test Data with Thermal Model Results (Bgr 3, Mass Flow = 12.8 lbs/sec, Inlet Temp = -305°F) | 5-106 |
| 5.6.22 | Comparison of Test Data with Thermal Model Results (Bgr 4, Mass Flow = 12.8 lbs/sec, Inlet Temp = -305°F) | 5-107 |
| 5.7.1 | Displacement of Outer Race with Inner Race Fixed | 5-109 |
| 5.7.2 | Change in Contact Angle as a Function of Outer Race Misalignment and Azimuth Location | 5-110 |
| 5.7.3 | Bearing Torque as a Function of Axial Load | 5-112 |
| 5.7.4 | Bearing Deflections and Contact Angle as a Function of Axial Load | 5-113 |
| 5.7.5 | Temperature vs Depth Below Surface of Inner Race Track | 5-118 |
| 5.7.6 | Total Frictional Heat Rate vs ΔT Across Bearing | 5-120 |
| 5.8.1 | N ₂ Film Thickness Estimates | 5-122 |
| 5.8.2 | Change in Radial Stiffness as Function of Ball Wear | 5-127 |
| 5.8.3 | Safe Operating Range for LN ₂ | 5-129 |
| 5.9.1 | Maximum Surface Shear Stress as Function of Friction Coefficient | 5-132 |
| 5.9.2 | Maximum Principal Stresses in Surface vs Friction | 5-133 |
| 5.9.3 | Maximum Tensile Surface Stress vs Friction | 5-134 |
| 5.9.4 | O ₂ Viscosity | 5-136 |
| 5.9.5 | Estimated Film Thickness vs Temperature for O ₂ | 5-137 |
| 5.10.1 | Carrier Tilt in Housing | 5-139 |
| 5.10.2 | Outer Race Misalignment as Function of Bearing Carrier Diametrical Clearance | 5-140 |
| 5.10.3 | Radial Stiffness vs Azimuth Angle | 5-141 |
| 5.10.4 | Operating Misalignment vs Initial Misalignment and Axial Load | 5-143 |
| 5.10.5 | Bearing Radial Reaction vs Deflection | 5-145 |
| 5.10.6 | Inner Race Contact Angle vs Radial Load | 5-147 |
| 5.10.7 | Maximum Contact Stress vs Axial and Radial Reactions | 5-148 |
| 5.10.8 | Load vs Time | 5-150 |
| 5.11.1 | Bearing Radial Reaction vs Deflection | 5-151 |
| 5.11.2 | Maximum Contact Stress vs Axial and Radial Reaction | 5-152 |
| 5.11.3 | Fluid Outlet Temperature and Heat Input vs Coolant Flow Rate | 5-154 |
| 5.11.4 | Fluid Outlet Temperature and Heat Input vs Coolant Flow Rate | 5-155 |

LIST OF FIGURES (CONTINUED)

| NUMBER | TITLE | PAGE |
|-----------|--|-------|
| 5.12.1 | Comparison of Nucleate Boiling Correlations | 5-158 |
| 5.12.2 | Component Temperature as a Function of Wall Superheat at Max Flux Conditions | 5-161 |
| 5.12.3 | Temperature Distribution in the Inner and Outer Races . . . | 5-164 |
| 5.12.3(a) | Detail of Tract Temperature Distribution in the Inner and Outer Races | 5-165 |
| 5.12.3(b) | Rolling Element Temperature Distribution | 5-166 |
| 5.12.4 | Temperature Distribution in Inner and Outer Races | 5-167 |
| 5.12.4(a) | Detail of Track Temperature Distribution in the Inner and Outer Races | 5-168 |
| 5.12.4(b) | Rolling Element Temperature Distribution | 5-169 |
| 5.12.5 | Temperature Distribution in the Inner and Outer Races . . . | 5-170 |
| 5.12.5(a) | Detail of Track Temperature Distribution in the Inner and Outer Races | 5-171 |
| 5.12.5(b) | Rolling Element Temperature Distribution | 5-172 |
| 5.12.6 | Temperature Distribution in the Inner and Outer Races . . . | 5-173 |
| 5.12.6(a) | Detail of Track Temperature Distribution in the Inner and Outer Races | 5-174 |
| 5.12.6(b) | Rolling Element Temperature Distribution | 5-175 |
| 5.13.1 | Tester Configuration and Lubricant Properties | 5-176 |
| 5.13.2 | Heat Transfer Regimes for LOX | 5-180 |
| 5.13.3 | Heat Transfer Regimes for LN ₂ | 5-181 |
| 5.13.4 | Force and Heat Distribution in Rolling Contacts (Inner Race) | 5-183 |
| 5.13.5 | Force and Heat Distribution in Rolling Contacts (Outer Race) | 5-184 |

LIST OF TABLES

| NUMBER | TITLE | PAGE |
|--------|--|-------|
| 5.6.1 | Shaft/Component Material Properties and Geometry | 5-82 |
| 5.7.1 | Summary of Bearing Thermal Model Data Base | 5-115 |
| 5.7.2 | Preliminary Temperature Iteration Results for 2500 Pound Axial Reaction | 5-116 |
| 5.7.3 | Preliminary Temperature Iteration Results for 6000 Pound Axial Reaction | 5-119 |
| 5.8.1 | Nitrogen Viscosity | 5-126 |
| 5.8.2 | Summary of Computer Runs Required to Generate Data for Figure 5.8.3 | 5-130 |
| 5.10.1 | Conditions Investigated for Bearing Misalignment Effects | 5-142 |
| 5.13.1 | Lubricant Properties | 5-178 |

1.0 INTRODUCTION

This report describes the work accomplished during the past year (July 1982 - July 1983) in support of the MSFC Bearing and Materials Tester (BMT) Program. The objective of this activity is to support the development and operation of the BMT including data reduction and evaluation. Since the Shuttle Main Engine (SSME) turbopump bearings operate in an environment considerably more severe than conventional bearing systems, traditional analysis methods and bearing life models are not directly applicable.

The MSFC BMT Program is therefore directed toward a better understanding of the various parameters that effect/or determine the SSME turbopump bearing operational characteristics and service life and to develop and verify design tools applicable to these systems. Support of this program involves a broad spectrum of engineering analysis activities including static analysis of the BMT Shaft Bearing System, high-speed bearing system analysis, contact stress evaluation, bearing failure mode evaluation and thermal modeling of the bearing and cryogenic flow system. The tasks described in this report do not represent the total analysis effort for the design and development of the BMT. The enclosed work was done to support the development of the BMT in specialized areas as problems occurred and to support the stated objectives. BMT test data are reduced, evaluated, and correlated with analyses where applicable. Since test data applicable to the turbopump bearing system are absent and the system and operating conditions are of such complexity that theoretical modeling requires unprecedented extrapolations, data from the BMT are required to substantiate turbopump bearing analysis and bearing life predictions.

2.0 SUMMARY

During this annual reporting period, significant progress has been made in the understanding and use of the Shaberth bearing analysis computer program. This program was developed for the analysis of jet engine shaft/bearing systems operating above room temperature with normal hydrocarbon lubricants. Through continued analysis effort, it has been possible to adapt this tool to the evaluation of shaft bearing systems operating in cryogenics.

Effects such as fluid drag, radial temperature gradients, outer race misalignments and clearance changes have been simulated and evaluated. In addition, the speed and preload effects on bearing radial stiffness has been evaluated. The Shaberth program has also been used to provide contact stresses from which contact geometry has been calculated to support other analyses such as the determination of cryogenic fluid film thickness in the contacts and evaluation of surface and subsurface stresses necessary for bearing failure evaluation. This program has been a vital tool for the thermal analysis of the bearing in that it provides the heat generation rates at the rolling element/race contacts for input into a thermal model of the bearing/shaft assembly.

Although the SHABERTH (41)* computer code has a thermal subroutine, it is not capable of accommodating varying thermal properties and two phase flow. A bearing thermal model with this capability has been developed using the SINDA thermal analyzer. The bearing/shaft assembly and cryogenic coolant flow are thermally simulated by a nodal network and the model provides a detailed description of the bearing and assembly component temperatures and gradients. The model accounts for the various heat transfer regimes encountered in a two phase flow system and allows the assessment of parameters such as load, speed, flow rate, fluid subcooling, etc. on bearing component temperatures. Bearing contact surfaces are modeled in detail, to assess the maximum surface temperatures, and complete descriptions of component temperature gradients are provided. This can be important in assessing the characteristics such as fluid film thickness, film lubricant requirements, and effects on contact friction. Test data from the BMT has been used when possible to calibrate/verify the thermal model.

A complete analyses of the bearing shaft assembly requires iteration between the SHABERTH bearing and SINDA thermal models. This is necessary due to the strong coupling between bearing component temperatures and internal operating clearances. As the inner race temperature exceeds that of the outer race, thermal growth reduces or eliminates the operating clearances. This in turn increases the contact stresses and forces which increase the frictional heat generated. This is a cycle that will cause premature bearing failure if it proceeds unchecked. This condition has been simulated by utilizing the SHABERTH bearing program and the SINDA bearing thermal model. By this analysis method, preliminary bounds have been established for stable operation in LN₂. These limits have been established in terms of fluid flow, fluid inlet temperature, and axial load for a shaft speed of 30,000 RPM as indicated in Figure 5.8.3.

The major conclusions from this reporting period are summarized below:

(1) The importance of understanding and developing reliable analysis tools for estimating the mechanical/thermal interactions of the bearing system and the effects on bearing performance and life cannot be over emphasized. There are many deficiencies in the analytical methods available and applicable test data is nonexistent. Therefore, these gaps must be filled with additional BMT test and operational data before reliable

* Refers to Reference on page 6-1.

predictions concerning Shuttle Main Engine turbopump bearing performance and life can be made.

(2) There is a strong mechanical/thermal interaction in the turbopump shaft/bearing system. This is especially critical in these cryogenically cooled systems because of the drastically changing cooling ability as the fluid changes from liquid to vapor. As an example, an increase in load can cause transition from forced convection liquid cooling to forced convection vapor cooling with a significantly large increase in component temperatures. Such increases can rapidly eliminate internal clearances, increase contact stresses and frictional heat causing further heating until failure occurs. This unstable condition can further be aggravated by extremely high temperatures in the contact areas which can cause breakdown of the dry film lubricant, significantly increasing the frictional heat generation. An example of these temperatures are shown in Figures 5.12.3 - 5.12.6. In addition to rapid bearing failure, less severe cases can cause failures different from the subsurface fatigue failures experienced by conventional oil lubricated bearings. As will be discussed later, increased surface friction moves the maximum shear stresses to the surfaces and therefore, the failure occurs in the surface rather than below the surface. Furthermore, the high temperatures predicted will significantly degrade the material properties in the surface and this, combined with loss of lubricant, allows surface wear to become a potential failure mode. Due to the steep thermal gradients at the bearing contact surfaces, there is a strong possibility that thermally induced stresses are significant contributors to bearing failure. These conditions and failure modes are vastly different from those experienced by conventionally operated and lubricated rolling bearings. Therefore, the data base for conventional bearing life predictions has severely limited validity when extrapolated to high-speed bearings operating in cryogenics.

(3) Estimating coolant flow requirements for cryogenically cooled bearing systems, typical of the SSME turbopumps, requires consideration of mechanical/thermal coupling of the system. Analysis has shown that system heat generation is not a simple function of applied load. As previously discussed, the establishment of a temperature gradient across the bearing will increase the frictional heat generated. For example, the coolant outlet temperature is essentially linear with flow for a constant heat input which, for a bearing of uniform temperature, would indicate a constant load. However, for a condition (this could be a low-flow case) that allows an adverse temperature gradient to establish itself across the bearing, the heat generated will be considerably greater for the same axial load causing a higher coolant outlet temperature. Therefore, rather than a linear coolant outlet temperature increase with decreasing flow, the outlet coolant temperature increase can become exponential with decreasing flow. Typical examples of this condition are shown in Figure 5.11.3 and 5.11.4. The required coolant flow should be specified to maintain the essentially linear relationship between flow and outlet coolant temperature for given load and bearing speed conditions.

(4) Contact stress analyses show that the maximum shear stress occurs in the surface of the contact for friction factors greater than 0.19. Results of these analyses are shown in Figure 5.9.1. For marginally lubricated bearings operating in cryogenics, it is very likely that the contact friction factor is greater than 0.19. This is especially true when the bearing contact temperatures are significantly above the cryogen saturated temperature. This condition precludes any liquid film support between the contacts. In addition, many dry film lubricants fail at temperatures approaching 500-700°F. Consequently, surface failure modes are strong candidates for bearings operating in these environments.

(5) Further research is needed to characterize the performance of dry film lubricants operating in cryogenics and the effects of contact surface temperature on the performance of these lubricants. The contact lubrication and traction, for bearing systems similar to those studied in this report, probably vary considerably with operation time and contact temperature. A key part of the bearing thermal analysis is the determination of the friction heat generated in the bearing contacts. This requires knowledge of local friction forces and slip velocities and the interdependency of these variables for the specific lubrication system being analyzed. For example, the friction coefficient is generally a function of slip velocity and may be enhanced by metal oxide formation when operating in liquid oxygen. Additional test data characterizing these effects are required before reliable contact heat generation estimates can be made.

(6) Further work is also needed to characterize the heat transfer mechanisms for high-speed bearings operating in high-flow, subcooled, cryogenic systems. No data has been found in the literature that is directly applicable to these conditions.

3.0 LISTING OF TASKS ACCOMPLISHED

3.1 JULY, 1982

- o Investigation of variables affecting wear tracks generated during tester operation,
- o Comparison of predicted and measured ball pass counts,
- o Investigation of thermal and flow characteristics that could have contributed to the LOX test incident, and
- o Determination of energy and flow balance estimates for the Bearing and Materials Tester (BMT).

3.2 AUGUST, 1982

- o Investigation of bearing temperature gradients on operational contact angle,
- o Modeling the effect of viscous drag on bearing rolling elements,
- o Development of a technique for modeling the thermal contact resistance between bearing rolling and stationary elements,
- o Continued thermal model development, and
- o Graphics capability development for data reduction and display.

3.3 SEPTEMBER, 1982

- o Continued investigation of bearing temperature gradients on bearing operating characteristics,
- o Estimates of ball drag forces, torques, and heat generated,
- o Correlation of tester internal power dissipated with bearing temperature differences, and
- o Continued bearing thermal model development.

3.4 OCTOBER, 1982

- o Effects of bearing preload on cage slip and friction heat generation,
- o Recommendations for temperature cutoff values for the LN₂ bearing tests, and
- o Continued thermal model development.

3.5 NOVEMBER, 1982

- o Bearing life prediction analysis,
- o Stiffness characteristics of the turbine and LOX pump bearing,
- o Heat transfer coefficients for bearing thermal model, and
- o Preliminary results of bearing thermal model.

3.6 DECEMBER, 1982

- o Evaluation of bearing operating preloads in LN₂,
- o Bearing axial reactions resulting from carrier axial loading,
- o Interference fit between bearing inner race and shaft, and
- o Results of bearing thermal model.

3.7 JANUARY, 1983

- o Possible effects of outer race misalignment on shaft assembly balancing,
- o Bearing radial stiffness analysis,
- o Evaluation of viscous heat loads and bearing friction factors in LN₂ for input to bearing thermal model, and
- o Results of bearing thermal model.

3.8 FEBRUARY, 1983

- o Film thickness estimates for 57 mm bearing operating in LN₂,
- o Evaluation of radial stiffness of 57 mm bearing as a function of ball wear,
- o Status and results of bearing thermal model, and
- o Investigation of outer race misalignment effects.

3.9 MARCH, 1983

- o Effect of friction on rolling element contact and subsurface stresses,
- o Bearing thermal modeling and analysis, and
- o Estimation of film thickness of 57 mm bearing operating in O₂.

3.10 APRIL, 1983

- o Evaluation of bearing carrier to housing clearance and the effect of bearing operating characteristics,
- o Bearing thermal analysis,
- o Investigation of the radial stiffness of the BMT 57 mm bearings, and
- o Cumulative load assessment for BMT bearing life.

3.11 MAY, 1983

- o Analysis of the radial stiffness of the BMT 57 mm bearings at 10,000 RPM,
- o Continued bearing thermal analysis, and
- o BMT bearing life modeling.

3.12 JUNE, 1983

- o Update of bearing thermal model surface-to-fluid heat transfer coefficients,
- o Sensitivity of bearing component temperatures to transition to film boiling, and
- o Bearing life modeling.

3.13 JULY, 1983

- o Fluid film thickness estimates for material fatigue tester,
- o Fluid heat transfer regimes and film coefficients for LOX coolant, and
- o Status of thermal model.

4.0 SYNOPSIS OF RESULTS

The following is a summary of results and conclusions from the monthly progress reports submitted during this 12 month period.

JULY, 1982

- 1) Observed bearing wear tracks can be simulated with the SHABERTH bearing program. However, the uncertainty in the tester loading due to unknown pressure-induced loads and the combined axial and radial load profiles cloud the results of this effort. Proposed loading sequences for upcoming tests and evaluation of the pressure-induced loads should overcome these problems. Instrumentation to determine ball pass counts is important in the evaluation of cage speed and potential ball slip due to fluid drag.
- 2) Evaluation of the BMT incident in LOX produced the following conclusions: (a) Parallel coolant flow paths can produce unequal flow and cooling causing potential overheating and thermal run away especially in two phase coolants, consequently "dedicated" coolant flow should be provided to each bearing pair in the BMT; (b) Coolant subcooling should be as large as practical to preclude major surfaces of the bearing from operating above the coolant saturation temperature; (c) The overall energy balance across the tester provides valuable data for assessing the heat generated in the BMT. Therefore, coolant inlet and outlet temperature and pressure measurements are important along with flow rate measurements. Measurement of bearing torque is also highly desirable as a guide for estimating the traction in the contact areas.

AUGUST, 1982

- 1) Initial analyses were performed to evaluate the effects of bearing radial temperature differences on contact angle, normal forces, contact stresses, operating clearances and heat generation. Assumptions were made concerning the bearing temperature gradient although later analyses used the bearing thermal model to determine the average temperature of the inner race, ball and outer race. These assumed gradients illustrated the coupling between the thermal and mechanical characteristics of the bearing/shaft assembly. For example, it was shown that internal clearances could be lost, forces and stresses increased, contact angles decreased, and heat generation significantly increased as the inner race temperature was assumed to increase over the outer race temperature. Therefore, an unstable situation could be created that would lead to thermal and mechanical instability causing bearing failure.
- 2) A technique was developed to estimate the thermal conductance between the ball and races of a high-speed rolling bearing for simulation in the nodal network thermal model.

SEPTEMBER, 1982

- 1) Analyses of bearing temperature gradient effects were continued and extended to evaluate the effects on the ball spin-to-roll ratio. Results show that an increase in temperature gradient reduces the ball spin. This effect alone should increase life. The other effects such as increased stresses and load, however, overshadow the gains of reduced ball spin.

- 2) The effect of coolant drag and friction coefficient on ball slippage or skidding was simulated with SHABERTH. Results for LOX indicated that lightly preloaded bearings ~ 400 lbs could experience increased heat generation, wear, and reduced life due to ball skidding. Reduction in friction coefficient caused increased ball skid.
- 3) The sources and magnitudes of heat generated in the BMT were defined. The total amount calculated was compared to the amount determined by the tester measurements. Assumption of a relatively high bearing temperature difference was required to match the measured BMT energy dissipation. As there are several unknown factors affecting the energy dissipation such as fluid vortexing, contact friction, loads, etc., additional measurements such as coolant outlet temperature for each bearing pair, bearing torque, carrier and bearing temperature, and loads are needed to narrow the uncertainty in the heat generation values.

OCTOBER, 1982

- 1) The ball skidding analysis was repeated for LN_2 coolant. Essentially the same results as described in paragraph 2 of the September 1982 summary were obtained.
- 2) Analyses were made to establish initial temperature red lines for the BMT operating in LN_2 . The outlet fluid temperature, based on a minimum recommended flow of 12.6 lbs/sec, and maximum inlet temperature of $160^\circ R$ should not exceed $178^\circ R$. The outer race temperature should not exceed $200^\circ R$ for the initial no-load runs. As more experience is gained with the BMT, these temperature limits can be relaxed.
- 3) The thermal model of the BMT bearing and shaft assembly was successfully executed using the SINDA thermal analyzer. Although this was an initial checkout run, the temperatures for the contact surfaces were significantly above the fluid saturation temperature, indicating that vapor rather than liquid was present in the contact areas. Consequently, it is unlikely that a fluid film thick enough to partially separate the contacts exists, and even though the bulk fluid is at cryogenic temperature, the dry film lubricant must perform at elevated temperature in the bearing contacts.

NOVEMBER, 1982

- 1) Techniques for adjusting the bearing life predictions due to lubrication film thickness-to-surface roughness ratio were extracted from both SHABERTH I and SHABERTH II. SHABERTH I lubrication factor is <1 and is therefore never a life improver. SHABERTH II allows a life improvement factor to account for full film lubrication. Since a life improvement factor for improved materials can be input to the program, and all reduction and improvement factors are multipliers of the Lundberg - Palmgren life model, the results of the two programs can be made to coincide with the proper selection of these factors. These lubricant life adjustment factors are not likely to be applicable to bearings operating in cryogenics.
- 2) Radial stiffness characteristics were evaluated for the turbine end LOX pump bearing. In general, radial stiffness increases with axial load and decreases with shaft speed. These results are shown in Figures 5.5.3 and 5.5.5.

- 3) Preliminary data from the bearing thermal model indicated several "hot spots" near the ball race contacts where frictional heat generation is high, indicating local boiling and/or vapor blanketing. Efforts, including an extensive literature survey, were undertaken to establish the heat transfer correlations most applicable for the conditions in the BMT. No published correlation was found to match the flow conditions in the tester. Based on a review of the literature, a Dittus - Boelter equation was selected for prediction of the forced convection heat transfer coefficient, and Rohsenow's correlation for pool nucleate boiling was used to predict the boiling heat transfer coefficient. As will be discussed later, significant changes were made as more work was done to evaluate the two phase heat transfer problem. Thermal analyses were conducted assuming no boiling heat transfer. Results showed the need for additional temperature measurements to verify the analyses. Recommendations were made for additional measurements on the outer surface of the bearing carriers.

DECEMBER, 1982

- 1) An analysis was done to estimate the change in bearing preload, from the assembled preload value, as the bearing shaft assembly is cooled from room temperature to LN₂ temperature and rotated to a speed of 30,000 RPM. Results show that room temperature preload is not significantly changed by cryogenic temperature (LN₂) and a speed of 30,000 RPM.
- 2) The unloaded bearings (1 and 4) will maintain sufficient preload to prevent skidding for carrier axial loads up to 8,000 lbs. The preload spring hysteresis introduces a maximum uncertainty of about 20% in the preload value.
- 3) An evaluation of bearing/shaft clearances show that an interference fit between inner race and shaft is maintained during steady operating conditions at 30,000 RPM. There is a potential for loss of interference during start transients when the bearing is suddenly loaded and rotated to speed. Even if this occurs, there should be no rotation of the inner race relative to the shaft because the assembly is held together by a highly torqued nut at the load end of the shaft and a balancing cap at the drive end.
- 4) Preliminary thermal analyses for an axial reaction of 2500 lbs and an assumed temperature difference between inner race and outer race of 200°C (this assumption was made to determine the frictional heat generated) show that bearing temperatures are more sensitive to coolant subcooling than changes in flow for flow rates greater than 10 lbs/sec per bearing set. The temperatures become more sensitive to flow at rates less than 10 lbs/sec per bearing set. This analysis does not iterate between the bearing dynamic model and thermal model to obtain the frictional heat generated and therefore should be considered highly preliminary.

JANUARY, 1983

- 1) An investigation was initiated to evaluate the effect of carrier face run out on apparent shaft assembly unbalance. The carrier run out can in effect produce an angular misalignment on the bearing outer race. For this to simulate a synchronous unbalance, the radial stiffness of the bearing would have to significantly vary in the azimuth direction. Results show that for the misalignments expected, the radial stiffness did not vary significantly in the azimuth direction and therefore, the carrier run out should not be a problem.

- 2) Using heat balance data from BMT tests, measured torque data viscous and frictional heat loads were estimated for the BMT thermal model. A dry friction coefficient of 0.2 was determined from the torque data. The data was for low-speed room temperature operation and considerable uncertainty remains concerning the true friction coefficient at the bearing operating temperature and speed.
- 3) Coupling of the mechanical and thermal characteristics of the bearing shaft system were simultaneously evaluated to simulate a thermal run away condition. This was done for a 6000 lb axial reaction, coolant flow of 3.2 lbs/sec per bearing set and an inlet coolant temperature of -285°F. For these conditions, there was a progressively increasing heat generation rate and bearing temperature indicating that over-temperature failure would occur.

FEBRUARY, 1983

- 1) Estimated film thickness for bearings operating in LN₂ indicate very little contribution of the fluid to contact lubrication. This is especially true when the contact surfaces exceed the fluid saturation temperature. This emphasizes the importance of dry film transfer lubrication.
- 2) The radial stiffness of the 57 mm bearing was estimated as a function of ball wear. Reduction in ball diameter of ~1 mil reduced the radial stiffness of the bearing by half.

MARCH, 1983

- 1) Contact stress analyses show that traction forces significantly affect the magnitude and location of the surface and subsurface stresses. The magnitude of friction forces are important in determining failure modes for rolling element bearings.
- 2) Estimates of fluid film thickness for the 57 mm bearings operating in LOX show that the fluid film is insufficient to provide appreciable separation and/or lubrication of the loaded contacts.
- 3) Thermal and dynamic analyses indicate that steady state axial reactions of 10,000 lbs will cause thermal run away in the 57 mm bearing operating in LN₂.

APRIL, 1983

- 1) Effects of carrier to housing clearances on outer race misalignment and bearing operating characteristics produced the following results: (a) Diametrical carrier to housing clearance of 1.3 mil caused an initial outer race misalignment of 2.25 minutes; (b) This misalignment was reduced to an operating value of 1.68 to 1.8 minutes depending on axial load; (c) Azimuth variations in radial stiffness and contact stresses as a result of these misalignments are negligible; (d) Highest ball speed orbital variations occurred for an axial reaction of 500 lbs - variation was 20 rad/sec which should cause no problem; (e) Steady state thermal analysis (for an axial load of 2500 lbs, 6.2 lbs/sec bearing coolant flow) indicate a 27°F difference between carrier housing - this causes a 0.1 mil interference in these components.
- 2) Results of a preliminary evaluation of the BMT 57 mm bearing are as follows: (a) Radial stiffness is nonlinear with radial load; (b) There is a strong dependence

of radial stiffness on axial load; (c) Since the inboard (2 and 3) and outboard (1 and 4) bearings have different axial loads, the radial stiffness for the bearings is considerably different when the tester is axially loaded; the inboard bearings are stiffer radially than the outboard bearings; (d) Radial loads greater than 4000 lbs/bearing may over-stress the bearing contacts; (e) For these high stresses, thermal run away of the bearings is possible; (f) Evaluation of BMT load variation effects on bearing life can probably be done using the cumulative damage approach.

MAY, 1983

- 1) Radial stiffness evaluation for the BMT at a shaft speed of 10,000 RPM show stiffness values ranging from 650,000 lbs/inch to 2.4×10^6 lbs/inch depending on axial and radial loads. The greatest effect of speed on radial stiffness occurs for the unloaded bearings (1 and 4) for radial loads up to about 850 lbs. Consequently, the BMT bearing radial stiffness varies considerably depending on the loading condition and, for the load range specified, on shaft speed.
- 2) Results of the thermal analysis of the bearings show a complex relationship between bearing coolant temperature, coolant flow and load. Reduction in coolant flow does not provide the normal linear increase in coolant outlet temperature expected of a constant heat rate system. Although some nonlinearities are the result of coolant heat capacity variations with temperature, a significant increase in coolant temperature is caused by the increase in heat load due to the loss of bearing internal clearances as bearing component temperatures increase. This thermo/mechanical interaction becomes increasingly more pronounced at the higher loads, higher coolant inlet temperatures, and reduced coolant flows.
- 3) The double linear damage rule is being considered as a tool for investigating rolling bearing fatigue life. This technique, if applicable, will allow load sequencing to be considered in estimating bearing fatigue life.

JUNE, 1983

- 1) Numerical convergence problems with the thermal model of the BMT have been solved.
- 2) Techniques for estimating surface-to-fluid heat transfer coefficients, the surface temperature at incipient nucleate boiling, and superheat ($T_w - T_s$) temperature at the peak flux condition for high-flow, subcooled LN_2 have been updated. These methods have been programmed for computer solution and initial analyses have been made to estimate bearing component temperatures.
- 3) Sensitivity analyses have been conducted to show the effect of wall superheat ($T_w - T_s$) at the burnout point on bearing component temperatures. Comparison of calculated and test temperatures indicate that the technique for determining the transition from nucleate boiling to film boiling provides reasonable results. More test data is required for complete confirmation.
- 4) The bearing thermal model is being updated to allow the heat rate to be distributed in the contact areas. The current model has the contact track represented as a single node (for each component). The updated model will have the tracks represented by several nodes, allowing the frictional heat to be distributed in the contact area. Representative analyses with the current model show high temperature in the bearing track areas. Although the analyses were done for LN_2

coolant, it indicates a potential high temperature lubrication problem for the SSME turbopump bearings.

- 5) A NASTRAN nodal analysis of the bearing inner race has been initiated.

JULY, 1983

- 1) Lubricant film thickness estimates have been made for the MSFC materials fatigue tester. Analysis shows that the film thickness-to-roughness ratio allows marginal boundary lubrication of the contacts ($h/\sigma < 1$). According to this analysis, surface distress should occur which may cloud the results of fatigue testing.
- 2) The two phase heat transfer regimes, for high-flow subcooled liquid oxygen, have been defined for inclusion into the bearing thermal model. This analysis shows that the heat transfer mechanism should change from liquid forced convection to vapor forced convection at a wall superheat of about 13°R.
- 3) The SHABERTH bearing analysis program has been modified to print the frictional heat distribution in the bearing contacts. This will be used in the SINDA thermal model to predict the temperature distribution in the rolling element contacts.

5.0 DETAILED TASK DESCRIPTIONS AND RESULTS

This section provides detailed descriptions of the tasks accomplished and the results.

5.1 JULY, 1982

5.1.1 WEAR TRACK AND BALL PASS COUNT ANALYSIS

A 57 mm bearing was modeled on the SHABERTH computer program with maximum clearances and an arbitrary temperature distribution radially across the bearing. The purpose was to determine if the observed bearing wear tracks could be matched within the known loads applied to the bearing tester. As shown in Figure 5.1.1, a fairly good match can be obtained with an axial load of 6500 pounds. For comparison, the calculated tracks for a uniform bearing temperature and nominal clearances are shown. The temperature gradient used was an assumed one which was selected to investigate the sensitivity of contact angle to increased diametrical clearances due to temperature differences. This information shows that the bearing tracks can be influenced by temperature and clearance as well as applied loads.

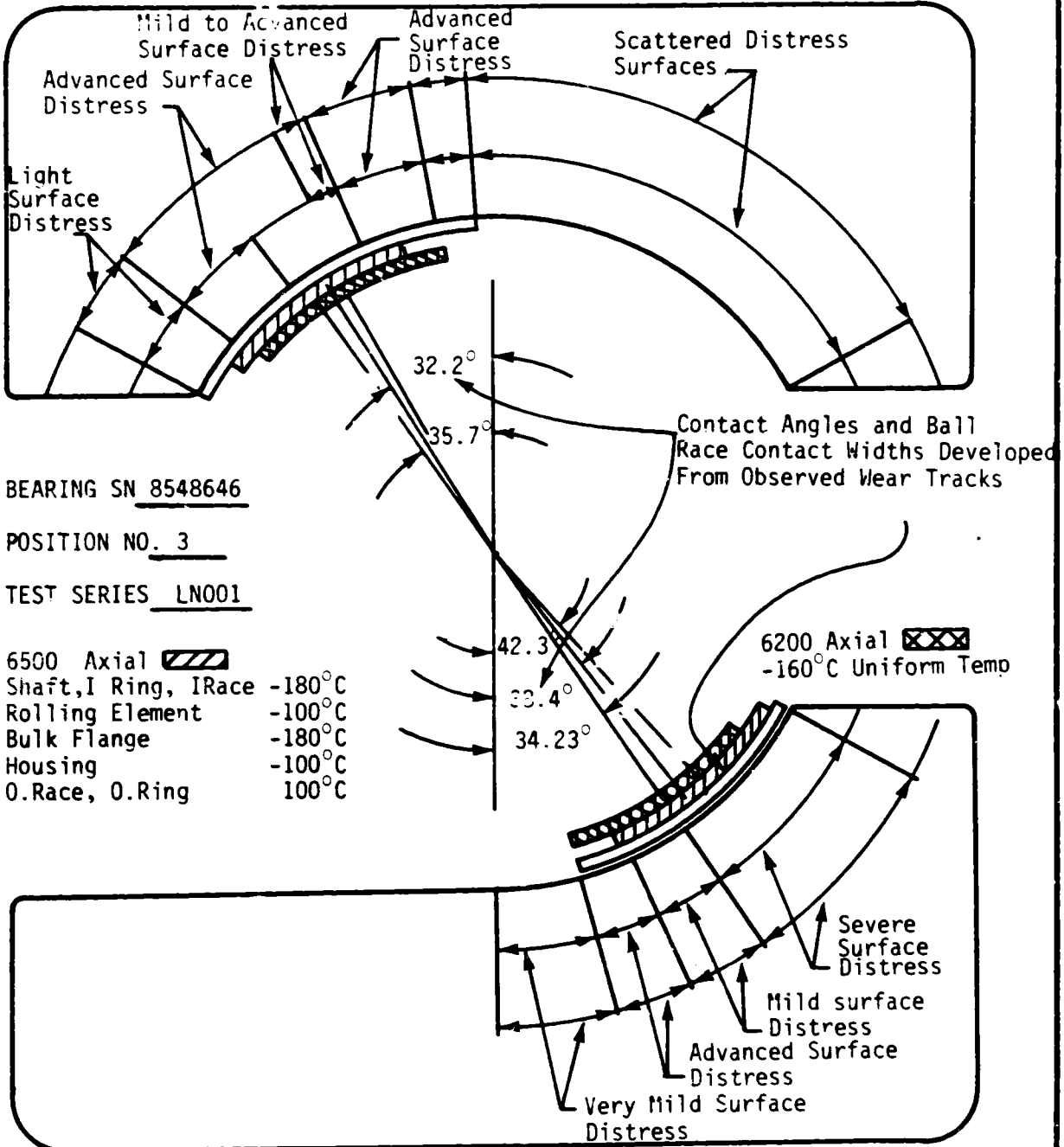
Cage speed data generated from SHABERTH was used to generate inner and outer race ball passes per minute. This data was compared with the data measured during tester operation. The comparisons, shown in Figure 5.1.2, indicate good agreement with the measured and calculated values. Also shown is the ball spin speed compared with the data derived from the tests. As illustrated, the above parameters are plotted as a function of the bearing axial reaction load.

5.1.2 LOX TEST INCIDENT ANALYSIS

In support of the Bearing and Material Tester (BMT) incident investigation, a scenario has been developed which describes the potential hazards associated with operating the tester bearings in the temperature regimes that produce two phase conditions in the coolant flow. The synergism of heating rate and flow pressure losses is much more pronounced in the two phase flow regime than in the single phase regime. A simplified flow network for the BMT is shown in Figure 5.1.3. Since each pair of bearings is cooled by flow circuits in parallel, the flow resistances of each circuit must be equal for equal flow and pressure loss. Furthermore, any flow losses upstream of the bearings must be the same in each circuit.

As indicated in the figure, this is not the case for the seal leakage. This is probably not a serious factor since the absolute value of the real leakage is small. However, if the bearing component temperatures exceed the saturation temperature of the LOX coolant flow, vapor generation can significantly increase the resistance to flow through the hot bearing. This in turn can cause a reduction in flow, reduced cooling, and further increases in bearing temperature.

The effect of increased vapor generation on flow pressure loss is shown in Figure 5.1.4. This is the correlation for steam/water mixtures developed by Martinelli and Nelson. Although the correlation is for steam/water flow, it is general in the sense that the same effect is experienced with other two phase mixtures. As shown in the figure, there is a significant increase in pressure loss over the single phase value as the percentage of vapor is increased. In a parallel flow network similar to the BMT



1 DEGREE = 0.04625 INCH AT 10X
MAGNIFICATION
BEARING 57-MM, P/N - RS007955 TURBOPUMP

FIGURE 5.1.1 COMPARISON OF CALCULATED AND OBSERVED WEAR TRACKS

FIGURE 5.1.2 COMPARISON OF ESTIMATED AND TEST RESULTS

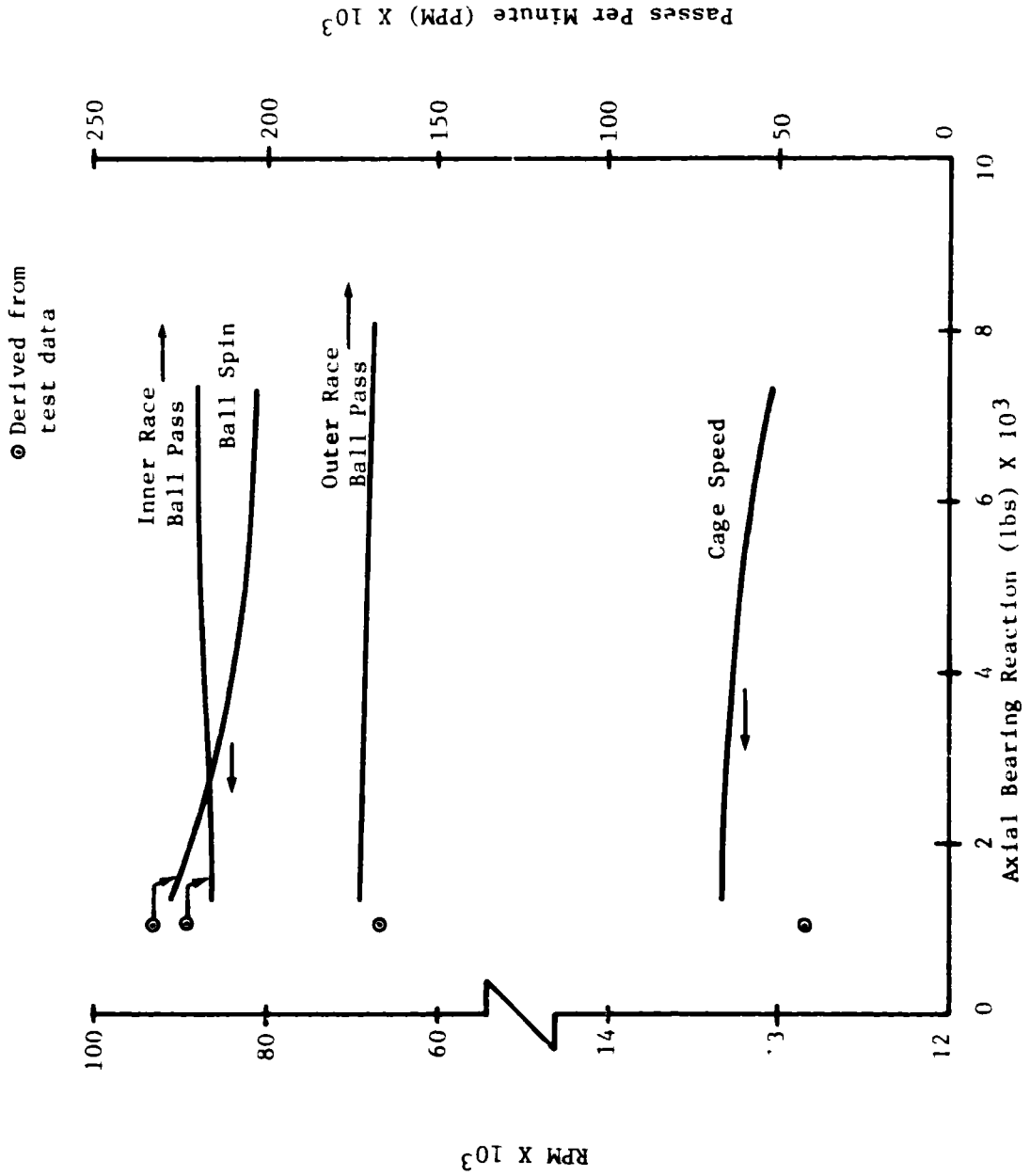
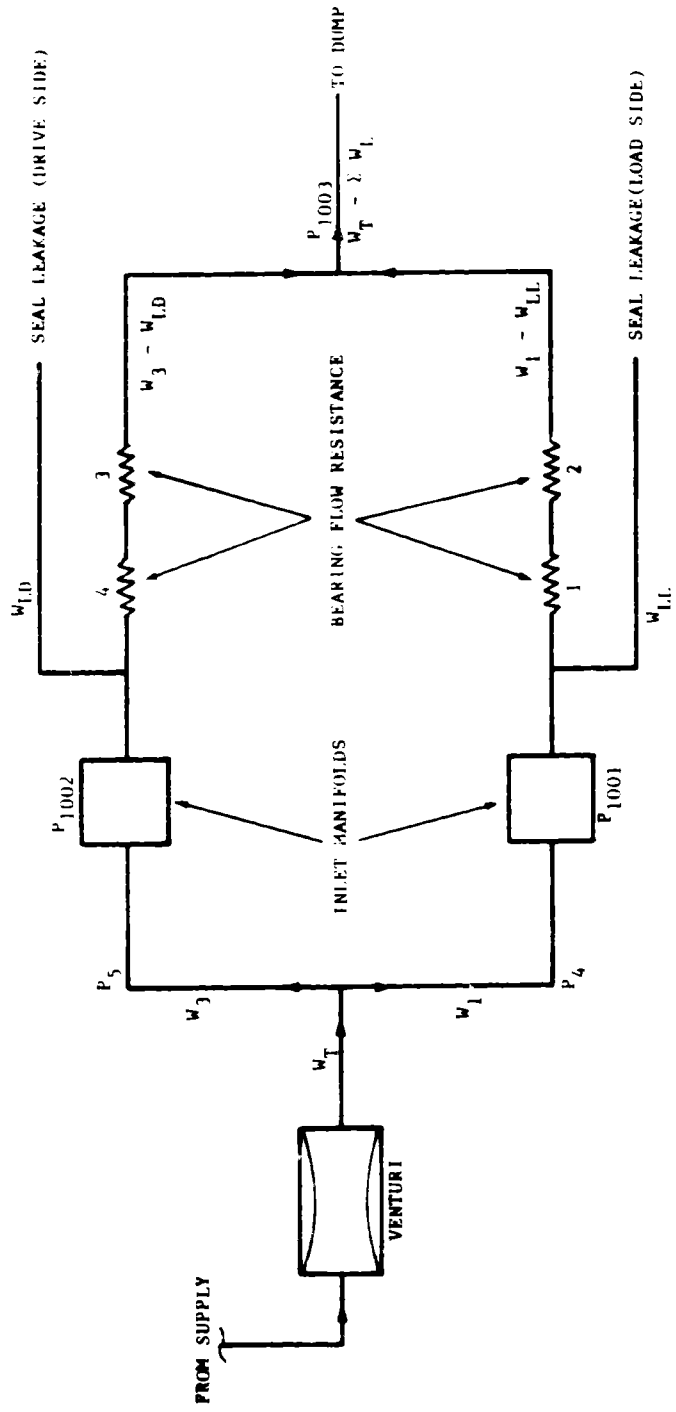


FIGURE 5.1.3

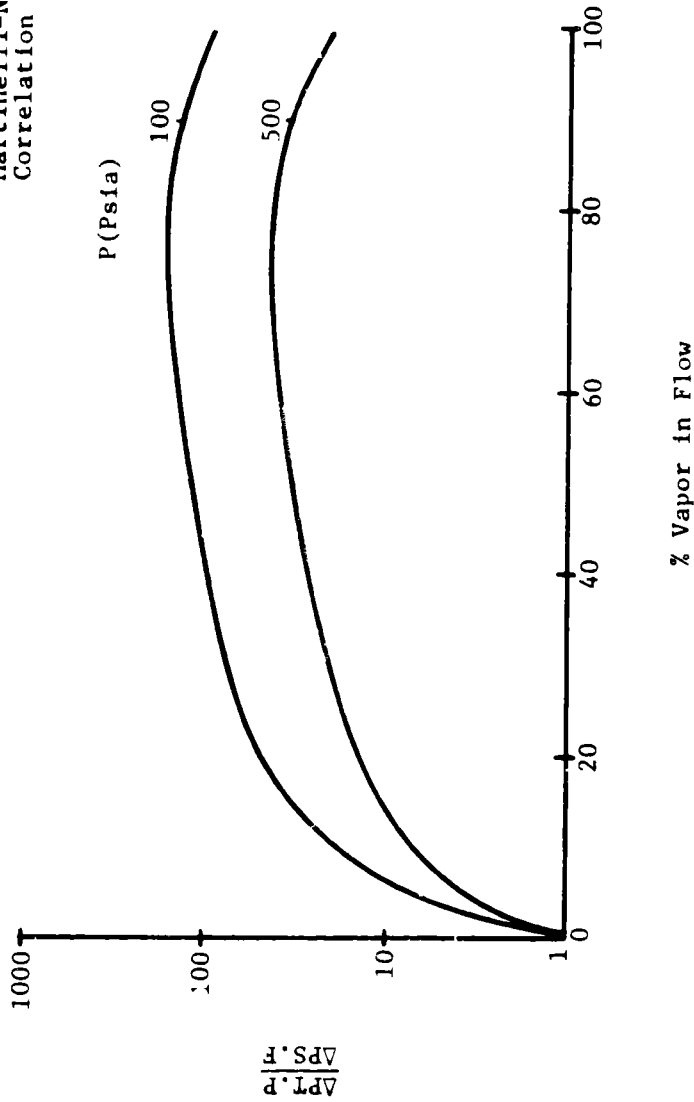
SIMPLIFIED PRESSURE/FLOW NETWORK



- o RATIO OF LOAD END TO DRIVE END SEAL LEAK PRESSURE = $14/8.25$
- o RATIO OF LOAD END TO DRIVE END LEAK RATE $\sim \sqrt{14/8.25} = 1.30$
- o INDICATES ABOUT 30% MORE LEAKAGE ON LOAD END, WITH CORRESPONDING LESS FLOW TO BEARINGS 1 & 2

FIGURE 5.1.4 INFLUENCE OF VAPOR GENERATION ON PRESSURE LOSS

Martinelli-Nelson Pressure loss
Correlation



GROUP 1 - HIGH
OF HIGH QUALITY

• $\frac{\Delta P_{T.P.}}{\Delta P_{S.F.}}$; Ratio of two phase pressure loss to single phase pressure loss

coolant circuit, this will reduce the flow to the bearing running the hottest and producing the most vapor.

Another problem with operating in the two phase regime is the possibility of exceeding the critical heat flux for nucleate boiling. This can cause a rapid increase in component surface temperature. An example of this characteristic is shown in Figure 5.1.5. Shown in this figure is the measured outer race temperature for the failed bearing superimposed on the pool boiling curve for oxygen. The bearing temperature shown is for the outer race which is the lowest expected temperature for any of the bearing components (inner race, balls, etc.). The other bearing components will be running at a temperature in excess of the measured outer race temperature.

Referring to Figure 5.1.5, it is evident that a small increase in load (heat flux) will cause the operating conditions to immediately shift to point E with a corresponding large increase in component temperature. The shift from C to D is not reversible. A reduction in load will cause the operating point to follow the path E to D and then move to the solid part of the curve horizontally across from point D. It is recognized that the boiling curve shown is for pool boiling and does not completely describe the high velocity flow through the bearings. In general, the velocity effect will be to increase the critical heat flux point. However, as stated previously, the measured temperature is the lowest expected for any bearing component. These two opposing factors will tend to cancel and the possibility of the operating point shifting as previously described is highly probable.

Supporting data indicating possible effects of vapor generation in the load side coolant path are shown in Figures 5.1.6 and 5.1.7. This data represents the LOX inlet manifold pressure for the flow circuits indicated. The mean steady pressure for the load side (P_{1001}) is about 440 psi, and the equivalent value for the drive side is about 419 psf. There is, however, a bias difference of about 7 psi at the no rotational point (time=0). Considering the bias, there is about a 14 psi difference between the two pressures with the load side being the greater. This could be caused by vapor generation in the load side circuit (bearings 1 and 2).

Based on the above discussion, the following conclusions can be stated:

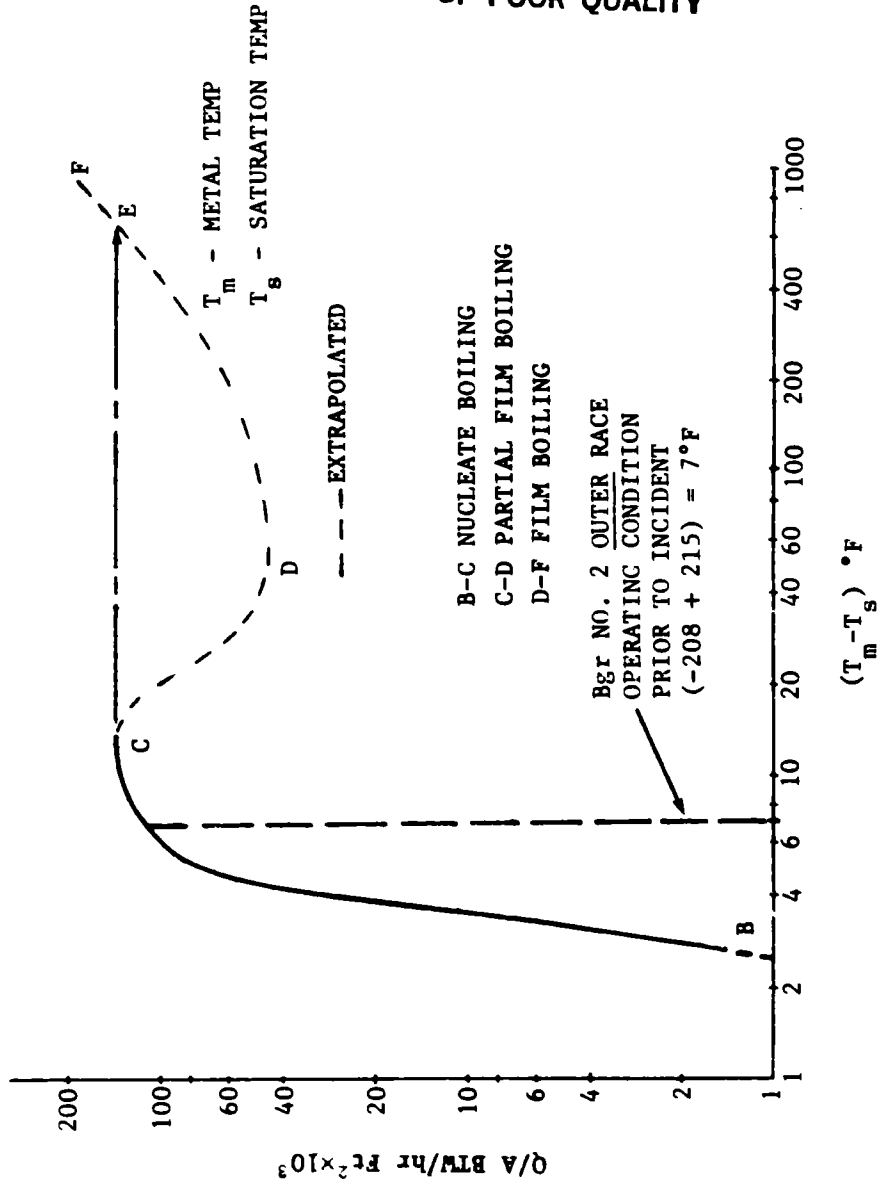
(a) First order instabilities can occur when operating in a two phase regime near the peak flux region. This can cause a rapid increase in component temperature with a small increase in heat load. It appears, as a first order approximation, that bearing 2 was operating near this condition prior to the incident.

(b) The parallel flow arrangement in the BMT requires stable flow resistances in both paths for equal coolant flow. Large variations in flow resistance can occur due to unequal heat generation in the bearings if the flow is two phase.

(c) The combination of coolant flow reduction, increased vapor generation, and loss of cooling efficiency can cause a "run away" situation causing rapid increase in component temperature and subsequent failure.

(d) Based on the above, the BMT bearing components should not be operated above the coolant saturation temperature unless absolutely necessary. If operating above the saturation temperature is required, the operating condition should be evaluated with respect to the peak flux condition to assure adequate cooling margin and sufficient coolant flow to each flow circuit.

FIGURE 5.1.5 BOILING CURVE FOR OXYGEN
(Pressure=377 Psia)



ORIGINAL PAGE IS
OF POOR QUALITY

- The region of multivalued temperature difference should be avoided because of possible sudden increase in surface temperature
- Example: If point C is reached and the heat flux is increased, a first order instability occurs and the stable point rapidly shifts to point E.

SRS

FIGURE 5.1.6 LOX INLET CAVITY PRESSURE (LOAD SIDE)

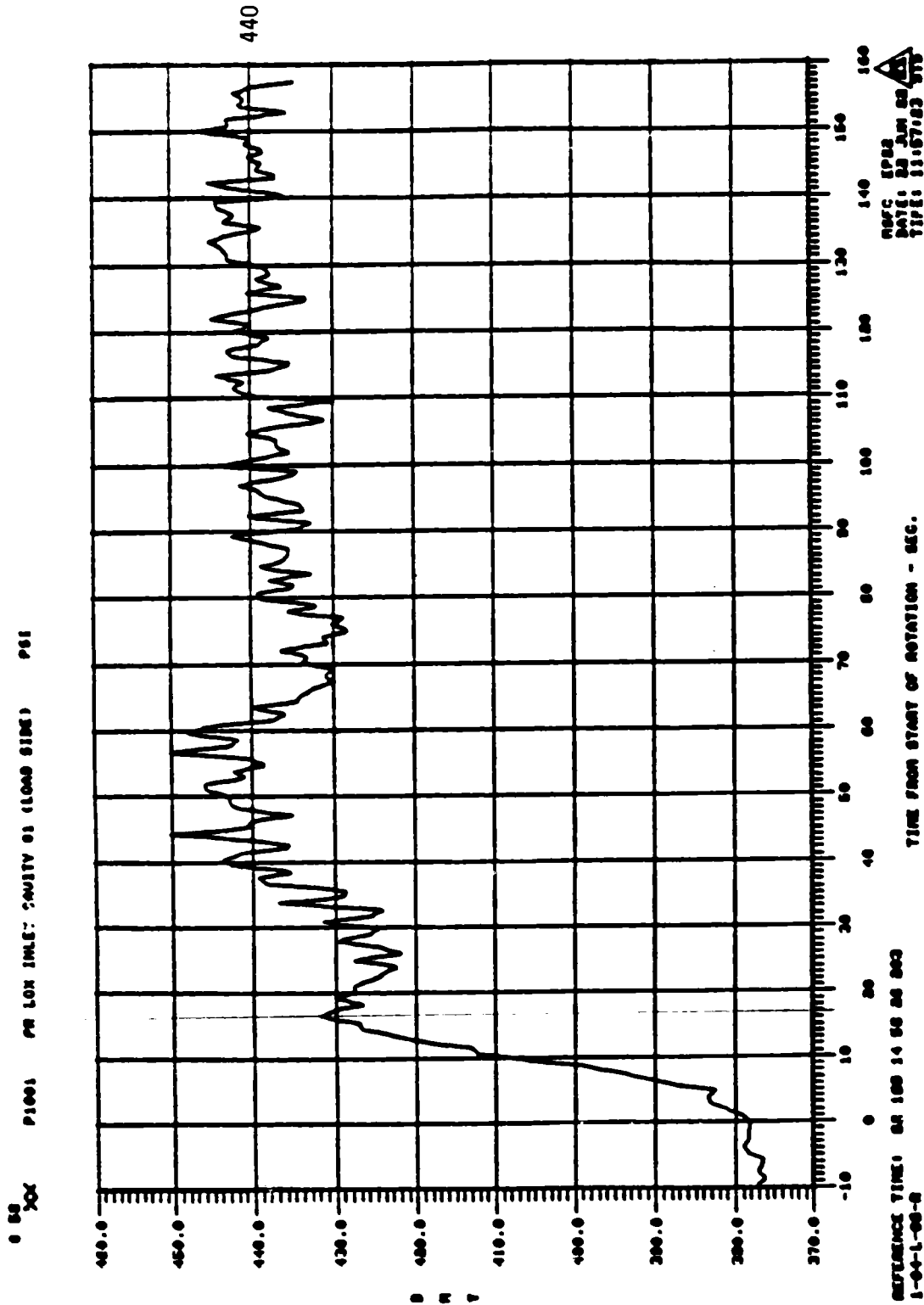
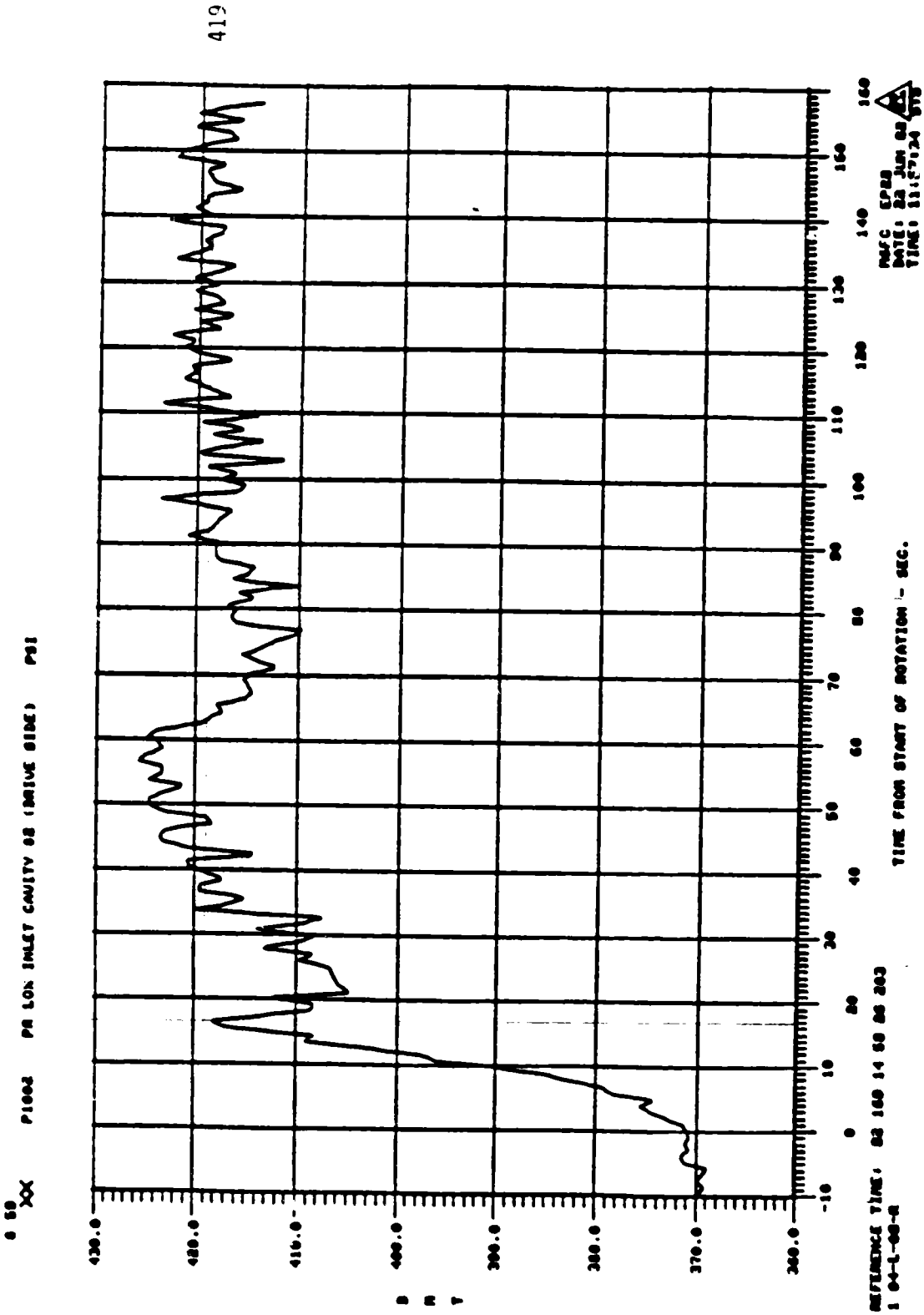


FIGURE 5.1.7 LOX INLET CAVITY PRESSURE (DRIVE SIDE)



SRS

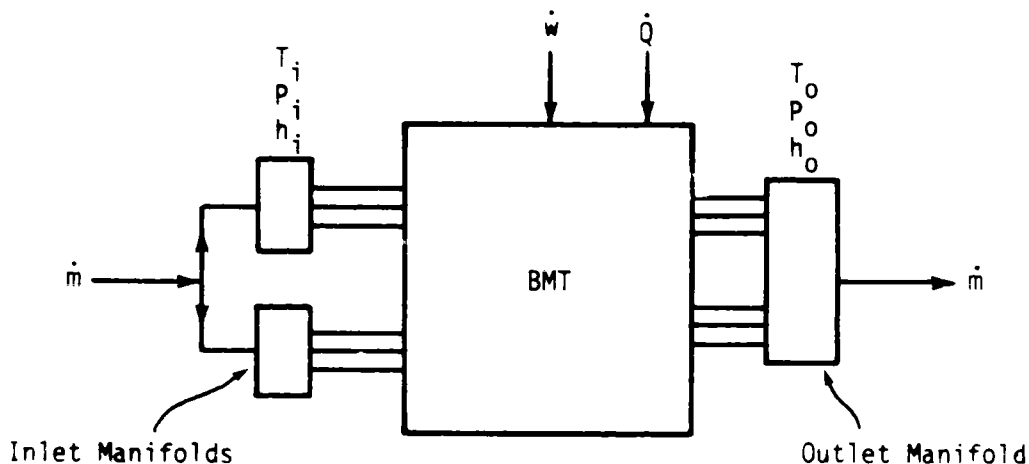
5.1.3 ENERGY AND FLOW BALANCE ESTIMATES FOR THE BEARING AND MATERIALS TESTER

Energy and flow balance analyses were conducted to investigate the differences in energy flow into and out of the tester during the LN_2 tests and LOX tests. In addition, inlet and outlet pressure measurements were evaluated in an attempt to compare tester flows during the LN_2 and LOX tests. Four test conditions were evaluated: (1) LOX flow, (2) LOX rotational, (3) LN_2 flow, and (4) LN_2 rotational. The flow tests were evaluated to judge the validity of pressure and temperature readings and to estimate the heat gain of the tester flow from the atmosphere. Figures 5.1.8, 5.1.9, 5.1.10, and 5.1.11 provide a summary of the four test conditions. These figures show the test values and schematically locate the instrumentation of interest. Test identification information is shown in the upper right corner of each figure.

The flow test data (tester not rotating) are shown in Figures 5.1.8 and 5.1.9. As indicated in the lower left corner of Figure 5.1.8, temperature measurements T_{1001} through T_{1003} are resistance bulb (RB) thermometers and the other temperature measurements are thermocouples. There appears to be a problem with the RB's during the LOX test since they show a decrease in temperature across the tester in the flow direction (see Figure 5.1.8). They also read about $6^\circ F$ lower than the thermocouples in comparable locations. The RB's are in fair agreement with the thermocouples during the LN_2 flow tests (Figure 5.1.9). Since the RB's appeared to be in error during the LOX tests, the thermocouple measurements at the entrance and exit manifolds were used to estimate the heat flow.

Pressure measurement P_6 is inconsistent with the upstream and downstream pressure measurements for both LOX test conditions. T_{1002} is not provided for the LOX tests and T_4 is a bad measurement. As stated above, the LOX flow test data were evaluated to determine the ambient heat flow into the tester. As shown in Figure 5.1.8, there is very little temperature gain as the flow moves from the inlet to the exit manifold. Using the stated LOX flow rate of 9.1 lbs/sec. and the inlet and outlet temperature difference, an ambient heat input of about .5 Btu/sec was calculated from the LOX flow test data.

The BMT thermal system was defined as follows:



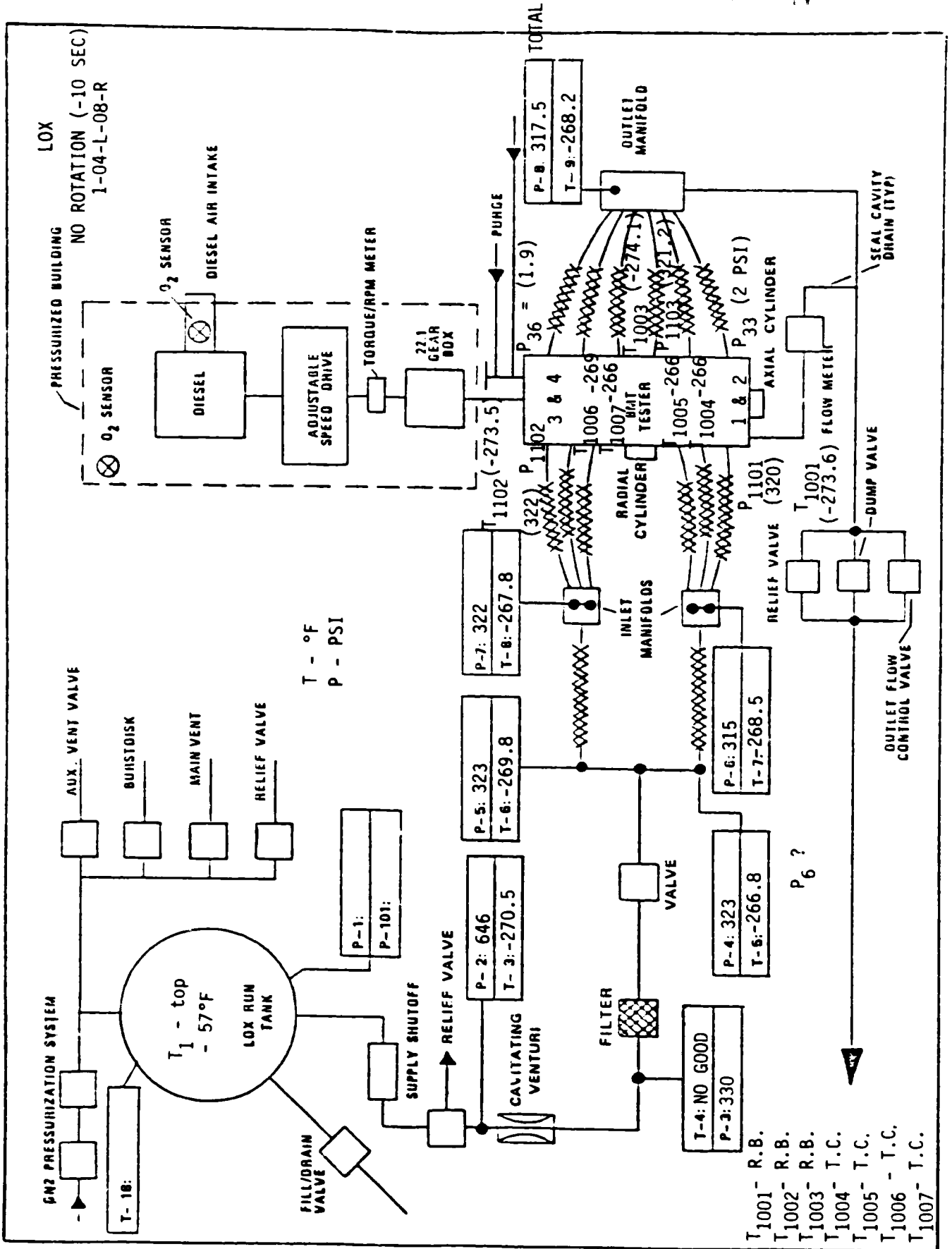


FIGURE 5.1.8 LOX TEST CONDITIONS (T = -10 SEC)

FACILITY SCHEMATIC

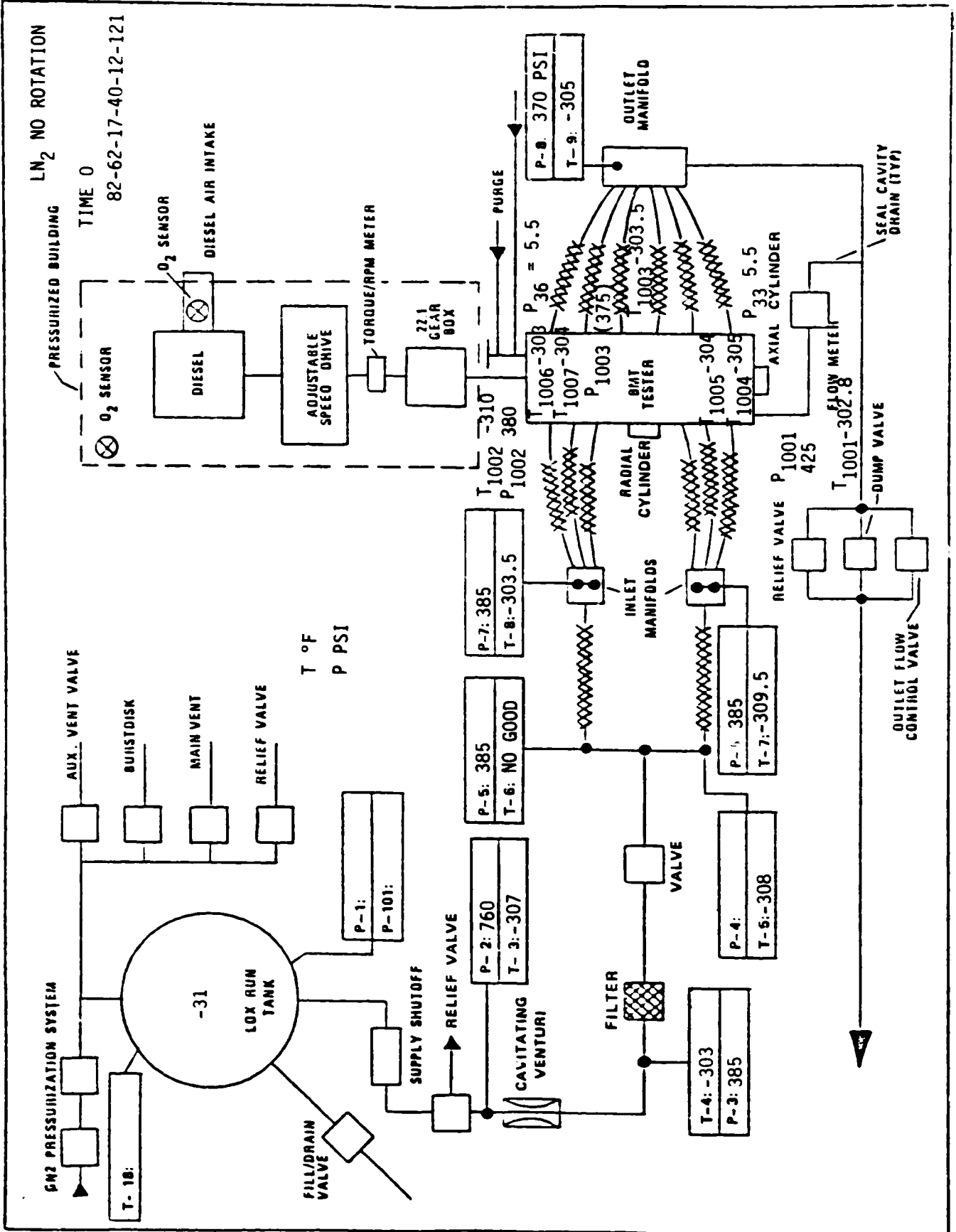


FIGURE 5.1.9 LN₂ TEST CONDITIONS (T = 0)

where: \dot{m} mass flow rate
 T temperature
 P pressure
 \dot{Q} heat rate
 \dot{w} power
subscripts: h fluid enthalpy
 i inlet conditions
 o outlet conditions

An energy balance on the system defined above is as follows:

$$\dot{w} + \dot{Q} = \dot{m}(h_o - h_i) + \frac{dE}{dt}$$

where: $\frac{dE}{dt}$ is the time rate of change of internal energy assumed to be zero, thus implying steady state conditions.

The power term (w) is determined from the torque and speed measurements and, as stated previously, the ambient heat flow term was evaluated from the flow test data and assumed to be the same for the rotating tests. Shown on Figure 5.1.12 are the terms of the above heat balance for the four test conditions. As shown in the figure, there is an excess of energy not accounted for in the steady state energy balance. The LOX test gives about 20 Btu/sec and the LN₂ test about 8.4 Btu/sec excess energy input into the system. This is a maximum error of 12% and 4% for the LOX and LN₂ heat balances.

Although this is fairly good agreement, there are several possible explanations for the energy imbalance. The calculation of power input to the tester is questionable because the torque is measured at the gear box input. This requires the gear box torque to be determined at no load conditions and subtracted from the test value. Since the loaded gear box torque is very likely greater, and the gear box torque can be affected by gear box temperature, etc., this method of determining the BMT torque has several uncertainties. A torque measurement at the gear box outlet is needed to eliminate these questions.

Other sources of potential error are the temperature and flow measurements, and the storage of energy in the tester hardware. Since the tester housing temperature does increase during the rotation tests, some energy is being stored. An accurate estimate of the amount is difficult due to the complicated geometry of the tester. Assuming for the moment that the energy storage term is small and the power input is correct, it is interesting to note that the energy input to the coolant flow ($m\Delta h$) is about 11% greater during the LN₂ runs as compared to the LOX tests. Because of the higher LOX density it would be expected that the viscous work done on the LOX would be considerably greater than done on the LN₂. This could suggest higher bearing friction in the LN₂.

Based on the preceding evaluation, the following conclusions can be stated:

- 1) An overall system energy balance is a valuable tool for evaluating the validity of the temperature, pressure, torque, speed, and flow data.
- 2) To improve the capability of this technique several changes should be made in the tester instrumentation as suggested below:

FIGURE 5.1.12 ENERGY BALANCE SUMMARY

| | | POWER INPUT W (WATTS) | AMBIENT HEAT INPUT Q (WATTS) | ENERGY REMOVED BY FLOW (mWh) (WATTS) | ENERGY UNBALANCE FOR STEADY CONDITIONS (WATTS) $\dot{W} + Q - W\dot{h}$ |
|-----------------|------------------------|--------------------------|---------------------------------|---|---|
| LOX | NON-ROTATING (FLOW) | 0 | 572 | 0 | 0 |
| | ROTATING | 202.8×10^3 | 572* | 182.1×10^3 | 21.2×10^3 |
| LN ₂ | NON-ROTATING (FLOW) | 0 | 572* | 0 | 0 |
| | ROTATING | 210.9×10^3 | 572* | 202×10^3 | 9.5×10^3 |

* ASSUMED TO BE THE SAME DURING ALL TESTS.

SRS

spectra research systems

- a) Provide a torque measurement at the drive end of the BMT.
- b) Add additional temperature and pressure measurements at the entrance and exit manifolds of the tester to assure more than one measurement at these critical locations. The temperature measurements should be that of the fluid and not the metal.
- 3) It is highly desirable to determine the flow rate to each pair of bearings as well as the total flow through the tester. Since flow is such a critical parameter, redundant measurements need to be considered.

5.2 AUGUST, 1982

5.2.1 INVESTIGATION OF BEARING TEMPERATURE GRADIENTS ON OPERATIONAL CHARACTERISTICS

A single 57 mm ball bearing has been modeled on the SHABERTH computer program. Several temperature gradients were imposed and their effects on contact angle, normal forces, contact stresses, operating clearances, and heat generation were determined.

Figure 5.2.1 shows the variation of inner and outer race contact angles and stresses as a function of bearing temperature difference. The positive temperature gradient is from the shaft to the bearing housing. The shaft and inner race are assumed to be at the high temperature and the ball temperature is assumed to be the average of the inner and outer race. As shown, the operating contact angles exhibit a significant decrease at the higher temperature differences with a corresponding increase in contact stresses. Figure 5.2.2 shows the effect of the temperature differences on the bearing operating clearances. As the clearances go from positive to negative, an internal preload is introduced which in effect increases the bearing preload. As shown, this occurs for a rather small temperature difference. It should be pointed out, however, that these analyses were made using the worst case stack up of tolerances to minimize the bearing clearances.

Shown in Figure 5.2.3 are the normal forces per ball for the inner and outer races as they are influenced by the bearing temperature differences. The forces appear to be approximately linear up to a temperature difference of 150°C and become a power function or exponential function as the ΔT increases. Shown in Figure 5.2.4 is this effect on the increase in heat generated at the contact surfaces. After about 200°C ΔT , there is a sharp rise in heat generated as the ΔT across the bearing is increased. The increase in heat generated will increase the bearing ΔT and, in turn, the ΔT effects will increase the heat generated. This can result in an unstable condition causing premature bearing failure.

5.2.2 MODELING THE EFFECTS OF BALL DRAG ON BEARING OPERATING CHARACTERISTICS

The SHABERTH computer program does have the capability of evaluating the effects of ball drag. Unfortunately, the treatment of the hydrodynamic effects have been programmed considering the properties of lubricants operating in a nominal temperature range of -60 to 600°F. For example, the temperature correction for the lubricant density is given as:

$$\rho(T) = \rho(60^{\circ}\text{F}) - G(T - 60^{\circ}\text{F})$$

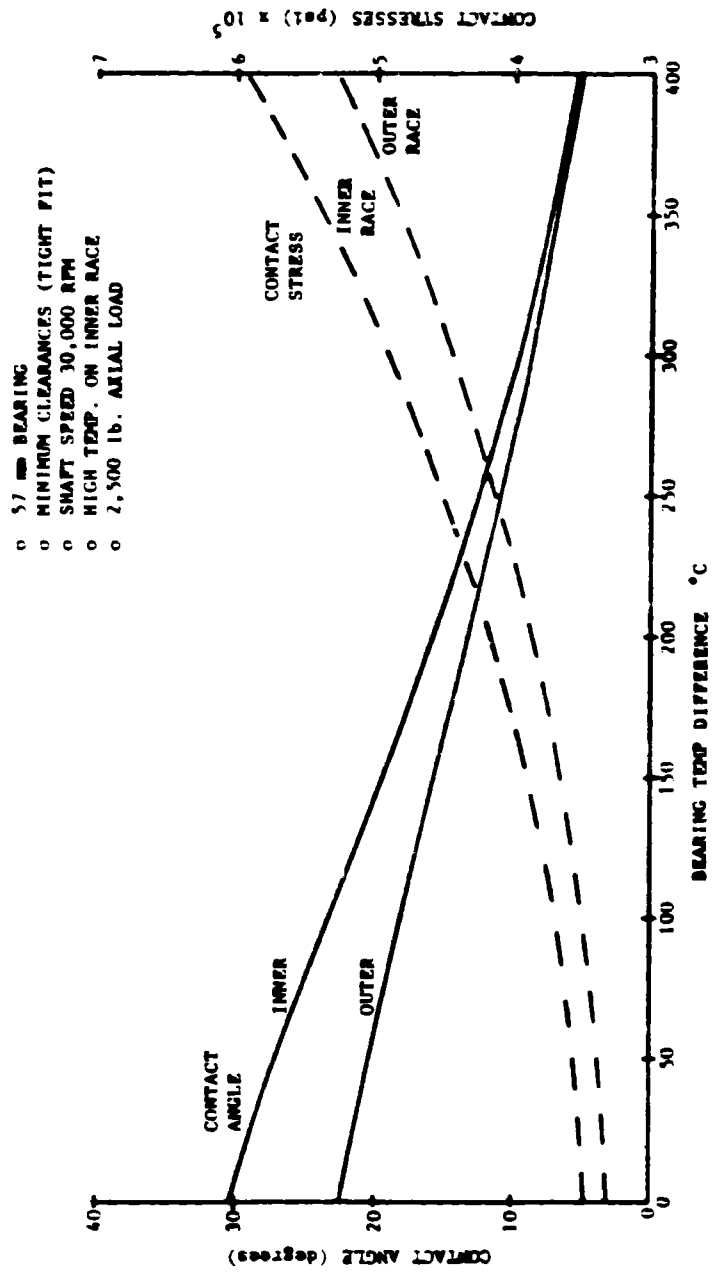
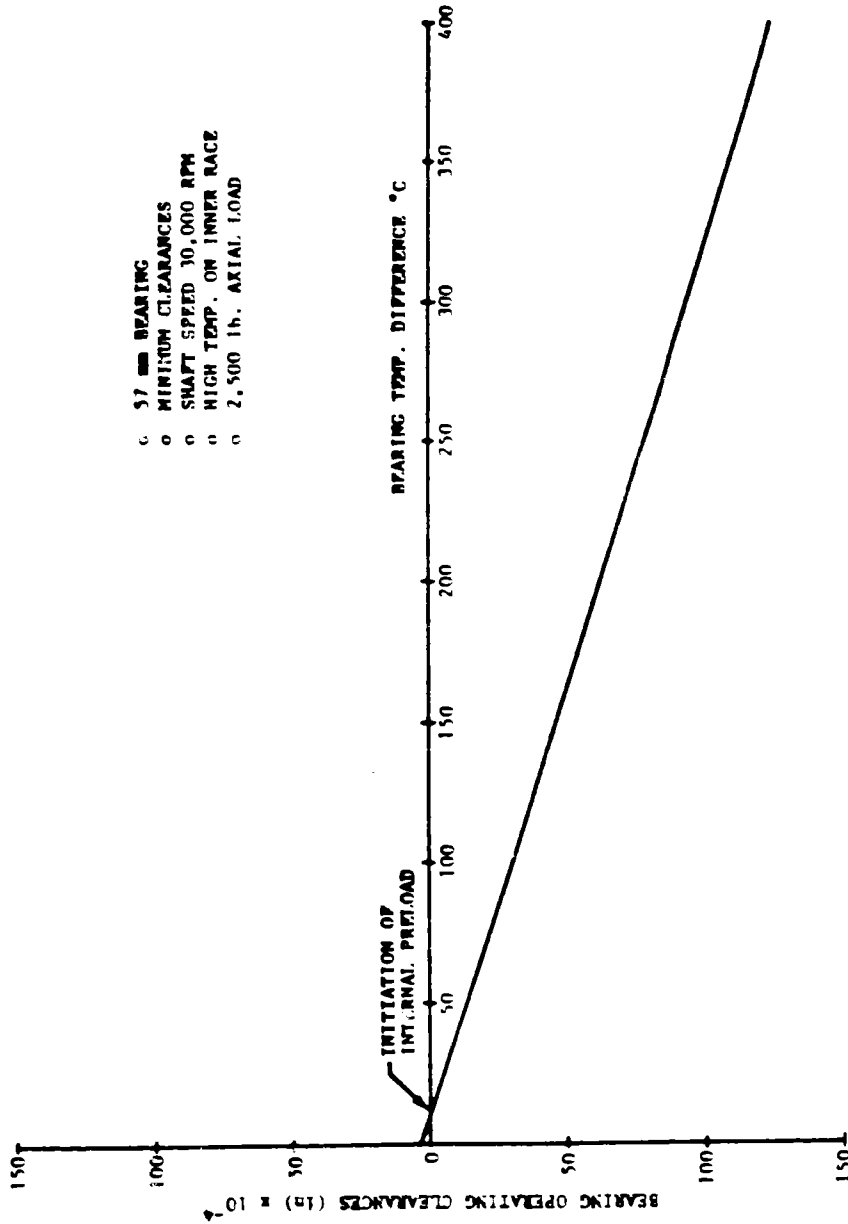


FIGURE 5.2.1 CONTACT ANGLE AND STRESSES vs. BEARING TEMPERATURE DIFFERENCE

ORIGINAL PAGE IS
OF POOR QUALITY



- 6 57 - BEARING
- 0 MINIMUM CLEARANCES
- 0 SHAFT SPEED 30,000 RPM
- 0 HIGH TEMP. ON INNER RACE
- 0 2,500 lb. AXIAL LOAD

FIGURE 5.2.2 BEARING OPERATING CLEARANCES vs. TEMPERATURE DIFFERENCE

SRS

2.3 TRACTION COEFFICIENT - EXPERIMENTAL DETERMINATION

One of the key parameters used in the bearing computer dynamic simulation is the traction coefficient, i.e., the ratio of the transverse force required to cause the ball to slip on the raceway (F_S) and the normal ball-to-raceway load (W). A special test fixture was used to determine this coefficient. This test machine is shown schematically in Figures 2 and 3 and pictorially in Figures 4 and 5. The test machine consists of two of the 100-mm bearing inner races mounted on parallel precision spindles with a single ball loaded between them and maintained in this location by a segment of the ball separator consisting of one of the ball pockets. By rotating the two precision spindles at precisely controlled speed, a small differential speed between the two spindles can cause ball slipping on the raceways. The ball pocket segment is mounted on a three-axis force transducer which permits measurement of the slip force required to maintain the ball in position, centered between the two races. A detail drawing of the ball pocket/transducer mount is included in Appendix C. By plotting the measured traction force

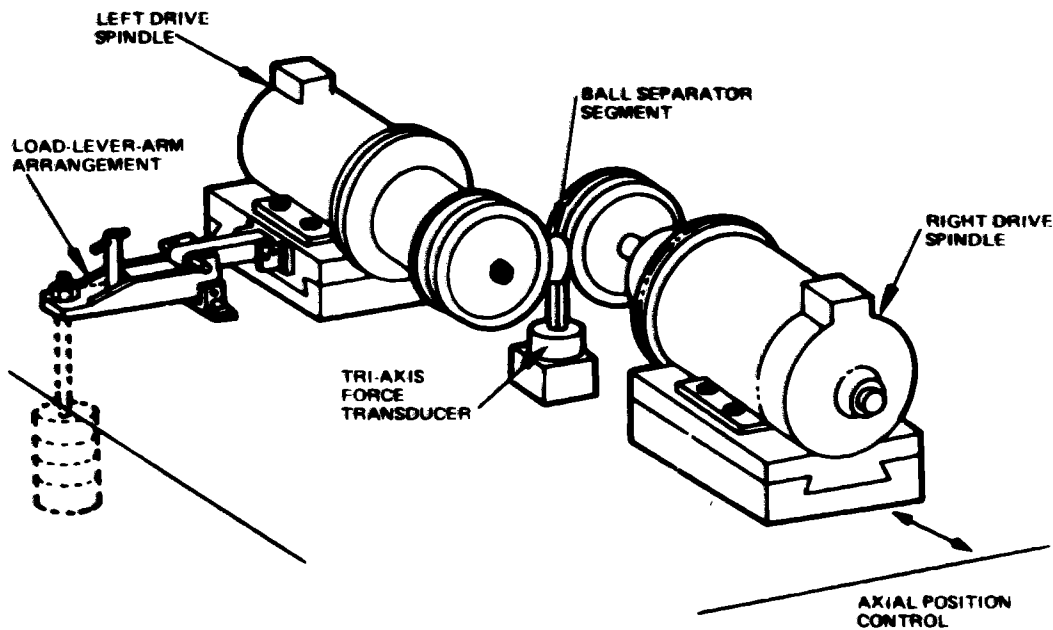


Figure 2. Ball/race traction test machine schematic.

where $\rho(60)$ and G can be input or a lubricant can be selected that has its properties already programmed. Obviously, O_2 does not exist as a liquid at $60^\circ F$ and the above equation does not account for a phase change from gas to liquid. Therefore, a fictitious value for $\rho(60)$ can be used or a lubricant selected that has a density range covering LOX, when the appropriate temperature is used in the above equation.

Another problem associated with LOX as a fluid is caused by the way the program accounts for viscosity variations with temperature. Typical lubrication viscosity data have been correlated with the following expression:

$$\log_{10} \log_{10} (V + 0.6) = A - B \log_{10} (T + 460)$$

where A and B are constants determined by substituting the known values of viscosity (V) at $T = 100^\circ F$ and $T = 210^\circ F$ and solving the two resulting equations for A and B . For a low viscosity fluid such as LOX, the term $(V+0.6)$ is less than one thus requiring taking the log of a negative number.

To work around the above problems, SHABERTH was run at LOX temperature using a dry lubricant friction coefficient. The purpose was to determine the operating clearances at LOX temperature. These clearances will be used as input for a higher temperature run (temperature selected to obtain a match of lubricant and LOX density) with a fluid to determine the drag force on the balls.

The ball drag force is determined by:

$$F_w = \frac{A_v C_v (d_m W_o)^2}{8g}$$

A_v = ball frontal area

C_v = drag force; determined as a function of Reynolds Number

d_m = bearing pitch diameter

W_o = ball orbital velocity (cage speed)

ρ = density of fluid in the bearing cavity

The density of the fluid in the bearing cavity is determined by:

$$\rho = XCAV \rho_0$$

ρ_0 is the density of the liquid and $XCAV$ is an input variable defining the percent liquid in the bearing cavity. Obviously, the ball drag force can be varied by varying the value of $XCAV$. The technique for using SHABERTH for estimating ball drag effects is as follows:

- 1) Run SHABERTH at LOX temperatures to establish operating clearances.
- 2) Run SHABERTH at appropriate temperature to provide a lubricant density equivalent to LOX density.
- 3) Use the values of viscosity to calculate a Reynolds Number to determine the drag coefficient C_v , and calculate the drag force used by the program. Any value of drag force can be investigated by varying $XCAV$.

To date, successful runs have been made using this technique. The results are provided in Section 5.3.2.

5.2.3 EQUIVALENT THERMAL CONDUCTANCE BETWEEN ROLLING ELEMENTS AND RACES OF HIGH SPEED BEARINGS

Finite element modeling of the thermal characteristics of high speed rolling bearings requires developing a technique for thermally connecting the finite elements of the rolling components with the finite elements of the stationary race and rotating race. Rigorously describing the time dependent physical picture of the rolling contact conductance is not considered practical, or necessary. A LOX bearing tester (57 mm) shaft speed of 30,000 RPM produces a ball speed of 85,000 RPM and a cage speed of about 13,000 RPM. A contact on the ball encounters a contact on the outer race about 5.3×10^5 times per second with a contact residence time of approximately 3.2×10^{-5} sec. To account for the effect of each contact would require a computer time step $< 3.2 \times 10^{-5}$ sec. This was not considered practical in terms of computer time for a model consisting of a large number of elements. The desirability of a well defined temperature gradient near the surface of the bearing elements dictated a fine element breakdown, resulting in a relatively large number of model elements. Since the shaft bearing system is rotating at steady speed, the highly transient rotating effects can be resolved into a more manageable "quasi static" condition for thermal modeling.

The SHABERTH computer program provides a method for estimating the thermal resistance between bearing elements. This method essentially replaces the actual rotating system with a thermally equivalent static model. In this system, the temperature is assumed uniform in the angular direction on each contact surface (i.e., there is no thermal gradient along the length of the contact surface). The thermal resistance is therefore taken to be equivalent to the resistance obtained by suddenly exposing the end of a perfectly insulated rod initially at zero temperature to a source of finite temperature. The solution of this problem is given in "Heat Transfer", Volume 1, page 359 by Jakob. The referenced expression for the heat transfer to the rod is:

$$1) \quad q_0 = \frac{kA t_0}{\sqrt{\pi \alpha \tau}}$$

k = thermal conductivity

A = contact area

α = thermal diffusivity

τ = period of contact

t_0 = difference in hot body and rod temperature

From the above expression the thermal resistance can be expressed as:

$$2) \quad \Omega = \frac{\sqrt{\tau \alpha \tau}}{kA}$$

As will be shown, this is equivalent to the value given in SHABERTH. The following parameters are defined as indicated:

A = πab ; Area of contact ellipse

a, b = semi-major and minor axis of contact ellipse

$$\tau = \frac{2b}{r_B w_B} = \frac{2b}{V}$$

r_B = ball radius

w_B = ball rotational speed

Substitution of this parameter into equation 2 gives:

$$3) \beta = \frac{\sqrt{\pi \alpha 2b}}{k \pi a b}$$

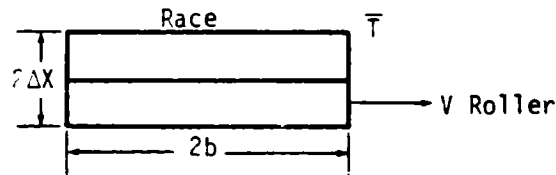
Equation 3 can be rearranged to give:

$$4) \beta = \frac{1}{1.57 ka} \sqrt{\frac{\pi \alpha}{2bV}}$$

This is equivalent to the expression given on page 15 of the SHABERTH operation manual.

The concern with using the above expression in the finite element modeling arises from the fact that the model bearing requires two finite elements to be in contact. Therefore each element has a resistance associated with it and both element temperatures are changing with time. Other simplifying assumptions such as the perfectly insulated surfaces of the rod require all the heat to flow in one direction.

An alternate technique for estimating the effective thermal resistance is developed as follows. Assume a control volume consisting of an element in the race contacting an element in the roller:



Further, assume the only heat transferred is between the race and ball elements, no temperature gradients exist in the elements, and \bar{T} is a constant average temperature for the time of contact.

The heat gained by the rolling element is:

$$5) dq = dm C_p \frac{dT}{d\theta}$$

The heat lost by the race element is:

$$6) dq = -\frac{k}{\Delta X} (\bar{T} - T) dA$$

$$7) \dot{M} C_p dT = -\frac{k}{\Delta X} (\bar{T} - T) dA; \dot{M} = \frac{dm}{d\theta}$$

$$8) T_o = T - (\bar{T} - T_i) e^{-kA/\Delta X \dot{M} C_p}$$

$$9) \frac{kA}{\Delta X \dot{M} C_p} = \frac{\alpha \sqrt{\pi b}}{[\Delta X] \sqrt{V}}$$

$$10) \dot{M} C_p (T_i - T_o) = C_1 (\bar{T} - T_i)$$

spectra research systems

where C_1 is the thermal conductance between the elements. Combining equation 8, 9, and 10 gives:

$$11) C_1 = MCp (1 - e)^{-\alpha_v \pi b / \Delta X^2 V}$$

$$12) \dot{M} = \rho \Delta X v \pi a V$$

ρ = density
 V = velocity of rolling element

Combining equations 11 and 12 gives the contact resistance in terms of the bearing physical and operating parameters.

$$13) \Omega = \frac{1}{C_1} = \frac{1}{\rho \Delta X v \pi a V (1 - e)^{-\alpha_v \pi b / \Delta X^2 V}}$$

A quantitative comparison of resistance values calculated from the preceding methods and the standard static values of resistance is provided as follows. The values used are for a 57 mm, 440 C steel bearing rotating at a shaft speed of 30,000 RPM with a ball speed of 85,000 RPM.

Using the procedure provided in SHABERTH, the contact resistance is calculated as follows:

$$\Omega = \frac{1}{1.57 k a} \sqrt{\frac{\pi \gamma}{2 b V}}$$

$$\Omega = \frac{12}{(1.57)(16.92)(.07)} \sqrt{\frac{(\pi)(.321)(12)}{(2)(.035)(.25)(3.2 \times 10^7)}} = .03 \frac{\text{hr}^\circ\text{F}}{\text{Btu}}$$

The method developed herein gives:

$$\Omega = \frac{1}{\rho \Delta X v \pi a V (1 - e)^{-\alpha_v \pi b / \Delta X^2 V}}$$

$$\Omega = \frac{144}{(479)(.005) \sqrt{\pi} (.07) (.11) (6.67 \times 10^5) [1 - e^{-\frac{(.321)(\sqrt{\pi})(.035)(12)}{(.005)^2 (6.67 \times 10^5)}}]}$$

$$\Omega = \frac{6.605 \times 10^{-3}}{1 - .9858} = 0.464 \frac{\text{hr}^\circ\text{F}}{\text{Btu}}$$

The resistance for a static case can be expressed as:

$$\Omega = \frac{\Delta X}{k \pi a b}$$

$$\Omega = \frac{(.005)(12)}{(16.92)(\pi)(.035)(.07)} = 0.461 \frac{\text{hr}^\circ\text{F}}{\text{Btu}}$$

ORIGINAL PAGE IS
OF POOR QUALITY

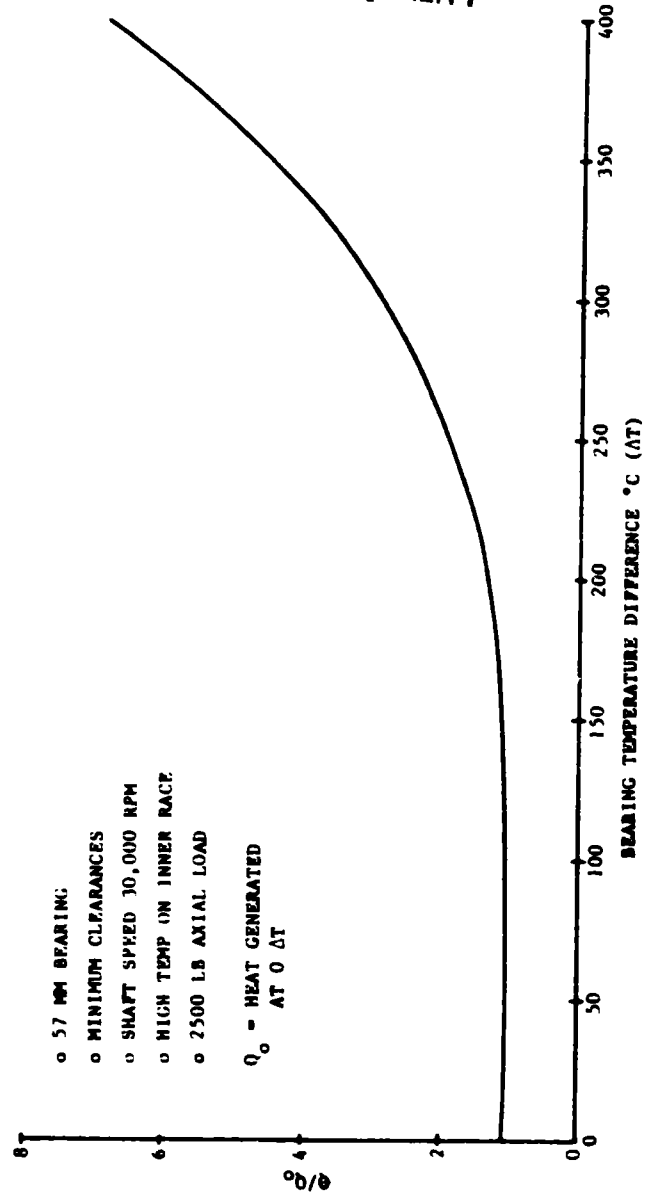


FIGURE 5.2.4 INCREASE IN HEAT GENERATED vs. BEARING TEMP. DIFFERENCE

spectra research systems

It is evident that the method derived herein gives essentially the same resistance values as would be used on modeling a stationary system, when representative values of contact area and velocities are used. Since the stationary resistance is higher than the value calculated from the equation in SHABERTH, and will consequently yield higher ΔT 's across the bearing, it is conservative in its effects on bearing clearances and element temperature gradients. For these reasons, the stationary resistances will be used in the development of the bearing model. As operating speeds, bearing size, etc. change, these charges will be incorporated in the "quasi-static" resistance calculation to be sure the static case remains in good agreement.

5.2.4 STATUS OF BEARING THERMAL MODEL DEVELOPMENT

A thermal model of the LOX BMT bearing set is being developed using the SINDA thermal modeling program. At this point in time, all nodes in the rolling element, inner raceway, and outer raceway have been determined for detailed temperature analysis in the areas of particular interest.

Data (i.e., cross sectional area of flow path, length of path, thermal conductivity, heat sources, etc.) is currently being assimilated into card formats which will be used to run the SINDA program. This program is already fully operational on the MSFC UNIVAC 1100 and therefore should require no modifications.

5.2.5 GRAPHICS CAPABILITY DEVELOPMENT FOR DATA REDUCTION AND DISPLAY

During the past month, the development of software to plot data from the BMT has progressed. The capability for conversion of raw data from the Engineering Units Tape is complete. Current tasks being pursued will allow plotting of selected data in a report-ready form on remote terminal CRT's which will then be hard-copied directly from the screen.

The routines to be used are found in the Tektronix PLOT 10 Terminal Control System User's Manual (4010A01) and the Advanced Graphing II User's Manual (062-1530-00). Copies of these documents have been obtained and studied.

End product specifications have been completed and data tapes have been logged on the system. A duplicate data tape (label #10315) has been created with a six month save option. An attempt has been made to mount the tape containing the conversion routine but an incompatibility existed. This is expected to be a minor problem that will be solved shortly.

Requirements that the software have the capability to plot any single data channel against any of the other channels have been established. Additionally, the software is to be developed so that it may be easily expanded at a later date to plot several lines on a single graph and provide multiple scales. Plots produced for the STS Data base are to be the general model for plot style from the instrument measurement system.

5.3 SEPTEMBER, 1982

5.3.1 CONTINUED INVESTIGATION OF BEARING TEMPERATURE GRADIENT EFFECTS ON OPERATIONAL CHARACTERISTICS

The development and initial checkout of a detailed finite element computer thermal model of the bearing pair used in the LOX turbopump turbine end has been completed. This model can be exercised for both transient and steady state operating conditions

spectra research systems

and provides a level of detail allowing the determination of thermal gradients at the rolling element contact surfaces. This model, coupled with SHABERTH, allows a complete dynamic and thermal analysis to be made for a shaft/bearing system. The capability to provide detail thermal gradients to support metallurgical, fatigue, and stress analysis is now available.

In the previous report, August 1982, the results of imposing several temperature gradients on a 57 mm ball bearing model were given. Due to inadvertent use of input data, these results are for a bearing with .0036 inch radial play at a contact angle of 20°. Since the test bearing has zero radial play at this contact angle, the input was modified and the analysis repeated. These results are shown in Figures 5.3.1 through 5.3.4. In comparing Figure 5.3.1 with Figure 5.2.1, it is evident that eliminating the radial play reduces the contact angle and increases the contact stresses, as should be expected. Comparison of the operating clearances (Figure 5.3.2) indicates a slight reduction in clearance for the case of no radial play. This results in an increase in frictional heat generated at the contact surfaces as can be seen by comparing Figure 5.3.4 with Figure 5.2.4.

The conclusions reached in the August report are unchanged. Elimination of the radial play slightly increased the sensitivity of operating conditions to bearing temperature differences. The previously discussed charts are labeled "minimum clearances". However, there may be other combinations of clearances that produce slightly tighter operating clearances. Although significant changes are not expected, this possibility is being investigated along with clearance combinations that provide maximum operating clearances. It should also be stated that the lower range of operating temperature for these analyses was -180°C or 168°R, which is representative of the LH₂ test environment. The higher temperature of the LOX (193°R) will have a slight effect on the clearance values.

An important factor in bearing life is the amount of slip occurring between the ball and races. The Lundberg - Palmgren method (Reference 1, page 411) for evaluating rolling bearing fatigue life is based on the assumption that bearings are lubricated and operated "properly". Proper operation means proper alignment, adequate loading to preclude skidding, free of contaminants such as dirt, etc. When the bearing is operated properly, sliding occurs in the contact area due to deformation of the surfaces. Since the Lundberg-Palmgren fatigue model is based on empirical data, this type of sliding is assumed to be accounted for in the fatigue life equations. Sliding which occurs because of skidding is not accounted for. According to Reference 1, the following expression can be used to reduce the dynamic capacity of the point contact due to ball spin.

$$\dot{Q}_c = \left[1 - \frac{b}{a} \frac{W_s}{W_{roll}} \right] \dot{Q}_c$$

Presumably ϕ must be determined experimentally, and

- b = Semi minor axis of contact ellipse
- a = Semi major axis of contact ellipse
- W_s = Ball spin normal to contact surface
- W_{roll}^s = Ball roll relative to contact surface.

FIGURE 5.3.1 CONTACT ANGLE AND STRESSES VS BEARING TEMP. DIFFERENCE

- o 57 mm Bearing
- o Minimum Clearances
- o Shaft Speed 30,000 RPM
- o High Temp. on Inner Race
- o 2500 Lb. Axial Load
- o Dry Friction

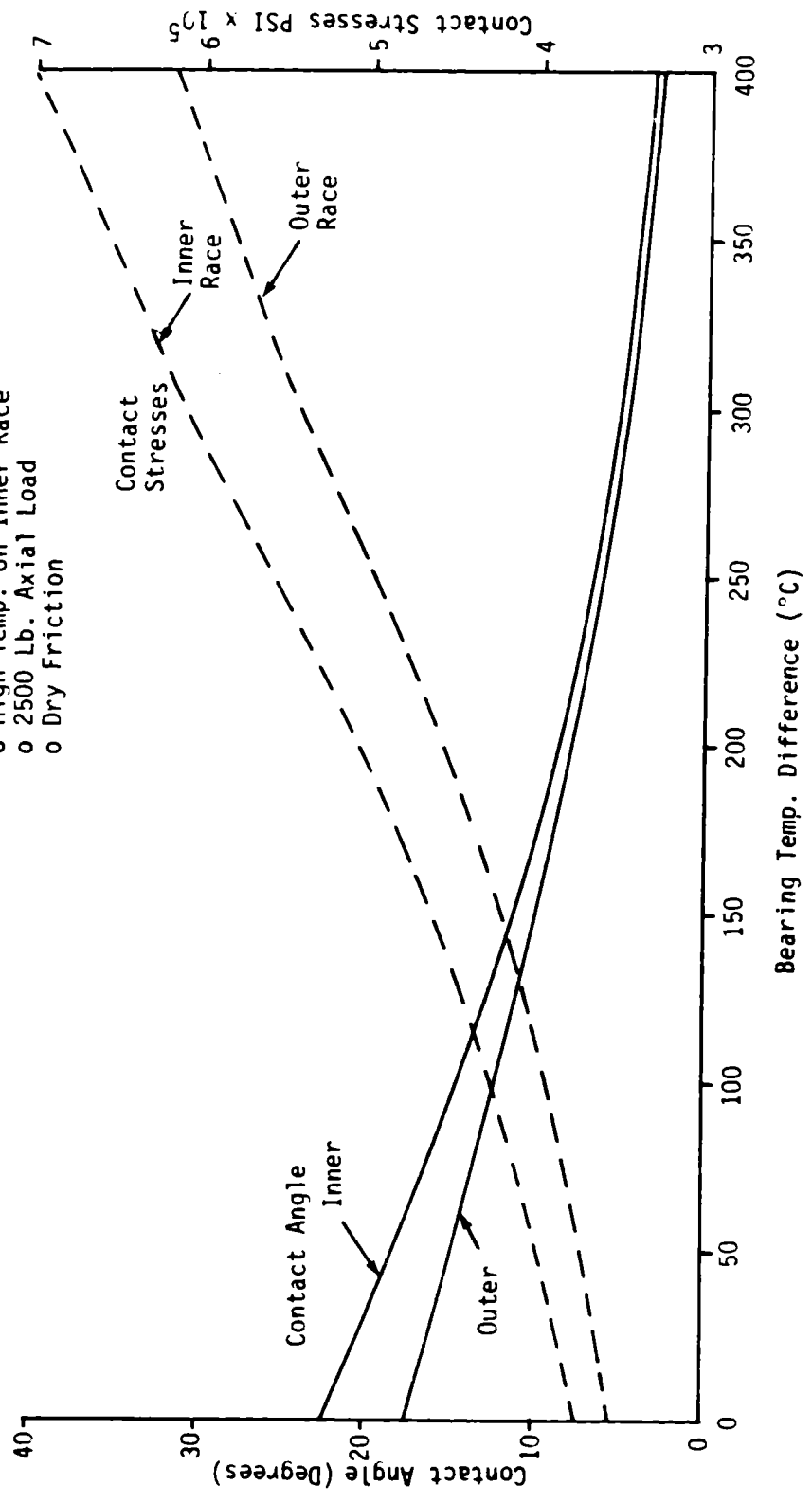
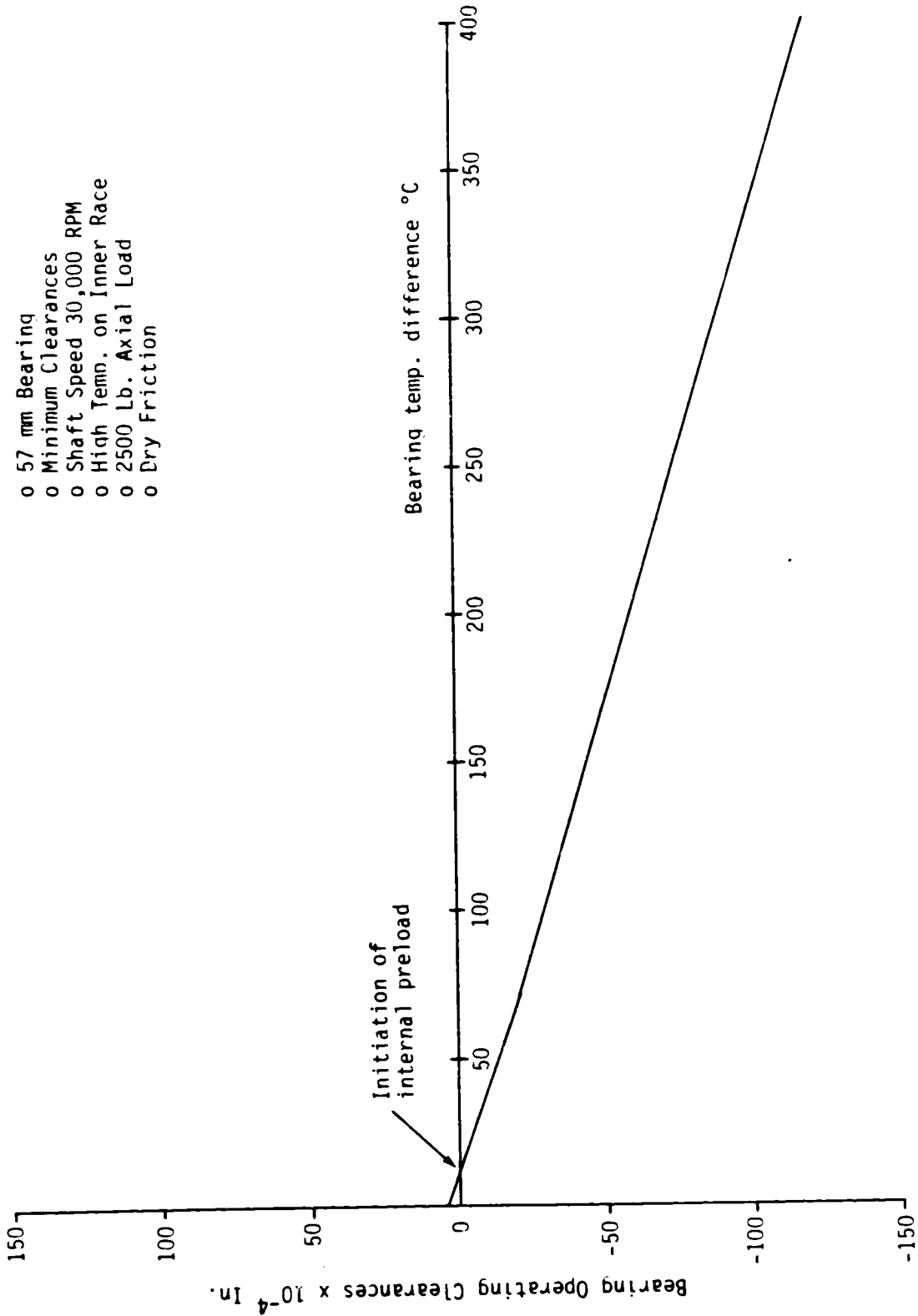


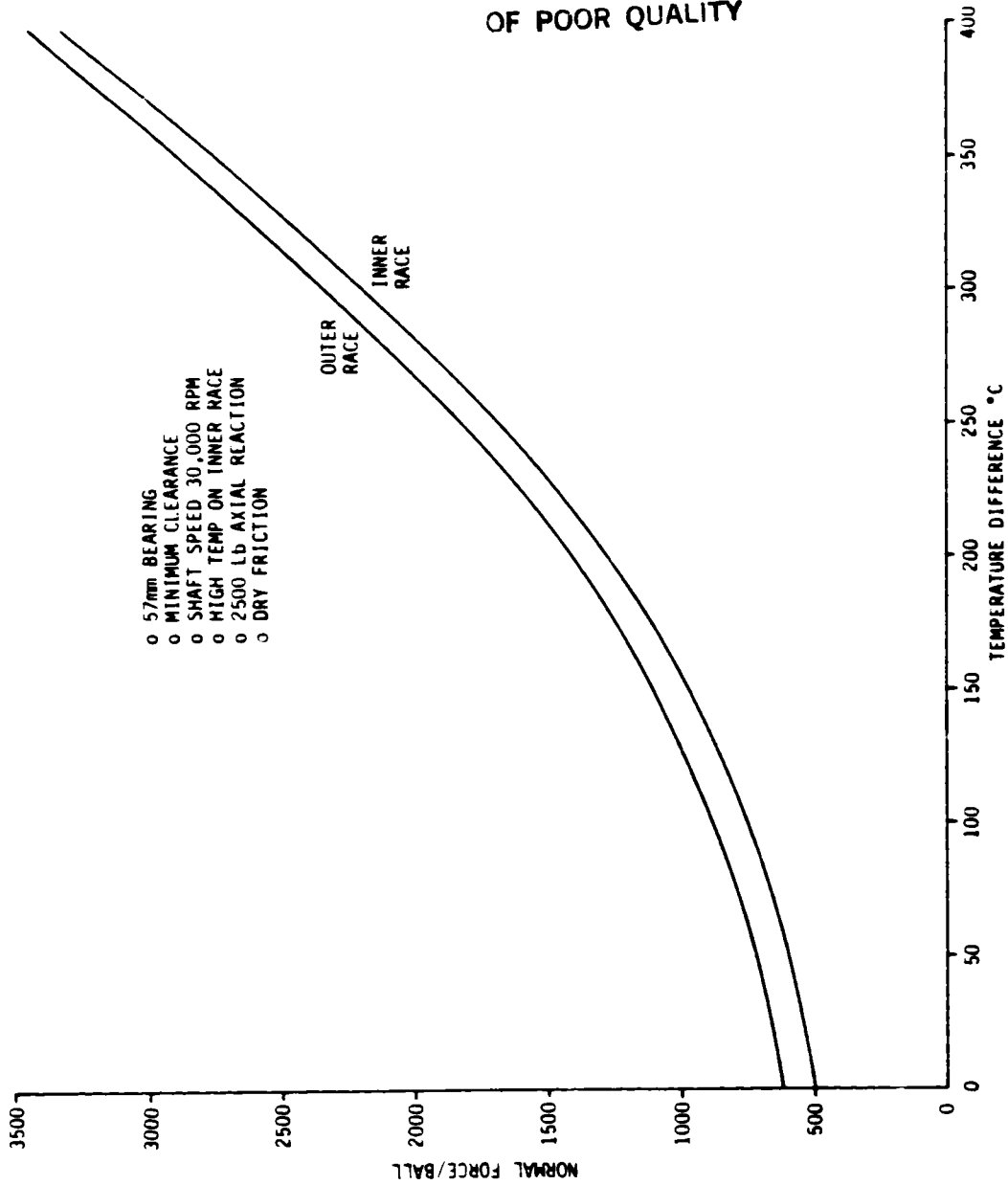
FIGURE 5.3.2 BEARING OPERATING CLEARANCE VS TEMPERATURE DIFFERENCE

- o 57 mm Bearing
- o Minimum Clearances
- o Shaft Speed 30,000 RPM
- o High Temp. on Inner Race
- o 2500 Lb. Axial Load
- o Dry Friction



SRS

FIGURE 5.3.3
 NORMAL FORCES VS. BEARING TEMP DIFFERENCE

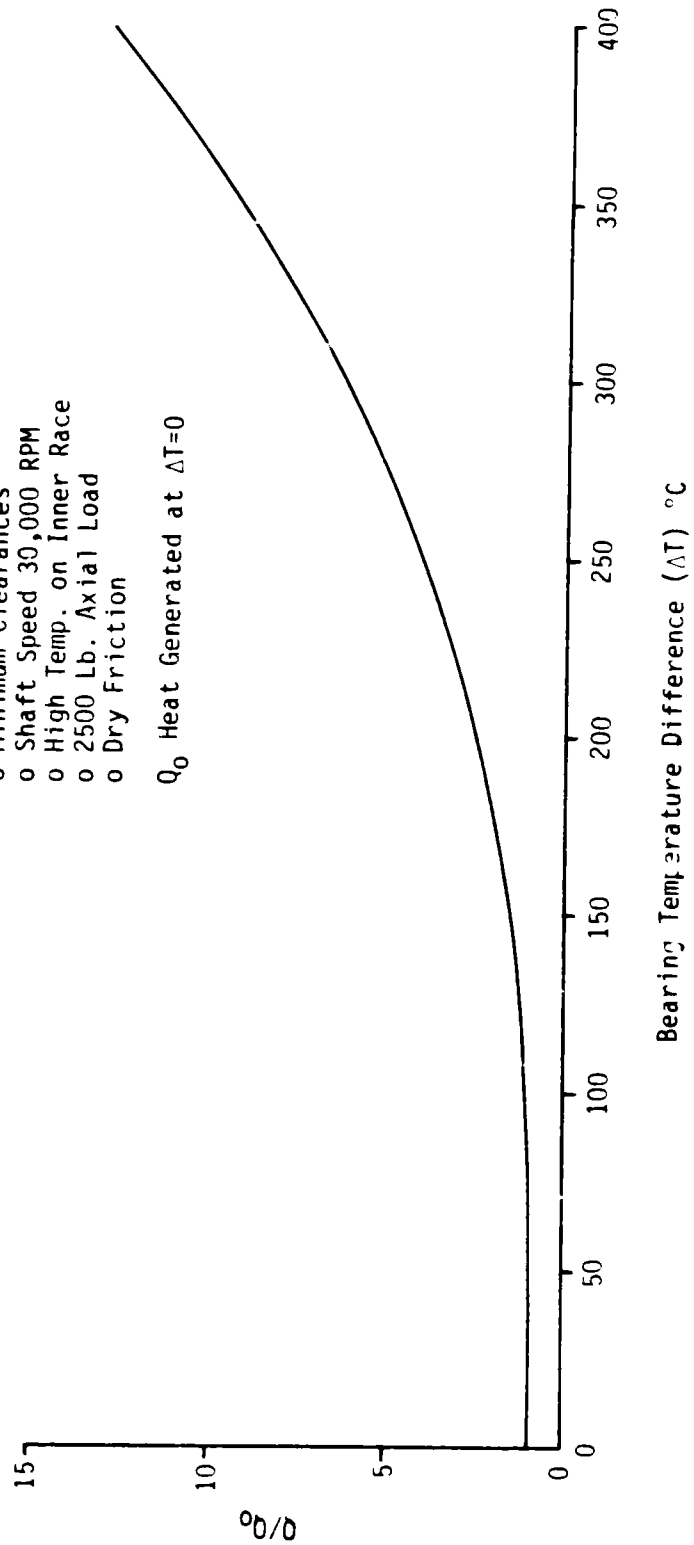


ORIGINAL PAGE IS
 OF POOR QUALITY

SRS

FIGURE 5.3.4
INCREASE IN HEAT GENERATED VS BEARING TEMP. DIFFERENCE

- o 57 mm Bearing
 - o Minimum Clearances
 - o Shaft Speed 30,000 RPM
 - o High Temp. on Inner Race
 - o 2500 Lb. Axial Load
 - o Dry Friction
- Q_0 Heat Generated at $\Delta T=0$



spectra research systems

As a start in investigating this effect, the ball spin to roll ratio for the 57 mm bearing was calculated as a function of ΔT across the bearing. Since the SHABERTH computer program does not provide this calculation directly, additional computations were performed. The necessary ball rotational information generated by SHABERTH is as follows:

$$\begin{aligned} W_x &= x \text{ component of ball speed} \\ W_y &= y \text{ component of ball speed} \\ W_z &= z \text{ component of ball speed} \end{aligned}$$

Using this information, the ball spin (W_s) and roll (W_r) can be determined by constructing a vector diagram as shown in Figure 5.3.5. From Figure 5.3.5, the following expressions can be obtained:

Ball Spin:

$$\begin{aligned} W_{si} &= (W_s - W_o) \sin \alpha_i + W_x \sin \alpha_i - W_y \cos \alpha_i \\ W_{so} &= W_{so} = -W_o \sin \alpha_o + W_x \sin \alpha_o - W_y \cos \alpha_o \end{aligned}$$

Ball Roll:

$$\begin{aligned} W_{ri} &= (W_s - W_o) \cos \alpha_i + W_x \cos \alpha_i + W_y \sin \alpha_i \\ W_{ro} &= W_o \cos \alpha_o - W_x \cos \alpha_o - W_y \sin \alpha_o \end{aligned}$$

Where: W_{si} , W_{so} = Ball spin normal to inner and outer races respectively.

W_s = Shaft speed

W_o = Ball orbital speed

α_i , α_o = Inner and outer contact angles

W_{ri} , W_{ro} = Ball roll speed relative to inner and outer races

The spin-to-roll ratios can therefore be expressed as follows:

Inner Race:

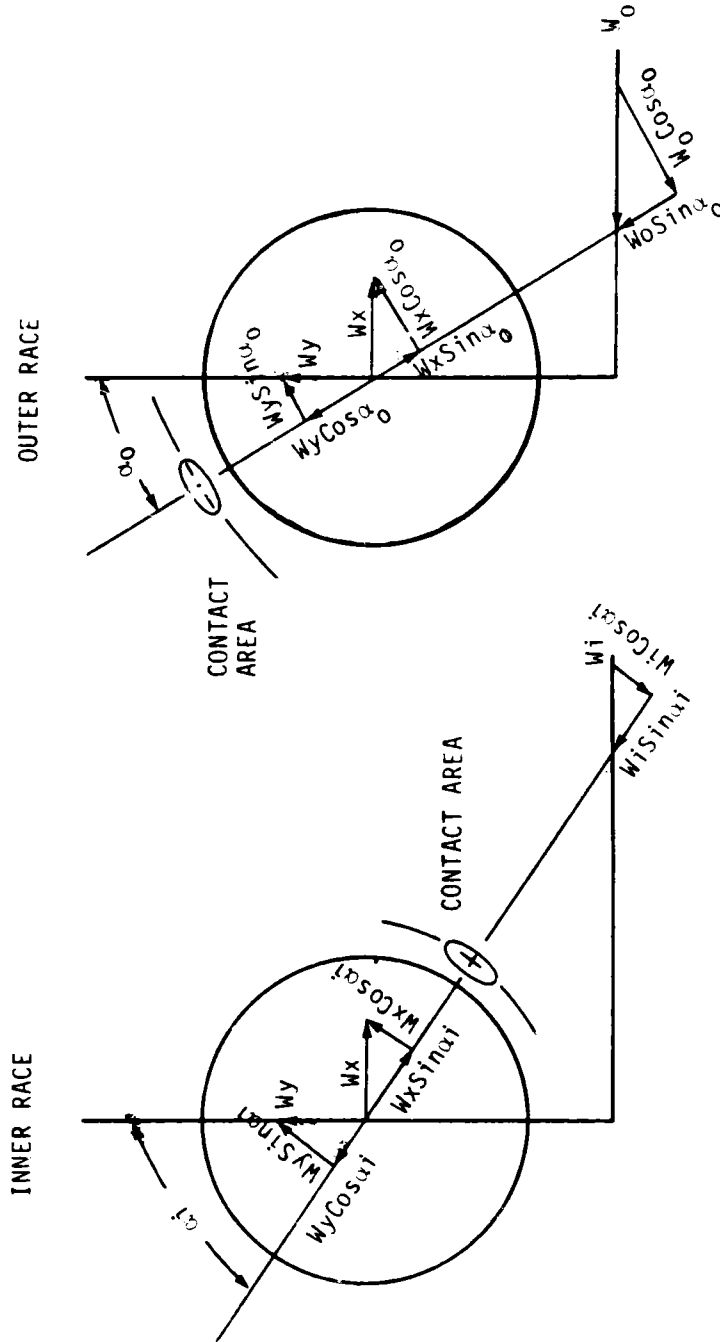
$$\frac{W_{si}}{W_{ri}} = \frac{(W_s - W_o) \sin \alpha_i + W_x \sin \alpha_i - W_y \cos \alpha_i}{(W_s - W_o) \cos \alpha_i + W_x \cos \alpha_i + W_y \sin \alpha_i}$$

Outer Race:

$$\frac{W_{so}}{W_{ro}} = \frac{-W_o \sin \alpha_o + W_x \sin \alpha_o - W_y \cos \alpha_o}{W_o \cos \alpha_o - W_x \cos \alpha_o - W_y \sin \alpha_o}$$

The inner and outer race ball spin-to-roll ratios are shown in Figure 5.3.6 as a function of bearing temperature difference. As shown, the ball spin is reduced as the

FIGURE 5.3.5 BALL SPIN VECTOR DIAGRAM



INNER RACE BALL SPIN NORMAL TO CONTACT AREA
 $W_{si} = (W_s - W_0) \sin \alpha_i + W_x \sin \alpha_i - W_y \cos \alpha_i$

OUTER RACE BALL SPIN NORMAL TO CONTACT AREA
 $W_{so} = -W_0 \sin \alpha_o + W_x \sin \alpha_o - W_y \cos \alpha_o$

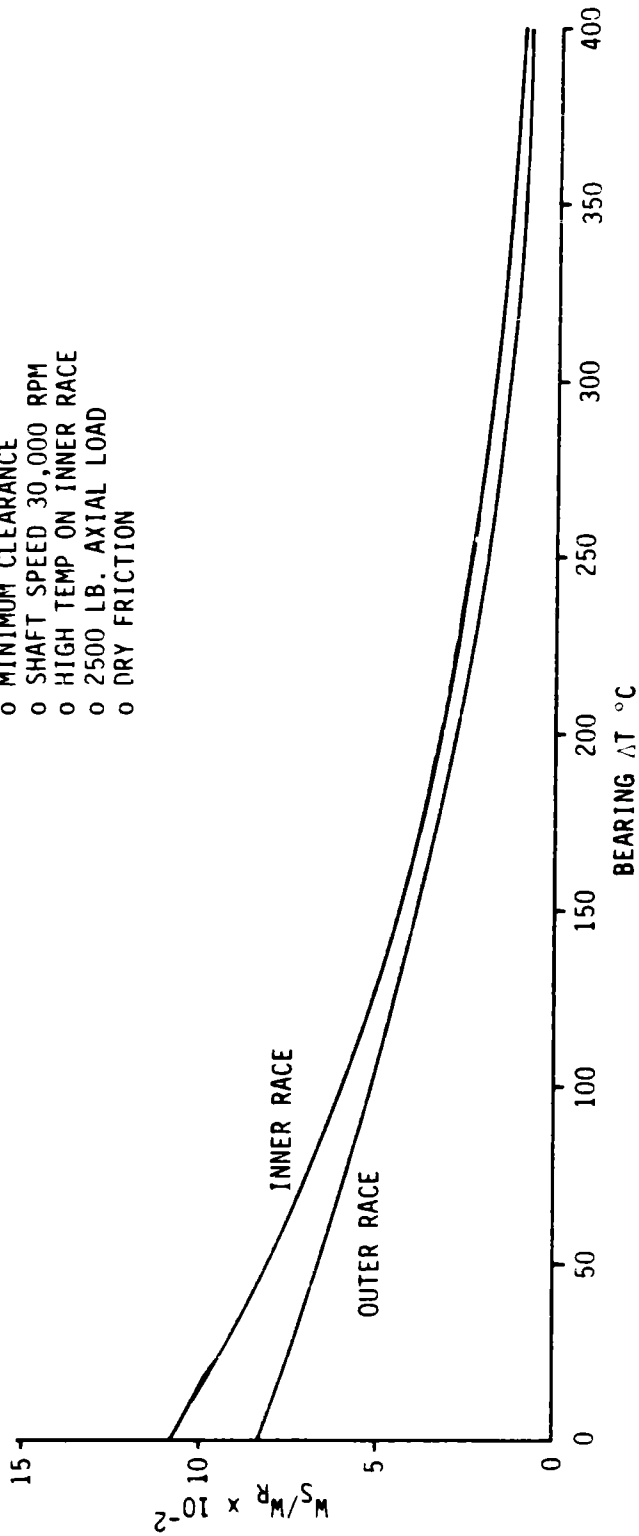
W_s = Shaft Speed
 W_0 = Cage Speed
 W_i = Relative Speed

FIGURE 5.3.6
BALL SPIN/ROLL RATIO vs. BEARING ΔT

W_S = BALL SPIN NORMAL TO
CONTACT SURFACE

W_R = BALL ROLL SPEED
RELATIVE TO RACES

- o 57 mm BEARING
- o MINIMUM CLEARANCE
- o SHAFT SPEED 30,000 RPM
- o HIGH TEMP ON INNER RACE
- o 2500 LB. AXIAL LOAD
- o DRY FRICTION



SRS

temperature difference is increased. This is the result of increased normal loads and friction forces and the reduced differences in inner and outer contact angles. It is evident that for a given set of conditions; load, speed, friction coefficients, etc., there is an optimum bearing configuration, contact angle, inner and outer race curvature, etc., that will minimize the combined effects of ball spin and heat generation and maximize bearing life.

These analyses have been conducted using a clearance stack producing a minimum contact angle. Similar analyses will be made using a clearance stack to maximize the contact angle. This will provide a band of information over the possible range of contact angle variations.

5.3.2 ESTIMATES OF BALL DRAG FORCES, TORQUES, AND HEAT GENERATION

Proper manipulation of the input data allows the SHABERTH bearing program to calculate the heat generated due to viscous and form drag on the orbiting balls in a low viscosity fluid such as LOX. This technique was explained in Section 5.2.1. Estimates of ball drag, torque, and heat generation can be made as a function of the percent liquid assumed to be in the bearing cavity. Shown in Figure 5.3.7 are the preliminary results of an analysis on the 57 mm bearing. As noted, the data are for a single bearing assumed to be operating in a stagnant fluid. The percent fluid in the cavity can be interpreted either as a low density fluid or the partial filling of the cavity with liquid.

Although bearing characteristics such as contact angle were not affected by ball drag, the fluid drag on the balls does cause ball slippage or skidding in a lightly loaded bearing. This effect is shown in Figure 5.3.8 which gives the ratio of cage-to-shaft speed as a function of bearing reaction, percent fluid in the cavity, and friction coefficient. Although this information should be considered preliminary due to convergence problems with the machine solution, the trends are believed to represent the physical characteristics. This problem should be overcome by going to a higher level of solution in the SHABERTH program.

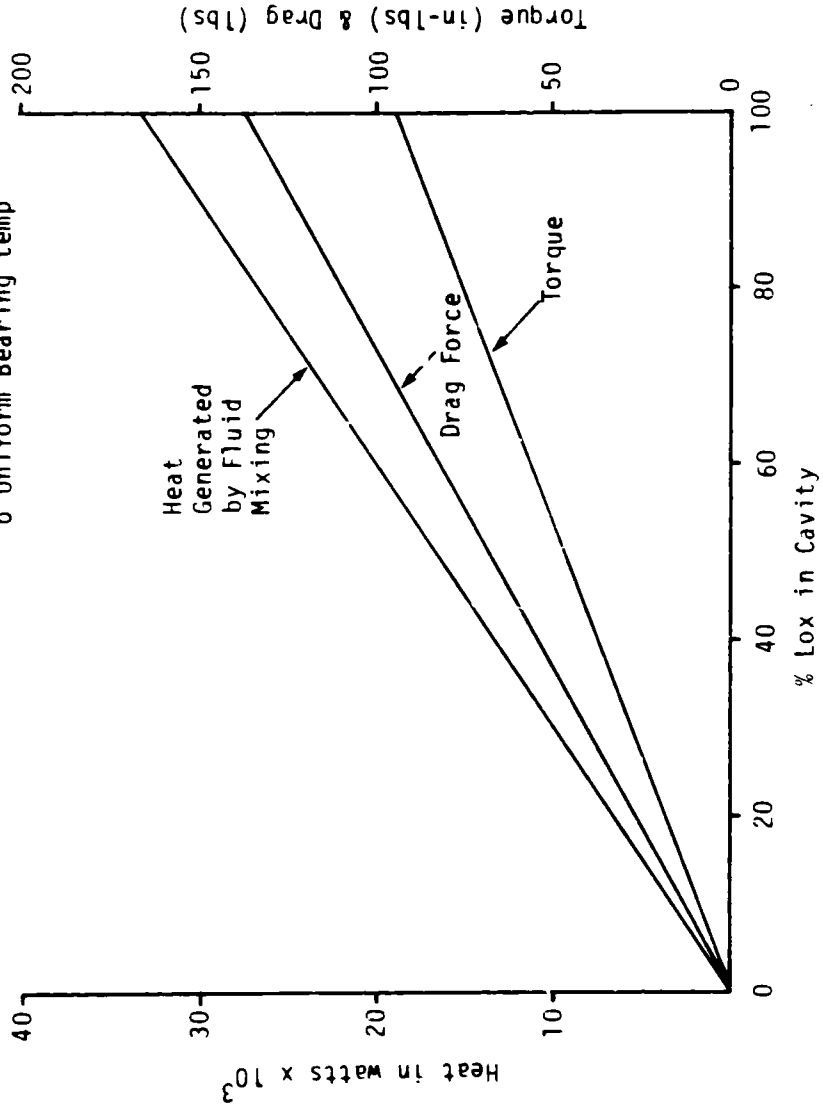
As shown, the effect of increased flooding of the bearing cavity is to slightly reduce the cage rotational speed at bearing reaction loads above approximately 150 pounds. Below 150 pounds there is a significant reduction in cage speed indicating bearing slip on the inner race. A reduction in friction coefficient increases the ball slip which further reduces the cage speed as shown. This indicated that a combination of low axial load and high fluid drag can cause significant slip between the rolling elements and the inner race. The consequence of this is increased heat generated, wear, and shorter bearing life. The fluid density used in these analyses is representative of LOX.

The effects on bearing frictional and viscous heat generation are shown in Figures 5.3.9 and 5.3.10. Figure 5.3.9 provides data for a 50% flooded cavity and Figure 5.3.10 is data representing a 100% flooded cavity. As shown, the fractional heat generated increases, after passing through a minimum point, as the bearing reaction load is reduced. The effect is more severe for the 100% flooded cavity. These effects could be considerably more severe than indicated for some combinations of axial and radial loading. For instance, if a bearing is lightly loaded in the axial direction with significant slip between rolling elements and inner race, a sudden application of radial load will cause the friction forces between the ball and race to increase. Since the ball/cage mass cannot be instantaneously accelerated to the cage equilibrium speed, considerable damage can be done to the balls and races due to slippage under

FIGURE 5.3.7

HEATING AND BALL DRAG VS % FLUID IN CAVITY
(Single Bearing)

- o 57mm Bearing
- o Minimum Clearances
- o Shaft Speed 30,000 RPM
- o 2500 Lb. Axial Load
- o Uniform Bearing temp



ORIGINAL PAGE IS
OF POOR QUALITY

SRS

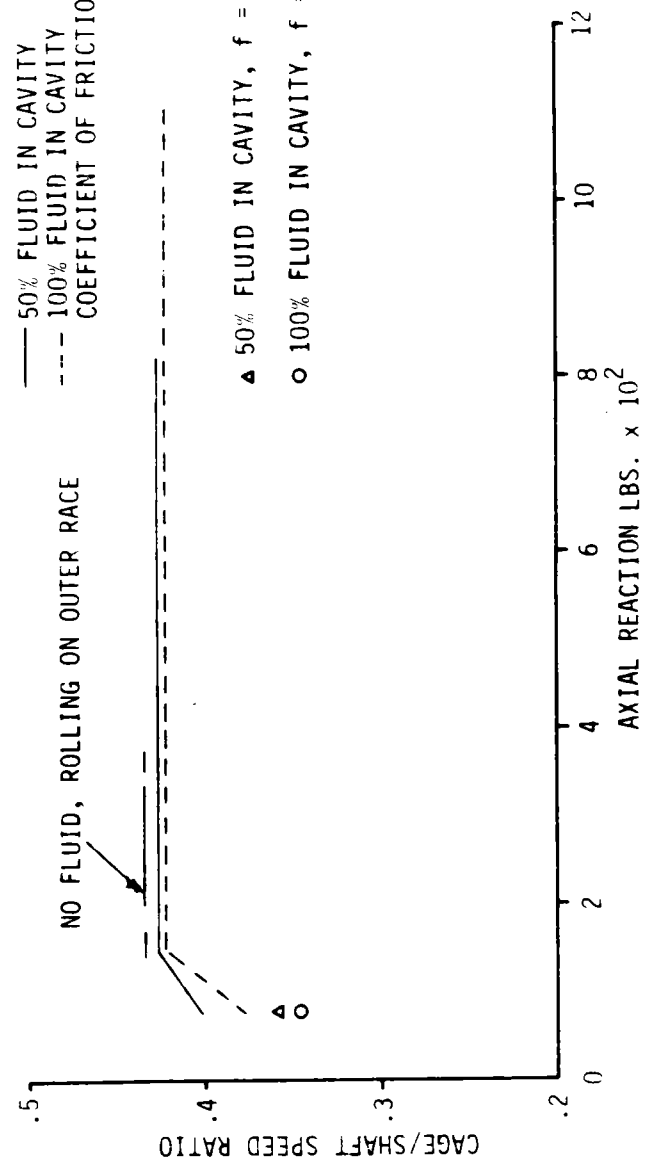
ORIGINAL PAGE 09
OF POOR QUALITY

FIGURE 5.3.8
CAGE/SHAFT SPEED RATIO vs. AXIAL LOAD, % LOX IN BEARING CAVITY AND FRICTION COEFFICIENT

o 57 mm BEARING
o SHAFT SPEED - 30,000 RPM
o MINIMUM CLEARANCE

— 50% FLUID IN CAVITY
- - - 100% FLUID IN CAVITY
COEFFICIENT OF FRICTION (f) = 0.14

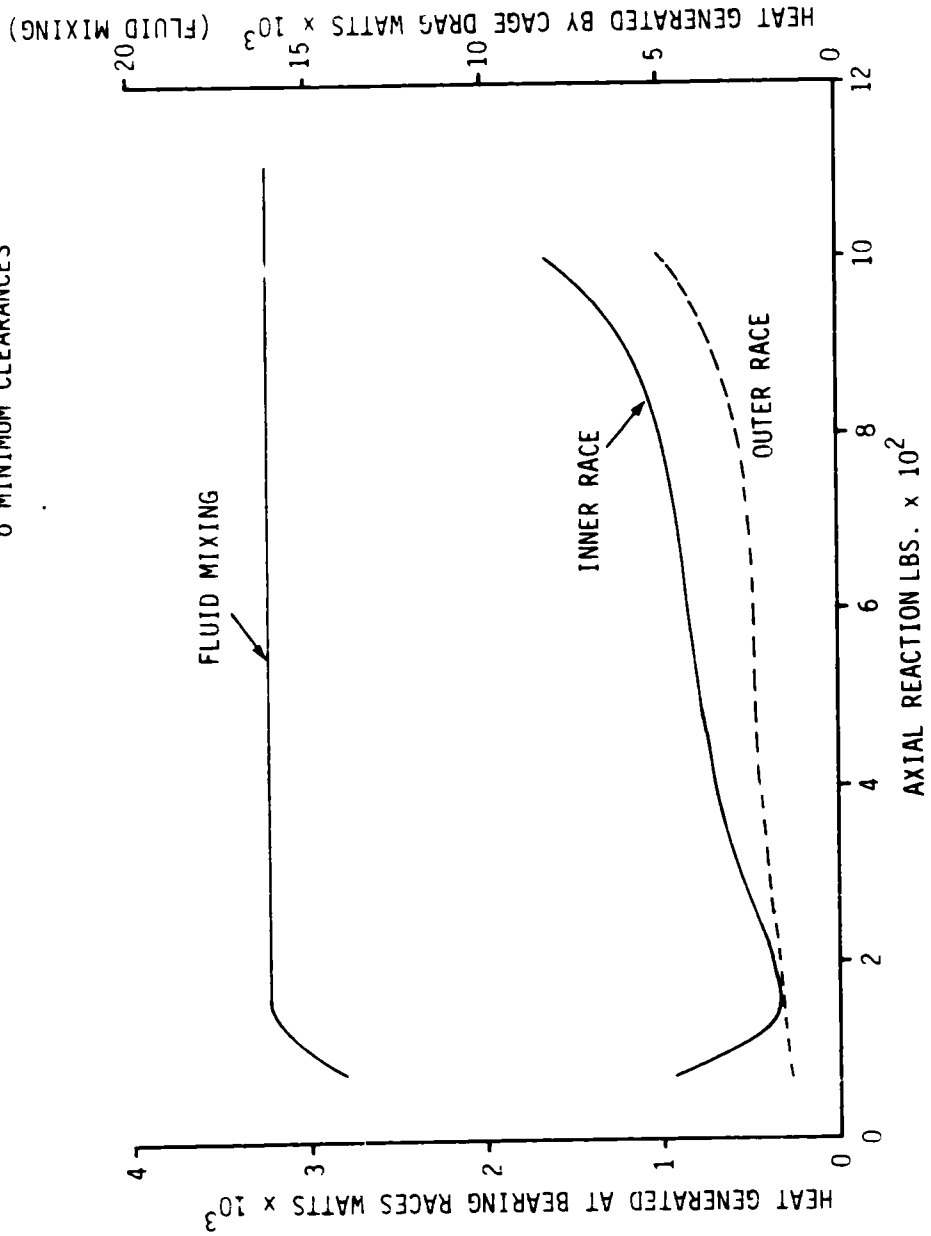
▲ 50% FLUID IN CAVITY, f = 0.1
o 100% FLUID IN CAVITY, f = 0.1



SRS

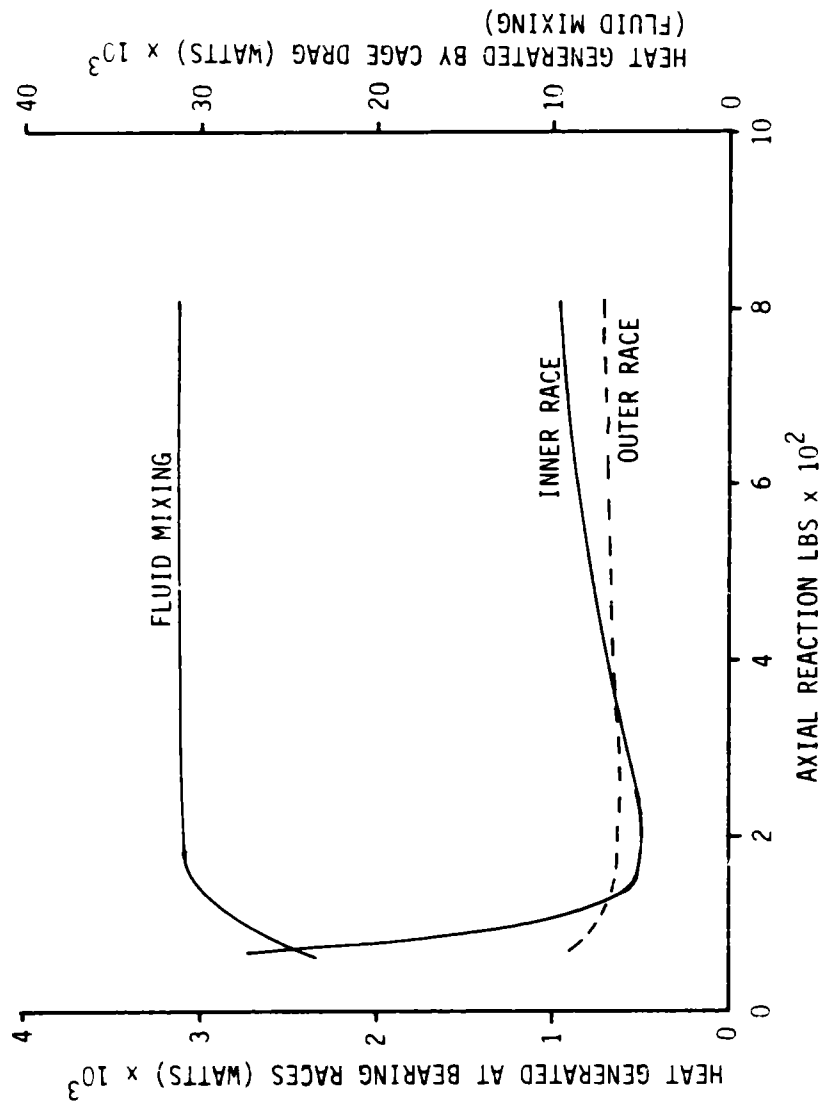
FIGURE 5.3.9
HEAT GENERATED vs. AXIAL LOAD (SINGLE BEARING) 50% FLUID IN CAVITY

- o 57 mm BEARING
- o SHAFT SPEED 30,000 RPM
- o FRICTION COEFFICIENT 0.14
- o MINIMUM CLEARANCES



ORIGINAL PAGE :
OF POOR QUALITY

FIGURE 5.3.10
HEAT GENERATED vs. AXIAL LOAD 100% FLUID IN CAVITY



SRS

high loading. This input could explain the abnormal wear observed in the LN₂ tests for bearings 1 and 4 of the BMT. Efforts are under way to extend these analyses² to include other friction factors and modify the fluid density to represent LN₂.

5.3.3 CORRELATION OF TESTER INTERNAL POWER DISSIPATION WITH BEARING TEMPERATURE DIFFERENCES

To determine the sources and magnitudes of heat generated in the BMT, each component was evaluated and an estimate of the amount of energy dissipated was made. The total amount dissipated was then compared to the total energy transferred to the LOX coolant flowing through the bearings. As will be shown, the total energy estimated from the component analysis is less than the energy transferred to the LOX coolant. The LOX coolant and component energy can be balanced, however, by assuming a temperature gradient across the bearing. As discussed previously, the temperature gradient causes increased internal loading and heat generation.

The power estimates for each component in the BMT is shown in Figure 5.3.11. This information was calculated using semiempirical relationships provided in Reference 2 and viscous ball drag obtained from the bearing computer program. Several assumptions were necessary to complete the power estimates. The most significant are as follows:

- 1) The fluid has no rotational speed prior to entering bearings 1 and 4.
- 2) Front faces (face to shaft shoulder) of bearings 2 and 3 are rotating in stagnant fluid.
- 3) Fluid is rotating at cage speed between bearings 1 and 2 and between bearings 3 and 4.
- 4) The power dissipated by the shaft section between bearings 2 and 3 was determined by averaging the power estimates based on inlet fluid properties and exit fluid properties.
- 5) The power estimated for disks and cylinders can be superimposed to obtain the combined slinger-shaft power.

As shown in Figure 5.3.11, only the bearing frictional power for the loaded bearings (2 and 3) was varied as a function of bearing temperature differences. Energy values for other components downstream of bearings 2 and 3 would vary as additional heat is added to the coolant. This effect was considered secondary in view of the other uncertainties in the analysis. The other side of the energy balance is the energy absorbed by the bearing coolant flow. This was estimated in the July 1982 progress report and the summary results are provided in Figure 5.3.12. As shown, 182.1 kW of energy was estimated to be absorbed by the bearing coolant flow. Since this is in excess of the 165.7 kW estimated to be generated, it is suggested that a temperature gradient across the bearings could explain the discrepancy. Figure 5.3.13 illustrates, in graphical form, the information provided in Figure 5.3.11. Also shown in Figure 5.3.13 is the temperature gradient across the bearings (2 and 3) necessary to achieve an overall energy balance.

In summary, the results of the analysis strongly indicate that the inner races of bearings 2 and 3 are considerably higher in temperature than the outer races. This condition can become unstable causing excessive internal loads and temperatures resulting in rapid deterioration and failure of the bearing. In addition, careful consideration must be taken to ensure the unloaded bearings (1 and 4) do not become

ORIGINAL PAGE IS
OF POOR QUALITY

FIGURE 5.3.11 POWER GENERATION VS. TEMPERATURE DIFFERENCE ACROSS BEARING
POWER IN (KW)

ΔT °C ACROSS BEARINGS 2 & 3

| COMPONENT* | 0 | 100 | 200 | 300 |
|---------------------------|--------|-------|-------|-------|
| Slinger (Smooth Sides) | 31.9 | 31.9 | 31.9 | 31.9 |
| Spacers | 10 | 10 | 10 | 10 |
| Shaft | 42.9 | 42.9 | 42.9 | 42.9 |
| Sub Total | 84.8 | 84.8 | 84.8 | 84.8 |
| BEARINGS | | | | |
| Viscous | | | | |
| 1 & 4 | **65.9 | 65.9 | 65.9 | 65.9 |
| 2 & 3 | ***2.0 | 2.0 | 2.0 | 2.0 |
| Sub Total | 67.9 | 67.9 | 67.9 | 67.9 |
| FRICTION | | | | |
| 1 & 4 | 2.2 | 2.2 | 2.2 | 2.2 |
| 2 & 3 | 10.8 | 13.0 | 27.5 | 68.7 |
| Sub Total | 13.0 | 15.2 | 29.7 | 70.9 |
| Total | 165.7 | 167.9 | 182.4 | 223.6 |

**Although the Component Power & Viscous Power will be reduced as the fluid temperature increases, this effect was assumed to be within the uncertainties introduced by the assumption made in the power calculations.

***Assumes no fluid rotation prior to entering the bearing.

****Assumes fluid enters bearings 2 & 3 with rotational velocity equal to cage speed.

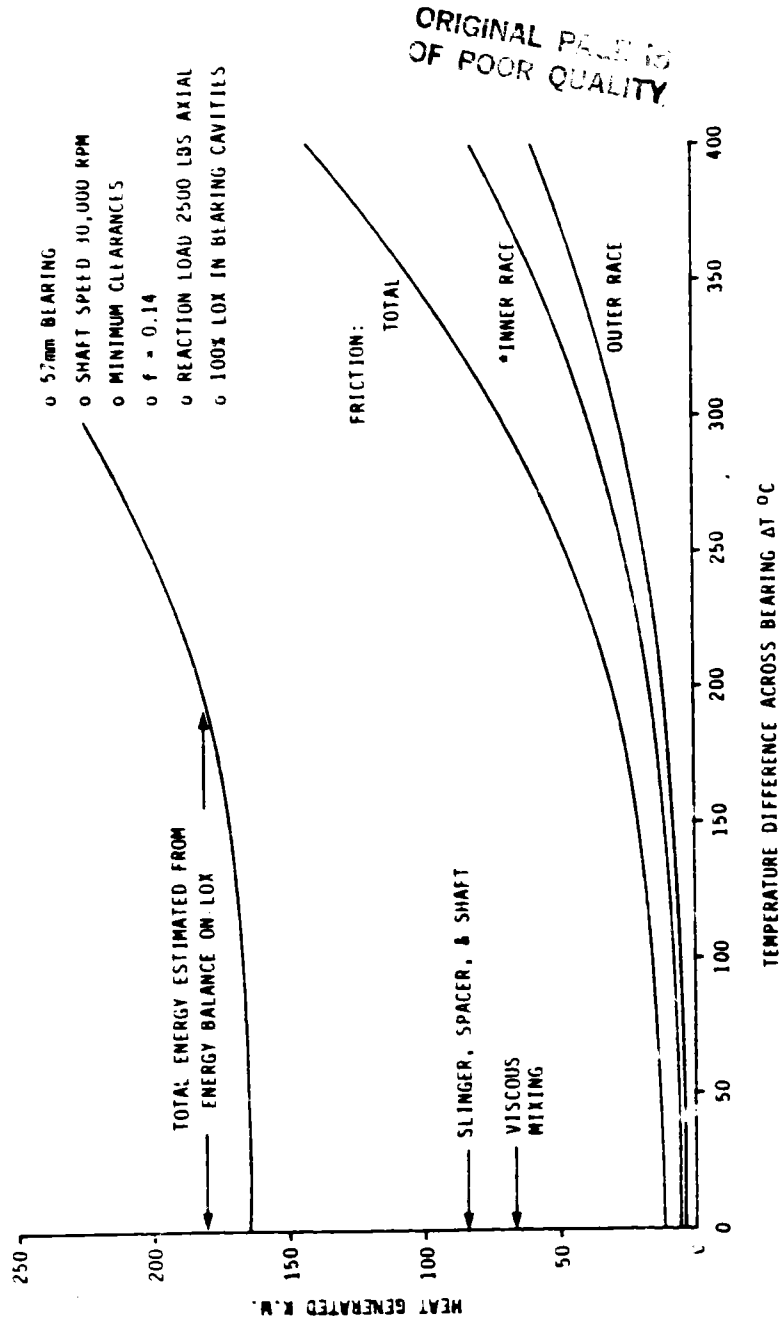
FIGURE 5.3.12 ENERGY BALANCE SUMMARY

| | | POWER INPUT W (WATTS) | AMBIENT HEAT INPUT Q (WATTS) | ENERGY REMOVED BY FLOW (mWh) (WATTS) | ENERGY UNBALANCE FOR STEADY CONDITIONS (WATTS) $\dot{W} + \dot{Q} - W\Delta h$ |
|-----------------|------------------------|--------------------------|---------------------------------|---|--|
| LOX | NON-ROTATING (FLOW) | 0 | 572 | 0 | 0 |
| | ROTATING | 202.8×10^3 | 572* | 182.1×10^3 | 21.2×10^3 |
| LN ₂ | NON-ROTATING (FLOW) | 0 | 572* | 0 | 0 |
| | ROTATING | 210.9×10^3 | 572* | 202×10^3 | 9.5×10^3 |

* ASSUMED TO BE THE SAME DURING ALL TESTS.

SRS

FIGURE 5.3.13 ENERGY VS. BEARING ΔT



- o 57mm BEARING
- o SHAFT SPEED 30,000 RPM
- o MINIMUM CLEARANCES
- o $f = 0.14$
- o REACTION LOAD 2500 LBS AXIAL
- o 100% LOX IN BEARING CAVITIES

* INNER & OUTER RACES OF BGRS. 2 & 3. BGMS 1 & 4 WERE UNLOADED; A CONSTANT RATE OF 2.2 K.M. WAS ESTIMATED FOR THE RACE FRICTION HEAT.

unloaded to the extent that significant slip or skidding can occur between the balls and inner races.

5.3.4 BEARING THERMAL MODEL DEVELOPMENT

The development of the thermal model for the LOX BMT Bearing Set is progressing and a summary of the work accomplished is shown in Figure 5.3.14.

The area of the tester under consideration with respect to the model is illustrated in Figure 5.3.15 by the slashed boundary lines and includes the shaft, inner races, outer races, bearing spaces, cages, carrier, and housing. Two back-to-back mounted duplex bearings will be analyzed. Figure 5.3.16 shows the cross-sectional view of the tester. The slashed lines in the figure indicate the boundary lines for the model from this prospective. Each pie shaped slice is identical and all thirteen will be connected by parallel resistors to model the heat flow for the entire bearing.

Figure 5.3.17 and 5.3.18 are included to illustrate the methodology used in the finite element or node analysis of the bearing components. Figure 5.3.17 shows one-eighth of the surface area of the rolling element. The nodal break-up below the surface in Section 1 (the ball track area) is represented in Figure 5.3.18. The other bearing components are partitioned into nodes in a similar manner.

During the past month, the capacitance data for the tester components, as shown in Figure 5.3.14, has been calculated and arranged in a format to be used in the "SINDA" (Systems Improved Differencing Analyzer) thermal modeling program. This task included computing the volume of more than 200 irregularly shaped nodes. The capacitance of each node was determined using a constant value of specific heat for the material over a range of 32^oF to 212^oF. The process of obtaining the specific heat and thermal conductivity data for each material as a function of temperature has been initiated. This information will be input into the SINDA program in array form and used to calculate the current capacitance and conductance values of the respective nodes during each iteration of the heat transfer equations.

The calculation of more than 800 conductance values was also accomplished in the past month. These values were determined using thermal conductivity data for a temperature range of 32^oF to 212^oF. When further data is obtained for the thermal conductivity of the materials as a function of temperature in the range of consideration, it will be utilized as described in the previous paragraph.

The heat-transfer coefficients (convective film coefficient) for forced convection to the coolant from the rolling element and races have also been calculated during this reporting period. Several analogies between heat and momentum transfer in turbulent flow were investigated including the Reynold's analogy for turbulent flow inside a pipe and along a flat plate. The Prandtl analogy for momentum and heat transfer for turbulent flow in a pipe was determined to be the best approximation for the situation to be modeled. The bearing thermal model is continuously being improved, and as will be discussed in later reports, extensive updating of nodal structure and fluid film coefficients have been made.

The SINDA is a software system which possesses the capabilities that make it well suited for solving lumped parameter representations of physical problems governed by diffusion-type equations. The system was designed as a general thermal analyzer accepting resistor-capacitor network representations of thermal systems.

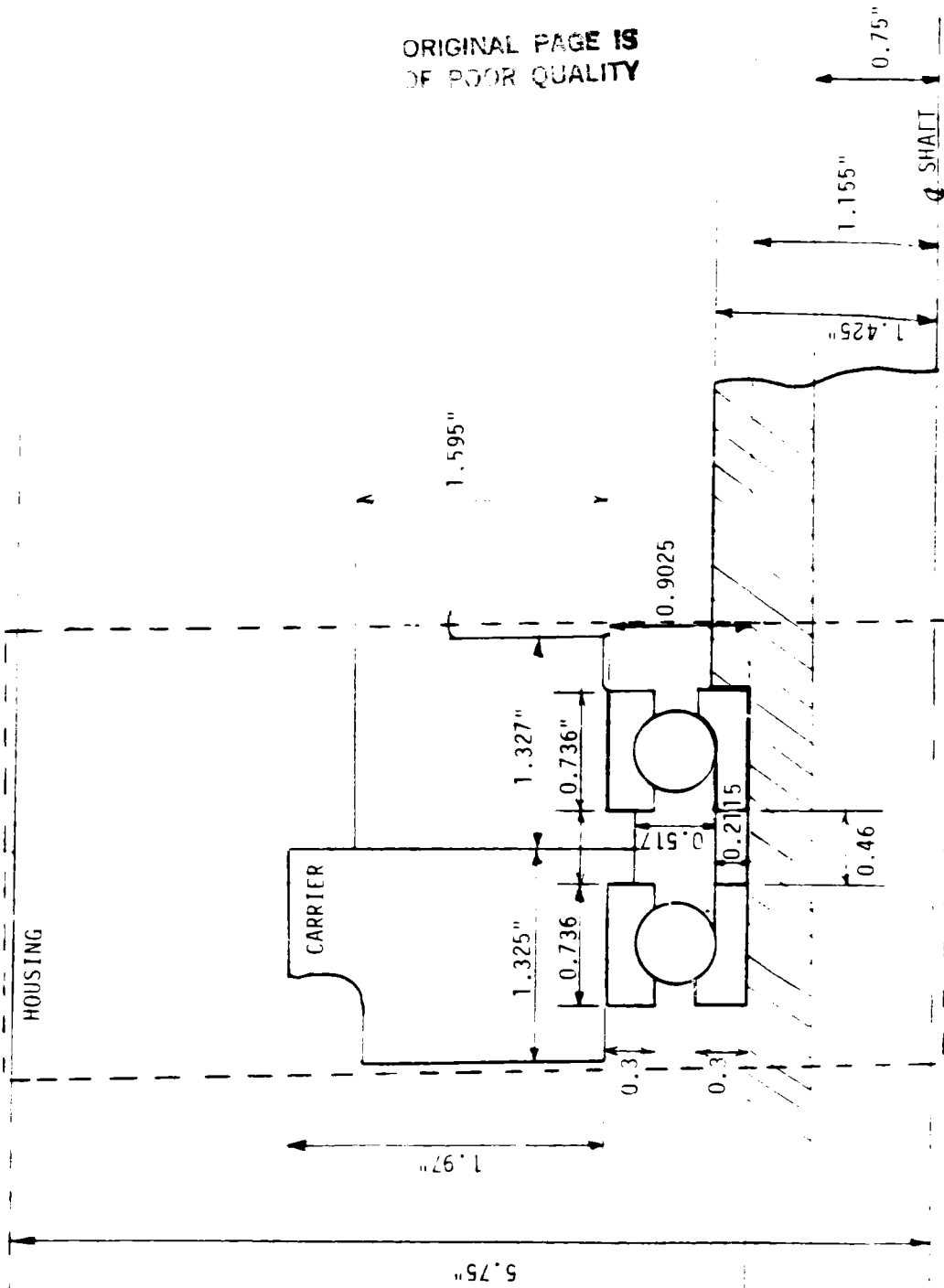
ORIGINAL PAGE IS
OF POOR QUALITY

FIGURE 5.3.14
STATUS OF BEARING THERMAL MODEL

| | ASSIMILATION OF THERMAL DATA | FINITE ELEMENT ANALYSIS | CALCULATION OF CAPACITANCE FOR EACH NODE | CALCULATION OF CONDUCTANCE FOR EACH HEAT TRANSFER PATH | GENERATION OF DATA | IMPLEMENTATION OF DATA INTO CARD FORMATS | RUN AND DEBUG MODEL |
|-------------------|------------------------------|-------------------------|--|--|--------------------|--|---------------------|
| ROLLING ELEMENT | ✓ | ✓ | ✓ | ✓ | ✓ | ✓ | |
| CAGE | ✓ | ✓ | ✓ | ✓ | N/A | ✓ | |
| BEARING SEPARATOR | ✓ | ✓ | ✓ | ✓ | N/A | ✓ | |
| COOLANT | ✓ | ✓ | ✓ | ✓ | ✓ | ✓ | |
| INNER RACE | ✓ | ✓ | ✓ | ✓ | ✓ | ✓ | |
| OUTER RACE | ✓ | ✓ | ✓ | ✓ | ✓ | ✓ | |
| SHAFT | ✓ | ✓ | ✓ | ✓ | N/A | ✓ | |
| CARRIER | ✓ | ✓ | ✓ | ✓ | N/A | ✓ | |
| HOUSING | ✓ | ✓ | ✓ | ✓ | N/A | ✓ | |

SRS

FIGURE 5.3.15 SCHEMATIC OF BEARING SET



ORIGINAL PAGE IS
OF POOR QUALITY

SCALE 1:1

SRS

FIGURE 5.3.16 CROSS-SECTIONAL VIEW OF SHAFT, BEARING,
CARRIER AND HOUSING

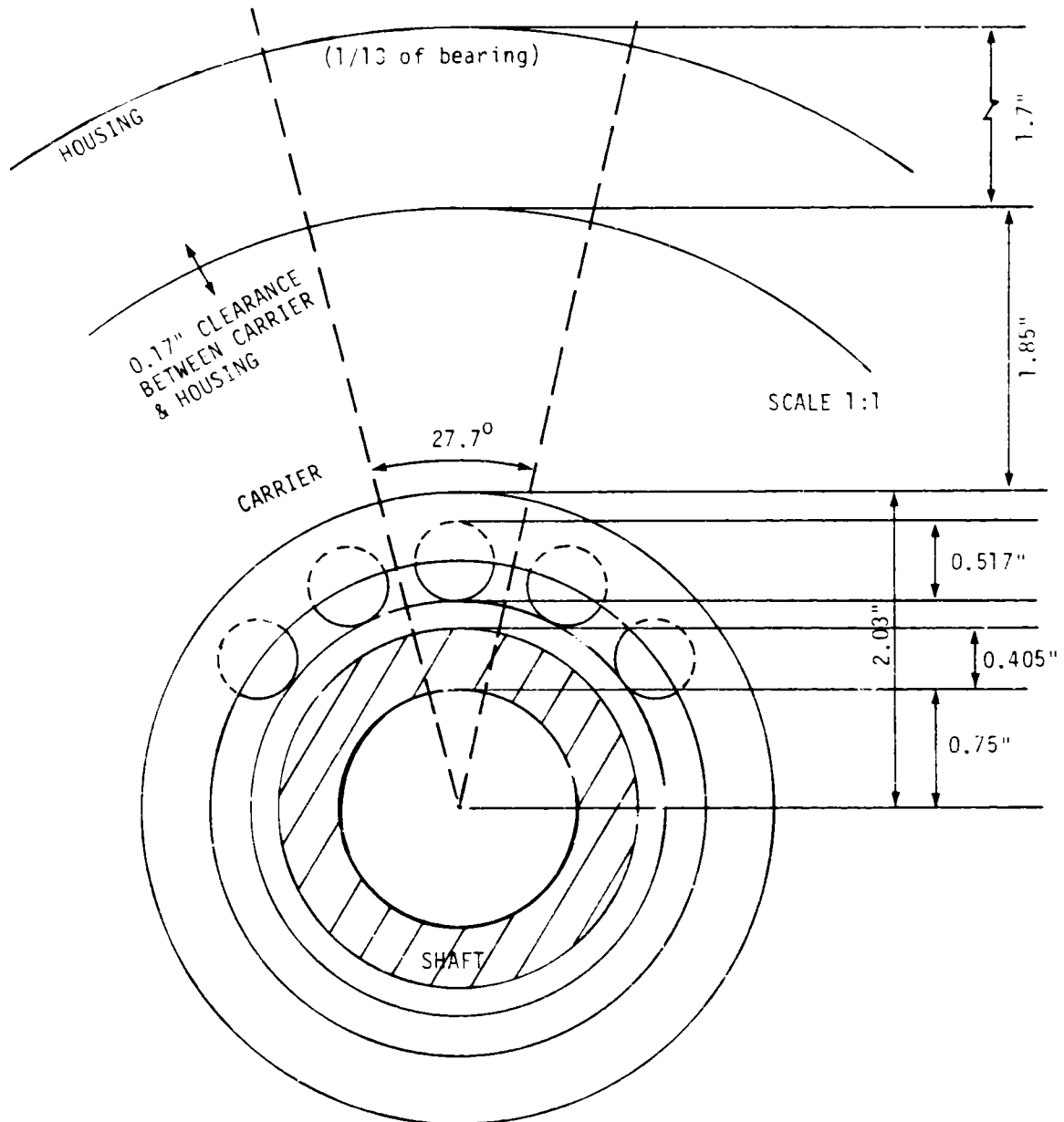
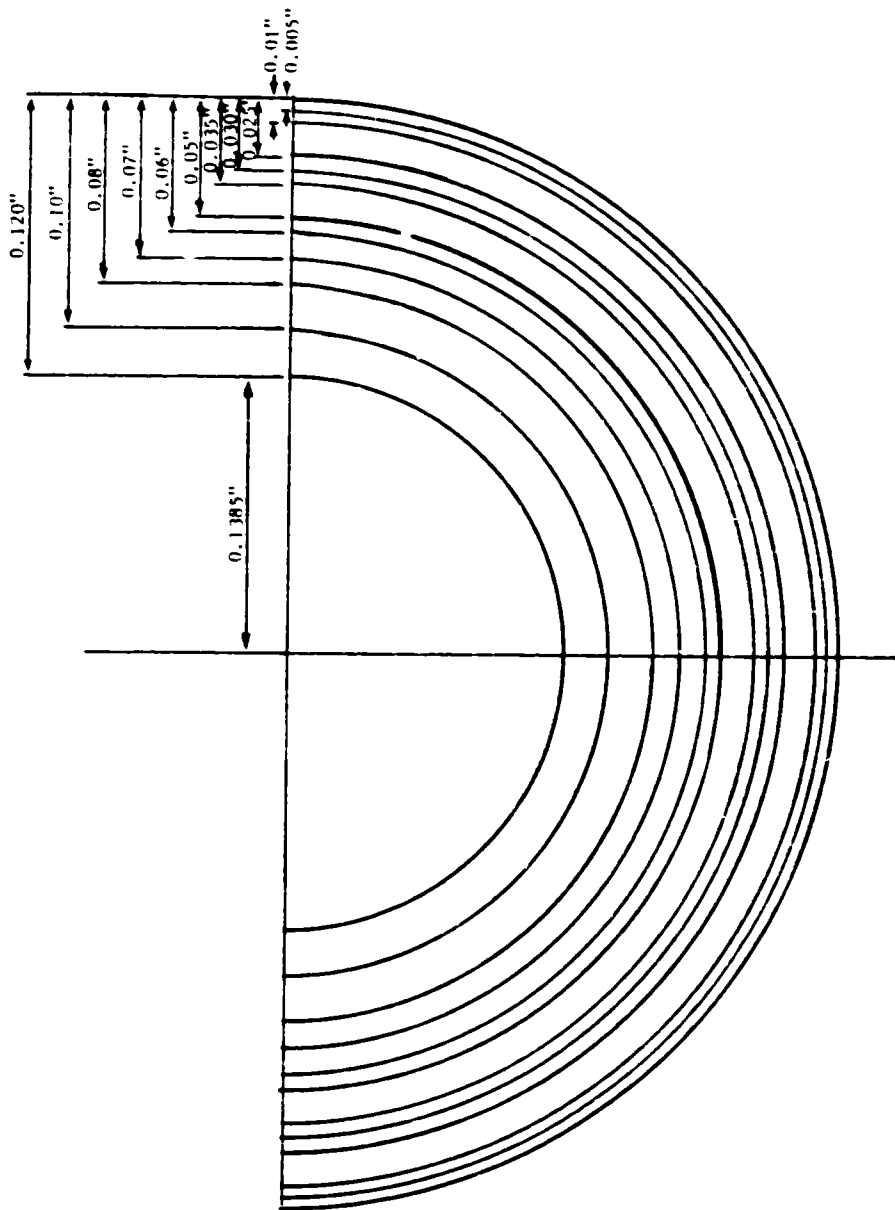


FIGURE 5.3.18 CENTER SECTION 1

DEPTH BELOW SURFACE



SRS

spectra research systems

At this time, a simplified, sample thermal problem is being exercised using the SINDA software to investigate all parameters and peculiarities of the package.

5.4 OCTOBER, 1982

5.4.1 EFFECTS OF BEARING PRELOAD ON CAGE SLIP AND FRICTIONAL HEAT GENERATION

An analysis has been made to evaluate the effects of axial load on bearing cage speed and heat generation rates due to rolling element slip with respect to the inner race. The effects of viscous drag, due to the rolling elements rotating in the LN₂ coolant, was accounted for in modeling the 57 mm LOX turbopump bearing for analysis using the SHABERTH Bearing Analysis Computer Program.

The objective was to determine the axial load that would allow the viscous drag force to overcome the contact friction forces to the extent that significant slippage could occur at the rolling element/face interfaces causing appreciable increases in inner race heat generation. Since the friction force is directly proportional to the coefficient of friction, which is not conclusively known, the friction coefficient was varied over a range from 0.08 to 0.22. The results of the investigation are shown in Figures 5.4.1 and 5.4.2. The data shown in Figure 5.4.1 for a friction coefficient of .08 indicate that, below a specific value of axial load, the heat generated at the inner race decreases to a minimum and then increases to a maximum. The same characteristic should occur for the other friction coefficients.

Inability of the computer program to converge to a solution at the lower levels prevented completing these curves in the low load region. It should also be observed for the friction coefficient of .08 that the heat generated by cage drag begins to decrease as the heat generated at the inner race begins to increase. Shown in Figure 5.4.2 is the cage/shaft speed ratio as a function of axial reaction, friction factor, and fluid drag. The upper horizontal line represents the case for no fluid drag. For these conditions, the cage to shaft speed ratio is about 43%. As shown, a decrease in friction force (friction coefficient) reduces the cage speed. Furthermore, a reduction in axial load reduces the cage speed dramatically at loads below about 300 lbs.

The results of this analysis provide a better understanding of why bearings 1 and 4 of the BMT were degraded even though they were lightly loaded in the axial direction. Based on these results, a design requirement should be to provide at least 400 lbs of preload in the bearings at all operating conditions.

5.4.2 RECOMMENDED COOLANT TEMPERATURE LIMITS FOR 57 mm BEARING OPERATING IN LN₂

Since the liquid density of LN₂ is approximately 43% less than LOX at the nominal operating temperatures and pressures for the BMT, the viscous work done on the LN₂ is estimated to be approximately 43% less than the work done on the LOX, provided the tester configuration was identical for the LN₂ and LOX tests. The overall energy balances (Figure 5.3.11) for the LN₂ and LOX tests show that the energy input to the coolant is about 11% higher for the LN₂ tests. This apparent contradiction may be due to any of the following:

- a) Changes made to the BMT following the LN₂ tests. Changes were made to the slinger and could account for part of the apparent high heat input during the LN₂ tests.

FIGURE 5.4.1
HEAT GENERATION VS AXIAL REACTION

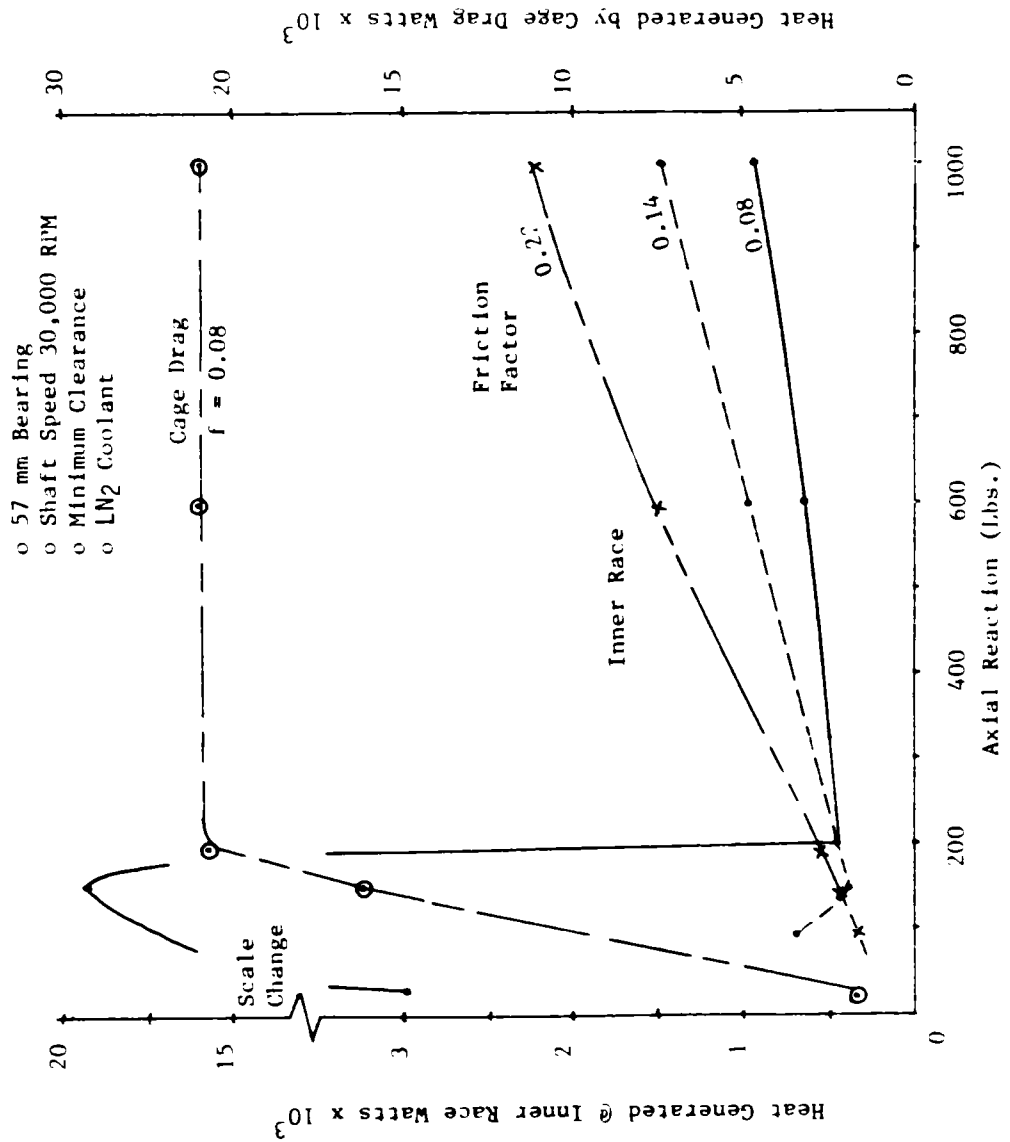
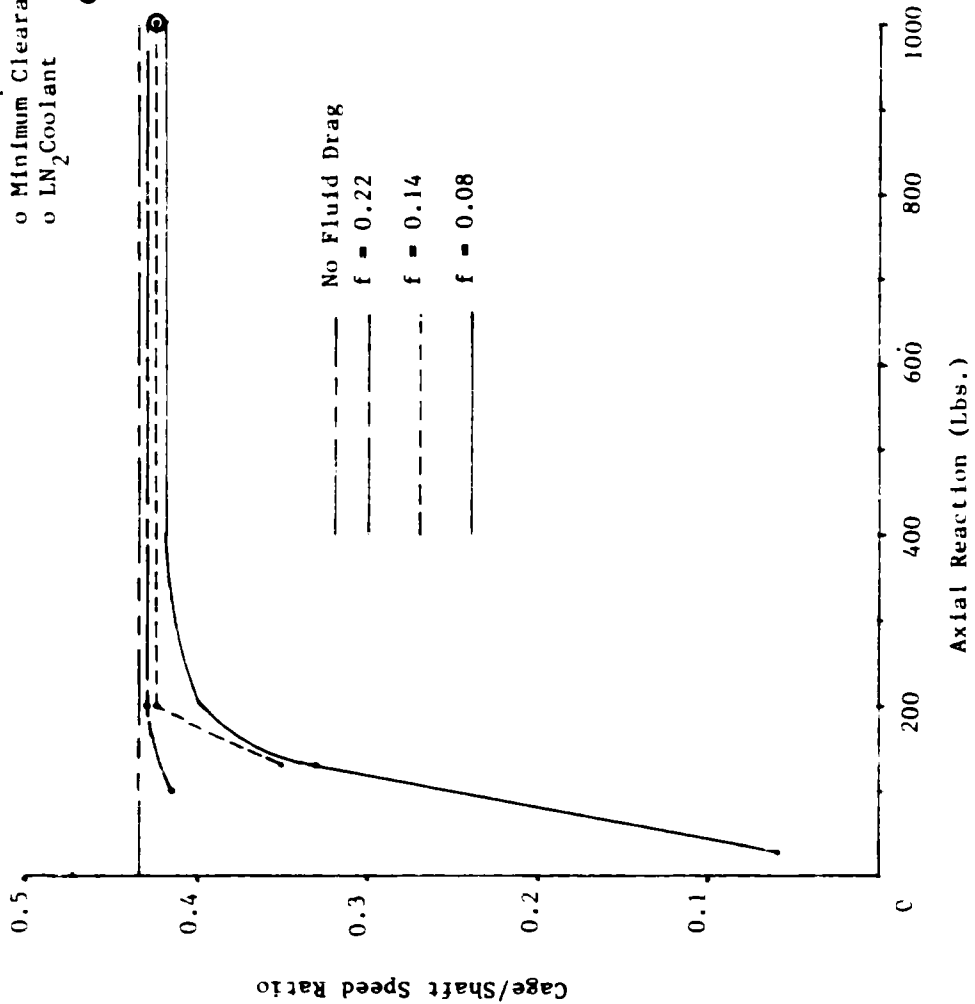


FIGURE 5.4.2
CAGE TO SHAFT SPEED RATIO

- o 57 mm Bearing
- o Shaft Speed = 30,000 RPM
- o Minimum Clearance
- o LN₂ Coolant

o FROM BALL
PASS DATA



ORIGINAL PAGE IS
OF POOR QUALITY

SRS

spectra research systems

- b) The LOX may provide a better lubrication medium than the LN₂. Since LN₂ is inert, any oxide films would not be reformed once worn away. Such films could improve the friction coefficient.
- c) Inaccurate measurement of coolant temperature and flow.

The conservative approach is to assume that the tester changes will reduce the viscous work by the density ratio (43%) and therefore the heat generated in the bearing should be limited such that a maximum value of contact stresses (~425 K psi) will not be exceeded. The value selected corresponds to a 100°C temperature difference across the bearing, as shown in Figure 5.4.3. This is a relative high value for sustained operation (For sustained running, the Hertz stress should be limited to ~350 K psi) but should be adequate for establishing cutoff limits.

Reducing the previously estimated viscous energy for LOX (Figure 5.3.11) to account for the lower LN₂ density, gives a value for LN₂ viscous work of 106.3 kW. The frictional heat generated by the bearings at 100°C ΔT is 15.2 kW. This gives a total heat input into the LN₂ of 121.5 kW. Based on the above values, the data provided in Figure 5.4.4 can be generated. At flow rates less than 10 lbs/sec, the limiting criteria is to maintain the coolant outlet temperature about 30° below the saturation temperature. Since the outlet temperature for the second LN₂ tests (see Figure 5.4.5) rose about 30°F, restricting average inlet flow to 160°R would give an outlet temperature of 190°R which is approximately 30° below the saturation temperature of LN₂ at 400 psia. This provides a safety factor of 2 with regard to the outlet flow conditions.

The above values provide limits based on an overall energy balance. It is also necessary to monitor and limit the energy generated by each bearing pair. To establish the limiting ΔT across the bearing, the bearing viscous work and friction heat were estimated assuming a 100°C radial temperature difference across the bearing (limits Hertz stress to ~450 K psi). The combined viscous and friction heat for one bearing pair was estimated to be 32 kW. Based on this value, the data provided in Figure 5.4.6 were generated. The curves in Figures 5.4.5 and 5.4.6 are cut horizontally (dashed lines) at specific values of ΔT available across the tester. The available ΔT is approximately 60°R ($T_{SAT} - T_{IN}$). Thirty degrees of this value was used as a safety factor. At a flow rate of 1010S/sec (total), about 12 degrees ΔT occurs across the bearing. This would allow about 18° for viscous work on the fluid excluding that done by the bearing. This is the minimum flow that will meet the imposed temperature restrictions. However, since a new tester configuration is being tested for the first time, flow rates less than those previously used, 12.6 lbs/sec, are not recommended. Based on a flow of 12.6 lbs/sec, an inlet temperature of 160°R, and a limiting ΔT of 18°R across the tester, the cutoff outlet temperature should be 178°R or -282°F, and the ΔT across the bearing should not exceed 9°R.

To gain a clearer understanding of the magnitudes of the viscous and bearing frictional heat generation and to minimize the risk to the BMT, it is recommended that a low speed (~10,000 RPM) test be performed with no applied load prior to runs at design speed. Data from this test could be used to verify heat generation estimates for updating temperature cutoff values. In view of the uncertainties in the analysis, the cutoff values provided should be considered preliminary for design speed and load tests. These analyses should be verified and/or updated based on additional data from the recommended low speed test. These cutoff values should be adequate for the low speed tests. In addition, it is recommended that the outer race temperatures be limited to 200°R. This is about 20°R below the saturation temperature at 400 psia.

SRS

FIGURE 5.4.3 CONTACT ANGLE AND STRESSES VS. BEARING TEMP DIFFERENCE

- 57mm Bearing
- Shaft Speed 30,000 RPM
- High Temp on Inner Race
- 2500 lb Axial Load
- Dry Friction

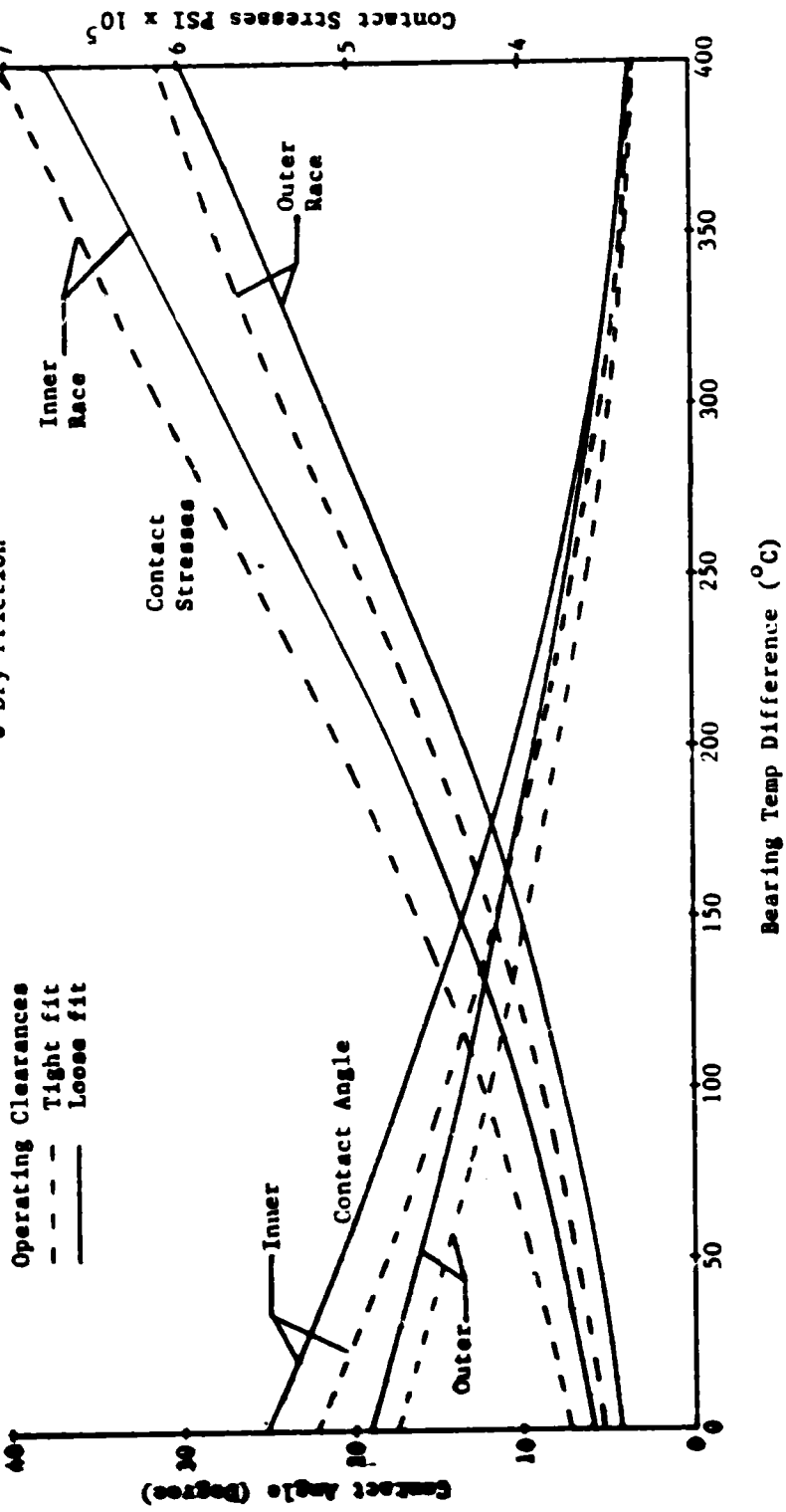


FIGURE 5.4.4 LIMITING TEMPERATURE ACROSS BEARING AND MATERIALS TESTER

- SPEED: 30,000 RPM
- 57mm BEARINGS
- LN2 COOLANT

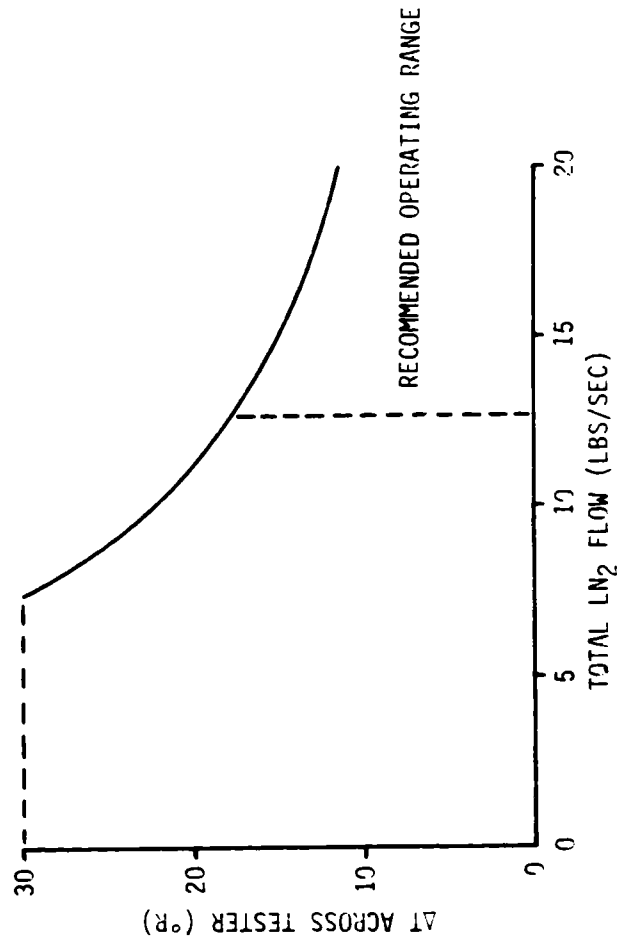
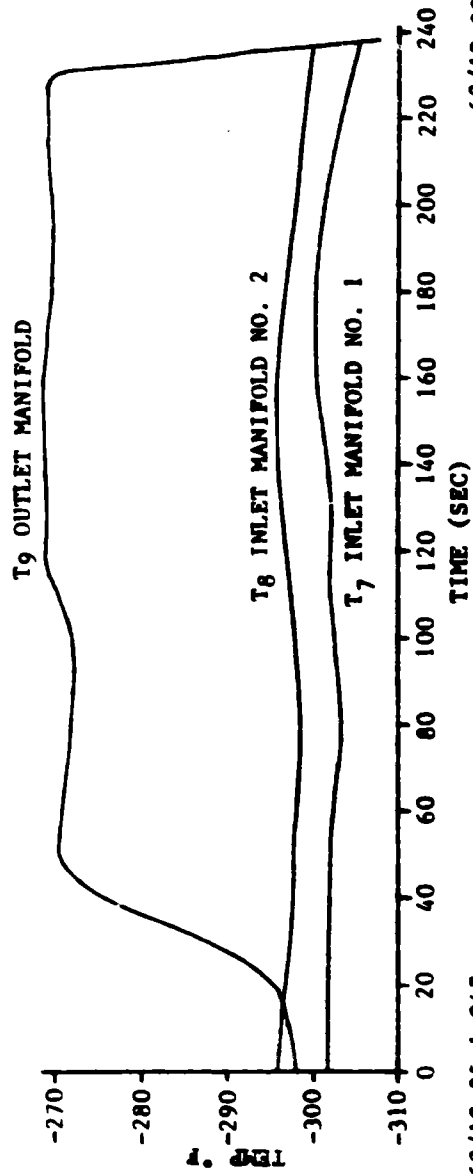


FIGURE 5.4.5
RUN NO. 2 INLET AND OUTLET TEMPERATURE vs. TIME



ORIGINAL PAGE IS
OF POOR QUALITY

62/18:39:0.094

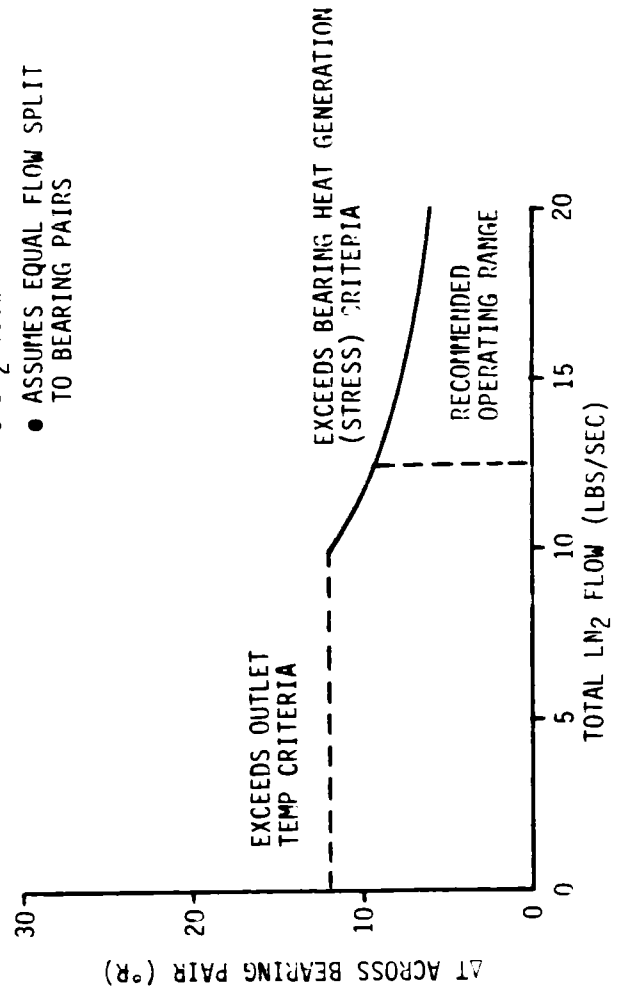
62/18:35:1.047

SRS

ORIGINAL PAGE IS
OF POOR QUALITY

FIGURE 5.4.6 LIMITING TEMPERATURE DIFFERENCE ACROSS SINGLE BEARING PAIR

- SPEED: 30,000 RPM
- 57mm BEARINGS
- LN₂ COOLANT
- ASSUMES EQUAL FLOW SPLIT TO BEARING PAIRS



5.4.3 BEARING THERMAL MODEL DEVELOPMENT

The thermal model for the LOX BMT bearing set has been successfully executed using SINDA. This preliminary model has been exercised using representative numbers for the imposed load, heat generation rate, etc.

Figure 5.4.7 illustrates the overall schematic of the bearing set with pertinent temperatures as obtained from SINDA. The representative thermal model was developed and executed for a 57 mm back-to-back mounted duplex bearing set with an imposed axial load of 6500 pounds and an unmounted contact angle of 20.5 degrees. This information was input into a SHABERTH run which produced heat generation data for the bearing set due to the turbulent mixing of the coolant and friction generated between the rolling elements and races. This input data was selected solely to check out the bearing thermal model, and does not represent conditions present during the LOX test incident.

The heat generation data thus obtained was then input in the SINDA model and steady-state temperature values for all nodes were calculated by the program as illustrated in Figure 5.4.8. The temperature gradient data across the bearing may now be input into SHABERTH in an iterative process to obtain more accurate heat generation data which will be used in the SINDA thermal program. This iterative process will be useful for analyzing the effects of temperature gradients across the bearings.

Figure 5.4.9 shows the outer race, rolling element, and inner race node breakdown for bearing 1 of the set. The temperatures shown are in degrees Fahrenheit and were obtained from the execution of SINDA utilizing the representative bearing setup described previously. Figures 5.4.10 and 5.4.11 illustrate the detailed nodes located in the inner and outer races, and the rolling element, respectively.

The next step in the model development will be to develop and integrate convective film coefficient data for the coolant at temperatures above the boiling point and to exercise the thermal model using LN_2 as the coolant.

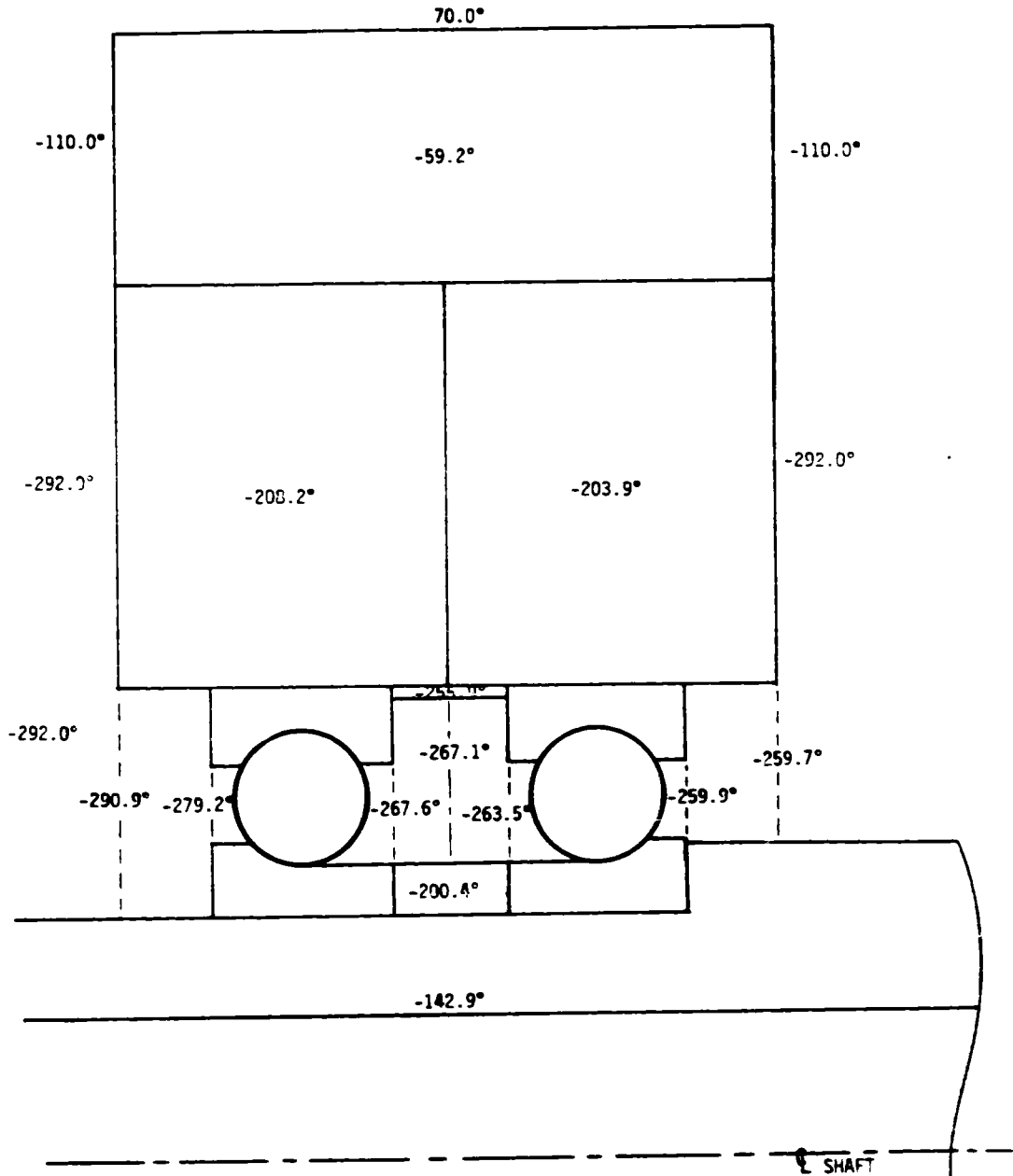
5.5 NOVEMBER, 1982

5.5.1 BEARING LIFE PREDICTION ANALYSIS

Efforts are continuing to investigate the potential for modifying current bearing life formulas for rolling bearings operating in a cryogenic environment. Although accepted techniques (4, 6, 12) have been developed to predict life for well lubricated bearings, these techniques lack experimental verification for high-speed rolling bearings operating in cryogenics. Typical cryogenics (LH_2 , LN_2 , LOX) have good heat removal characteristics; however, they lack the viscous properties necessary to provide a fluid film of sufficient strength to prevent metal-to-metal contact between the rolling elements and the race. The degree these films support the interface loads has not been experimentally determined.

Another uncertainty is the role cryogen film lubrication plays when solid lubricants are used to provide a lubricating surface film. The interaction between the solid film and fluid film are not known. This can be further complicated when the contact surface temperature exceeds the saturation temperature of the coolant to the extent that the surfaces become vapor blanketed and the surface film is that of a gas. Some experiments (15) indicate that LOX is potentially a better lubricant than non-reactive cryogens such as LH_2 and LN_2 . This results from the formation of surface films (oxides) that provide a measure of protection for the metal surfaces in contact.

FIGURE 5.4.7 BMT BEARING SET



SRS

SYSTEMS IMPROVED NUMERICAL DIFFERENCING ANALYZER - - - SINDA - - - UNIVAC-1108 FORTRAN-V VERSION PAGE 25

BEARING TESTER THERMAL MODEL(157M110)

| Y | 411 | -1.10000+02 | Y | 419 | -1.10000+02 | Y | 410 | 7.00000+01 | YEMPECC | 01 | 0.00000 | RELKCC | 681 | 9.96952-07 |
|-------|---------|-------------|---|-----|-------------|---|-----|-------------|---------|-----|-------------|--------|-----|-------------|
| ***** | | | | | | | | | | | | | | |
| TIME | 0.00000 | | | | | | | | | | | | | |
| Y | 10 | -2.87009+02 | Y | 18 | -2.57325+02 | Y | 11 | -2.53899+02 | Y | 17 | -2.64921+02 | Y | 12 | -2.35571+02 |
| Y | 13 | -1.96839+02 | Y | 15 | -2.04871+02 | Y | 20 | -2.76896+01 | Y | 21 | -2.61713+00 | Y | 22 | -2.61713+00 |
| Y | 24 | -6.36841+01 | Y | 25 | -8.49122+01 | Y | 26 | -1.03899+02 | Y | 27 | -1.70306+02 | Y | 28 | -1.26085+02 |
| Y | 30 | -1.48506+02 | Y | 33 | -1.74523+02 | Y | 34 | -1.81618+02 | Y | 40 | -1.86667+02 | Y | 35 | -1.70017+02 |
| Y | 36 | -1.88489+02 | Y | 42 | -1.49752+02 | Y | 37 | -2.11601+02 | Y | 43 | -2.21568+02 | Y | 38 | -2.05541+02 |
| Y | 39 | -2.31795+02 | Y | 45 | -2.40600+02 | Y | 200 | -2.48753+02 | Y | 208 | -2.45203+02 | Y | 201 | -2.54265+02 |
| Y | 202 | -2.42127+02 | Y | 204 | -2.45257+02 | Y | 203 | -2.10384+02 | Y | 205 | -2.12477+02 | Y | 210 | -2.08875+01 |
| Y | 212 | -1.36685+01 | Y | 213 | -1.67871+01 | Y | 214 | -4.34357+01 | Y | 215 | -6.74329+01 | Y | 216 | -8.96666+01 |
| Y | 218 | -1.15387+02 | Y | 219 | -1.29335+02 | Y | 220 | -1.41172+02 | Y | 223 | -1.69508+02 | Y | 224 | -1.85478+02 |
| Y | 225 | -1.67834+02 | Y | 231 | -1.68978+02 | Y | 226 | -1.82222+02 | Y | 232 | -1.83303+02 | Y | 227 | -2.11701+02 |
| Y | 228 | -2.05731+02 | Y | 239 | -2.11680+02 | Y | 229 | -2.13269+02 | Y | 235 | -2.45775+02 | Y | 50 | -1.52271+02 |
| Y | 52 | -2.08853+02 | Y | 53 | -2.28740+02 | Y | 54 | -1.11131+02 | Y | 55 | -4.66875+01 | Y | 56 | -6.00077+01 |
| Y | 58 | -5.63497+01 | Y | 59 | -7.14435+01 | Y | 60 | -7.32058+01 | Y | 61 | -5.47226+01 | Y | 62 | -1.86470+01 |
| Y | 64 | 5.26762+01 | Y | 65 | 8.32157+01 | Y | 66 | 1.21260+02 | Y | 67 | 1.40465+02 | Y | 68 | 2.44079+02 |
| Y | 70 | 3.49861+02 | Y | 71 | 4.40847+02 | Y | 72 | 5.04274+02 | Y | 73 | -1.78876+02 | Y | 74 | -1.86975+02 |
| Y | 76 | -2.49889+02 | Y | 77 | -7.56807+02 | Y | 78 | -2.82219+02 | Y | 79 | -2.08189+02 | Y | 80 | -1.72835+02 |
| Y | 251 | -1.74001+02 | Y | 252 | -1.49299+02 | Y | 253 | -2.11372+02 | Y | 254 | -4.13436+01 | Y | 255 | -6.54651+01 |
| Y | 257 | -8.73408+01 | Y | 258 | -4.35743+01 | Y | 259 | -3.48189+01 | Y | 260 | -5.46904+01 | Y | 261 | -4.63989+01 |
| Y | 263 | 2.97186+01 | Y | 264 | 6.87668+01 | Y | 265 | 9.48926+01 | Y | 266 | 1.37999+02 | Y | 267 | 1.96643+02 |
| Y | 269 | 2.49463+02 | Y | 270 | 4.71527+02 | Y | 271 | 6.72043+02 | Y | 272 | 4.28899+02 | Y | 273 | 1.54421+02 |
| Y | 100 | -2.10427+02 | Y | 101 | -2.43365+02 | Y | 102 | -2.32827+02 | Y | 103 | -2.30105+02 | Y | 104 | -2.74488+02 |
| Y | 106 | -1.63595+02 | Y | 107 | -1.99125+02 | Y | 108 | -1.23109+02 | Y | 109 | -9.78573+01 | Y | 110 | -1.04627+02 |
| Y | 112 | -2.56019+02 | Y | 113 | -2.31859+02 | Y | 114 | -2.23194+02 | Y | 115 | -7.35725+02 | Y | 116 | -2.55822+02 |
| Y | 118 | -2.57528+02 | Y | 119 | 2.50172+02 | Y | 120 | 2.01178+02 | Y | 121 | 1.57637+02 | Y | 122 | 8.456105+01 |
| Y | 124 | 2.25913+01 | Y | 125 | 1.66189+01 | Y | 126 | -4.17740+01 | Y | 127 | -6.14930+01 | Y | 128 | -8.49994+01 |
| Y | 130 | -1.22645+02 | Y | 131 | -2.14400+02 | Y | 132 | -2.14400+02 | Y | 133 | -2.27854+02 | Y | 134 | -2.16342+02 |
| Y | 305 | -1.82269+02 | Y | 306 | -1.35445+02 | Y | 307 | -1.39719+02 | Y | 308 | -1.11967+02 | Y | 309 | -8.69265+01 |
| Y | 311 | -2.49931+02 | Y | 312 | -2.30777+02 | Y | 313 | -2.17178+02 | Y | 314 | -2.11595+02 | Y | 315 | -2.23714+02 |
| Y | 317 | -2.40935+02 | Y | 318 | -2.56729+02 | Y | 319 | 2.56060+02 | Y | 320 | 2.18354+02 | Y | 321 | 1.51084+02 |
| Y | 323 | 7.64456+01 | Y | 324 | 3.51534+01 | Y | 325 | -4.08011+00 | Y | 326 | -3.03450+01 | Y | 327 | -5.06393+01 |
| Y | 329 | -1.66344+01 | Y | 330 | -1.19373+02 | Y | 400 | -1.42806+02 | Y | 401 | -2.40037+02 | Y | 402 | -2.55949+02 |
| Y | 402 | -2.03904+02 | Y | 403 | -1.91744+01 | Y | 1 | -2.69395+02 | Y | 2 | -2.79236+02 | Y | 3 | -2.67634+02 |
| Y | 5 | -2.63465+02 | Y | 6 | -2.45966+02 | Y | 7 | -2.59858+02 | Y | 8 | -2.79236+02 | Y | 9 | -2.67634+02 |
| Y | 411 | -1.10000+02 | Y | 419 | -1.10000+02 | Y | 410 | 7.00000+01 | Y | 500 | -2.42000+02 | Y | 412 | -2.92000+02 |

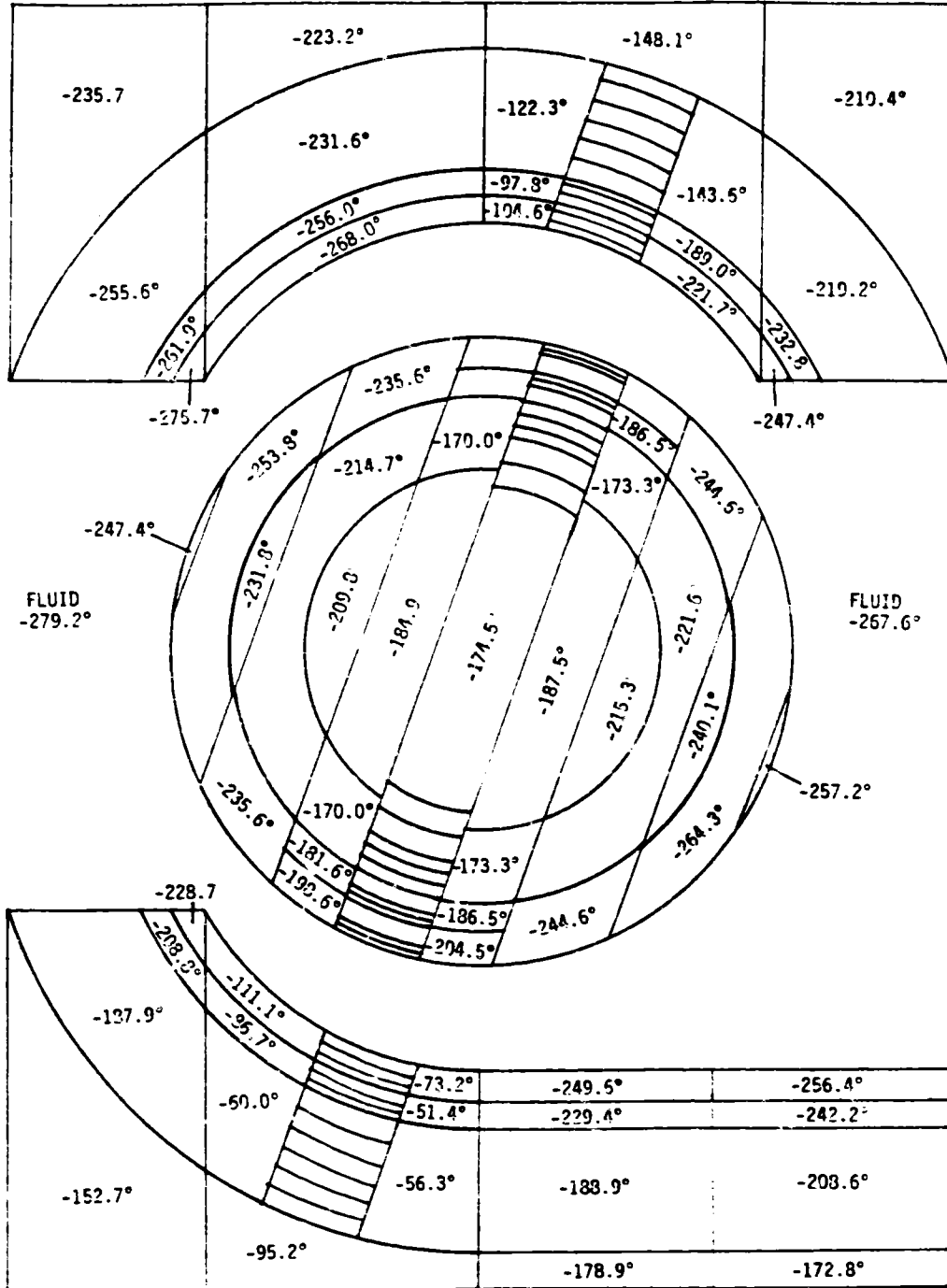
LOOPCT = 105 ENGRAL = .1663+05

END OF DATA

FIGURE 5.4.8 "SINDA" OUTPUT

ORIGINAL PAGE IS
OF POOR QUALITY

FIGURE 5.4.9
BEARING 1; OUTER RACE, ROLLING ELEMENT, AND INNER RACE TEMPERATURE
FOR 6500# AXIAL LOAD

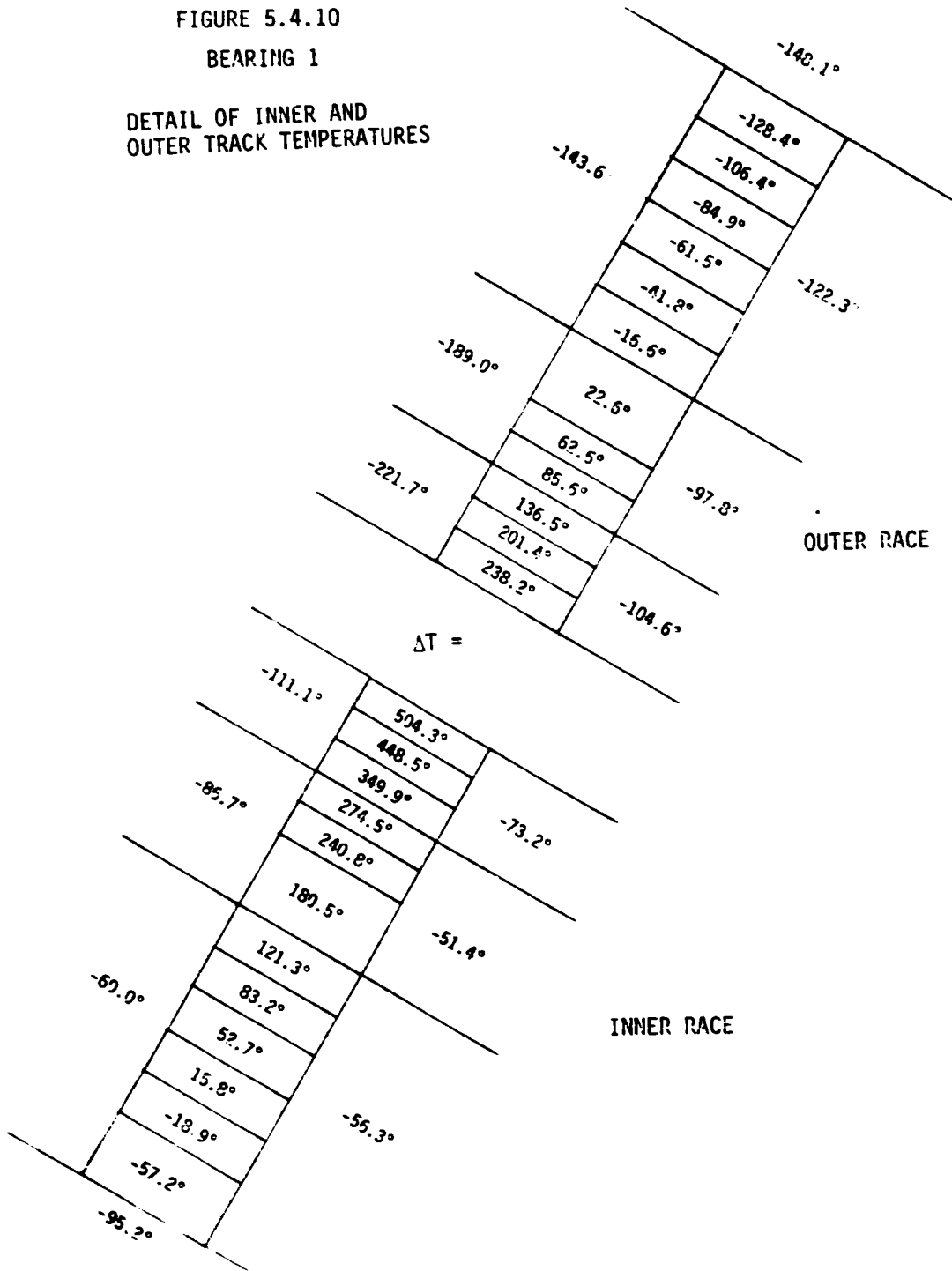


SRS

FIGURE 5.4.10

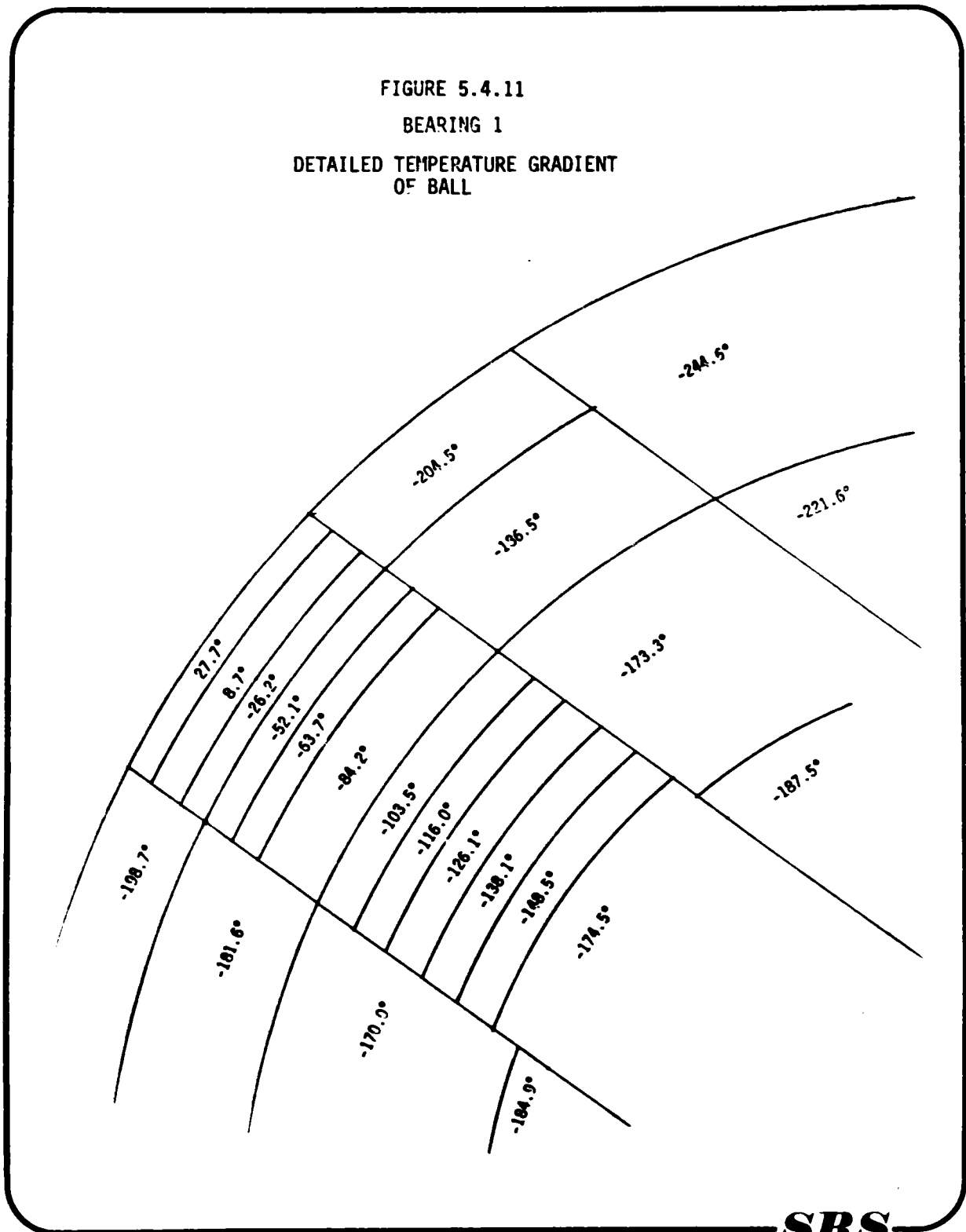
BEARING 1

DETAIL OF INNER AND
OUTER TRACK TEMPERATURES



ORIGINAL PAGE IS
OF POOR QUALITY

FIGURE 5.4.11
BEARING 1
DETAILED TEMPERATURE GRADIENT
OF BALL



SRS

spectra research systems

Here again, the rate of oxide formation can be a function of surface temperature and the degree of protection can be a function of the sliding velocity or rate of film removal. Considerably more work is needed to establish the film lubrication properties of various bearing materials and solid lubricants operating in cryogenics.

The classical failure mode of a rolling contact between hard steel surfaces is contact fatigue. The life formula as developed by Lundberg (4) is based on the assumption that the failure is initiated by a decisive stress amplitude located at some distance below the surface. The relationship between loads, stresses, and stress location is developed from the bearing dynamics and Hertz theory of contact stresses. Bearing life dispersion has been obtained by applying the Weibull distribution function to bearing life data. Experience has shown that this technique adequately predicts bearing life for well lubricated bearings. Since better lubricants and materials have become available, the original life formula has been modified by factors to account for the improved life derived from these improvements (6,12). These factors, however, do not account for the conditions encountered in cryogenic operation. As an example, the development of stresses from the Hertz theory does not account for tangential forces. Since the contact friction forces with cryogenic fluids is expected to be significantly larger than the forces encountered in oil lubricated bearings, the maximum shear force will probably be at, or near, the surface rather than below the surface. Furthermore, the solid film lubricant will enhance the asperity friction. Consequently the apparent contact friction force should fall somewhere between dry asperity friction and hydrodynamic film friction. This presents a problem in determining the life adjustment factor for lubrication that will account for the degradation of lubrication capability of the cryogenic.

Current plans are to use the SHABERTH I bearing analysis computer program as an aid in predicting bearing life. This program uses the life formula developed in reference 4 with life adjustment factors to account for improved materials and lubrication film thickness. The life adjustment factors will be adjusted to represent cryogenic operations as data becomes available from the bearing tester program.

SHABERTH I uses the following technique for estimating bearing life:

$$\text{Eq 1} \quad L_{10m} = \left(\frac{Q_{cm}}{Q_{em}} \right)^3$$

L_{10m} is the raceway fatigue life in millions of revolutions, as determined by Lundberg and Palmgren (4), and Q_{cm} is the dynamic capacity which is the load for which the bearing raceway will have 90% assurance of surviving one million revolutions. Q_{em} is the raceway equivalent load. Q_{cm} and Q_{em} are calculated by the SHABERTH computer program.

Since experience has shown, for ball bearings, that the races usually fail before the balls due to the changing axis of rotation as the balls orbit the shaft, the bearing fatigue life is based on the life of the races. The L_{10} life for a raceway is given by:

$$L_{10n} = a_2 a_3 a_3^* L_{10m} \quad \text{where}$$

a_2 is a life improvement factor to account for improved materials,

spectra research systems

a_3 is a life improvement factor to account for full film lubrication, and

a_3^* is a factor less than one when full film lubrication is not obtained.

a_3^* is a reduction factor accounting for the effect of surface asperity interaction and was deduced from a best fit to a large body of rolling contact life test data (12). This function was extracted from the SHABERTH I program and is shown in Figure 5.5.1. Also shown is the lubricant life factor used by SHABERTH II, which will be discussed later. As shown, the SHABERTH I lubrication factor is always ≤ 1 and is therefore never a life improvement factor. If the film thickness to surface roughness ratio (h/σ) is greater than about 3.5, a life improvement factor >1 can be input (a_2).

A limiting value of about 0.52 is shown for h/σ approaching zero, or zero film thickness. Since this condition is believed to be approached in LN_2 , LOX, and LH_2 , this is the value that would be applied with these fluids. The determination of this life factor did not, however, consider the benefits of the solid lubricant film transfer system used to lubricate the tester bearings. The effectiveness of this lubrication on bearing life can be evaluated from the bearing and materials tester data. SHABERTH II has, in effect, combined the life reduction and improvement due to lubrication into one function. This function is developed in reference 6. The important point is that for h/σ approaching zero, the life reduction factor is 0.21, which is less than 1/2 the factor used in SHABERTH I. This, again, illustrates the need for experimental data for cryogenic operation in these low film regions.

As stated earlier, the L_{10m} is the raceway fatigue life for 90% survivability. Since the bearing has two races the L_{10} life for the bearing is

$$\text{Eq 2} \quad L_{10b} = \left[L_{101}^{-e} + L_{102}^{-e} \right]^{-1/e}$$

where 1, 2 denote inner and outer races.

Since one bearing set consists of two bearings, the L_{10} life of the bearing set is:

$$\text{Eq 3} \quad L_{10bs} = \left[L_{10b1}^{-e} + L_{10b2}^{-e} \right]^{-1/e}$$

And the life of the total bearing system is

$$\text{Eq 4} \quad L_{10bst} = \left[L_{10bs1}^{-e} + L_{10bs2}^{-e} \right]^{-1/e}$$

Equation 4 is the 90% survivability life for all the bearings on the tester shaft. Since a 10% failure rate is not acceptable for Shuttle components, Equation 4 must be modified to predict probabilities of success greater than 99%. Techniques to correlate failure rates in these low regimes are addressed in references 5 and 1. These techniques suffer from the same deficiencies as discussed earlier when applied to bearings operating in low viscosity fluids such as LN_2 , LOX and LH_2 . However, they do provide a technique for evaluating the data derived from the Bearing and Materials Tester.

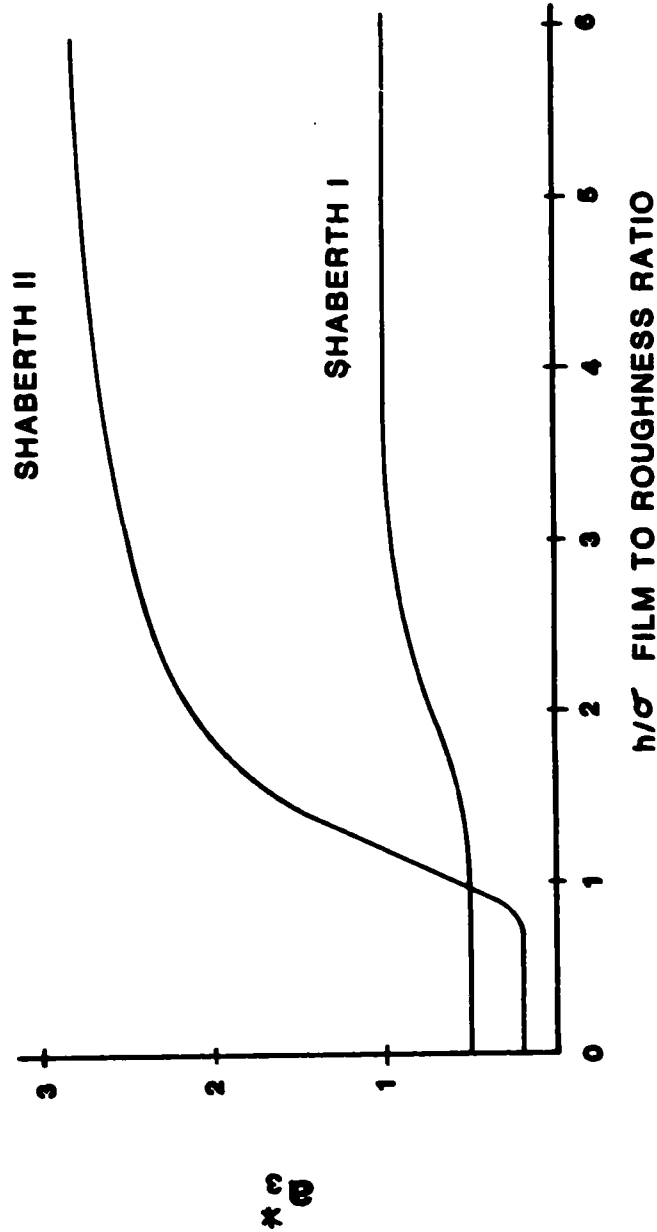


FIGURE 5.5.1 LUBRICATION LIFE ADJUSTMENT FACTORS

SRS

spectra research systems

The previous discussion has addressed fatigue type failures which is the dominant failure mode for well designed and lubricated bearings. Obviously, there are other type failures such as excessive wear, overheat cracking, overload cracking, destruction by material softening due to unstable overheating, etc. These type failures must be overcome before life data relating to bearing fatigue can be obtained.

The effort to date has provided a bibliography of reference material pertaining to bearing fatigue life (Reference 3 through 15). Life data relating to bearings operating in cryogenics is scarce and relating existing semi-empirical life formulas to these conditions require additional test data. The Weibull distribution does not represent the data in the region of 90% reliabilities. Techniques have been found that represent current data in these regimes and should, with modification, represent the data obtained from the cryogenic tests. The methods for adjusting the bearing life for lubrication film thickness and surface roughness used in both SHABERTH I and SHABERTH II have been extracted from the programs and explained.

5.5.2 STIFFNESS CHARACTERISTICS OF THE TURBINE END LOX PUMP BEARING

As requested, analyses were conducted to estimate the radial stiffness of the LOX pump turbine end bearing as a function of axial preload and shaft speed. The bearing radial stiffness is defined as the ratio of radial load to radial deflection ($dF/d\delta$).

Approximately 21 computer runs were made using the SHABERTH bearing analysis program. These runs were made to determine the relationship of load versus deflection as affected by axial load and shaft speed. The bearing stiffness was then determined as the slope ($dF/d\delta$) of the force versus deflection curves. The radial load was varied from 100 to 400 lbs. At higher loads these curves can become nonlinear, i.e., the deflection can decrease as the radial load increases. As shown in Figure 5.5.2, the relationship is linear for axial loads greater than 1136 lbs. For the axial load case of 607 lbs, the curve is linear to about 200 lbs radial load. Since the computer solution failed to converge at higher radial loads, it is not recommended to extrapolate the stiffness versus axial reaction curve shown in Figure 5.5.3 to axial loads below about 600 lbs and radial loads greater than 200 lbs when the axial reaction is less than approximately 1000 lbs. If it is of interest to further define the stiffness characteristics outside these limits (lower axial reactions, higher radial reactions), this can be done, within the convergence limits of the computer program, by additional analysis.

As expected, the radial stiffness of the bearing increased with increasing axial reaction or preload as shown in Figure 5.5.3. As previously discussed, the curve shown in Figure 5.5.3 represents the linear portion of the radial reaction versus deflection bearing characteristics shown in Figure 5.5.2. A similar analysis was done to determine the effects of shaft speed on bearing stiffness. Figure 5.5.4 provides the bearing radial deflection as affected by radial reaction and shaft speed. Shown in Figure 5.5.5 is the bearing radial stiffness as a function of shaft speed. As shown, the bearing becomes less stiff in the radial direction as the shaft speed increases. This is primarily due to the increase in centrifugal force effects on the outer ring.

5.5.3 HEAT TRANSFER COEFFICIENTS FOR BEARING THERMAL MODEL

In any attempt to predict failure using the bearing thermal model, the effects of surface boiling on the coolant performance must be considered. Preliminary SINDA runs showed, as expected, several 'hot spots' near the ball-race contact areas where frictional heat generation is high. Local boiling can occur here (even though the bulk of

FIGURE 5.5.2 RADIAL LOAD VERSUS RADIAL DEFLECTION

- SPEED 30,000 RPM
- 57 MM BEARING

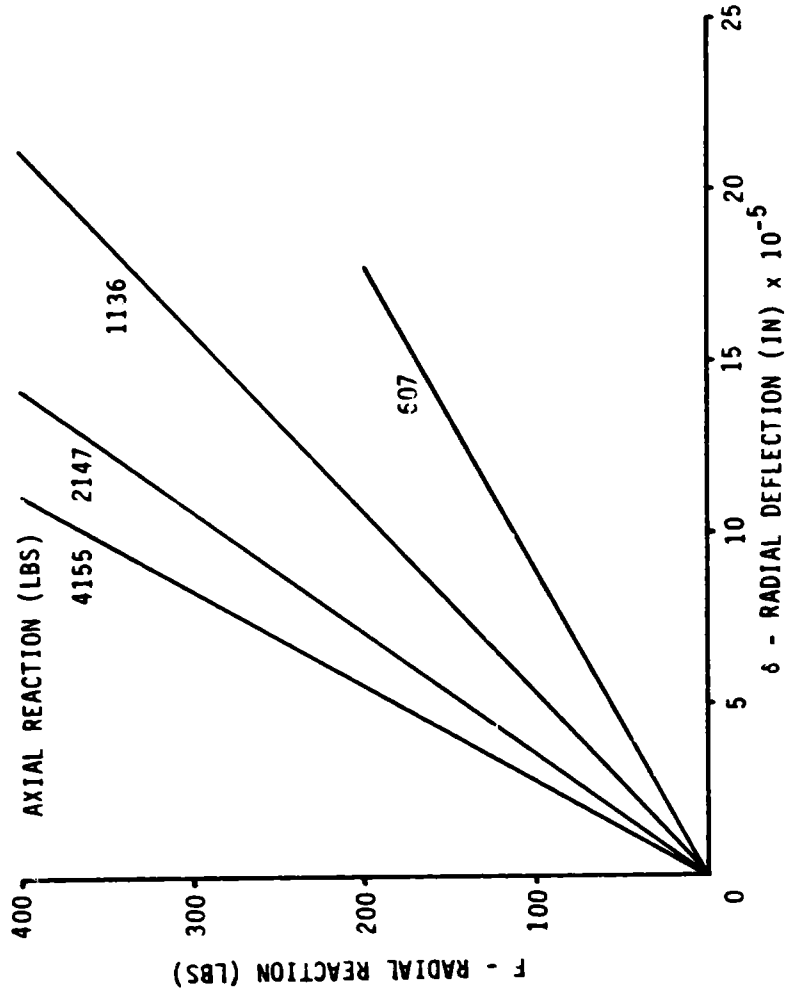


FIGURE 5.5.3 RADIAL STIFFNESS VERSUS AXIAL REACTION

- SPEED 30,000 RPM
- 57 MM BEARING
- RADIAL LOAD < 400 LBS FOR
AXIAL LOADS > 1000 LBS
- RADIAL LOAD < 200 LBS FOR
AXIAL LOADS ≥ 600 LBS AND
< 1000 LBS

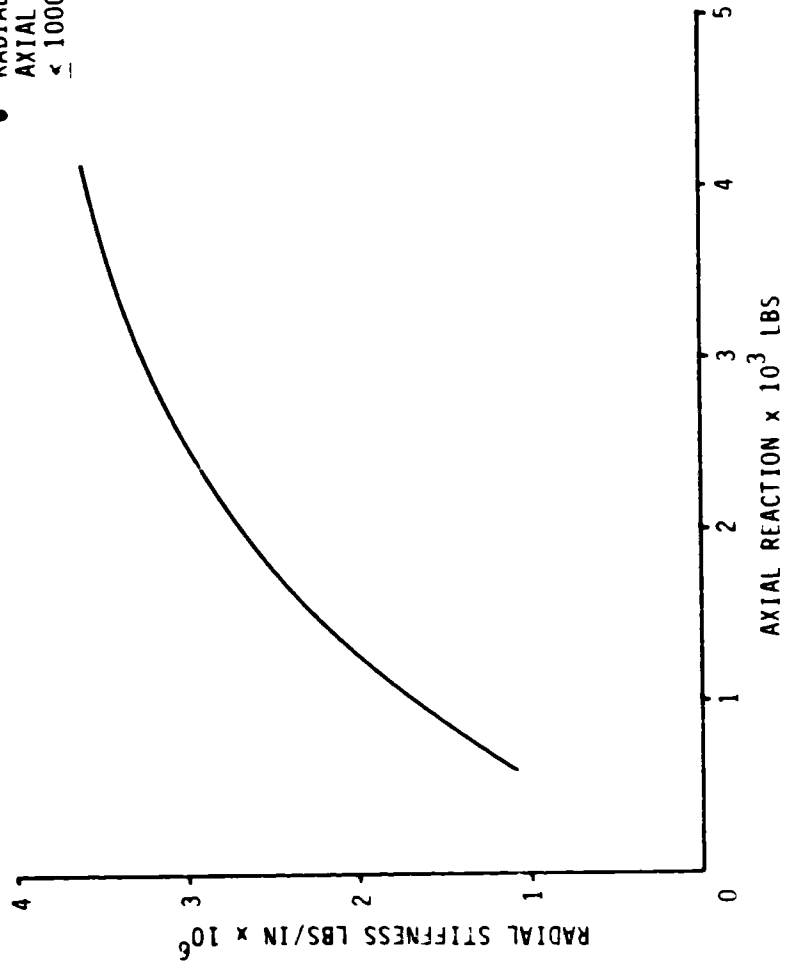
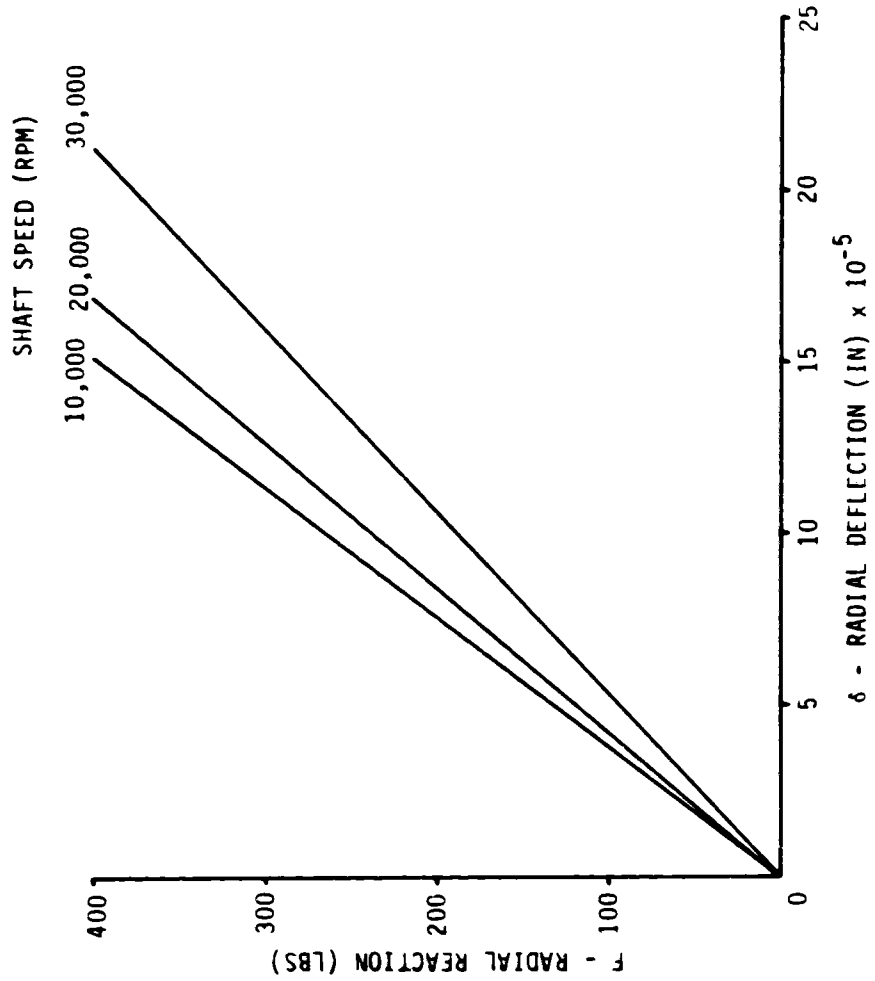


FIGURE 5.5.4 RADIAL LOAD VERSUS RADIAL DEFLECTION

- AXIAL REACTION 1000 LBS.
- 57 MM BEARING



ORIGINAL PAGE IS
OF POOR QUALITY

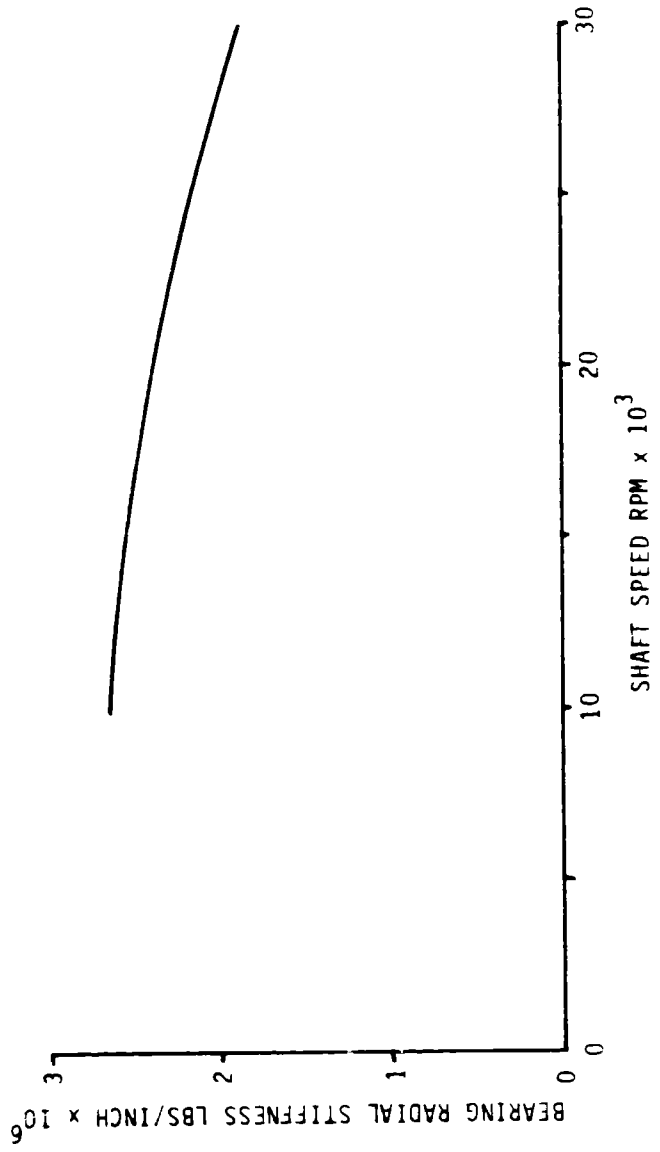
SRS

ORIGINAL QUALITY
OF POOR QUALITY

SRS

FIGURE 5.5.5 BEARING RADIAL STIFFNESS VERSUS SHAFT SPEED

- 57 MM BEARING
- AXIAL REACTION 1000 LBS



spectra research systems

the fluid is sub cooled) causing an abrupt reduction in the surface heat transfer coefficient and potential increases over the maximum heat flux temperature difference. Therefore, a boiling curve (heat transfer coefficient versus surface temperature) needs to be established.

So far no published correlation has been found to match the flow conditions in the bearing tester. Excellent reviews of most correlations can be found in references 22 and 27. Other material relevant to this subject can be found in References 16, 17, 18, 20, 21, 22, 23, 24, 25, 26, 27, 28, 29, 30, 31, 32, 33, 38, 39 and 40. The method chosen herein uses the more general relations so that it can be adjusted to fit the test data. The forced convection boiling process has been divided into three major categories:

- (1) Forced convection to single phase liquid,
- (2) Forced nucleate boiling, until some maximum heat flux is reached, corresponding to a particular surface temperature, and
- (3) Film boiling (vapor film at the wall).

The methods used to calculate the the transfer coefficient in each region is outlined below.

- (1) The Prandtl analogy (reference 17, page 260) using the Stanton number was rejected in favor of the Dittus-Boelter equation which gives more conservative values and is in more general use. A comparison of these two equations for the modeled flow conditions is shown in Figure 5.5.6. The form of the Dittus-Boelter equation is

$$Nu = \frac{hd}{k} = 0.023 Re^{0.8} Pr^{0.4}$$

- (2) In the nucleate boiling region, the superposition method of Kutateladze was used

$$\frac{h}{h_{conv}} = \sqrt{1 + \left(\frac{h_{npb}}{h_{conv}}\right)^2}$$

where h_{conv} (convective to single phase liquid) is given by the Dittus-Boelter equation. The h for nucleate pool boiling (npb) is calculated using the Rohsenow correlation;

$$\frac{C_{pl} \Delta T}{h_{fg} Pr_1^{1.7}} = C_{sf} \left[\frac{q}{h_{fg}} \sqrt{\frac{q_1}{g(\rho_l - \rho_v)}} \right]^{0.33}$$

The constant C_{sf} is empirical and depends on the "heating surface-fluid" combination. A value of 0.013 was used (water-stainless steel).

- (3) During film boiling at such high relative velocities, heat transfer to the film becomes close to that of a single phase vapor. Since no correlation has been found that does not require the fluid quality or heat flux, the Dittus-Boelter equation, evaluated for vapor flow, was used to set the lower limit after the peak heat flux was reached. Radiation through the film has not been considered.

ORIGINAL PLOTS
OF POOR QUALITY

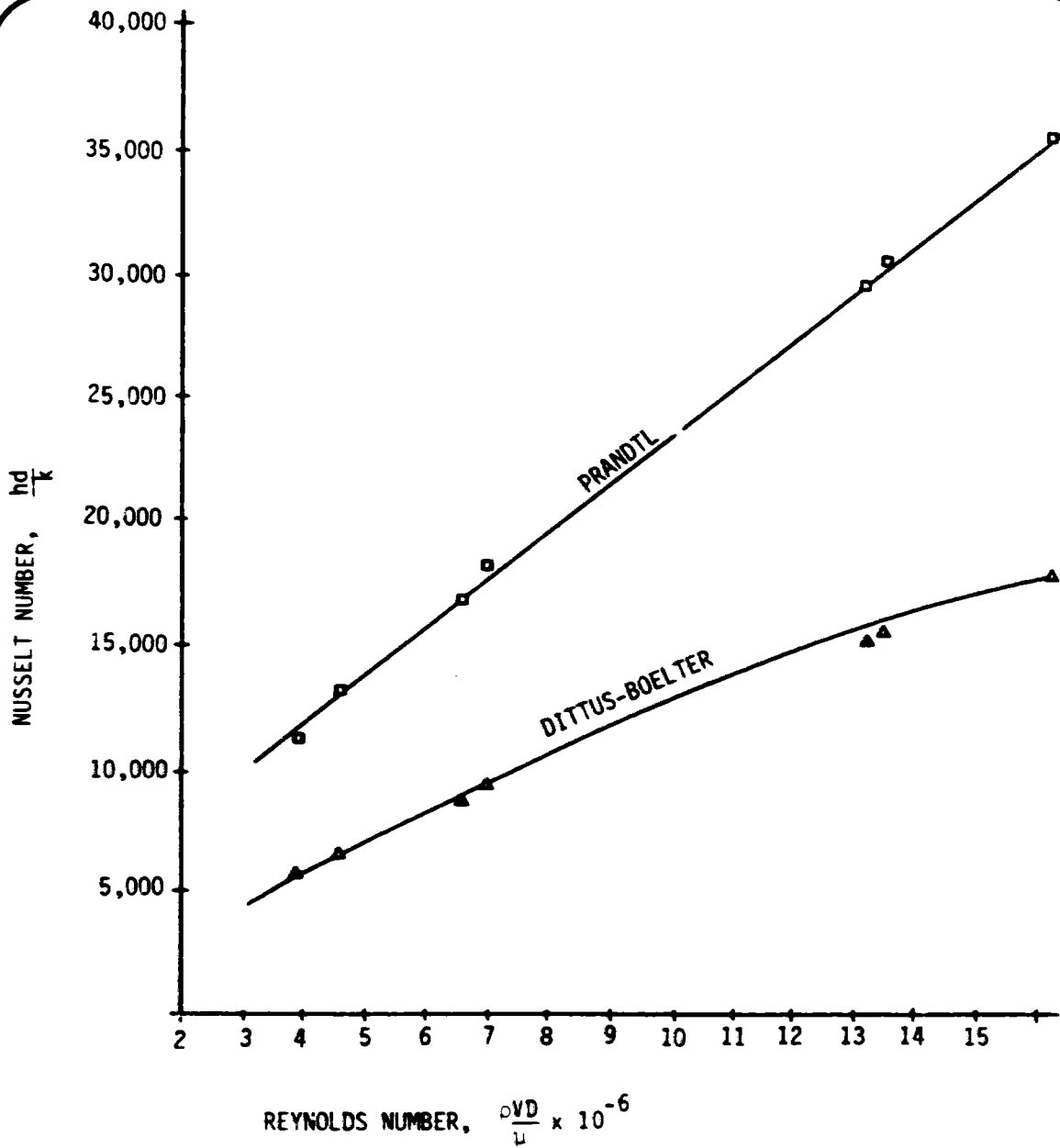


FIGURE 5.5.6
COMPARISON OF CORRELATIONS FOR SINGLE
PHASE FLOW IN THE BEARING MODEL

SRS

spectra research systems

Although a satisfactory method for determining at which surface temperature the maximum heat flux occurs has not been established, the following benchmarks are being used (reference 21, pages 261-277).

- (a) For inception nucleate boiling of cryogenics, $T_w - T_{sat}$ seldom exceeds 2°K.
- (b) The transition region between the peak heat flux and film boiling covers ~ 8°K in nitrogen and ~30°K in oxygen.
- (c) Wall to bulk fluid ΔT s to establish film boiling in cryogenics are low (< 50°K).

The following values were taken from the forced convection boiling curve developed for liquid nitrogen using the above method.

| <u>$\Delta T (T_w - T_{sat}), ^\circ K$</u> | <u>$h, \text{btu/hr.ft.}^2$</u> |
|--|--|
| 5 | 13,800. (nucleate boiling) |
| 10 | 25,000. (nucleate boiling) |
| 15 | 50,000. (q max) |
| -Transition Range- | |
| 24 | 1,500. (film boiling) |

In reality, the minimum heat flux for film boiling may not be established at these high velocities (see reference 21, pages 200-201) and burnout (rapid and large increase in the dry wall surface temperature) occurs after the peak heat flux is reached. This is highly undesirable. Burnout prediction will be made using these boiling curves in the SINDA thermal model.

The boiling curves for liquid nitrogen are presently being integrated into the conductor data of the SINDA thermal model and curves for liquid oxygen will also be constructed. A computer program to adjust these curves based on different flow rates and shaft speed is also planned. The literature search for better correlations will also continue.

5.5.4 STATUS AND PRELIMINARY RESULTS OF BEARING THERMAL MODEL

During this reporting period, the Bearing Thermal Model was refined, modified, and exercised utilizing the SINDA software program. Several different subroutines were examined to better understand the capability of the program including one which provides a detailed heat rate analysis into and from each node through a specific conductor. An example of this type of output is illustrated in Figure 5.5.7.

A data base has been established for both LOX and LN₂ coolant flow through the Bearing and Material Tester. This data base includes all node and conductor data along with temperature varying thermal property information and film coefficient data. At this time, the thermal model program is using film coefficient data obtained from the Dittus-Boelter equation and no film boiling conditions are being considered. The results from these preliminary runs will be used as a basis for comparison with the model using the complete heat transfer boiling curve to better understand and analyze its effect on resultant temperatures.

The LOX data base has been integrated to simulate tester conditions of a 2500 pound axial reaction with appropriate heat generation input. This iteration of the thermal model is representative of the conditions seen by bearings 2 and 3 during the

BEARING THERMAL MODEL157MILM2

GRATES INTO ACTUAL NODE 20 (RELATIVE NODE 9)
 IMPRESSED Q = 1.460E02
 C FROM ACTUAL NODE 13, THRU RELATIVE CONDUCTOR 1 = -3.326E00
 C FROM ACTUAL NODE 15, THRU RELATIVE CONDUCTOR 2 = -3.595E00
 C FROM ACTUAL NODE 21, THRU RELATIVE CONDUCTOR 43 = -4.658E01
 C FROM ACTUAL NODE 319, THRU RELATIVE CONDUCTOR 417 = 1.311E01
 C FROM ACTUAL NODE 7, THRU RELATIVE CONDUCTOR 418 = 2.269E01
 C FROM ACTUAL NODE 3, THRU RELATIVE CONDUCTOR 450 = -6.599E01
 C FROM ACTUAL NODE 2, THRU RELATIVE CONDUCTOR 460 = -6.431E01

GRATES INTO ACTUAL NODE 21 (RELATIVE NODE 10)
 IMPRESSED Q = 0.000
 C FROM ACTUAL NODE 13, THRU RELATIVE CONDUCTOR 3 = -3.187E00
 C FROM ACTUAL NODE 15, THRU RELATIVE CONDUCTOR 4 = -3.235E00
 C FROM ACTUAL NODE 20, THRU RELATIVE CONDUCTOR 43 = 4.638E01
 C FROM ACTUAL NODE 22, THRU RELATIVE CONDUCTOR 44 = -8.017E01

GRATES INTO ACTUAL NODE 22 (RELATIVE NODE 11)
 IMPRESSED Q = 0.000
 C FROM ACTUAL NODE 13, THRU RELATIVE CONDUCTOR 5 = -6.090E00
 C FROM ACTUAL NODE 15, THRU RELATIVE CONDUCTOR 6 = -6.228E00
 C FROM ACTUAL NODE 21, THRU RELATIVE CONDUCTOR 44 = 4.037E01
 C FROM ACTUAL NODE 23, THRU RELATIVE CONDUCTOR 45 = -2.744E01

GRATES INTO ACTUAL NODE 23 (RELATIVE NODE 12)
 IMPRESSED Q = 0.000
 C FROM ACTUAL NODE 34, THRU RELATIVE CONDUCTOR 7 = -1.606E00
 C FROM ACTUAL NODE 40, THRU RELATIVE CONDUCTOR 8 = -1.659E00
 C FROM ACTUAL NODE 22, THRU RELATIVE CONDUCTOR 45 = 2.784E01
 C FROM ACTUAL NODE 24, THRU RELATIVE CONDUCTOR 46 = -2.817E01

GRATES INTO ACTUAL NODE 24 (RELATIVE NODE 13)
 IMPRESSED Q = 0.000
 C FROM ACTUAL NODE 34, THRU RELATIVE CONDUCTOR 9 = -1.627E00
 C FROM ACTUAL NODE 40, THRU RELATIVE CONDUCTOR 10 = -1.679E00
 C FROM ACTUAL NODE 23, THRU RELATIVE CONDUCTOR 46 = 2.417E01
 C FROM ACTUAL NODE 25, THRU RELATIVE CONDUCTOR 47 = -2.086E01

GRATES INTO ACTUAL NODE 25 (RELATIVE NODE 14)
 IMPRESSED Q = 0.000
 C FROM ACTUAL NODE 34, THRU RELATIVE CONDUCTOR 11 = -3.072E00
 C FROM ACTUAL NODE 40, THRU RELATIVE CONDUCTOR 12 = -3.191E00
 C FROM ACTUAL NODE 24, THRU RELATIVE CONDUCTOR 47 = 2.076E01
 C FROM ACTUAL NODE 26, THRU RELATIVE CONDUCTOR 48 = -1.060E01

GRATES INTO ACTUAL NODE 26 (RELATIVE NODE 15)
 IMPRESSED Q = 0.000
 C FROM ACTUAL NODE 35, THRU RELATIVE CONDUCTOR 13 = -3.672E00
 C FROM ACTUAL NODE 41, THRU RELATIVE CONDUCTOR 14 = -3.736E00
 C FROM ACTUAL NODE 25, THRU RELATIVE CONDUCTOR 48 = 1.460E01
 C FROM ACTUAL NODE 27, THRU RELATIVE CONDUCTOR 49 = -1.119E01

ORIGINAL PAPER
 OF POOR QUALITY

FIGURE 5.5.7 EXAMPLE HEAT RATE ANALYSIS OUTPUT FROM "SINDA"

spectra research systems

tester incident with LOX coolant. The steady-state temperature results of this analysis are shown in Figure 5.5.8.

Comparison of the outer race temperatures of the LOX model, at nodes 300, 307, 314, and 315 (node locations and temperatures are shown in Figure 5.5.9), with experimental data is illustrated in Figure 5.5.10. Note that the temperatures obtained from the model bracket the curve obtained from the tester run. The temperature differential across the outer race shows the need for a thermocouple positioned across from the expected contact area. If the thermocouple was located in the center of the outer race during the test run, the hottest part of the race was not being measured. This being the case, the experimental curve could actually be closer to the temperature of node 307. To facilitate correlation of the thermal model with actual conditions, boundary temperatures of the carriers are needed. It is recommended that thermocouples be placed on the outer surface of each carrier as illustrated in Figure 5.5.11.

Although the experimental data for the outer race does seem to correspond to the LOX thermal model temperatures relatively well, further work is still being done on the model. The next step will be to add the heat transfer coefficient boiling curve data to the model and determine its effect on resulting temperatures.

5.6 DECEMBER, 1982

5.6.1 BEARING OPERATING PRELOADS

An analysis has been done to estimate the change in bearing preload, from the assembled room temperature value, as the bearing/shaft assembly is cooled from room temperature to LN₂ temperature and rotated to a speed of 30,000 RPM. At this point in the analysis, it is assumed that the shaft is not axially loaded; therefore, the bearing axial reactions are equal for all bearings and equal to the spring preload value at operating conditions.

Considering only the thermally induced axial loads and deflection, the following expressions can be written for the axial deflection of the shafts and components.

$$1) \quad dl_s = \alpha_s l_s \Delta T - \frac{F_T l_s}{A_s E_s}$$

$$2) \quad dl_c = F_T \sum_{i=1}^n \frac{l_{ci}}{A_{ci} E_{ci}} + \sum_{i=1}^n \alpha_{ci} l_{ci} \Delta T$$

- α - Thermal coefficient of expansion
- A - Cross sectional area under load
- E - Modulus of elasticity
- F_T - Thermally induced load
- l - Length
- s - Shaft
- c - Components on the shaft

Since $dl_s = dl_c$, these equations can be solved for the thermally induced force and the axial deflections due to the temperature changes. The axial deflection of interest

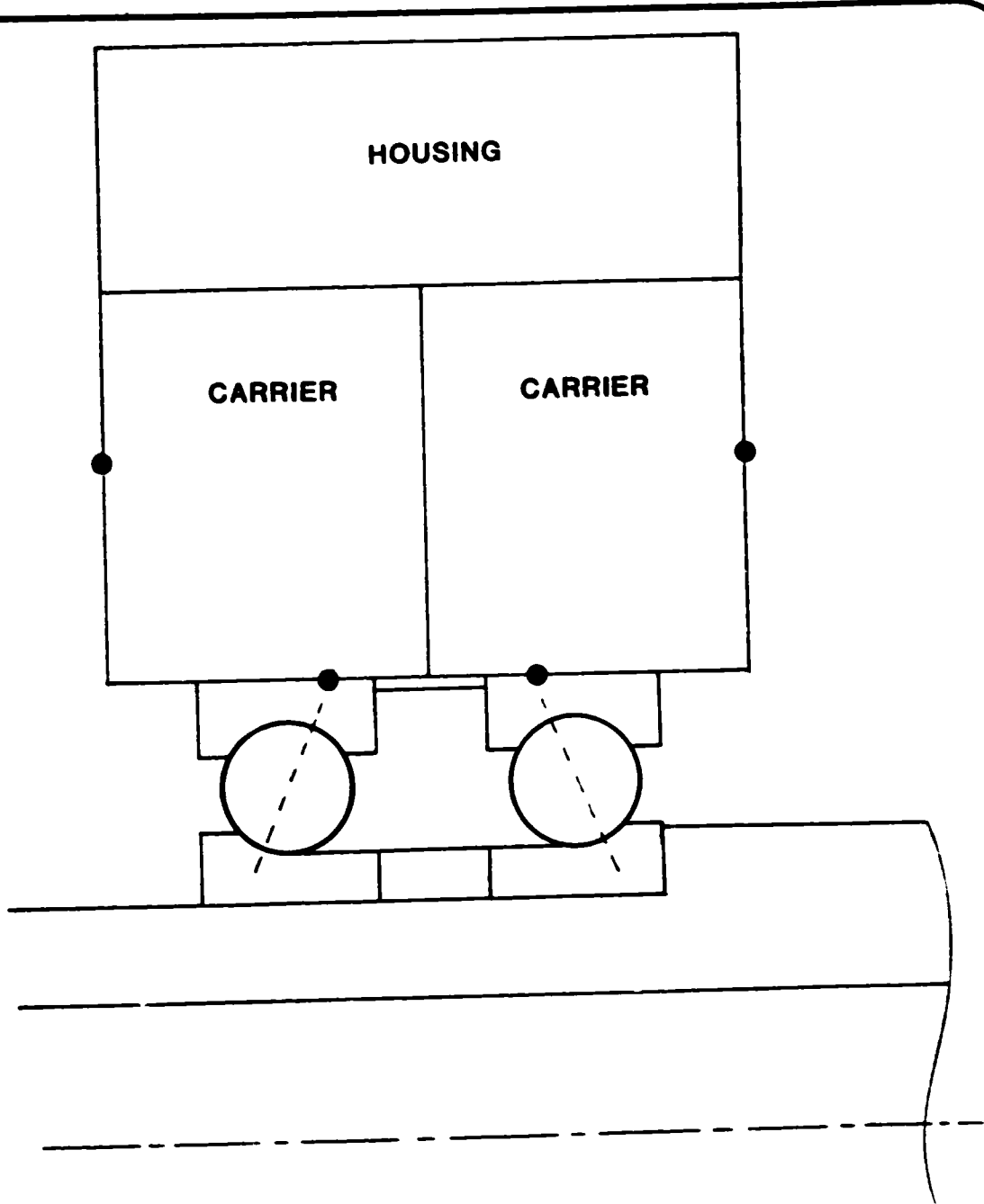


FIGURE 5.5.11 THERMOCOUPLE LOCATIONS

spectra research systems

is the net deflection between one-half the bearing separator, one-half the bearing race, the bearing spring, and the carrier tang. Using the data provided in Table 5.6.1, a net deflection of 0.1551 mils was estimated. This deflection is in the direction to compress the spring. Since the spring constant is between 55 and 65 lbs/mil (depending on direction of spring travel), this movement produces an insignificant change in preload.

An axial movement of the bearing can occur as a result of radial clearance changes caused by initial press fits, temperature changes, and shaft speeds. To assess these effects on bearing preload, bearing deflection curves at these different conditions were generated, as shown in Figure 5.6.1. Deflection curves are shown for three conditions; room temperature, cryogenic temperature, and cryogenic temperature and speed. As shown, fitting the bearing to the shaft causes an axial movement of the races which requires about a thousand pounds to return the races to their relative unmounted positions. Since the room temperature preload is approximately one thousand pounds, this is the initial condition from which the shaft/bearing system changes as the components are cooled down and brought up to speed. The effect of the cool down is shown, as well as the speed effect.

As indicated in Figure 5.6.1, the effect of cool down on bearing deflection is to release a small amount of preload, ~50 lbs. As shown in Table 5.6.1, the thermal coefficient of expansion for the shaft is about 10% larger than the value for the inner race; therefore, the shaft shrinks from the inner race reducing the interference fit. This, in turn, increases the internal clearance of the bearing, allowing the outer race to move in a direction to reduce the spring preload. As the shaft reaches operational speed (30,000 RPM), the centrifugal force causes the inner race to grow, reducing the bearing internal clearance, causing the outer race to move in the direction to increase the preload. As shown in Figure 5.6.1, these are compensating effects and the operating preload is very near the room temperature value. It is important to realize that these conditions have been estimated for uniform temperature conditions (i.e., all bearing elements, shaft, and carrier are assumed to be at the same temperature). Temperature gradients across the bearing and in the bearing carrier could change these results. In addition, the spring constant is the room temperature value. Further analyses are needed to evaluate these effects.

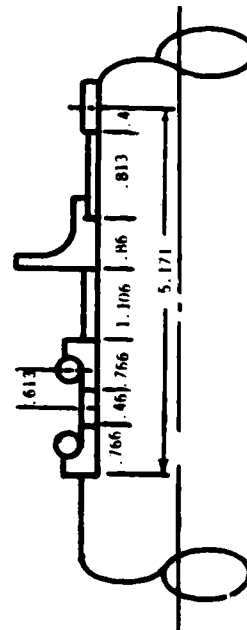
Another factor affecting bearing preload is the preload spring hysteresis. This effect is shown in Figure 5.6.2. As shown, the spring has a different spring constant depending on the direction of travel. It is estimated that the preload value will vary about 20% depending on the direction of the spring action.

5.6.2 BEARING AXIAL REACTIONS RESULTING FROM CARRIER AXIAL LOADS

The design of the Bearing and Materials Tester requires that bearing axial loads be applied by loading the bearing carrier rather than the shaft. The bearing carrier can be loaded by activating the axial load cells. Another source of loads on the carrier is the fluid pressure difference across the carrier. The fluid pressure over the carrier faces is difficult to estimate because of the uncertainty in the fluid rotation effects on local static pressure; therefore, the resulting pressure load is uncertain. Figure 5.6.3 provides the relationship of bearing carrier loads to bearing reactions. Since it is difficult, as explained above, to separate the load cell and fluid ΔP loads, the carrier loads in Figure 5.6.3 should be considered the sum of these loads. As shown, the preload spring constant uncertainty affects the initial preload about 20% and has a smaller effect as the carrier load is increased. Also of interest is the reduction in preload of bearings 1 and 4. Although the preload for these

| COMPONENT | MATRICE | LENGTHS (IN) | EFFECTIVE CROSS | | $\frac{1}{\sigma F}$ | $\bar{\epsilon}$ (Psi) @ -180°C | $\Delta T \cdot R$ |
|-------------------|--------------|--------------|-----------------|------------------------------------|-----------------------|------------------------------------|--------------------|
| | | | LENGTHS (IN) | SECTIONALS AREA (10 ²) | | | |
| BEARING RACE | 440C | .766 | | 1.621 | 4.86x10 ⁻⁶ | 30.74x10 ⁻⁶ | 373 |
| BEARING SEPERATOR | A286 | .46 | | 1.642 | 6.49x10 ⁻⁶ | 30.74x10 ⁻⁶ | 373 |
| SPACER | A286 | 1.106 | | 1.291 | 6.49x10 ⁻⁶ | 30.74x10 ⁻⁶ | 373 |
| SEAL | K-MONEL | .86 | | 1.853 | 6.22x10 ⁻⁶ | 26.4x10 ⁻⁶ | 373 |
| SEAL SPACER | A286 | .813 | | .91 | 6.49x10 ⁻⁶ | 30.74x10 ⁻⁶ | 373 |
| NUT | K-MONEL | .4 | | 1.362 | 6.22x10 ⁻⁶ | 26.4x10 ⁻⁶ | 373 |
| SHAFT | WASPALLOY | 5.171 | | 2.216 | 6.2x10 ⁻⁶ | 33.89x10 ⁻⁶ | 373 |
| SPRING | INCONNEL 718 | .115 | | - | 6.22x10 ⁻⁶ | 30.2x10 ⁻⁶ | 373 |
| CARRIER TANG | INCONNEL 718 | .103 | | - | 6.22x10 ⁻⁶ | - | 373 |

TABLE 5.6.1 SHAFT/COMPONENT MATERIAL PROPERTIES AND GEOMETRY



ORIGINAL PAGE IS
OF POOR QUALITY

SRS

ORIGINAL RANGE
OF FCOR QUALITY

- ROOM TEMP, ZERO SPEED
- - - SPEED + CRYO TEMP
- - - CRYO TEMP, ZERO SPEED

SINGLE 57mm BEARING
-180°C
SPEED 30,000 R.P.M.

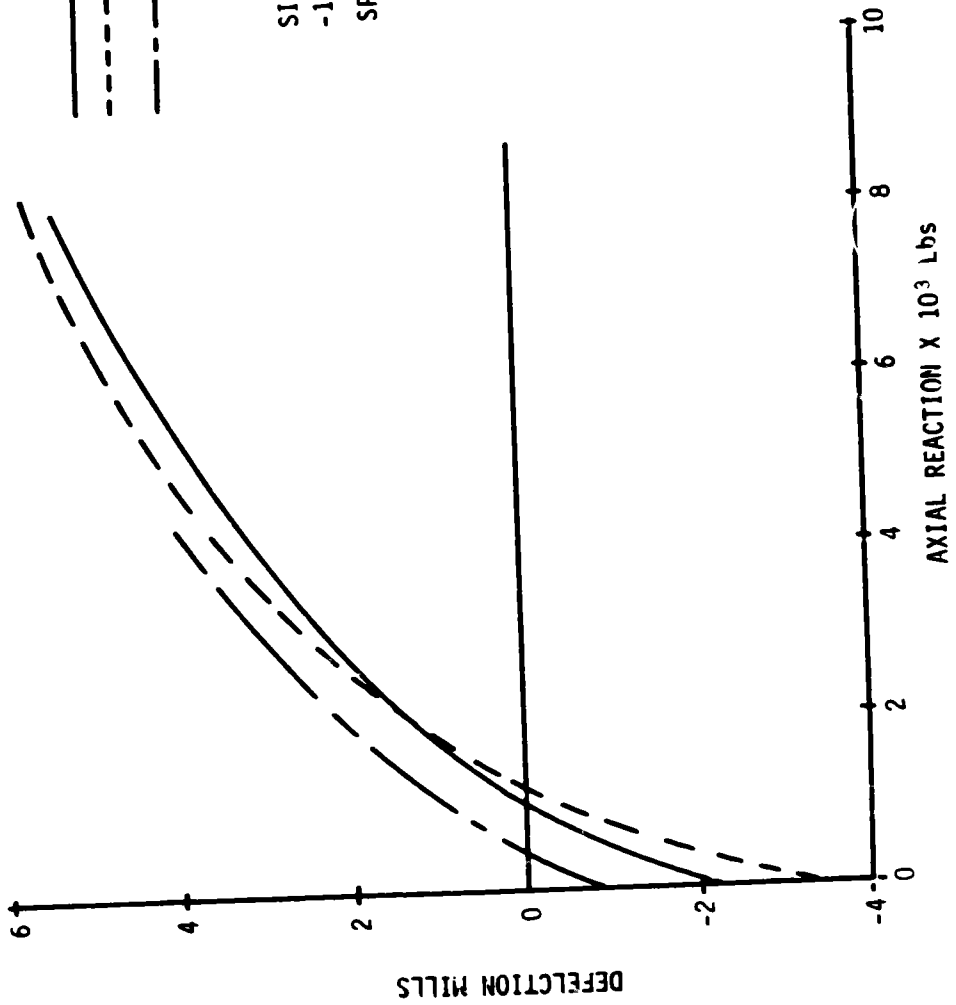
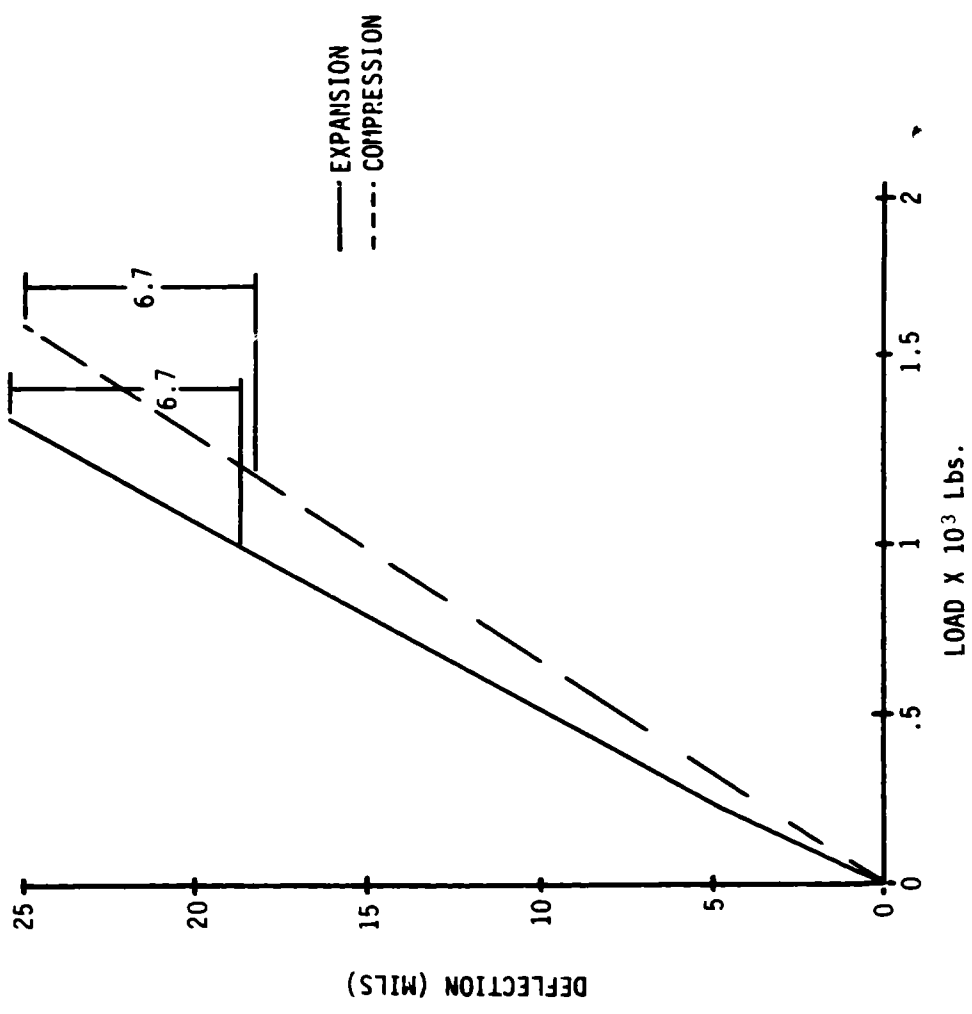


FIGURE 5.6.1
BEARING DEFLECTION VS AXIAL REACTION

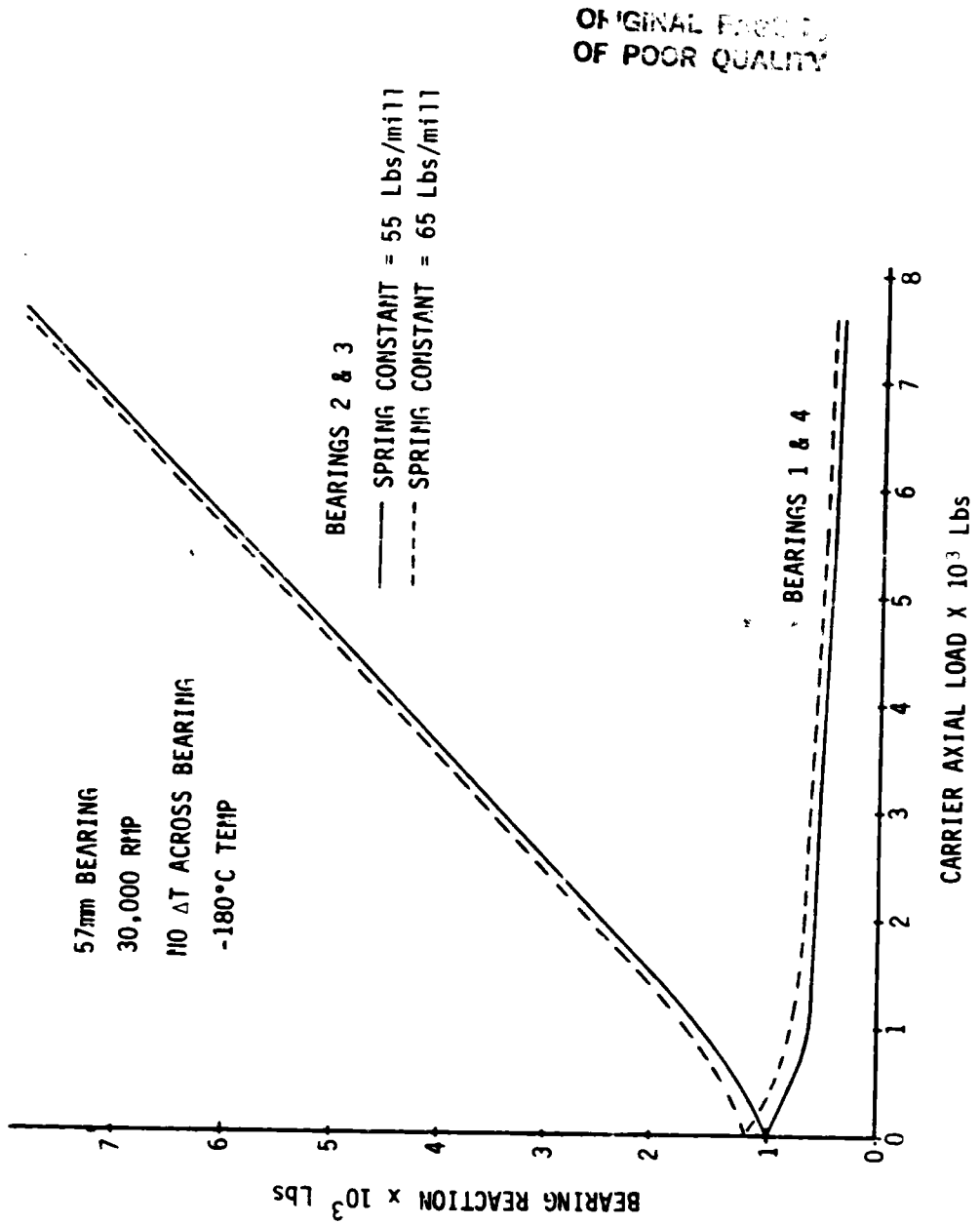
SRS

ORIGINAL PAGE IS
OF POOR QUALITY

SRS



PRELOAD (BELLEVILLE) SPRING DEFLECTION VS LOAD
FIGURE 5.6.2



BEARING REACTION Vs CARRIER AXIAL LOAD
FIGURE 5.6.3

bearings is reduced to about 400 pounds, it has been shown in a previous analysis (see Section 5.4.1) that this load is sufficient to prevent ball skid due to fluid drag.

5.6.3 INTERFERENCE FIT BETWEEN THE INNER RACE AND SHAFT

The bearing inner race is a force or interference fit on the tester shaft. This assembly is made at room temperature and the interference between the race and shaft changes as the tester is cooled to LN₂ temperature, rotated to test speed, and loaded. An analysis was done to estimate these changes at the various conditions from assembly to test.

Assuming that the assembly temperature is 20°C and the cold operating temperature is -180°C, the interference will change from 2.3 mils at room temperature to 1.2074 mils at -180°C. Rotation of the bearing shaft assembly to 30,000 per minute will reduce the interference to 0.6178 mils. A preload of 1000 lbs. will increase the interference to about 0.75 mils. Increased axial loading will "tighten" the interference of bearings 2 and 3 and loosen bearings 1 and 4. The interference for 1 and 4 will not be less than 0.6178 mils.

The above estimates are for uniform temperature of bearing race and shaft. This is not the case when bearing friction heat warms the inner race to a higher temperature than the shaft. The maximum temperature difference between the inner race and the shaft probably occurs during tester start when the heat generation, due to speed and load, is suddenly imposed on the chilled shaft and bearing. This transient condition has not been analyzed; however, a calculation was made to estimate the temperature difference between the inner race and shaft that would eliminate the interference fit. Assuming the shaft remained at -180°C, this analysis indicated about 38°C temperature difference between bearing inner race and shaft will cause the interference fit to be lost (i.e., if the inner race temperature attains an average temperature of -142°C, while the shaft average temperature remains at -180°C, the interference between inner race and shaft will be zero at 30,000 RPM and 1000 lbs axial reaction at the bearing).

Since the thermal model predicts an average temperature of only 28°C for an axial load of 2500 lbs and 30,000 RPM, there should be no problem in losing interference fit at steady operating conditions. However, as stated previously, the start transient could cause a temperature difference large enough to eliminate the interference fit for short periods of time. Although an increase in axial load tends to increase the interface pressure (between inner race and shaft), it also increases the heat generation rate. The steady conditions analyzed were for an axial load of 2500 pounds. It is expected, but not confirmed by analysis, that the increase in load will outweigh the thermal effects and the interference fit will be maintained at the higher load conditions. If the maintenance of an interference fit is critical to tester operation, a transient analysis should be done and additional higher loads investigated to verify that the interference is not lost for any possible operating condition.

The previous analyses show that the room temperature bearing preload is not significantly affected by cooling to LN₂ temperature and rotation of the shaft to 30,000 RPM. Temperature gradients across the bearing have been neglected and the temperature effect on bearing spring constant has not been included. Although the bearing internal clearances can be significantly affected, it is expected that temperature differences of less than about 150°F across the bearing will have little effect on the preload value. The temperature effect on spring constant will require further work. It should also be observed that the effect of speed is to increase the preload;

abstract research systems

therefore, at a shaft speed of 10,000 RPM, the preload will be slightly reduced (reduction will be less than ~65 lbs.) compared to the value at 30,000 RPM.

The analyses relating the carrier load to bearing reactions shows that the unloaded bearings (1 and 4) will retain sufficient preload to prevent excess skidding and internal heat generation. It also shows that the uncertainty in bearing reaction due to preload spring hysteresis is approximately 20% maximum.

The interference fit between the inner race and shaft has been evaluated to determine the effects of temperature and speed. Although an interference is maintained at uniform operating temperatures and speed, temperature differences between the bearing inner race and shaft can be large enough to eliminate the interference. It has been estimated that interference fit will be lost at speed if the inner race temperature is greater than the shaft temperature by about 38°C. This assumes the shaft to be operating at -180°C which is a representative temperature when operating in LN₂. It presently appears that this can possibly occur only during start transients when the shaft and bearing are chilled and a sudden load and speed is imposed which heats the bearing before the shaft temperature has time to respond.

5.6.4 STATUS OF BEARING THERMAL MODEL DEVELOPMENT

During this reporting period, emphasis has been placed on verification and validation of the bearing thermal model. This was done by comparing the results from the thermal model using test run conditions, to the extent that they are known, with experimental data. The test conditions considered include the flow rate of the coolant into the bearing set, the initial temperature of the coolant or the degree of subcooling and the axial load imposed upon the bearing. The coolant being considered was LN₂. During the course of this investigation, the sensitivity of selected node temperatures with respect to the flow rate of the coolant and inlet coolant temperatures was also examined.

To facilitate changes in operating conditions (i.e., flow rate, shaft speed, etc.) with regards to the thermal model, a computer program was developed to calculate the 657 metal-to-fluid conductances needed in the present model. The program calculates, for each surface node, a conductance-vs-temperature array and assembles the output in the format required by the thermal model computer program. The conductance values are calculated using a boiling curve (heat transfer coefficient-vs-surface temperature) for temperatures above the saturation temperature of the coolant. Various operating conditions such as flow rate, shaft speed, cage speed, and boiling temperatures can easily be changed. This program allows rapid modification of the thermal model and improves our capability for analysis of trends involving changes in operating conditions.

The LN₂ data base for the thermal model represents heat generation conditions to simulate a 2500 pound axial reaction in the tester for a 57 mm bearing set. This data base was set up to consider four different mass flow rates through the bearing set; 3.2, 6.3, 9.6, and 12.8 lbs/sec per bearing set. For each different mass flow rate, the thermal model was exercised for three different values of subcooled temperature; -285°F, -305°F, -331°F. The frictional heat generated was estimated based on a friction coefficient of 0.14 and a ΔT across the bearing of 200°C. Future analyses for LN₂ will use a friction coefficient of 0.2, and a ΔT calculated from the thermal model.

spectra research systems

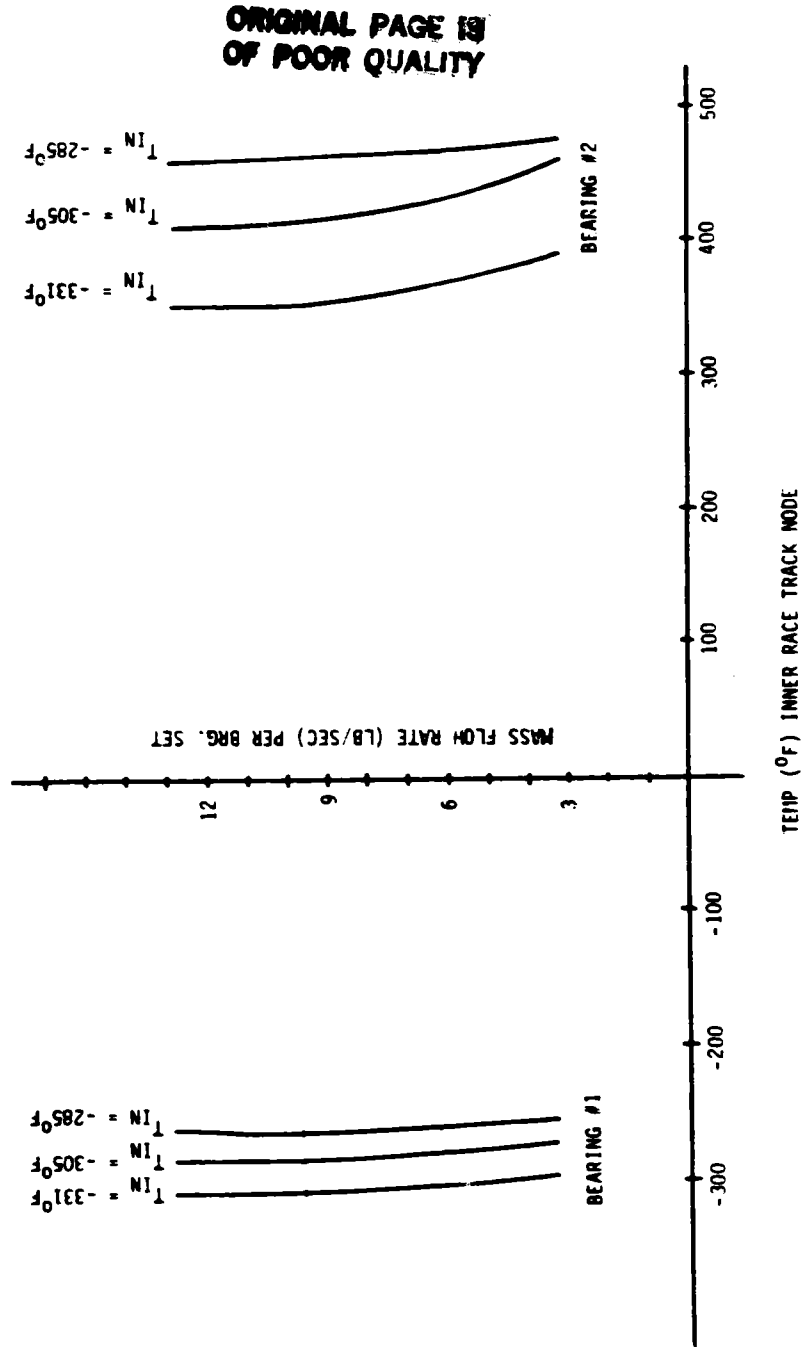
The sensitivity of several node temperatures was examined to determine the effect of changing mass flow rate and degree of subcooling. In Figure 5.6.4, a plot of the temperature of the ball track node on the inner race versus the mass flow rate of the coolant is shown for different degrees of subcooling. As can be seen, the degree of subcooling has a larger effect on the resultant node temperature than does the flow rate of the coolant through the bearing set. Figure 5.6.5 shows the effect of changing mass flow rates on the outer race temperature. Similar conclusions can be drawn from this figure. Node number 107 is located above the contact area, at the edge of the outer race, on bearing 1. Node number 307 is in the same location on bearing 2. A third node was examined in a similar manner, node number 403, which is a surface node located between bearings 1 and 2 as shown in Figure 5.6.6.

A comparative analysis was performed between the test data for an LN₂ run and the thermal model utilizing various operating conditions. The outer edge of the outer race is divided into four nodes in the bearing thermal model. These nodes are numbered 115, 114, 107 and 100 for bearing 1 and 315, 314, 307 and 300 for bearing 2. Nodes 107 and 307 are above the contact area of the bearing and therefore run the hottest. Figures 5.6.7 through 5.6.10 show the comparison of experimental to model outer race temperature for bearings 1 through 4. This comparison is for a mass flow rate of 3.2 lb/sec per bearing set and a -305°F inlet coolant temperature for the thermal model operating parameters. Figures 5.6.11 through 5.6.14 illustrate the same type of comparison with a flow rate of 6.3 lb/sec per bearing set which is representative of the BMT coolant flyout. Figures 5.6.15 through 5.6.18 compare outer race temperatures using a flow rate of 9.6 lb/sec for the thermal model and Figures 5.6.19 through 5.6.22 utilize a 12.8 lb/sec per bearing set flow rate for the model. It is significant to note that although temperatures for the model continue to become cooler with increasing mass flow rate, the effect of flow on cooling decreases with increasing flow. The model predicts temperatures well within the range of values for the experimental test runs as illustrated by Figure 5.6.7 through 5.6.18.

There appears to be little potential for using any one control node to determine acceptable operating conditions for the bearing tester. The next step will be to examine the operating clearances of the bearing as a function of the temperature difference across the bearing using average temperatures of the outer race, inner race and rolling element. The analysis will be extended to other loads in an effort to define an acceptable operating range for the tester in terms of flow and subcooling. The effect of changing the temperature at which film boiling begins will also be examined.

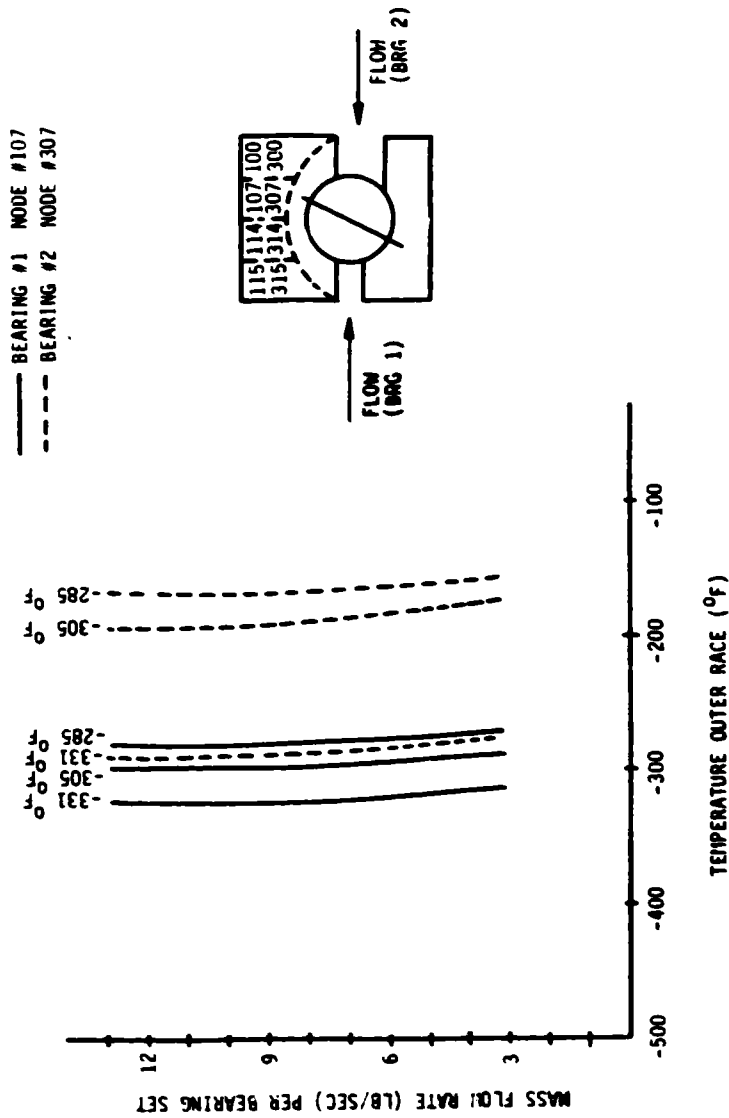
In summary, the temperature of the bearing contact surfaces (ball and race tracks) appear to be influenced more by reduced subcooling than by increased mass flow over the range of variables investigated. There does, however, appear to be a slight deflection in the temperature versus flow curve at about 10 lbs/sec where further reductions in flow allow the temperatures to begin increasing (for $T_{IN} = -305$ and -331°F). Although it is not clear at this point how to select a temperature node or series of nodes as a limiting temperature condition, further analyses on the influence of temperature differences across the bearing and the sensitivity of this difference to flow and subcooling will hopefully provide a criteria for selecting a safe operating range in terms of loads flow, and subcooling.

FIGURE 5.6.4 MASS FLOW RATE-VS-INNER RACE BALL TRACK TEMPERATURE FOR AXIAL REACTION OF 2500 POUNDS ON BEARING 2



SRS

FIGURE 5.6.5 MASS FLOW RATE-VS-TEMPERATURES ACROSS OUTER RACE FOR AN AXIAL REACTION OF 2500 POUNDS ON BEARING 2

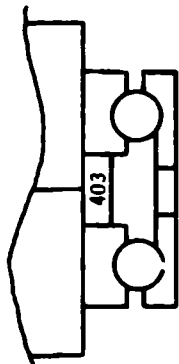
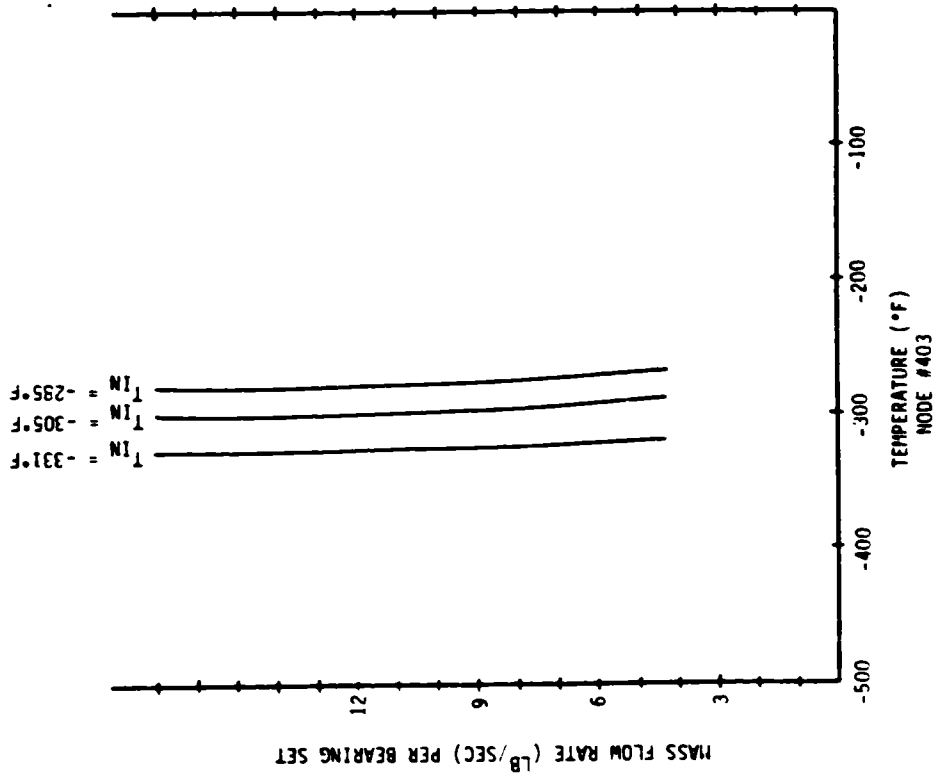


ORIGINAL PAGE IS
OF POOR QUALITY

SRS

ORIGINAL PAGE IS
OF POOR QUALITY

FIGURE 5.6.6
MASS FLOW RATE - VS - TEMPERATURE OF NODE #403 FOR AN AXIAL REACTION OF 2500 POUNDS



BEARING 1
MASS FLOW RATE = 3.2 LB/SEC
INLET FLUID TEMP = -305°F

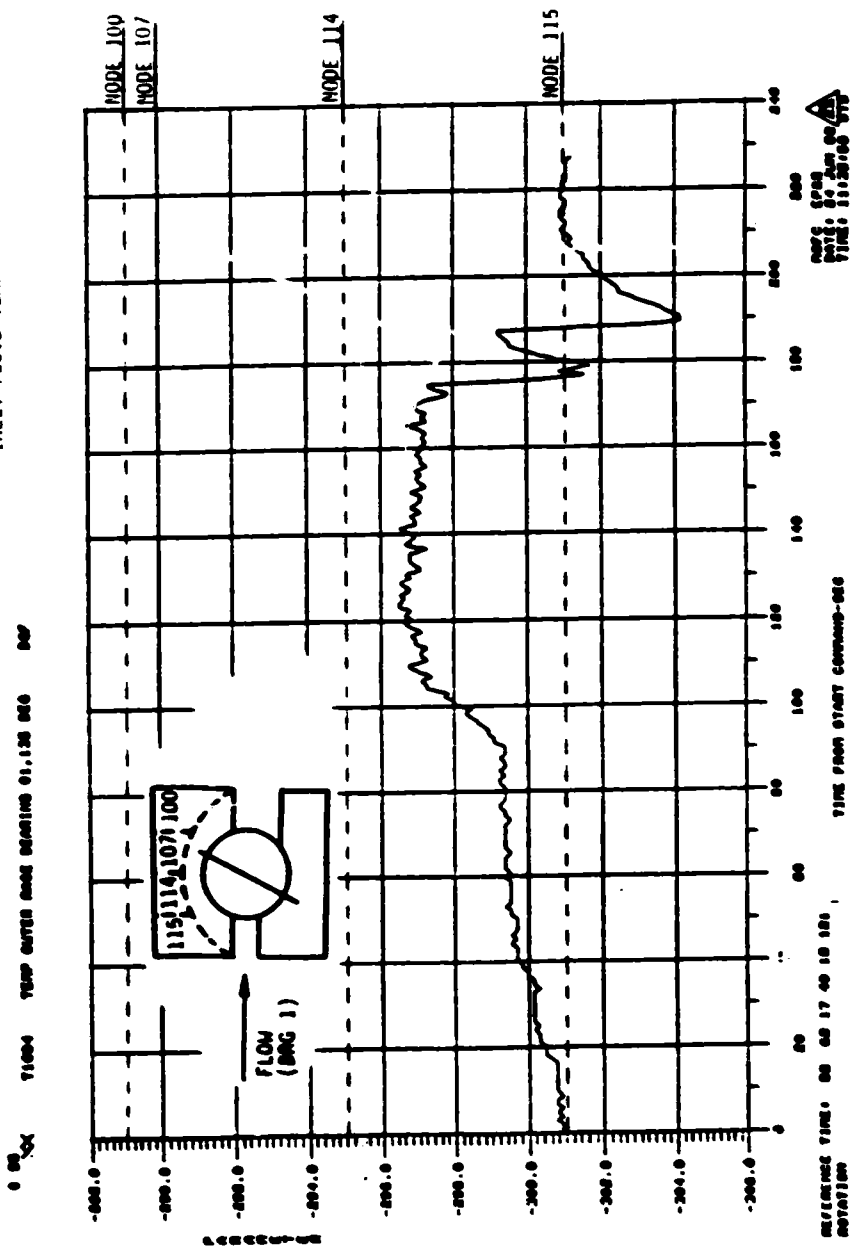


FIGURE 5.6.7 COMPARISON OF TEST DATA WITH THERMAL MODEL RESULTS

SRS

NODE #307
NODE #314

BEARING 2
MASS FLOW RATE = 3.2 LB/SEC
INLET FLUID TEMP = -305.

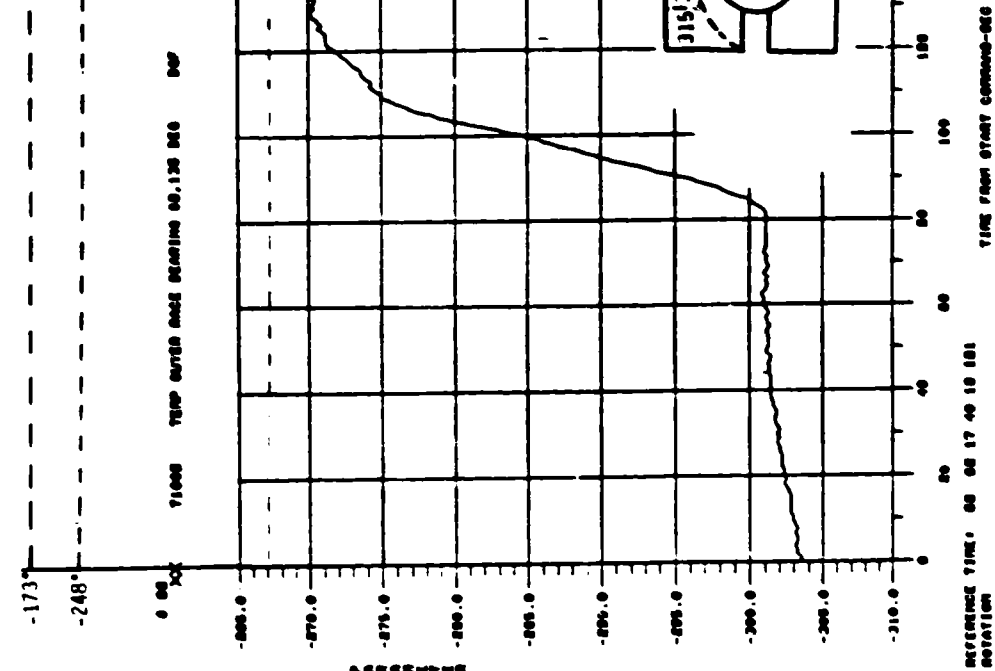


FIGURE 5.6.8
COMPARISON OF EXPERIMENTAL TEST DATA WITH THERMAL MODEL RESULTS (CONTINUED)

SRS

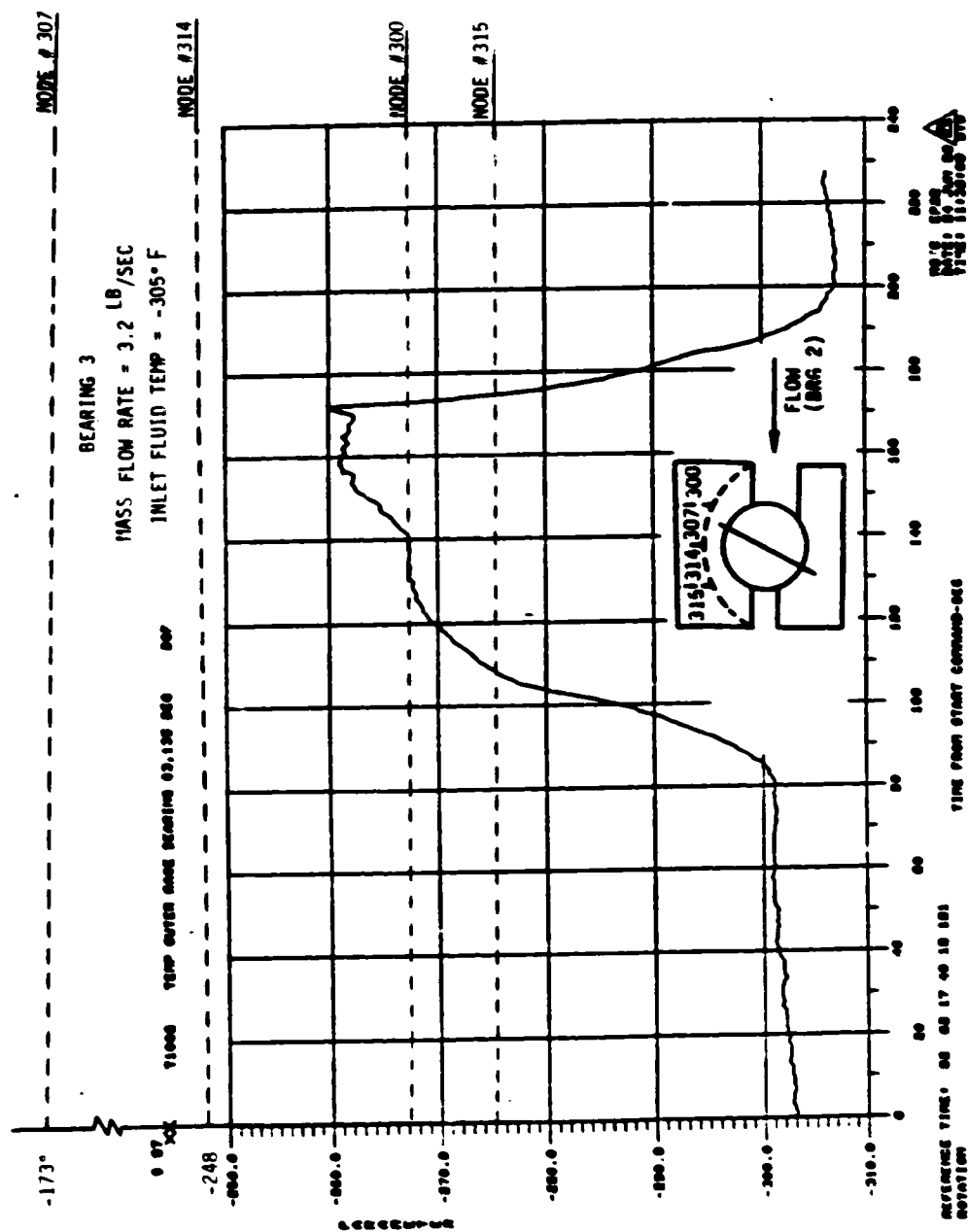


FIGURE 5.6.9
 COMPARISON OF EXPERIMENTAL TEST DATA WITH THERMAL MODEL RESULTS (CONTINUED)

SRS

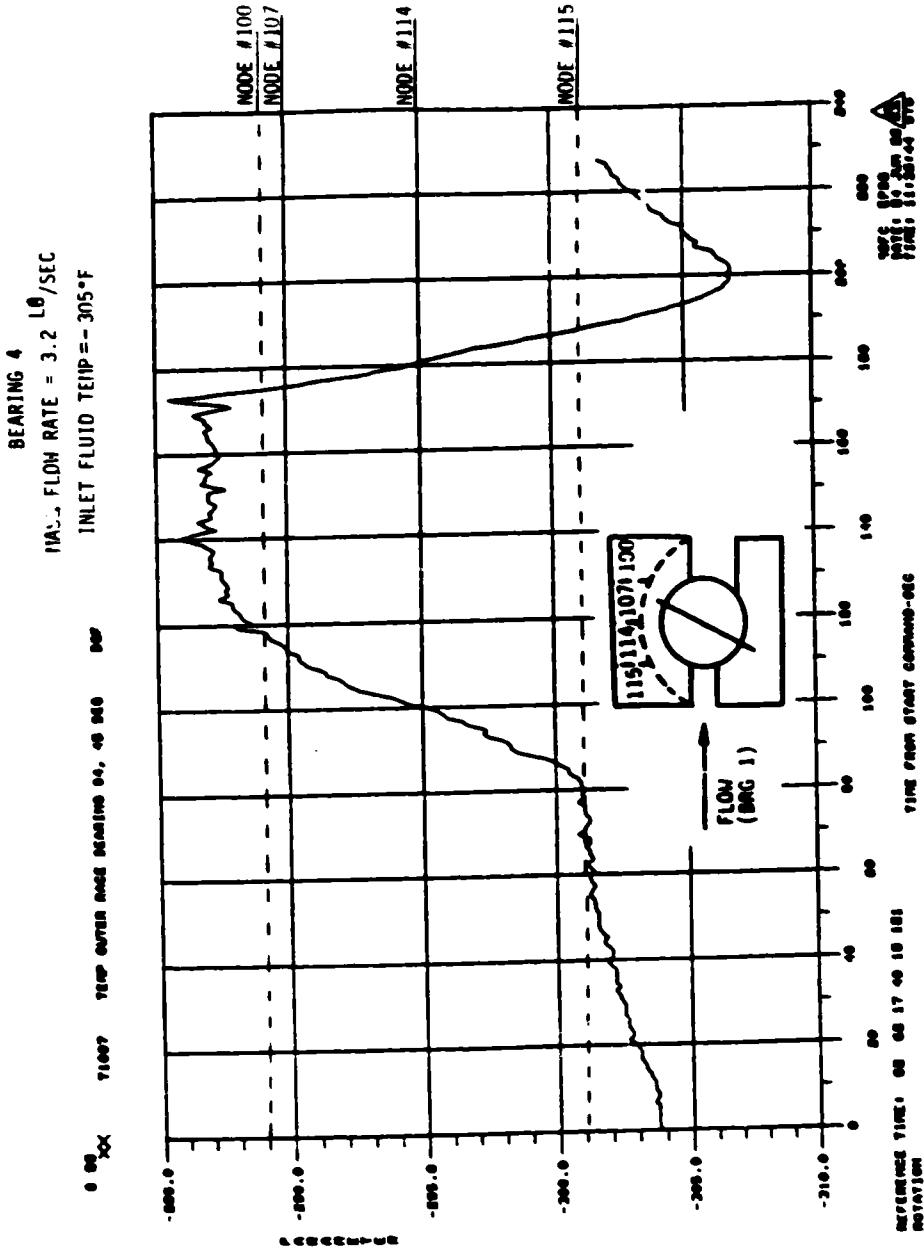


FIGURE 5.6.10
 COMPARISON OF EXPERIMENTAL TEST DATA WITH THERMAL MODEL RESULTS (CONTINUED)

BEARING 1
MASS FLOW RATE = 6.3 LB/SEC
INLET FLUID TEMP = -305° F

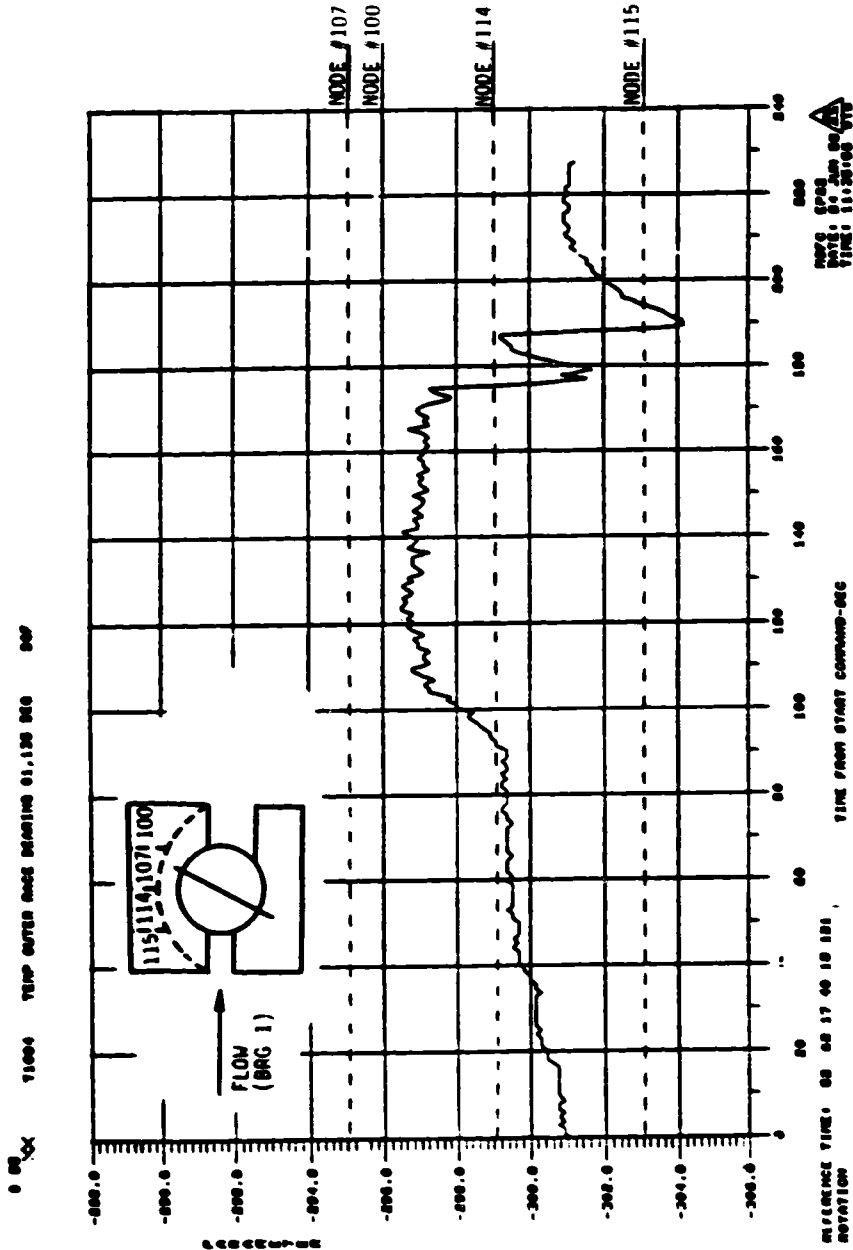


FIGURE 5.6.11
COMPARISON OF EXPERIMENTAL TEST DATA WITH THERMAL MODEL RESULTS (CONTINUED)

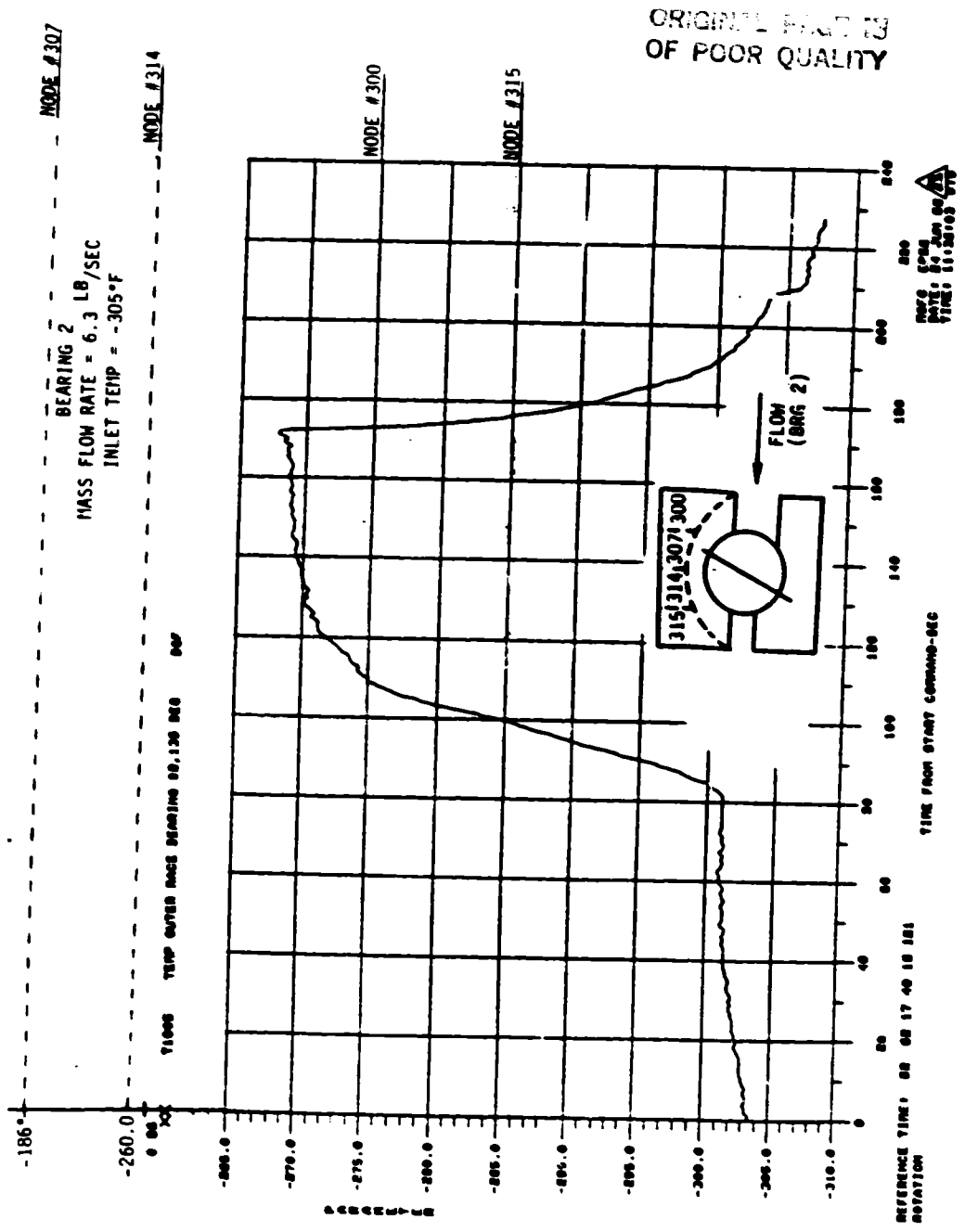


FIGURE 5.6.12
 COMPARISON OF EXPERIMENTAL TEST DATA WITH THERMAL MODEL RESULTS (CONTINUED)

MODE #307

BEARING 3
MASS FLOW RATE = 6.3 LB/SEC
INLET TEMP = -305°F

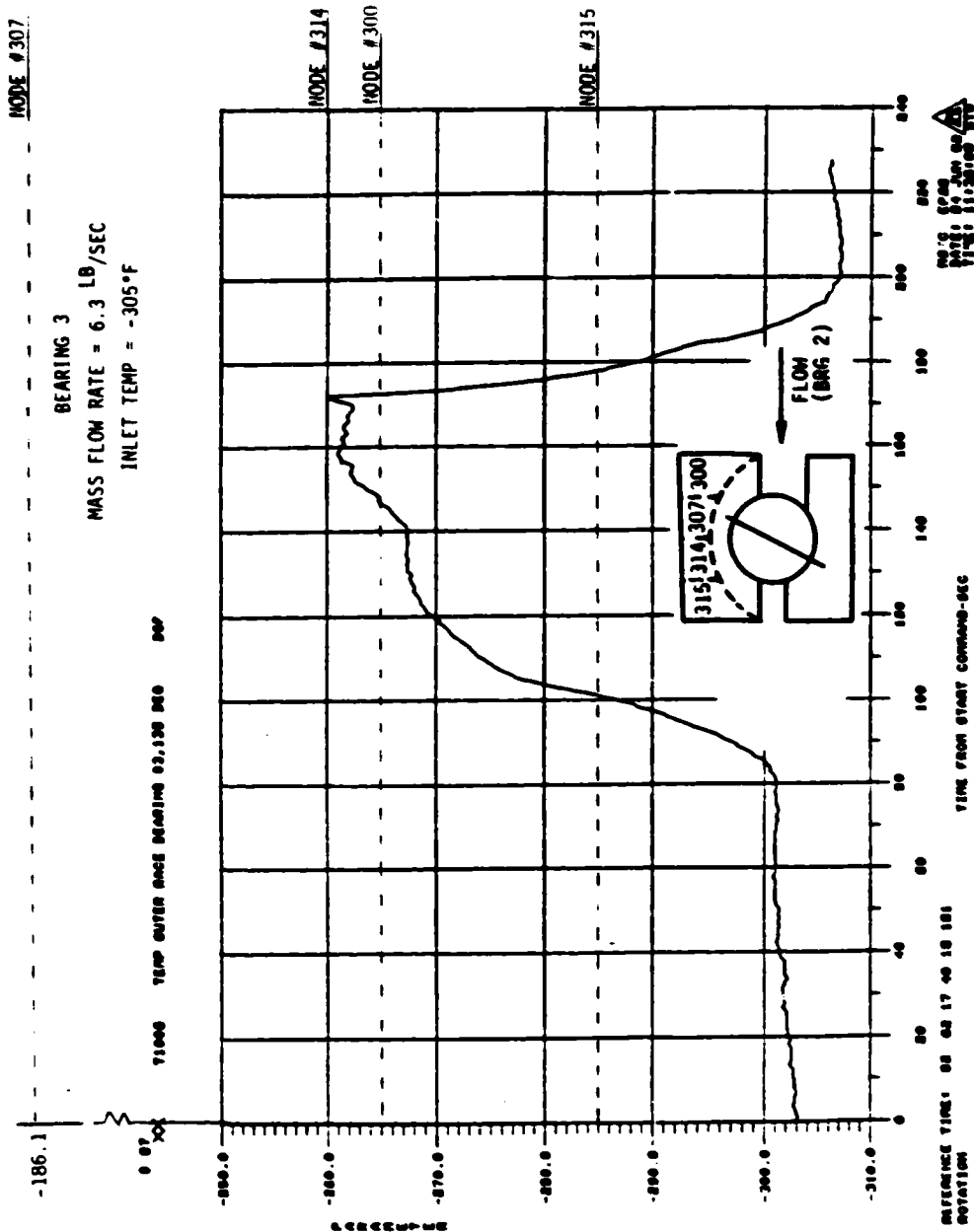


FIGURE 5.6.13
COMPARISON OF EXPERIMENTAL TEST DATA WITH THERMAL MODEL RESULTS (CONTINUED)

SRS

BEARING 4
MASS FLOW RATE = 6.3 LB/SEC
INLET FLUID TEMP 305

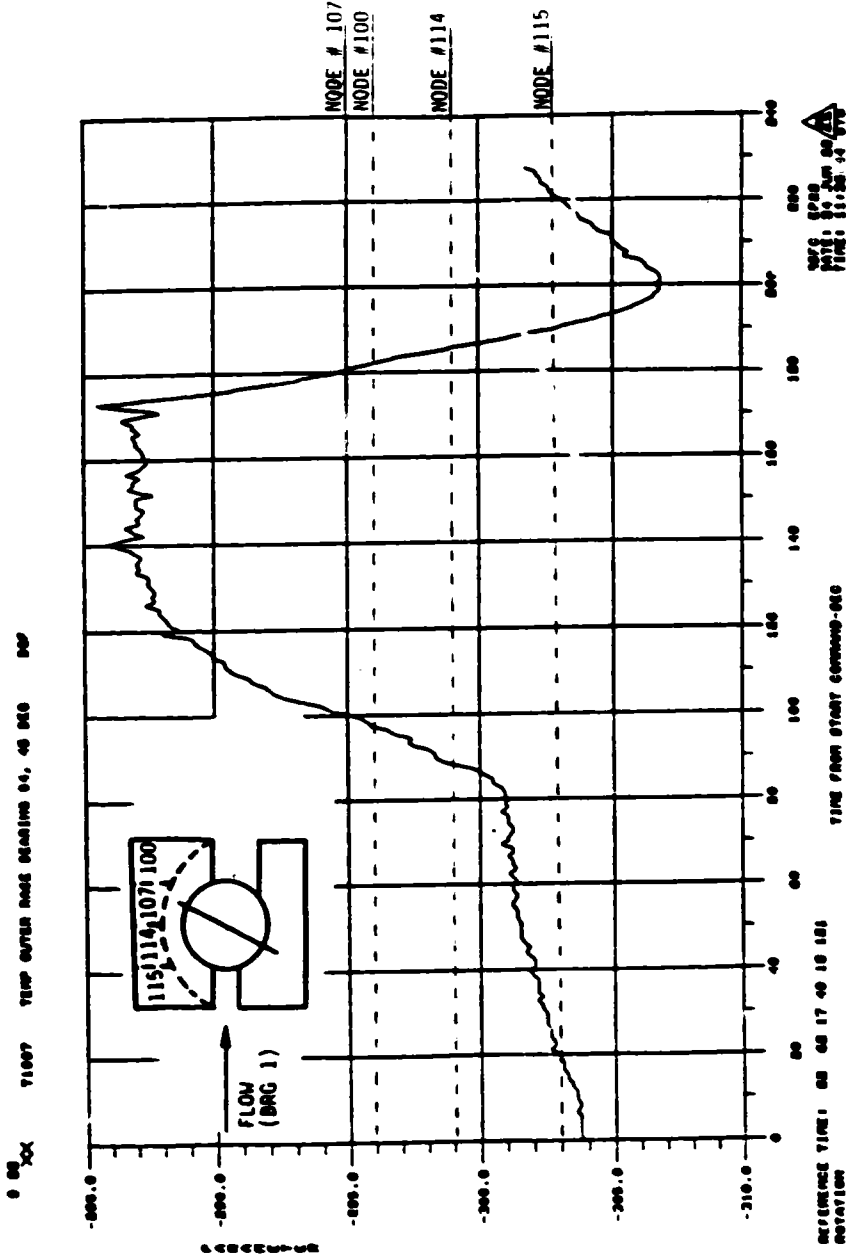


FIGURE 5.6.14
COMPARISON OF EXPERIMENTAL TEST DATA WITH THERMAL MODEL RESULTS (CONTINUED)

SRS

BEARING 1

MASS FLOW RATE = 9.6 LB/SEC
INLET FLUID TEMP = -305°F

0 00X 71004 TEMP ENTER MASS BEARING 01.126 DEG DEG

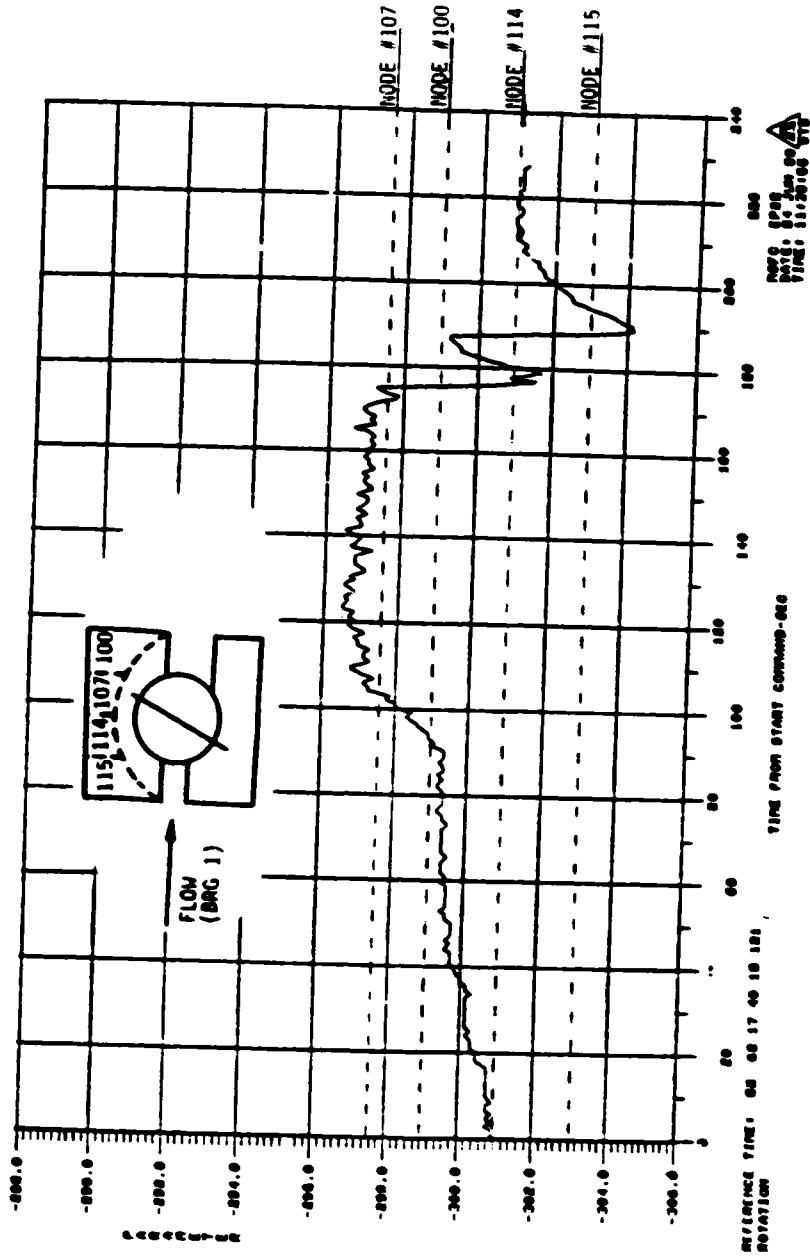


FIGURE 5.6.15
COMPARISON OF EXPERIMENTAL TEST DATA WITH THERMAL MODEL RESULTS (CONTINUED)

SRS

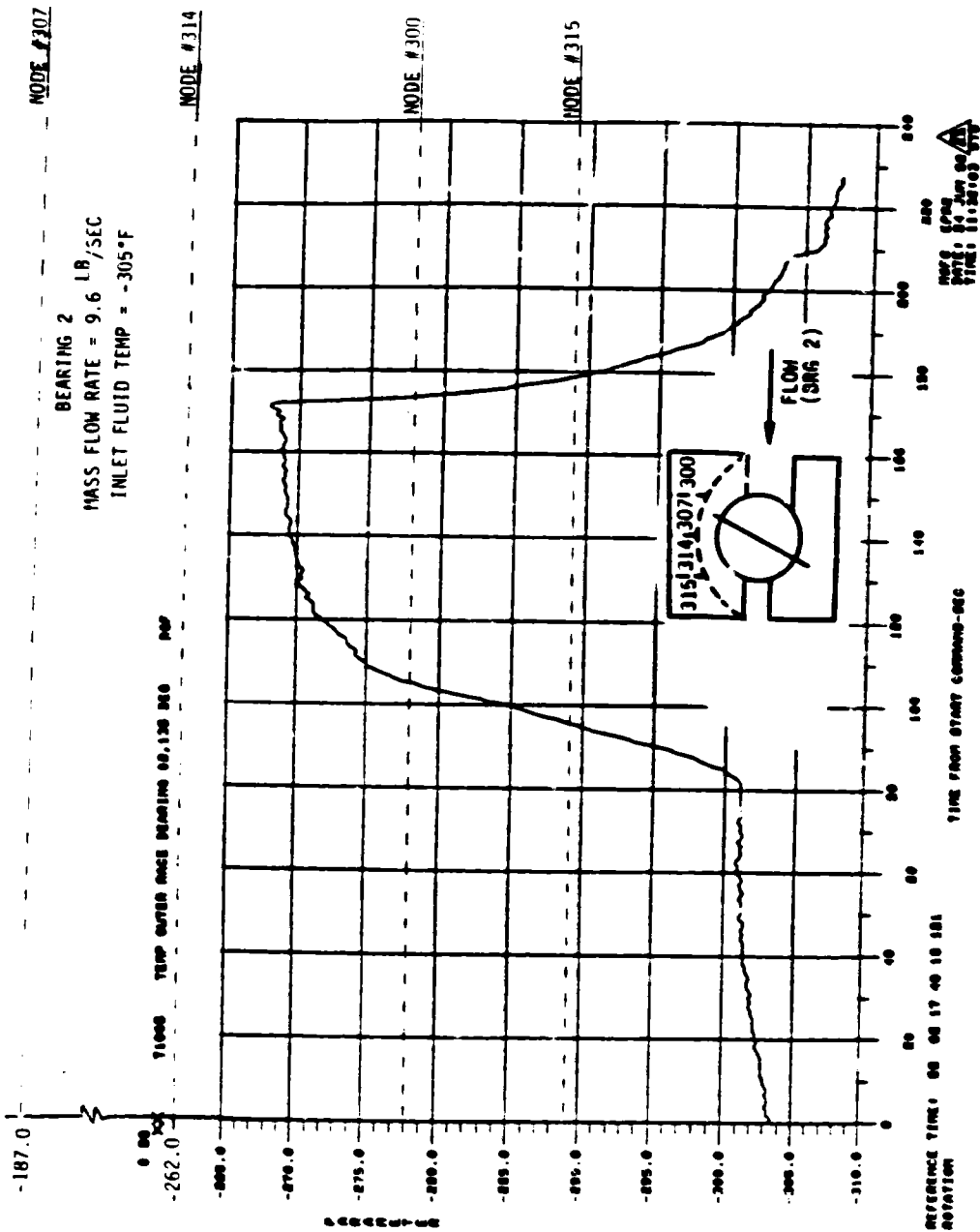
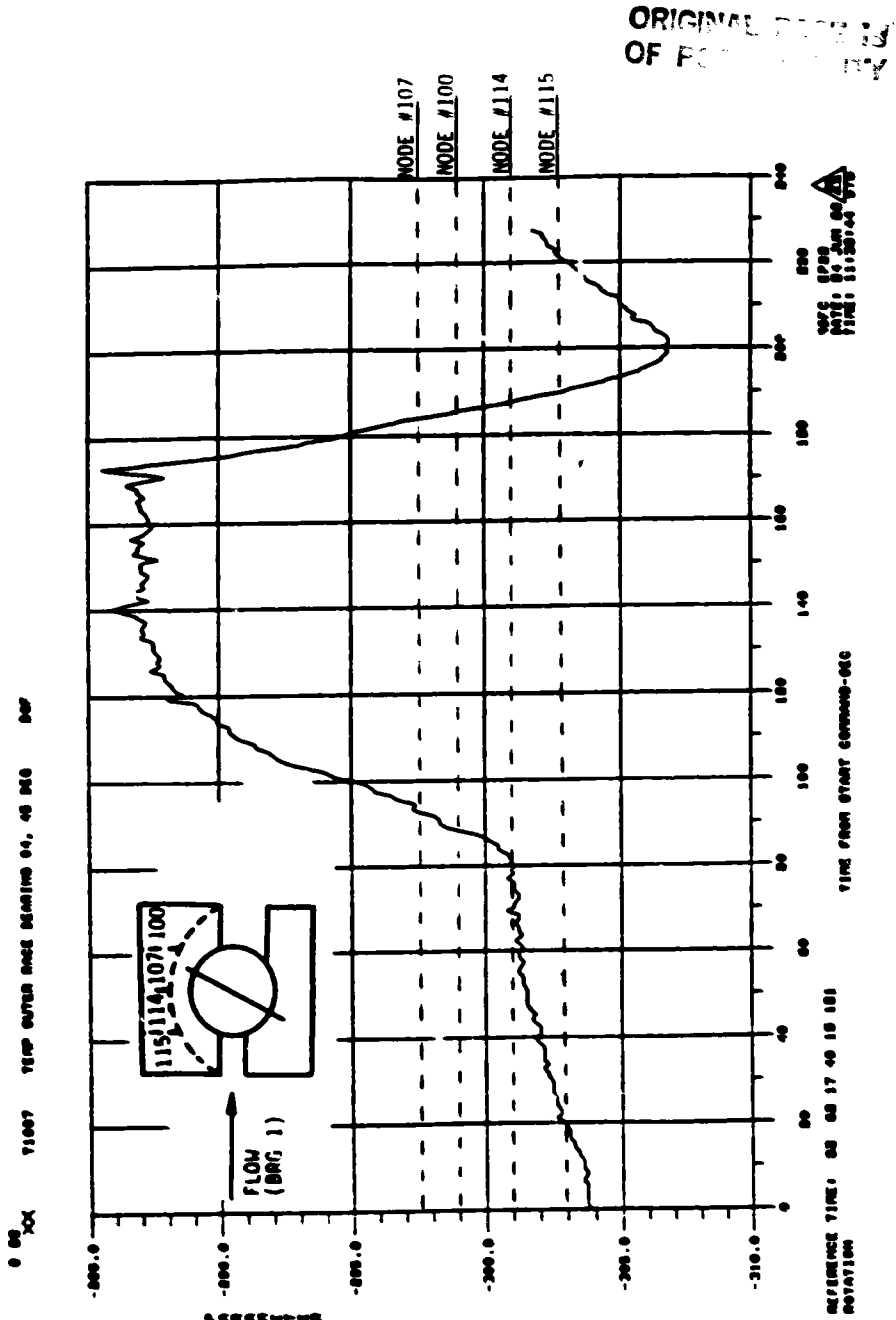


FIGURE 5.6.16
COMPARISON OF EXPERIMENTAL TEST DATA WITH THERMAL MODEL RESULTS (CONTINUED)

BEARING 4
 MASS FLOW RATE = 9.6 LB/SEC
 INLET FLUID TEMP = -305°F



ORIGINAL RECORD
 OF POC

FIGURE 5.6.18
 COMPARISON OF EXPERIMENTAL TEST DATA WITH THERMAL MODEL RESULTS (CONTINUED)

SRS

BEARING 1
MASS FLOW RATE = 12.8 LB/SEC
INLET FLUID TEMP = -305°F

0 00 71000 TEMP ENTER BEARING 01.130 DEG 000

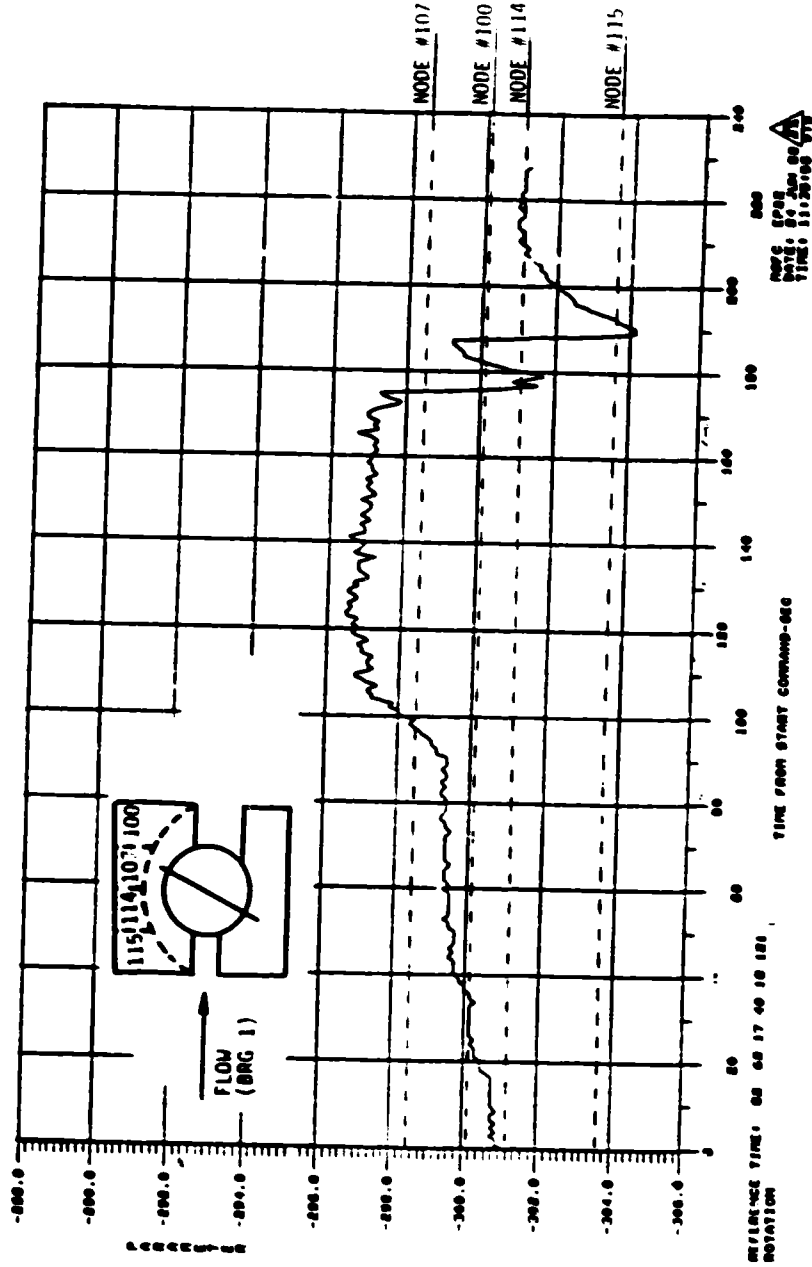


FIGURE 5.6.19
COMPARISON OF EXPERIMENTAL TEST DATA WITH THERMAL MODEL RESULTS (CONTINUED)

SRS

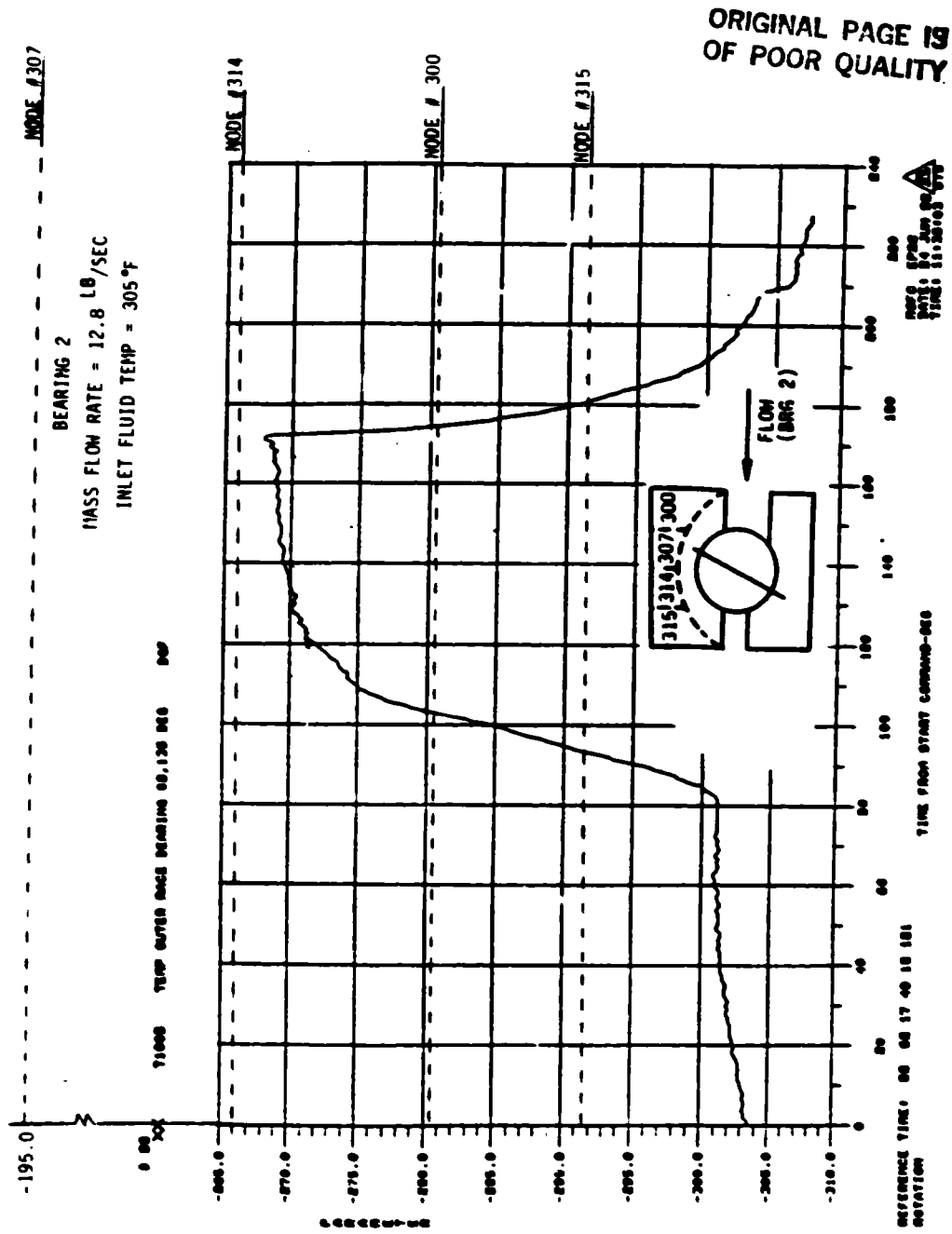


FIGURE 5.6.20
 COMPARISON OF EXPERIMENTAL TEST DATA WITH THERMAL MODEL RESULTS (CONTINUED)

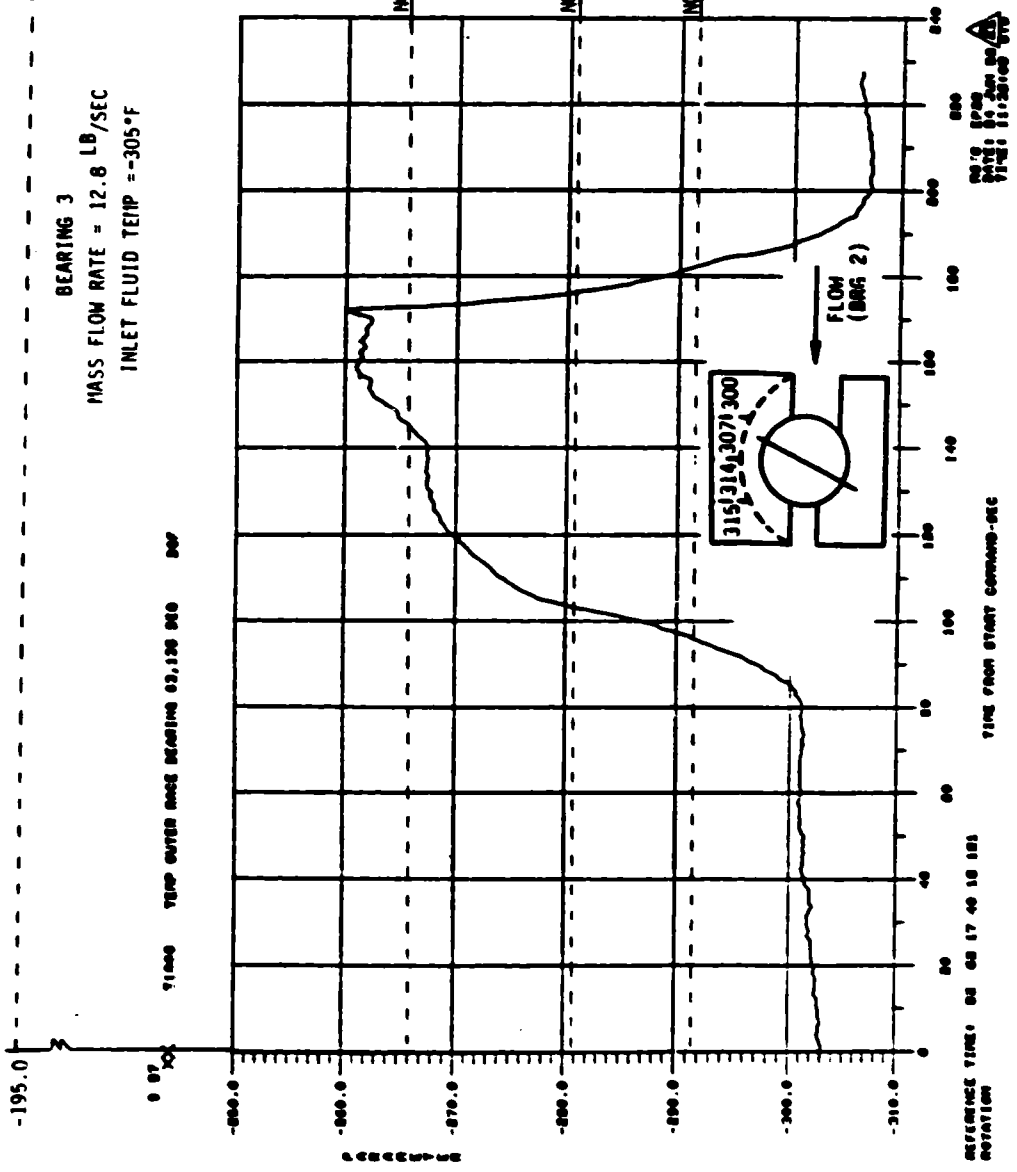
MODE #302

BEARING 3

MASS FLOW RATE = 12.8 LB/SEC

INLET FLUID TEMP = -305°F

TEMP OUTER AND BEARING 05.120 060 060



ORIGINAL PAGE 19
OF POOR QUALITY

FIGURE 5.6.21

COMPARISON OF EXPERIMENTAL TEST DATA WITH THERMAL MODEL RESULTS (CONTINUED)

SRS

BEARING 4
MASS FLOW RATE = 12.8 LB./SEC
INLET FLUID TEMP = -305°F

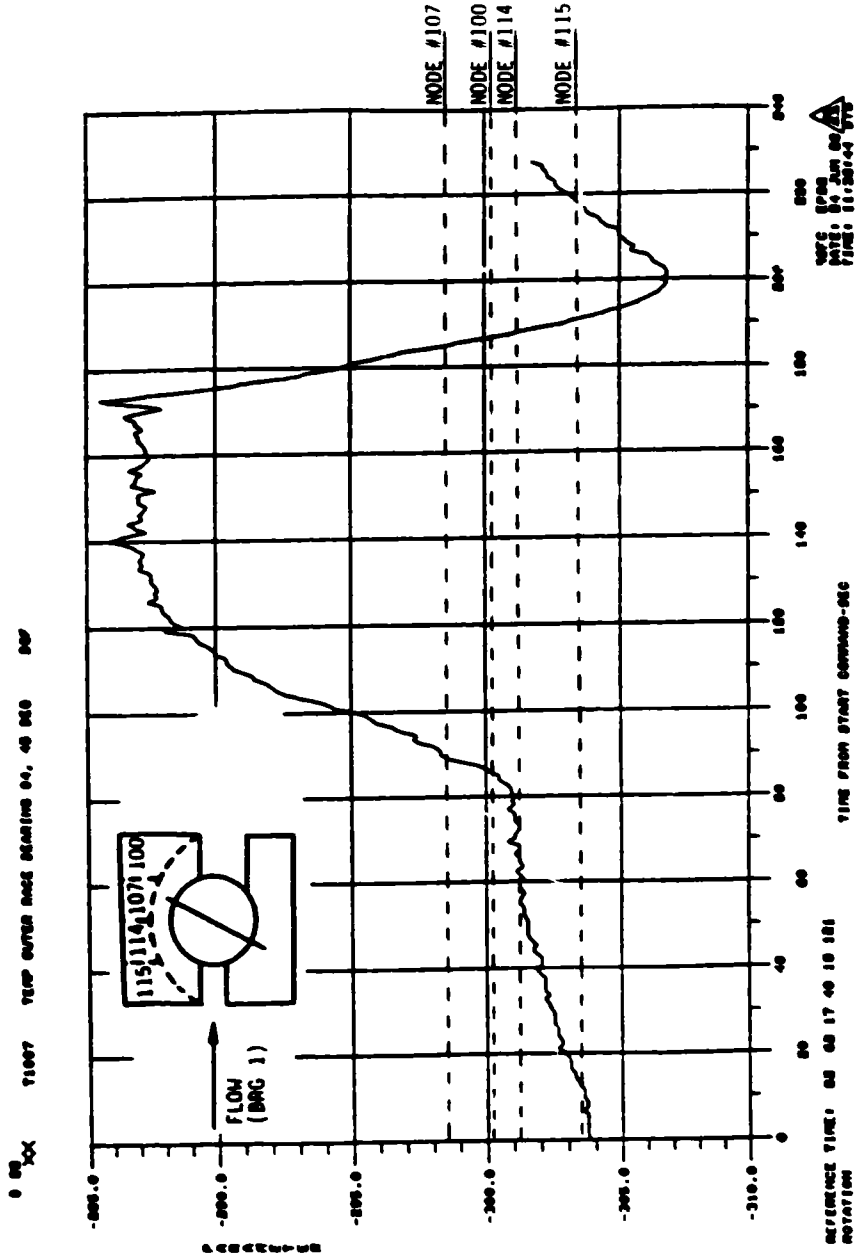


FIGURE 5.6.22
COMPARISON OF EXPERIMENTAL TEST DATA WITH THERMAL MODEL RESULTS (CONTINUED)

SRS

5.7 JANUARY, 1983

5.7.1 POTENTIAL EFFECTS OF OUTER RACE MISALIGNMENT ON SHAFT ASSEMBLY BALANCING

An apparent shaft assembly unbalance was observed during balancing of the BMT rotating assembly. The cause was determined to be bearing carrier face run out. The carrier run out can in effect produce an angular misalignment in the bearing outer race. The purpose of this investigation is to develop an explanation as to how the outer race tilt could produce a synchronous load effect, which would appear to be a grossly out of balance shaft assembly.

As a start, the geometry change in the bearing was evaluated as the outer race was displaced. Figure 5.7.1 illustrates the geometric representation. As the outer race is rotated counter clockwise, the right ball moves upward and to the right and the left ball moves down and to the right. The center of the pitch circle is displaced in the positive y direction. The center of the circle formed by the outer race curvative center is displaced in the y direction (k) and in the x direction (h). Normally this is a static condition and the ball pitch circle would be displaced from the shaft center line by a constant value and there should be no shaft dynamic effects. However, the contact angle changes as a function of the azimuth angle. The contact angle is increased in the $\psi = 0^\circ$ position and decreases when $\psi = 180^\circ$. At $\psi = 90^\circ$, the contact angle is not changed. Assume an out of balance shaft assembly producing a synchronous load in the radial direction. Since the contact angle changes with azimuth location, the bearing radial stiffness also changes in the azimuth direction. Therefore, with a variable stiffness, the shaft can move radially in a dynamic manner synchronous with shaft speed. Consequently, a small unbalance can be magnified into an apparent large unbalance by outer race misalignment. The geometry shown in Figure 5.7.1 is obviously for an unloaded, static bearing. Loads and speed will change the configuration. However by superimposing the outer race misalignment effects on the configuration assumed by the bearing at speed and under load, the above explanation should still be valid.

To investigate the sensitivity of the contact angle to outer race misalignment the following analysis was made. Assuming no deformation in the contact areas and very small axial displacement, $h \ll a$, the contact angle can be related to the misalignment angle as follows:

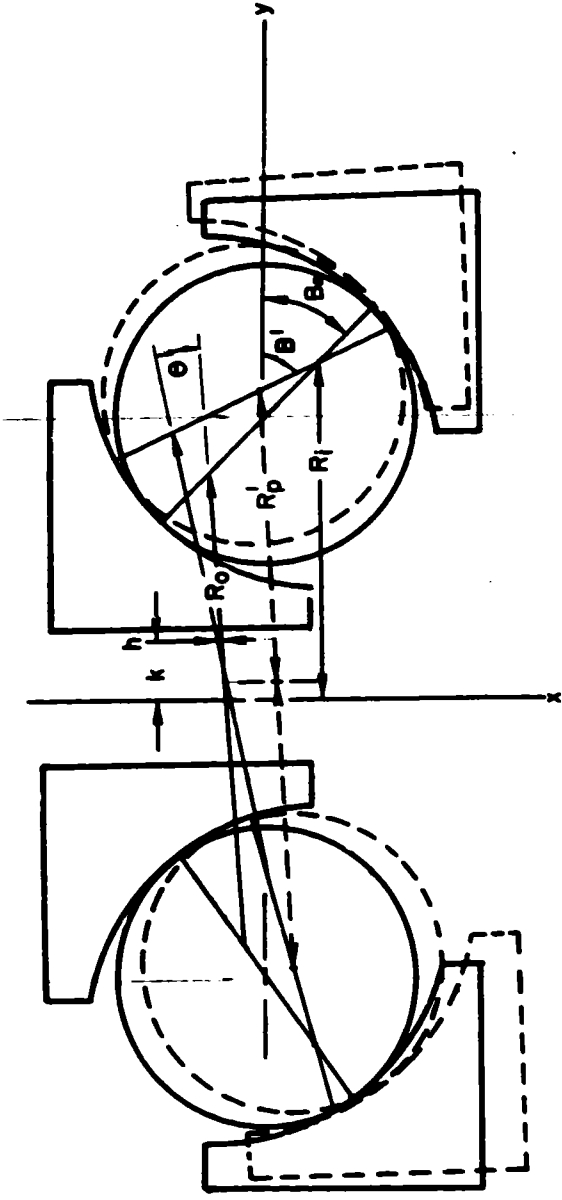
$$\text{SINB}' = \frac{R_0 \theta}{A} \text{COS}\psi + \text{SINB}_0$$

A is the distance between curvature centers.

The above equation is presented graphically in Figure 5.7.2. A one minute angle of misalignment introduces about 4.5% peak to peak variation in contact angle. The degree this affects radial stiffness and shaft assembly dynamics is yet to be determined.

An analysis to determine the stiffness variation is in work. "SHABERTH I" was coded to evaluate the stiffness variation with misalignment, but failed to run. "SHABERTH II" was subsequently coded to include outer race misalignment and it ran. Additional runs for "SHABERTH II" are being submitted and the results will be provided in the next progress report. These results will be bearing radial stiffness values that can be input to a bearing dynamic model for evaluating rotor/shaft dynamics.

ORIGINAL DESIGN
OF POOR QUALITY

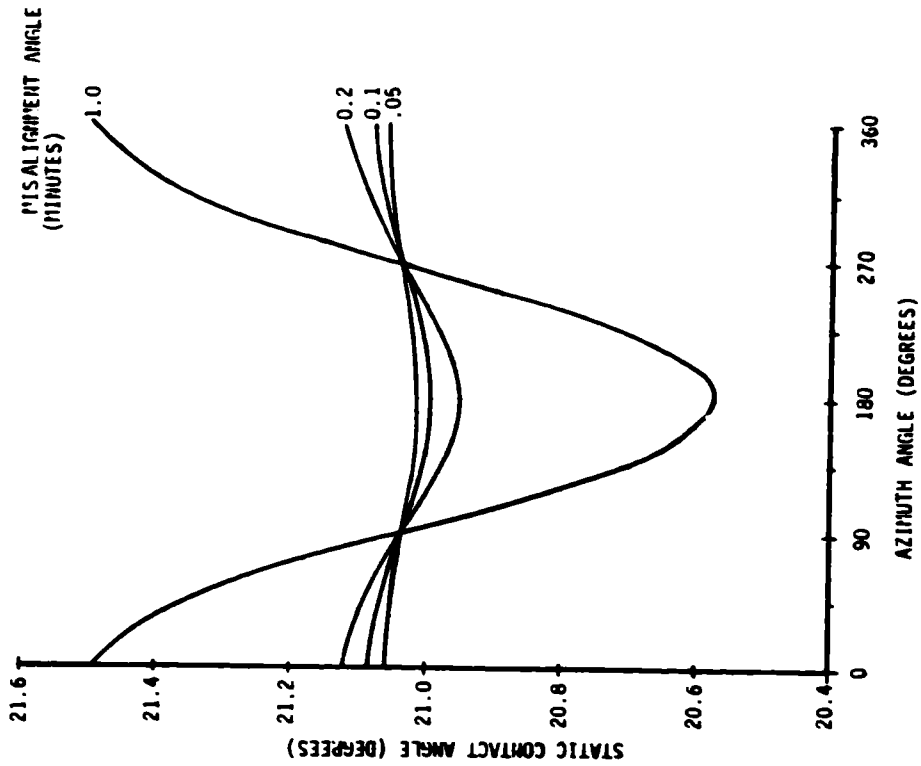


- R_i = INNER RACE RADIUS
- R_p = OUTER RACE RADIUS
- B_0 = INITIAL CONTACT ANGLE
- ψ = AZIMUTH ANGLE
- R'_p = PITCH RADIUS AFTER MISALIGNING OUTER RACE
- B' = CONTACT ANGLE AFTER MISALIGNMENT
- h = DISPLACEMENT OF OUTER RACE RADIUS ALONG X-AXIS
- k = DISPLACEMENT OF OUTER RACE RADIUS ALONG Y-AXIS
- θ = MISALIGNMENT ANGLE

FIGURE 5.7.1 DISPLACEMENT OF OUTER RACE WITH INNER RACE FIXED

SRS

FIGURE 5.7.2 CHANGE IN CONTACT ANGLE AS FUNCTION OF OUTER RACE MISALIGNMENT AND AZIMUTH LOCATION



ORIGINAL PAGE IS
OF POOR QUALITY

SRS

5.7.2 STATUS OF BEARING RADIAL STIFFNESS ANALYSIS

The analysis to evaluate bearing radial stiffness as function of ball wear has encountered a problem due to the Shaberth I computer program failing to converge for the cases of higher contact angles. The assumed ball wear increases the contact angle, reducing the radial stiffness, and causes larger deflections which in turn causes a convergence problem. Since Shaberth II has become operational, an attempt will be made to evaluate the problem with this computer code. Another option is to relax the convergence criteria, and see if the programs will run to completion.

5.7.3 ESTIMATION OF HEAT LOADS FOR THE BMT THERMAL MODEL

Heat is generated in the BMT from mechanical friction and viscous work done on the coolant. To realistically estimate bearing component temperature, this energy must be evaluated and applied correctly in the BMT thermal model. An estimate of the total energy generated can be obtained from an overall energy balance on previous test data. This was done in Section 5.3 and is shown in Figure 5.3.12. Once the total energy is determined, the problem remaining is to correctly evaluate the distribution of viscous and frictional energy. The bearing contact surface temperatures are obviously much more sensitive to frictional energy changes than changes in viscous energy.

The distribution of energy for the BMT thermal model, with LN₂ coolant, was evaluated as follows:

- 1) Estimate total energy generated from a heat balance on the coolant (see Figure 5.3.12 of Section 5.3.3).
- 2) Calculate the viscous energy generated by each component in the tester (see Figure 5.3.11 of Section 5.3.3).
- 3) Using measured torque values, estimate appropriate friction coefficients, and calculate friction energy distribution (i.e. inner race, outer race).
- 4) Adjust viscous energy distribution such that the total input matches the overall heat balance determined from test data.

Steps 1 and 2 had already been done and the results provided in Section 5.3.

Battelle (Reference 35) measured the bearing torque as a function of axial load and surface conditions. Figure 5.7.3 is a reproduction of their data. Also shown, for comparison, is the bearing torque predicted by Shaberth I. The predicted torque curve was generated using a friction coefficient of 0.2. The predicted curve is reasonably close to the PTFE burnished condition. The referenced value of friction coefficient for this surface condition is .08. The reason for this difference is not evident, however, since torque and heat are equivalent, a coefficient of friction of 0.2 in the Shaberth program provides a value reasonably close to the measurement. A further verification of the analysis is shown in Figure 5.7.4. This is data taken from the same reference, compared with results from the Shaberth I bearing analysis computer code. Although the calculated and measured axial deflections diverge with increased load, the contact angles agree fairly well. Consequently a friction coefficient of 0.2 was used in Shaberth to obtain frictional heat generation values required for the thermal model.

To complete the frictional heat evaluation the bearing load as well as the friction coefficient must be known. There is uncertainty in the axial load seen by the bearings due to the unknown pressure loss across the carriers. According to the

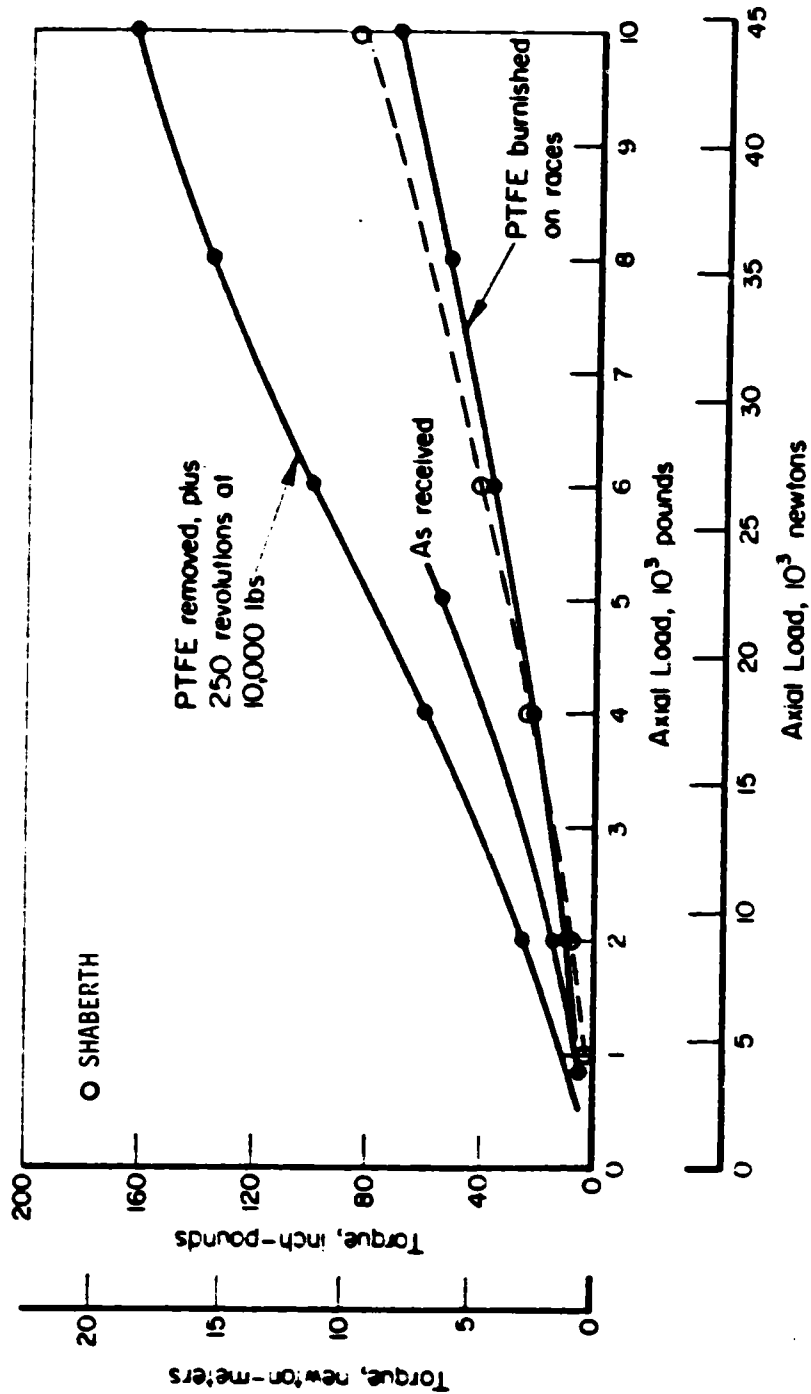


FIGURE 5.7.3 BEARING TORQUE AS A FUNCTION OF AXIAL LOAD

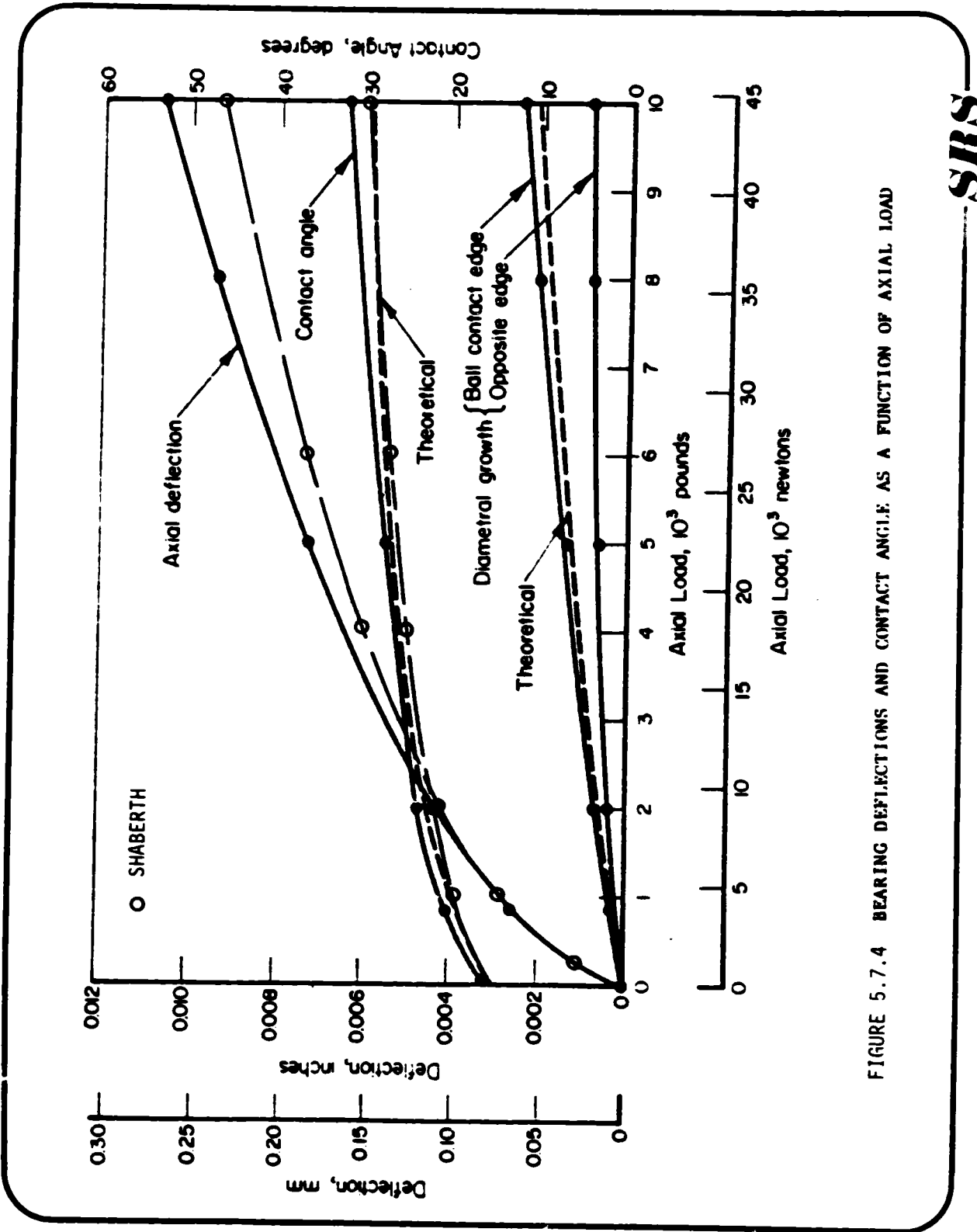


FIGURE 5.7.4 BEARING DEFLECTIONS AND CONTACT ANGLE AS A FUNCTION OF AXIAL LOAD

SRS

measured ΔP the axial load on the bearing should be about 2500 pounds. Although this value is suspect because of fluid vortices, it is probably the most representative at this time.

Therefore this axial load in combination with a friction value of 0.2 was used to estimate the frictional heat generated. The amount of friction energy was subtracted from the total measured energy, and the remainder was assumed to be viscous. The viscous energy was distributed in the proper proportions as indicated by the viscous work analysis done in Section 5.3. It was assumed that no lubrication was provided by the LN_2 coolant. This assumption will be reevaluated for the analyses of the LOX coolant.

Another important parameter, with a high degree of uncertainty, is the two phase heat transfer coefficient. There is no experimental data on this parameter that corresponds to the operating conditions of the bearing. Therefore, extrapolations have been made to estimate these parameters for the thermal model. The uncertainty in these extrapolations are unknown.

The above points out two critical areas of cryogenic bearing analysis requiring experimental work: 1) Evaluation of the friction coefficient for high speed bearings using film transfer lubrication in cryogenics, and 2) Evaluation of two phase heat transfer coefficients for high speed bearings in cryogenics.

5.7.4 STATUS AND RESULTS OF BEARING THERMAL MODEL

The Bearing Thermal Model has been refined to better represent actual thermal conditions in the tester. The modification consisted of changing several boundary nodes along the outer edge of the modeled portion of the bearing set. This change allows the Bearing Thermal model program to iteratively calculate a temperature for this boundary area rather than inputting a boundary temperature which would affect the steady state temperatures of surrounding nodes.

An iteration procedure has been developed to determine the temperature gradient across the BMT bearing utilizing the "SHABERTH" bearing program and the Bearing Thermal Model. A specific axial reaction is selected for analysis and put into the "SHABERTH" data base which is set up with configuration data for a 57 mm bearing. A first estimate temperature gradient across the bearing is assumed and added to the data base along with appropriate temperature varying thermal property data for the shaft, inner race, rolling element, outer race and housing. A friction coefficient of 0.2 was used for reasons outlined in Section 5.7.3. The "Shaberth" model is then exercised with this data base and the resultant information contains the frictional heat generated at the track areas of the races and rolling element for a specific axial reaction. This heat, generated from mechanical friction, is input into the Bearing Thermal Model data base along with heat generated from viscous work done on the coolant. At this time, there are twelve data bases for the Bearing Thermal Model, each reflecting a different mass flow rate through the bearing set and a different degree of subcooling or inlet coolant temperature as shown in Table 5.7.1.

spectra research systems

| Bearing Thermal Model Data Base Number | 1 | 2 | 3 | 4 | 5 | 6 | 7 | 8 | 9 | 10 | 11 | 12 |
|---|------|------|------|------|------|------|------|------|------|------|------|------|
| Inlet Coolant Temperature (°C) | -176 | -187 | -202 | -176 | -187 | -202 | -176 | -187 | -202 | -176 | -187 | -202 |
| Mass Flow Rate (LB/SEC) Per Bearing Set | 3.2 | 3.2 | 3.2 | 6.3 | 6.3 | 6.3 | 9.6 | 9.6 | 9.6 | 12.8 | 12.8 | 12.8 |

TABLE 5.7.1 SUMMARY OF BEARING THERMAL MODEL DATA BASE

The Thermal Model is then exercised for a specific data base with the resulting output being steady state temperatures for each node. The average temperature for each bearing component (i.e., shaft, inner race, rolling element, outer race, and housing) is then calculated as shown.

$$T_A = \frac{1}{N} \sum_{i=1}^N T_i V_i$$

T_i = Temperature of Node
 V_i = Volume of Node
 N = Total Number of Nodes

Presently, the steady state node temperatures are being manually input into a computer program which calculates the average temperature of each of the bearing components. The thermal property data is then manually computed from derived curve fit equations for each average temperature. Future plans include the implementation of coding into the Bearing Thermal Model to handle all of these calculations which will facilitate faster turnaround on each run.

The average temperature values for the bearing components are then placed back into the "SHABERTH" data base and replace the original assumed values. Appropriate temperature varying thermal property data is also replaced in the data base. The "SHABERTH" program is then executed again to determine new frictional heat generation data. This data is compared with the previously obtained values to determine whether another iteration is required. It is important to obtain not only the correct ΔT across the bearing, but also the correct bearing component temperatures. The ΔT across the bearing changes the bearing internal clearance. Reduced clearance results in a larger load on the bearing which in turn increases the frictional heat generated. The individual component temperatures are used to determine such thermal property data as the coefficient of thermal expansion and the modulus of elasticity, the values of which, also affect the bearing internal clearances.

The iteration procedure outlined above was performed for an axial reaction of 2500 pounds. The operating parameters; inlet coolant temperature of -176°C and mass flow rate of 3.2 LB/SEC per bearing set, were selected for a "worst case" situation. The results of this iteration are shown in Table 5.7.2. The preliminary frictional heat generation data was obtained from a "SHABERTH" run with an initial assumed ΔT across the bearing of 200°C . This temperature gradient was then resubmitted into the "SHABERTH" bearing data base along with a friction coefficient of 0.2. The first iteration frictional heat generation data is significantly smaller than the preliminary data. Therefore, the Bearing Thermal Model does not support the original assumption of a 200°C ΔT across the bearing. A second iteration shows the heat generation data holding relatively constant which supports a preliminary ΔT across the bearing of 25°C .

| BEARING COMPONENT | *PRELIMINARY FRICTIONAL HEAT GENERATION DATA (Btu/hr) | AVERAGE TEMPERATURES FROM BEARING THERMAL MODEL (°C) | FIRST ITERATION FRICTIONAL HEAT GENERATION DATA (Btu/hr) | AVERAGE TEMPERATURES FROM BEARING THERMAL MODEL (°C) | SECOND ITERATION FRICTIONAL HEAT GENERATION DATA (Btu/hr) |
|-------------------|---|--|--|--|---|
| INNER RACE | 1001 | -128 | 537 | -137 | 558 |
| ROLLING ELEMENT | 1805 | -44 | 954 | -122 | 953 |
| OUTER RACE | 804 | -137 | 416 | -162 | 395 |

TABLE 5.7.2

PRELIMINARY TEMPERATURE ITERATION RESULTS FOR 2500 POUND AXIAL REACTION MASS FLOW RATE = 3.2 LB/SEC PER BEARING SET INLET COOLANT TEMPERATURE = -176°C (-285°F)

(HEAT GENERATION DATA IS FOR 1/13 OF A BEARING; OR ONE ROLLING ELEMENT)

*DATA OBTAINED FROM PRELIMINARY SHABRETH RUN USING ΔT ACROSS THE BEARING OF 200°C AND A FRICTION COEFFICIENT OF 0.14

SRS

and average temperatures of -137°C , -122°C and -162°C for the inner race, rolling element, and outer race respectively. This indicates a stable set of thermal conditions, i.e., the heat generated and bearing temperatures do not increase without limit, as will be shown later, they do with these conditions at higher axial loads.

Figure 5.7.5 illustrates the temperature gradient of the inner race ball track area for an axial reaction of 2500 pounds, a mass flow rate of 6.3 LB/SEC per bearing set and a coolant temperature of -187.2°C (-305°F). This data indicates a rather large temperature gradient of approximately $1800^{\circ}\text{C}/\text{inch}$ in the inner race.

An iterative temperature analysis was also performed for a 6000 pound axial reaction using "worst case" operating conditions (mass flow rate of 3.2 LB/SEC per bearing set and inlet coolant temperature of -176°C). These results are shown in Table 5.7.3 and after five iterations, failed to converge. This diverging situation indicates incipient bearing failure due to a runaway thermal condition. Figure 5.7.6 shows the relationship between the ΔT across the bearing as a function of the total frictional heat generation rate for one rolling element (1/13 of a bearing). This graph indicates that Q could go catastrophically high for a ΔT as small as 100°C , for this loading condition. Therefore, a failure is predicted for these specific test conditions.

Further iterative analyses and temperature evaluations will be performed for the 6000 pound axial reaction situation utilizing higher flow rates and colder inlet coolant temperatures in an attempt to converge on an acceptable set of heat generation data and temperatures. Other axial reactions will also be evaluated over a range of operating conditions to assimilate the data necessary to construct a safe operating range envelope for the bearing tester.

In summary, the dynamic and thermal analyses of the BMT 57 mm bearing has simulated an unstable operating condition leading to thermal failure of the bearing. Obviously, as contact surfaces (raceways) become extremely hot, the question of temperature effects on lubrication and friction become extremely important, i.e., at what temperature does the dry film lubricant breakdown. This temperature may be the limiting temperature for acceptable bearing operation.

5.8 FEBRUARY, 1983

5.8.1 ESTIMATION OF FILM THICKNESS FOR 57 mm BEARING OPERATING IN LN_2

A cursory analysis was done to provide an "order of magnitude" estimate of the fluid film thickness for the 57mm bearing operating in LN_2 . Although the viscosity of N_2 is over two orders of magnitude less than typical lubricating oil, the high speed of the bearing could partially compensate and provide some measure of separation of the contact surfaces. This could be an aid to the solid film lubricant in providing contact lubrication.

There are several major drawbacks in using current techniques to estimate fluid film thickness in N_2 . These techniques have been developed for lubricating oils and such characteristics as compressibility, phase type, and extreme variations in temperature have not been considered. Furthermore, there is a lack of viscosity data for N_2 at the high pressures encountered in the contacts. Therefore, the error due to extrapolation to these pressures is not known. The assumption of incompressibility should provide optimistic values of film thickness. The assumed variation of viscosity with pressure (exponential law) could also be optimistic.

ORIGINAL PAGE IS
OF POOR QUALITY

| BEARING COMPONENT | INNER RACE | ROLLING ELEMENT | OUTER RACE |
|---|------------|-----------------|------------|
| *PRELIMINARY FRICTIONAL HEAT GENERATION DATA (Btu/hr) | 1448 | 2598 | 1151 |
| AVERAGE TEMPERATURES FROM BRG. THERMAL MODEL (°C) | -128 | -44 | -137 |
| FIRST ITERATION FRICTIONAL HEAT GENERATION DATA (Btu/hr) | 1726 | 3089 | 1363 |
| AVERAGE TEMPERATURES FROM BRG. THERMAL MODEL (°C) | -55 | 120 | -104 |
| SECOND ITERATION FRICTIONAL HEAT GENERATION DATA (Btu/hr) | 1858 | 3321 | 1463 |
| AVERAGE TEMPERATURES FROM BRG. THERMAL MODEL (°C) | -37 | 171 | -92 |
| THIRD ITERATION FRICTIONAL HEAT GENERATION DATA (Btu/hr) | 1945 | 3472 | 1527 |
| AVERAGE TEMPERATURES FROM BRG. THERMAL MODEL (°C) | -27 | 195 | -84 |
| FOURTH ITERATION FRICTIONAL HEAT GENERATION DATA (Btu/hr) | 2008 | 3584 | 1575 |
| AVERAGE TEMPERATURES FROM BRG. THERMAL MODEL (°C) | -22 | 212 | -80 |
| FIFTH ITERATION FRICTIONAL HEAT GENERATION DATA (Btu/hr) | 3813 | 6129 | 2316 |
| AVERAGE TEMPERATURES FROM BRG. THERMAL MODEL (°C) | 110 | 224 | 31 |

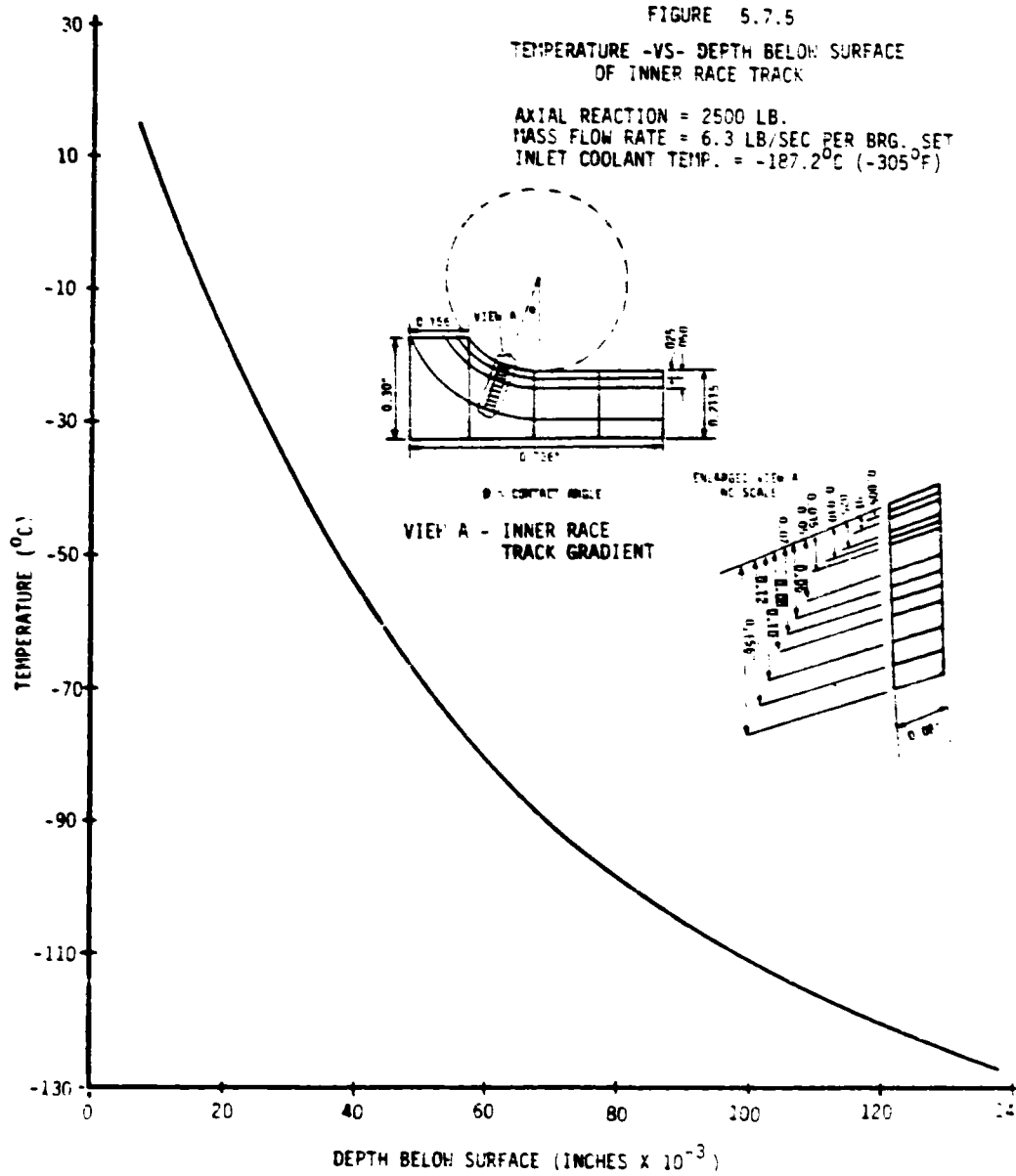
TABLE 5.7.3

PRELIMINARY TEMPERATURE ITERATION RESULTS FOR 6000 POUND AXIAL REACTION

MASS FLOW RATE = 3.2 LB/SEC PER BEARING SET
INLET COOLANT TEMPERATURE = -176°C (-285°F)

*DATA OBTAINED FROM SHABERTH RUN USING FINAL ITERATION ΔT ACROSS THE BEARING AND A FRICTION COEFFICIENT OF 0.2

SRS



ORIGINAL PAGE IS
OF POOR QUALITY

| BEARING COMPONENT | INNER RACE | ROLLING ELEMENT | OUTER RACE |
|---|------------|-----------------|------------|
| *PRELIMINARY FRICTIONAL HEAT GENERATION DATA (Btu/hr) | 1448 | 2598 | 1151 |
| AVERAGE TEMPERATURES FROM BRG. THERMAL MODEL (°C) | -128 | -44 | -137 |
| FIRST ITERATION FRICTIONAL HEAT GENERATION DATA (Btu/hr) | 1726 | 3089 | 1363 |
| AVERAGE TEMPERATURES FROM BRG. THERMAL MODEL (°C) | -55 | 120 | -104 |
| SECOND ITERATION FRICTIONAL HEAT GENERATION DATA (Btu/hr) | 1858 | 3321 | 1463 |
| AVERAGE TEMPERATURES FROM BRG. THERMAL MODEL (°C) | -37 | 171 | -92 |
| THIRD ITERATION FRICTIONAL HEAT GENERATION DATA (Btu/hr) | 1945 | 3472 | 1527 |
| AVERAGE TEMPERATURES FROM BRG. THERMAL MODEL (°C) | -27 | 195 | -84 |
| FOURTH ITERATION FRICTIONAL HEAT GENERATION DATA (Btu/hr) | 2008 | 3584 | 1575 |
| AVERAGE TEMPERATURES FROM BRG. THERMAL MODEL (°C) | -22 | 212 | -80 |
| FIFTH ITERATION FRICTIONAL HEAT GENERATION DATA (Btu/hr) | 3813 | 6129 | 2316 |
| AVERAGE TEMPERATURES FROM BRG. THERMAL MODEL (°C) | 110 | 224 | 31 |

TABLE 5.7.3

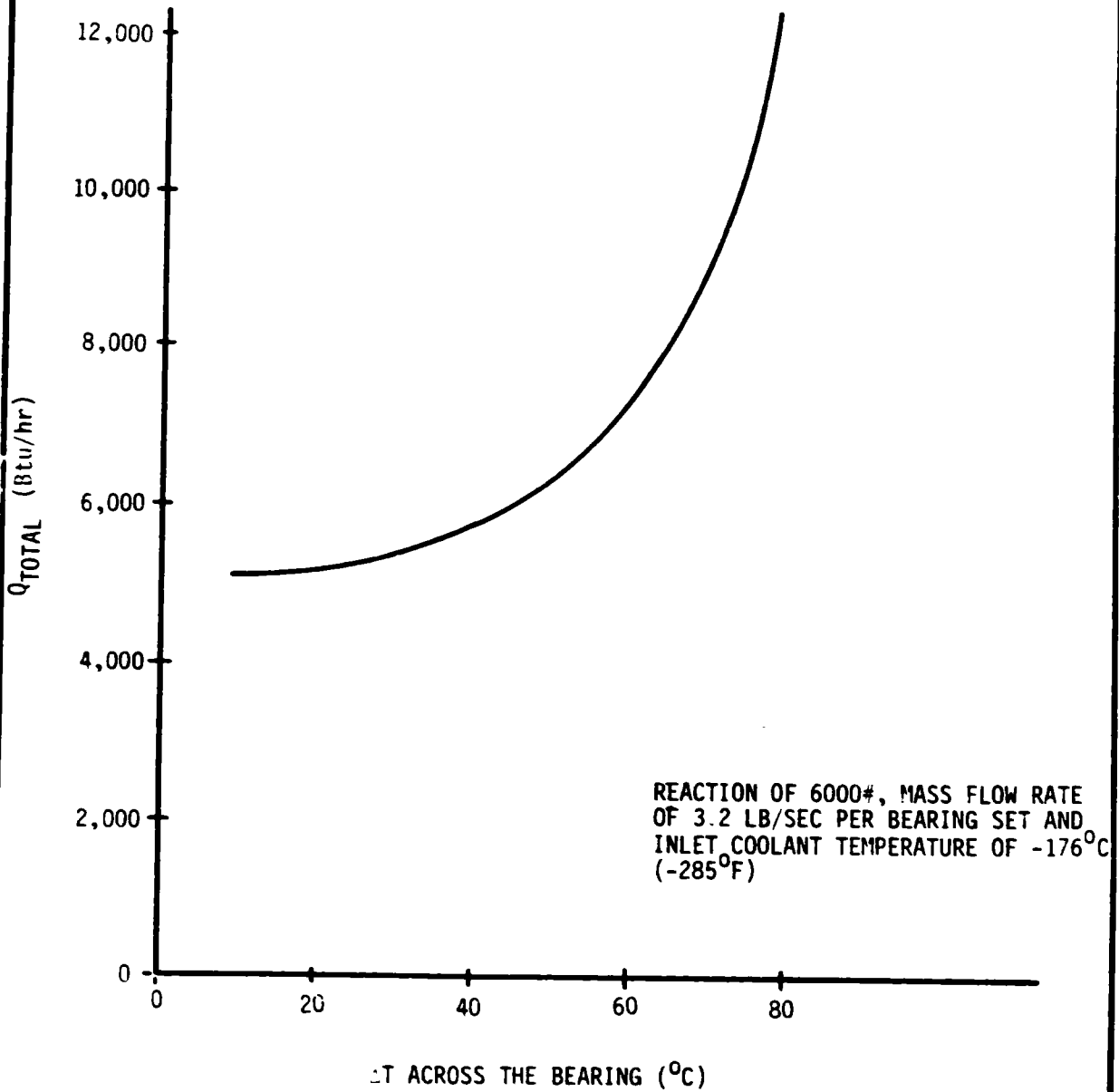
PRELIMINARY TEMPERATURE ITERATION RESULTS FOR 6000 POUND AXIAL REACTION

MASS FLOW RATE = 3.2 LB/SEC PER BEARING SET
INLET COOLANT TEMPERATURE = -176°C (-285°F)

*DATA OBTAINED FROM SHABERTH RUN USING FINAL ITERATION ΔT ACROSS THE BEARING AND A FRICTION COEFFICIENT OF 0.2

SRS

FIGURE 5.7.6 TOTAL FRICTIONAL HEAT RATE -VS- ΔT ACROSS THE BEARING



spectra research systems

The results of the film thickness estimates are shown in Figure 5.8.1. As the temperature increases, the film thickness decreases rather suddenly and then levels off. The sudden decrease is characteristic of a liquid, and the leveling off is similar to the behavior of a gas whose viscosity increases with temperature. The estimate was not carried past 1000°R since viscosity for higher temperatures was not available. Table 5.8.1 provides viscosity data at specified temperatures and pressures. Also shown are values for the pressure coefficient (λ) and μ'_0 . The significance of these parameters will be discussed later. Comparing μ'_0 with the viscosity values at 400 psia shows fairly good agreement at the lower and higher temperatures. Since the critical temperature of N_2 is 227°R, it is expected that the larger discrepancy at 300°R is due to rapidly changing properties near the critical point. N_2 properties were taken from Reference 35.

As shown, the film thickness varies from about 1.8μ to $.033\mu$ inches. Since the surface finish of the balls and races are 0.5μ and 6μ inches respectively, the ratio of film thickness to asperity height varies from 0.3 to 0.05. Furthermore, thermal analyses of the bearings indicate that the race way temperatures are considerably greater than 170°R. Consequently, the film thickness to roughness ratio would be considerably less than 0.3. Bearing life adjustment factors, due to lubrication, does not affect life predications for film thickness to roughness ratios less than about 0.08. In fact, SHABERTH I assumes dry friction for ratios less than 0.4. (See Section 5.5.)

Following is an outline of the method used to provide the estimated film thickness data shown in Figure 5.8.1.

Gurbin's formula for fluid film thickness is (see Reference 1):

$$h^3 = 1.95 R \frac{(GU)^{0.727}}{Q_z^{0.091}}$$

$$G = \lambda E'$$

λ = Pressure Coefficient of Viscosity

$$\bar{U} = \frac{\mu'_0 U}{E' R}$$

μ'_0 = Fluid Viscosity as Reference Pressure

$$\bar{Q}_z = \frac{Q_z}{4E'R}$$

R = Equivalent Radius

$$E' = \frac{E}{1-\nu^2}$$

U = Entrainment Velocity
= $(u_1 + u_2)/2$

E = Modulus of Elasticity

ν = Poisson's Ratio

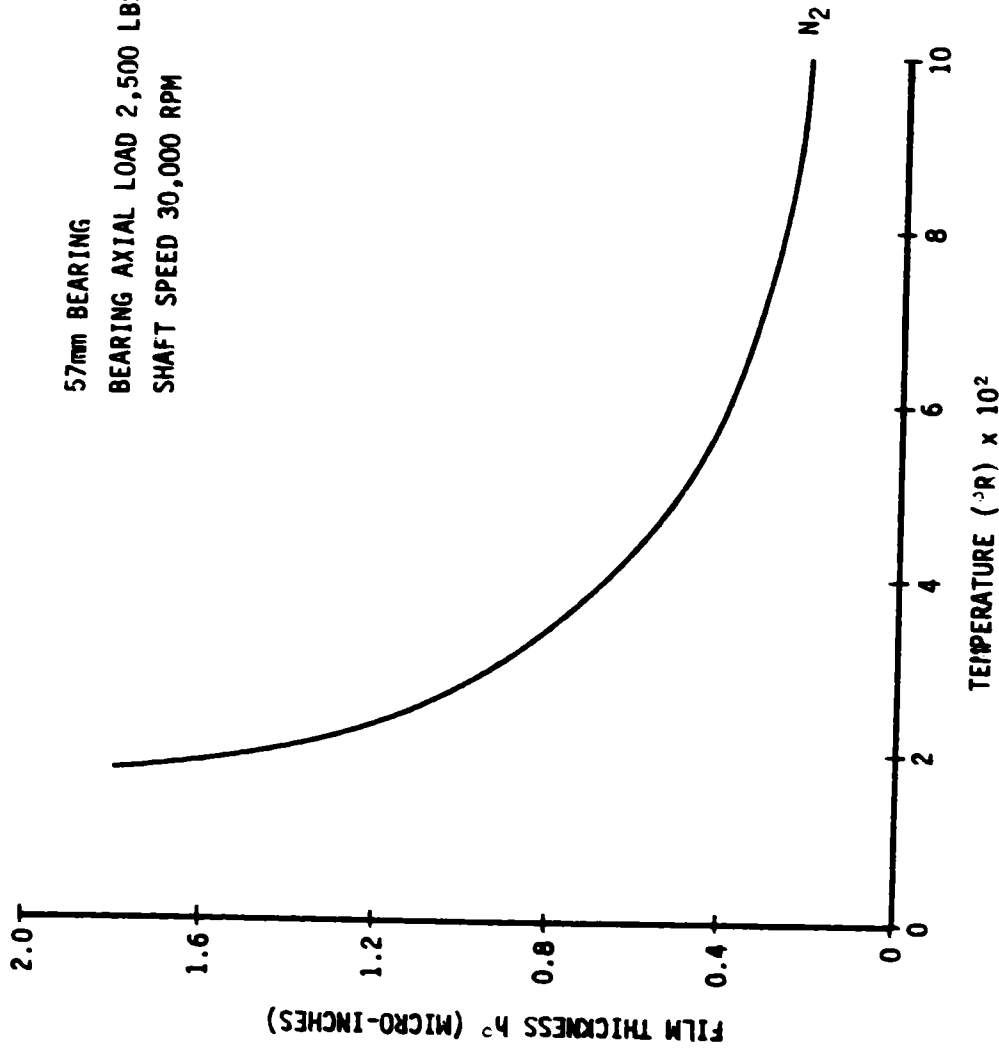
(For Rolling Elements
of Same Material)

This expression was developed from the incompressible Reynolds equation and elastohydrodynamic considerations including effects of contact surface deformation. The fluid viscosity is assumed to vary exponentially with pressure, and temperature is assumed to be constant. As given above, the expression is for line contact and must be slightly modified to represent ball bearings (point contact).

The terms in the above expressions are developed and grouped as follows:

FIGURE 5.8.1 ESTIMATED FILM THICKNESS vs. TEMPERATURE FOR N₂

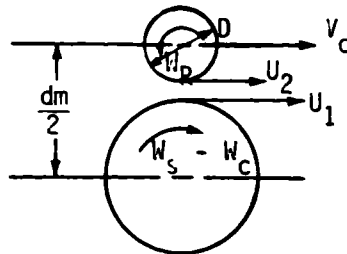
57mm BEARING
BEARING AXIAL LOAD 2,500 LBS
SHAFT SPEED 30,000 RPM



ORIGINAL DATA
OF POOR QUALITY

SRS

ENTRAINMENT VELOCITY



W_s = Shaft Speed

W_c = Cage Speed

α = Contact Angle

To determine the fluid entrainment velocity U refer to the above figure.

$$U_1 = 1/2 (dm - D \cos \alpha) (W_s - W_c)$$

$$U_2 = \frac{D}{2} W_c \cos \alpha$$

For pure rolling, $U_1 = U_2$, and

$$U = 1/2 (W_s - W_c) \left[\frac{1-\gamma}{\gamma} \right] D \cos \alpha ; \quad \gamma = \frac{D}{dm} \cos \alpha$$

to express W_c in terms of W_s note that the cage velocity V_c is 1/2 the absolute shaft velocity V_i , i.e.

$$V_c = 1/2 dm W_c = 1/2 V_i$$

$$V_i = W_s (dm/2 - D/2 \cos \alpha) = 1/2 W_s dm (1-\gamma)$$

$$1/2 dm W_c = 1/2 \left[1/2 W_s dm (1-\gamma) \right]$$

$$W_c = 1/2 W_s (1-\gamma)$$

Substitution of W_c in the expression for U gives:

$$U = \frac{D}{4} W_s \left[\frac{1+\gamma}{\gamma} \right] \left[1-\gamma \right] \cos \alpha$$

Therefore, the entrainment fluid velocity can be expressed in terms of bearing geometry, contact angle, and shaft speed.

EQUIVALENT RADIUS (R):

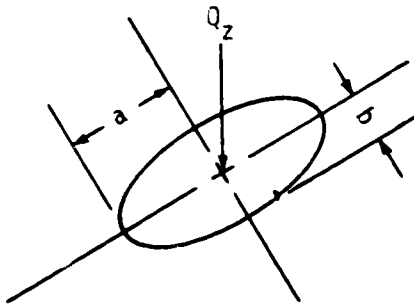
$$R = \frac{1}{\frac{1}{R_1} \pm \frac{1}{R_2}} = \frac{R_1 R_2}{R_1 \pm R_2} = \frac{1/2 D (1-\gamma) \cos \alpha}{(1-\gamma) \cos \alpha + \gamma}$$

For small values of α , $\cos \alpha \approx 1$, and

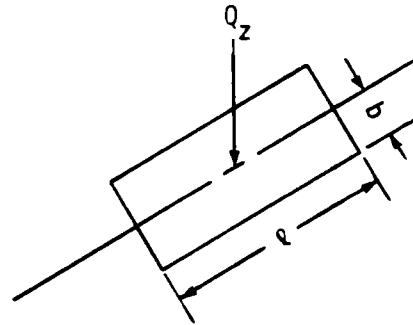
$$R = 1/2 D (1-\gamma)$$

LOAD PER UNIT LENGTH:

As stated earlier, the expression for Q_z is for line contact and, for use with ball bearings, should be modified to represent point contact. The following represents the two contact configurations.



Point Contact



Line Contact

The maximum Hertz Pressure for point contact and line contact are as follows:

$$\sigma_{mp} = \frac{3 Q_z}{2\pi ab} \quad (\text{Point Contact})$$

$$\sigma_{ml} = \frac{2 Q_z}{\pi l b} \quad (\text{Line Contact})$$

Assuming equal Hertz pressures and loads for both contacts gives an equivalent length l_E for the point contact.

$$l_E = \frac{4a}{3}$$

The dimensionless terms in Gurbin's equation can now be written as:

$$G = \gamma E'$$

$$U = \frac{W_s}{E'} \left[\frac{W_s}{2} \right] \left[\frac{1-\gamma}{\gamma} \right] \cos \alpha$$

$$P_z = \frac{3}{2} \frac{Q_z}{a E' D (1-\gamma)}$$

$$E' = \frac{E}{1-\nu^2}$$

and Gurbin's equation can be expressed as:

$$h^3 = 0.228 \left[1/2 D (1-\gamma) \right]^{1.091} \left[W_s \frac{1+\gamma}{\gamma} \cos \alpha \right]^{.727} \left[\mu'_0 \right]^{.727} \left[\frac{4aE'}{3 Q_z} \right]^{.091}$$

spectra research systems

ORIGINAL PAGE IS
OF POOR QUALITY

where W_s = shaft speed in RPM

λ = pressure coefficient (in²/lb)

μ_0' = viscosity (lbs-sec/in²)

$E' = 33 \times 10^{-6}$ psi for steel bodies

This arrangement of variables illustrates the effects of speed, viscosity, and load on film thickness. The speed and viscosity parameters are raised to the same power and, therefore, are equally influential. The lower power value for the term containing the load renders the film thickness rather insensitive to load changes. Although high shaft speed can offset low fluid viscosity, the viscosity for N_2 is so low that the high speed of the tester is still insufficient to provide an adequate film thickness.

ESTIMATION OF INITIAL VISCOSITY AND PRESSURE COEFFICIENT (λ):

The exponential law relating viscosity to pressure used in Gurbin's equation is as follows:

$$\mu = \mu_0 e^{\lambda P}$$

This implies that at $P=0$, $\mu = \mu_0$. Since the internal pressure of the bearing tester is approximately 400 psia, a correction was made to μ_0 to account for this pressure level.

$$\mu = \mu_0 e^{\lambda(P-P_0)} = (\mu_0 e^{-\lambda P_0}) e^{\lambda P}$$

The parameter $\mu_0' \equiv (\mu_0 e^{-\lambda P_0})$ is used as the ambient viscosity in the film thickness expression. The pressure coefficient for each temperature level was determined as follows:

$$\lambda = \frac{1}{(P_1 - P_2)} \ln \frac{\mu_1}{\mu_2}$$

The values of μ_1 , μ_2 , P_1 and P_2 are shown in Table 5.8.1. The estimated values of λ and μ_0' are also given in this table.

5.8.2 BEARING RADIAL STIFFNESS AS A FUNCTION OF BALL WEAR

The SHABERTH I computer code was used to evaluate bearing radial stiffness as a function of ball wear. Although the highest level solution would not converge, a lower level solution that still considered friction was obtained. Judging by the few third level computer runs that did converge, the calculated radial stiffness of the bearing did not differ significantly between solution levels.

Four radial loads (100, 200, 300, and 500 lbs) were applied to bearings at five different stages of ball wear. The results of these runs are shown in Figure 5.8.2. This analysis suggests that even a decrease in ball diameter of 0.0008 inches is enough to reduce the radial stiffness by half.

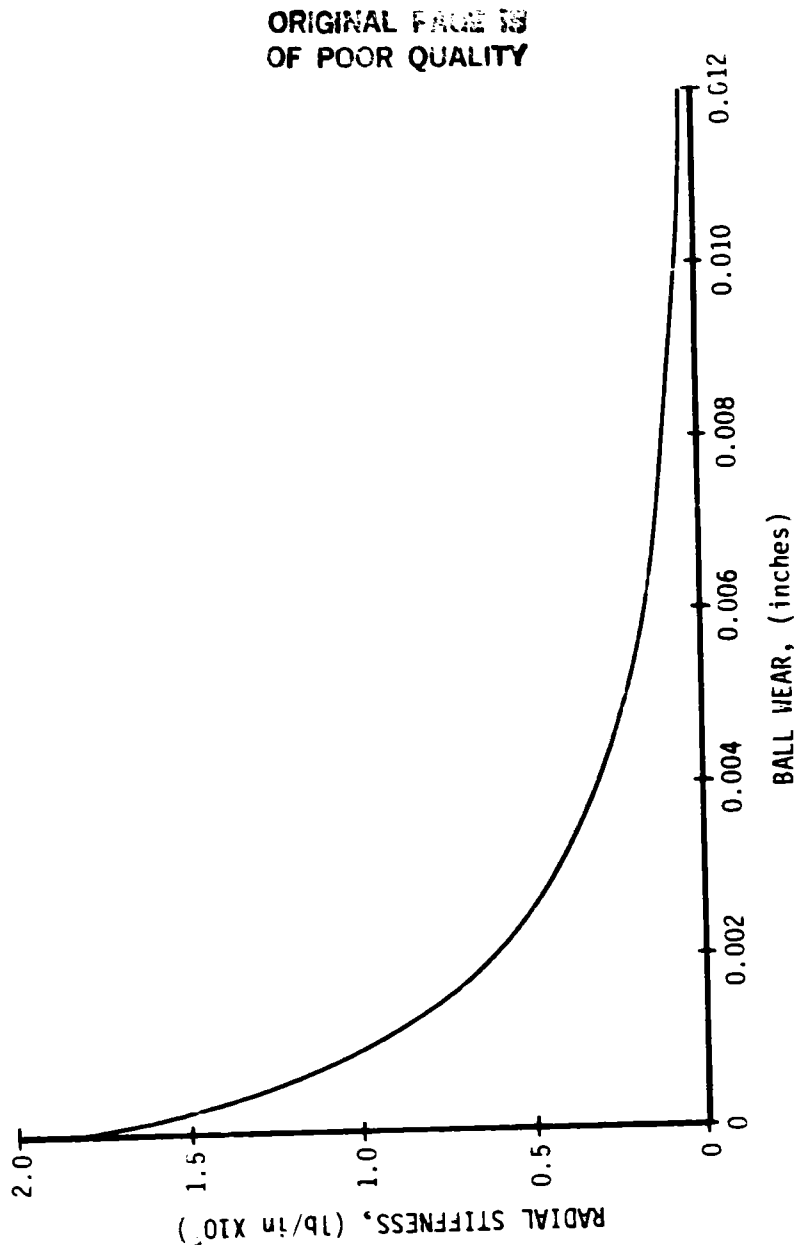
TABLE 5.8.1 (N₂) VISCOSITY

| TEMP °R | 400 | 4000 | 5000 | | $\mu_0 \times 10^{-8}$ |
|------------|---------|-------|-------|--|------------------------|
| 170 | * 1.497 | 2.31 | 2.55 | | 1.562 |
| 300 | 0.177 | 0.658 | 0.785 | | 0.3242 |
| 500 | 0.254 | 0.354 | 0.393 | | 0.233 |
| 1000 | 0.411 | 0.449 | 0.459 | | 0.41 |

* VISCOSITY $\left(\mu \times 10^{-8} \frac{\text{LB} \cdot \text{SEC}}{\text{IN}^2} \right)$

SRS

FIGURE 5.8.2 CHANGE IN RADIAL STIFFNESS AS A FUNCTION OF BALL WEAR



5.8.3 STATUS AND RESULTS OF BEARING THERMAL MODEL

During this reporting period, the assimilation of data necessary to construct a safe operating range envelope for the bearing tester has continued. The criteria for establishing the "safe" operating region is stable thermal operating conditions for the bearing. As the bearing temperature increases, internal clearances are reduced, thus increasing loads and generating additional heat and further increasing temperatures. If bearing coolant is insufficient to check this cycle, bearing temperatures will increase without bound and failure will occur. These analyses have assumed the friction coefficient to be invariant with temperature because data on temperature effects are not available. In some cases, the high race and ball track temperatures may invalidate this assumption due to breakdown of the dry film lubricant. Therefore, caution should be exercised in operating at the lower left hand corners of the regions shown in Figure 5.8.3 and at the higher loads.

The iterative procedure outlined in Section 5.7.4 was performed for an axial reaction of 6000 pounds. Four of the twelve cases examined resulted in an acceptable convergence upon heat generation data and bearing component temperatures. Each case consisted of a different combination of inlet coolant temperature and mass flow rate. This data is presented in Figure 5.8.3. The larger rectangle represents the 2500 pound axial reaction investigation in which all combinations of flow rates and inlet temperatures examined converged on an acceptable set of heat generation data and temperatures. Areas to the left and below the cross hatched lines in the large rectangle are areas of decreased flow rate and increased inlet coolant temperature and could be potentially hazardous operating areas for the bearing tester for an axial reaction of 2500 pounds. The dotted lines bound areas outside of which conditions being increased flow rate or decrease bearing component temperatures (these conditions being increased flow rate or decreased inlet temperatures).

The smaller rectangle in Figure 5.8.3 represents the safe operating area for an axial reaction of 6000 pounds. In this investigation, one case examined (flow rate of 6.3 lb/sec per bearing set and inlet coolant temperature of -331°F) was not clearly defined as a converging or diverging point in the number of iterations performed. Thus, an area of uncertainty exists as illustrated in Figure 5.8.3 by the lined triangular area attached to the smaller or 6000 pound rectangle. Further analysis will be performed on this case to clearly determine whether this case will converge on an acceptable set of heat generation data and bearing component temperatures.

Areas to the left and below the cross hatched lines on the smaller rectangle (6000 pound axial reaction case) could be potentially hazardous operating areas for the bearing tester for an axial reaction of 6000 pounds due to the effect of increasing inlet coolant temperatures and decreasing flow rate. Table 5.8.2 summarizes the total number of computer iterations required to generate the data necessary for Figure 5.8.3. A total of 100 different computer runs were executed for both the 2500 pound and 6000 pound axial reactions combined.

In summary, several potentially unstable operating areas have been identified for the bearing tester. Further dynamic and thermal analysis will be performed for other values of axial reactions to further generate data for the development of an acceptable operating envelope for the bearing tester. It should be emphasized that the "safe" operating regions, based on thermal runaway criteria, is for operation in LN_2 . This criteria may not apply to bearings operating in LOX . The criteria for LOX may be the race and/or ball track temperatures and the temperature limits of the dry film lubrication. In fact, caution should be exercised in operating near the lower left cross

ORIGINAL PAGE IS
OF POOR QUALITY

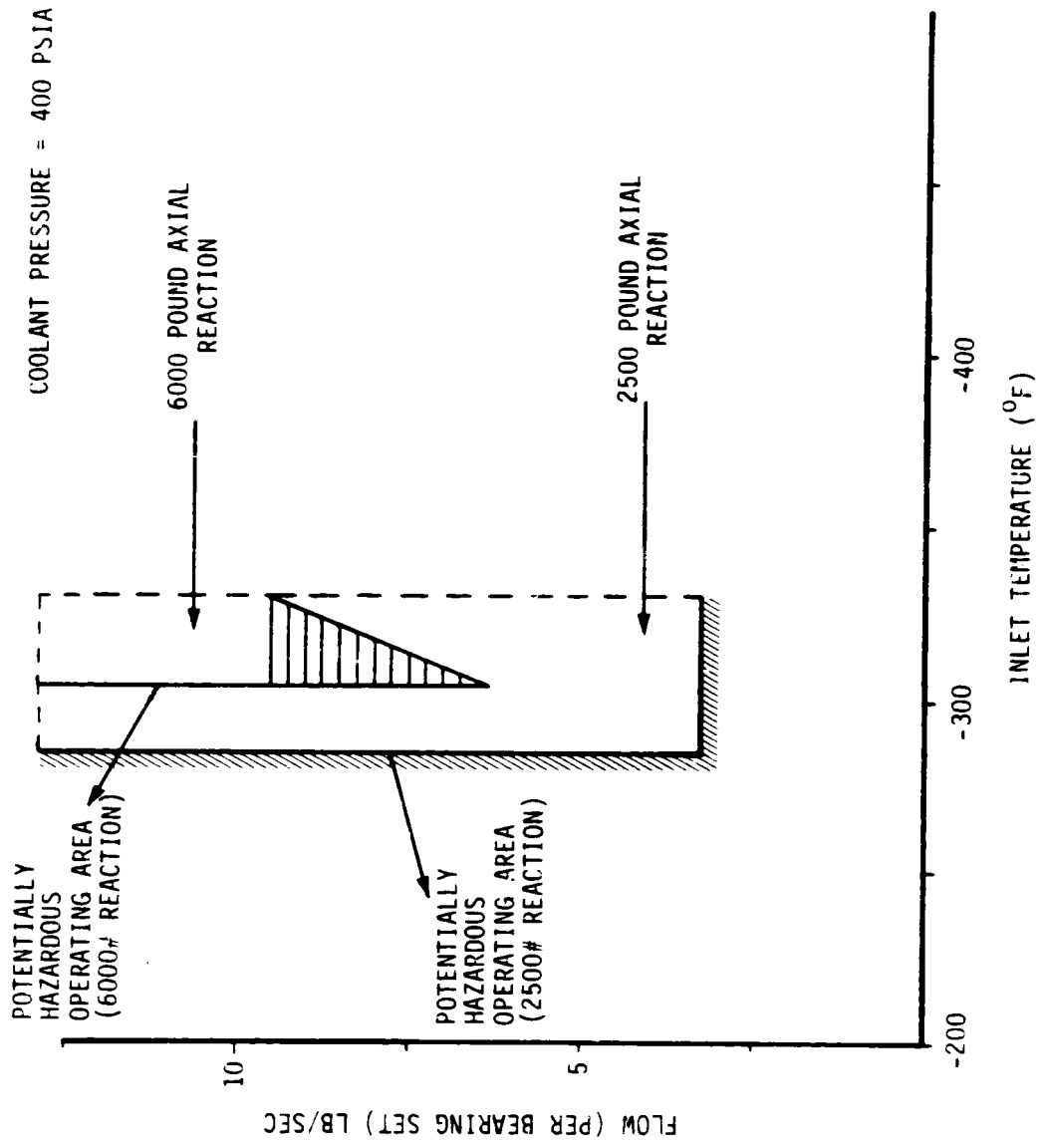


FIGURE 5.8.3
SAFE OPERATING RANGE IN LN₂ FOR 2500 POUND
AND 6000 POUND AXIAL REACTIONS

spectra research systems

hatched boundaries shown in Figure 5.8.3 as the analysis does not consider possible increased friction due to the potential for loss of dry film lubrication at high contact temperatures.

5.8.4 OUTER RACE MISALIGNMENT

An attempt has been made to determine the radial stiffness variation as a function of outer race misalignment. To date, a solution has not been obtained due to failure of the "SHABERTH" computer program to converge to a reasonable solution with outer race misalignment included. This problem was solved and results are given in Section 5.10.1.

5.9 MARCH, 1983

5.9.1 EFFECT OF FRICTION ON ROLLING ELEMENT CONTACT AND SUBSURFACE STRESSES

The effects of friction on the magnitude and distribution of normal and shear stresses in rolling element contacts has been investigated. Reference 37 contains general expressions for the normal and shear stresses for rolling elements producing line contact. Line contact allows the stress problem to be solved in closed form by the application of plane stress and plain strain assumptions. Although these assumptions do not hold for point contact, the trends identified in the line contact solutions should apply.

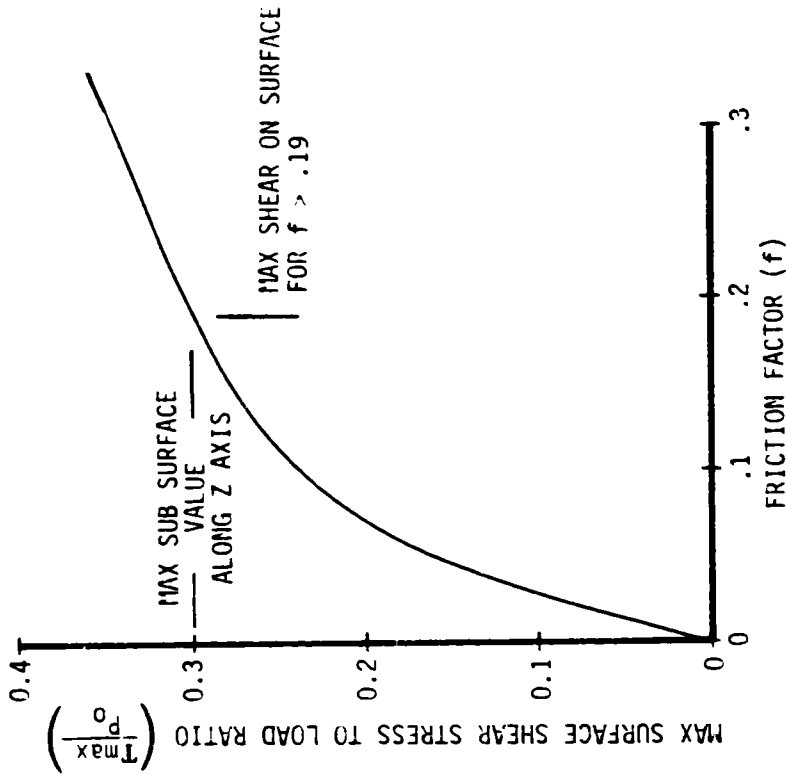
The effect of surface friction on the location of the maximum shear stress was determined by solving for shear stress and setting the derivative to zero. Figure 5.9.1 shows the results. As shown, the location of the maximum shear stress along the axis in the rolling direction (x axis) is a function of the coefficient of friction. Also shown is the expression of the maximum surface shear (T_{max}) as a function of friction. The maximum shear stress for zero friction occurs at a subsurface depth of ($z/a = 0.7861$), and the shear-to-load ratio is 0.3. This point is shown on the vertical axis of Figure 5.9.1. As shown in the figure, the maximum shear stress moves to the surface for friction factors greater than 0.19.

Shown in Figure 5.9.2 are the maximum surface principal stresses. As shown, these are all compressive stresses and occur in the surface (x/a) as a function of the friction factor. The maximum tensile surface stress is shown in Figure 5.9.3, and occurs at ($-x/a=1$) in the contact surface.

This analysis shows that the magnitude and location of the maximum contact stresses can be significantly affected by the friction force in the contact surface. Since these stresses increase with increased friction, this effect can be especially important for rolling elements with marginal lubrication such as high speed bearings operating in cryogenics. These trends may help explain the surface failures observed in cryogenic bearing tests as opposed to the more common subsurface failures observed in well lubricated bearings.

This analysis has been restricted to line contact, a similar analysis for point contact requires evaluation of a three dimensional stress field and can best be handled by finite element computer codes.

FIGURE 5.9.1 - MAXIMUM SURFACE SHEAR STRESS AS FUNCTION OF FRICTION COEFFICIENT
(LINE CONTACT)



a = HALF WIDTH OF CONTACT AREA
 P = NORMAL LOAD PER UNIT LENGTH
 MAX SURFACE SHEAR OCCURS AT

$$\left(\frac{x}{a}\right) = f \sqrt{\frac{1}{1+f^2}}$$

$$\frac{\tau_{max}}{P_0} = (.2) \left[\sqrt{1 + f^2} + 2.5f \right]$$

$$P_0 = \frac{2P}{\pi a}$$

COORDINATE SYSTEM

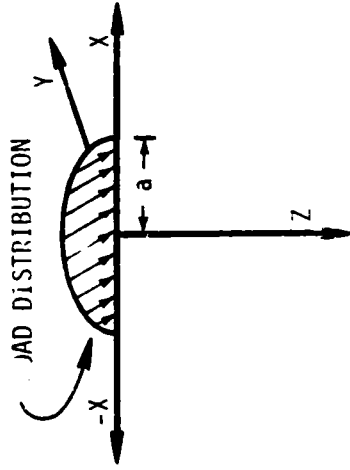


FIGURE 5.9.2 - MAXIMUM PRINCIPAL STRESSES IN SURFACE vs FRICTION
(LINE CONTACT)

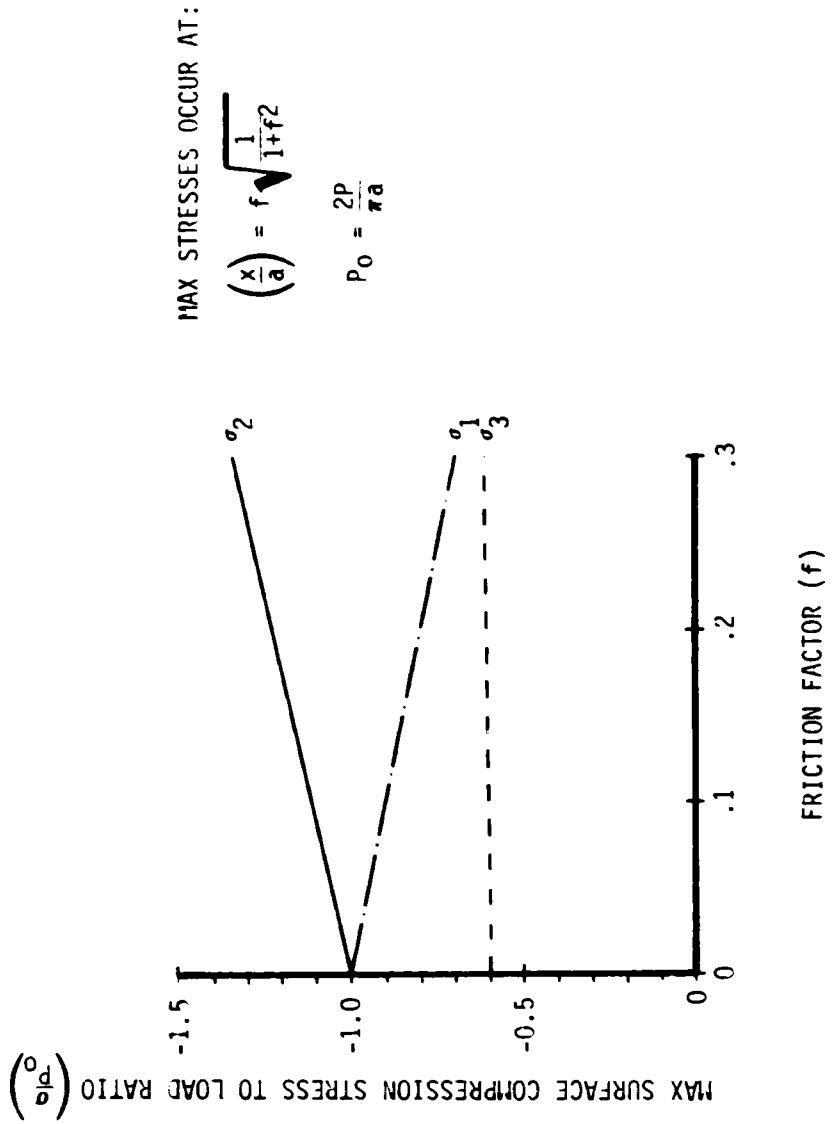
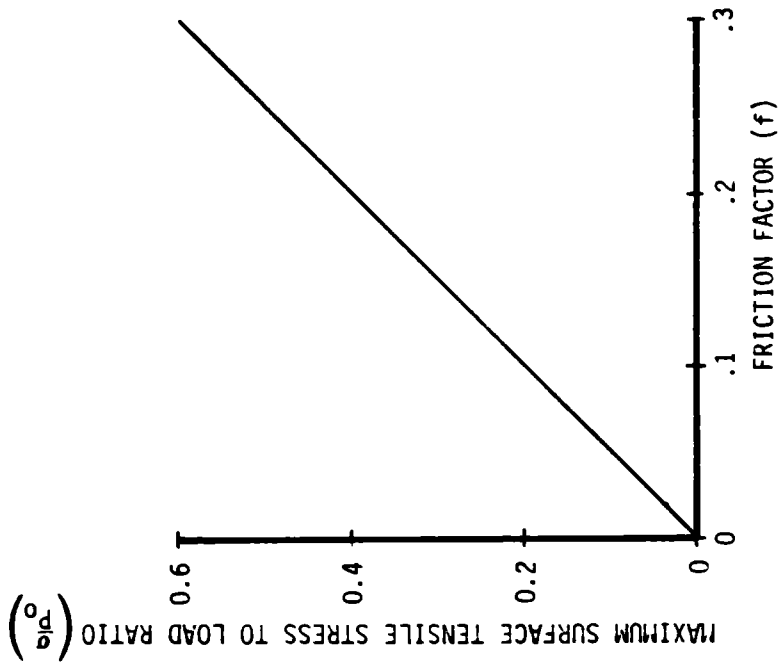


FIGURE 5.9.3 - MAXIMUM TENSILE SURFACE STRESS vs FRICTION
(LINE CONTACT)



MAX STRESSES OCCUR AT:

$$\left(\frac{x}{a}\right) = -1$$

$$\sigma_1 = 2(P_0)f$$

$$P_0 = \frac{2P}{\pi a}$$

ORIGINAL PAGE IS
OF POOR QUALITY

SRS

5.9.2 BEARING THERMAL MODELING AND ANALYSIS

The iterative analysis to determine a safe operating range envelope for the bearing tester, using LN₂ as a coolant, has continued during this reporting period. All cases examined for a 2500 pound axial reaction converged to stable bearing component temperatures. No points of convergence were found for an axial reaction of 10,000 pounds. A transient thermal analysis is being done on the 10,000 pound case to determine bearing component temperatures as a function of time. It is of interest to investigate the time necessary for thermal runaway to start for this high load condition. Iterations are continuing for the 6000 pound axial reaction to finalize the area of convergence that was provided in the February report. An analysis is also being conducted for an 8000 pound axial reaction but insufficient iterations have been completed at this time to determine any converging points.

In summary, with the identification of additional conditions for convergence the operating range for the tester is becoming more clearly defined. In addition, the ball track temperatures are being evaluated and the BMT modified operating region may be based on ball track temperatures rather than relying on thermal runaway criteria. All analyses thus far have been for a 57mm bearing operating with LN₂ as the coolant at 400 psia.

Future plans include performing the same analysis with varying axial reactions, flow rates, and coolant inlet temperatures using LOX rather than LN₂ as the coolant.

5.9.3 ESTIMATION OF FILM THICKNESS FOR 57mm BEARING OPERATING IN O₂

An analysis similar to the one reported in the February progress report was done to estimate the fluid film thickness for the 57mm bearing operating in oxygen. The details of the analysis are contained in the reference and will not be repeated here. The same assumptions and reservations discussed in the reference hold for this analysis. Figure 5.9.4 shows the fluid viscosity data, derived pressure coefficient, and estimated initial viscosity for O₂. Figure 5.9.5 shows the estimated fluid film thickness as a function of contact temperature. Lack of high temperature O₂ viscosity data limited the calculation to 600°R. As was shown with N₂, the film thickness for O₂ is too small to provide appreciable separation of the loaded contacts since typical surface finishes are on the order of 6μ inches.

5.10 APRIL, 1983

5.10.1 EVALUATION OF BEARING CARRIER TO HOUSING CLEARANCE AND THE EFFECT ON BEARING OPERATING CHARACTERISTICS

Maintaining bearing carrier to housing clearances is important to assure freedom of axial movement during axial load application to the BMT. Binding of the carrier could distort the applied load that actually reaches the bearings, introducing unknown errors in test results. Furthermore, a locked carrier could preclude rapid unloading as a contingency measure.

Currently, the BMT design allows for a 1.3 mil diametrical clearance between carrier and housing. Results from a typical bearing thermal analysis was used to estimate the differential movement between the carrier and housing due to thermal growth. The following conditions were assumed in the thermal analysis:

FIGURE 5.9.4 O₂ VISCOSITY

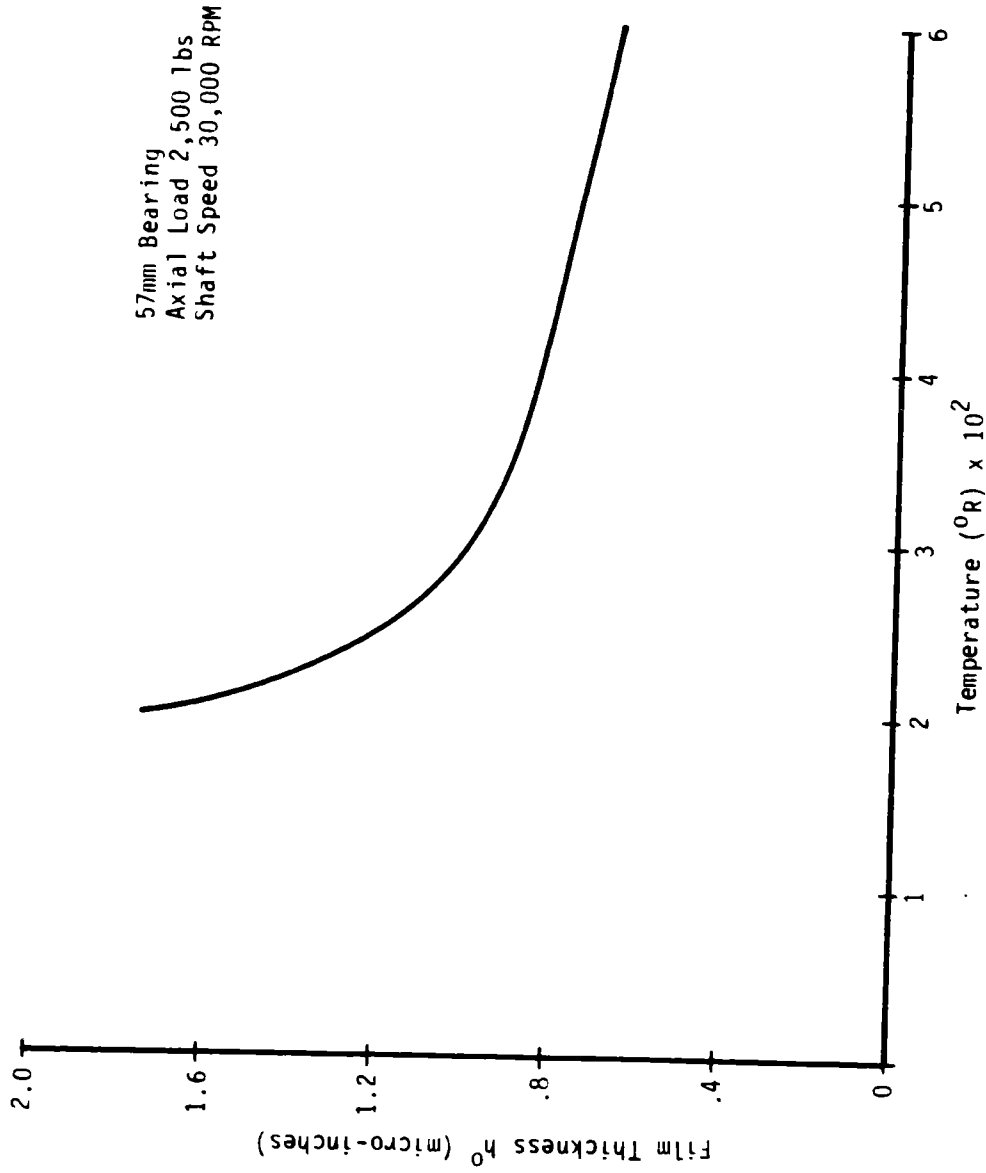
| Pressure Psia Temp °R | 350 | 4000 | 5000 | Pressure Coefficient $\lambda \times 10^{-8}$ | $\mu'_0 \times 10^{-8}$ |
|--------------------------------|-------|-------|-------|---|-------------------------|
| 200 | 1.731 | 2.388 | 2.579 | .769 | 1.756 |
| 300 | .233 | 1.124 | 1.208 | .721 | .842 |
| 500 | .305 | .576 | .651 | 1.224 | .353 |
| 600 | .345 | .543 | .597 | .941 | .373 |

*Viscosity $\mu \times 10^{-8} \frac{\text{lb-sec}}{\text{in}^2}$

ORIGINAL PAGE IS
OF POOR QUALITY

SRS

FIGURE 5.9.5 ESTIMATED FILM THICKNESS VS TEMPERATURE FOR O₂



spectra research systems

Inlet fluid temperature -305°F
Flow 6.3 lbs/sec per bearing set
Axial load 2500 lbs.

Results indicated an average temperature difference between carrier and housing of about 27°F with the carrier being the warmer of the two components. Based on this temperature difference, it is estimated that there will be an interference of about 0.1 mil (diametrical) between the carrier and the housing. These are steady operating conditions, therefore, there will be a clearance at the start and early part of the test run. In order to verify the thermal analysis and operating clearance, the previously requested carrier temperature measurements are essential.

As clearances will exist during the early part of the test, analyses were done to investigate the effects of misalignment on bearing operation characteristics. Angular misalignments were determined as a function of carrier to housing clearances and the effect of these misalignments on bearing radial stiffness, ball speeds, contact angles, contact stress, and contact heat generation was determined. These effects were investigated for axial loads from 500 lbs/brg to 6000 lbs/brg, and radial loads of 100 to 500 lbs.

Figure 5.10.1 shows the potential for the carrier to tilt in the housing. The tilt angle θ is a function of the carrier diametrical clearance (C). From the geometry of the figure the following relations can be written:

$$1) \quad M = \frac{W \cos \theta - D \sin \theta}{2}$$

$$2) \quad M = \frac{\sqrt{D^2 + W^2} - (D + C)}{2}$$

$$3) \quad D + C = D \cos \theta + W \sin \theta$$

Eliminating M and $\cos \theta$ from the above:

$$4) \quad \theta = \sin^{-1} \left[\frac{W(D + C) - D\sqrt{D^2 + W^2} - (D + C)^2}{D^2 + W^2} \right]$$

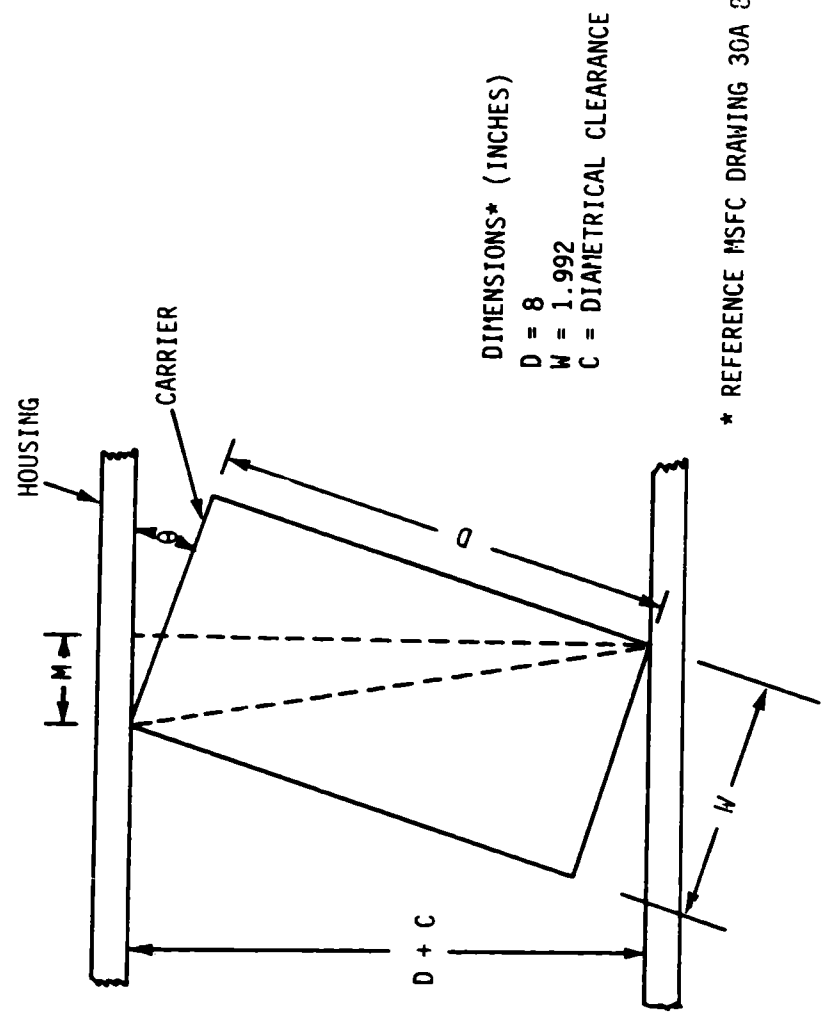
Equation 4 provides the tilt or misalignment angle as a function of carrier diametrical clearance. Figure 5.10.2 provides misalignment angle as a function of diametrical clearance. As indicated the maximum expected clearance is 1.3 mils (carrier and housing at same temperature) giving a maximum misalignment angle of 2.25 minutes (.0375°).

BEARING RADIAL STIFFNESS VARIATIONS

The bearing radial stiffness as a function of azimuth angle is shown in Figure 5.10.3. In this figure, the zero azimuth angle corresponds to the "pinch" point caused by the misalignment of the outer race [the results from the "SHABERTH" bearing analysis program, Table 5.10.1, are presented with the zero azimuth angle 180° out of phase from the "pinch" point]. The variation in stiffness shown is conservative because the reduction of the bearing misalignment angle as a function of axial load was not considered in the stiffness determination. These variations should not significantly affect synchronous radial motion of the shaft due to small rotor unbalance which was the main concern of possible large stiffness variations due to misalignment.

ORIGINAL DRAWING
OF POOR QUALITY

FIGURE 5.10.1 CARRIER TILT IN HOUSING



DIMENSIONS* (INCHES)
D = 8
W = 1.992
C = DIAMETRICAL CLEARANCE

* REFERENCE MSFC DRAWING 30A 24 009

SRS

ORIGINAL PAGE IS
OF POOR QUALITY

FIGURE 5.10.2 OUTER RACE MISALIGNMENT AS A FUNCTION OF BEARING
CARRIER DIAMETRICAL CLEARANCE

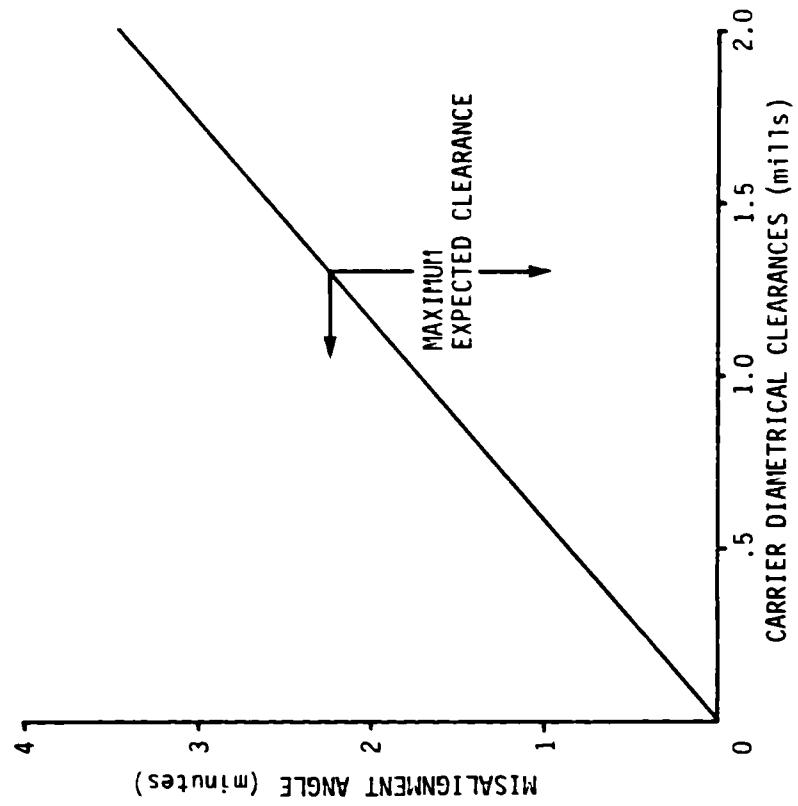
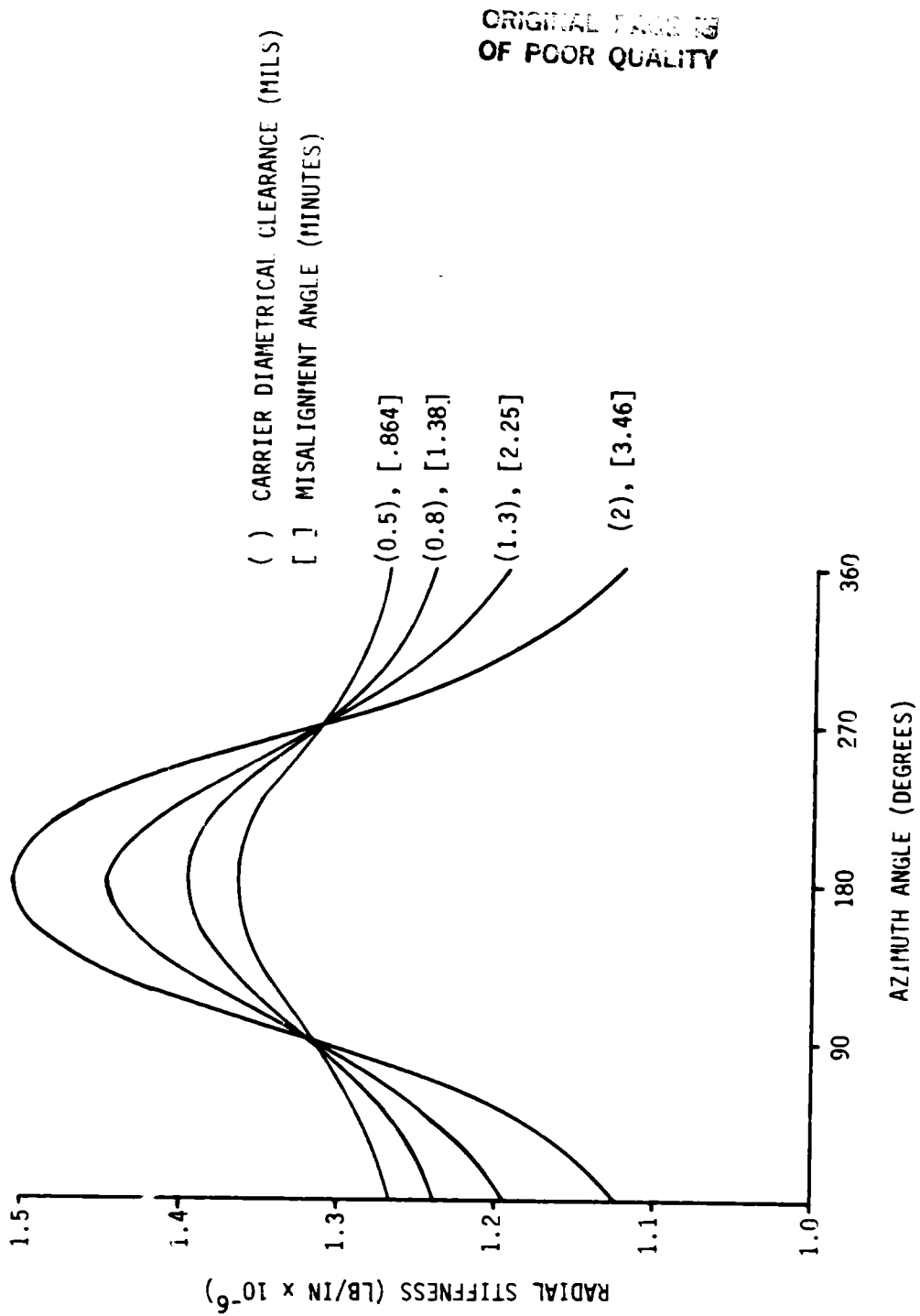


FIGURE 5.10.3 RADIAL STIFFNESS VERSUS AZIMUTH ANGLE



ORIGINAL PAGE IS
OF POOR QUALITY

SRS

BEARING OPERATION CHARACTERISTICS

The investigation of carrier misalignment on contact stresses, contact angles, ball speeds, and heat generated at the contacts required numerous "SHABERTH" computer runs with varying input parameters. The following conditions shown in Table 5.10.1 were investigated.

TABLE 5.10.1

| | | | | | |
|------------------|-------|--|--------|--------|-----------|
| Axial Load (lbs) | | Misalignment Angles (°) | | | |
| 500 | .0375 | .0229 | .01439 | .01 | |
| 2500 | .0375 | .0229 | .01439 | .01 | |
| 6000 | .0375 | .0229 | .01439 | .01 | |
| Axial Load (lbs) | | Radial Loads (lbs) (No Misalignment) | | | |
| 2500 | | 100 | 300 | 500 | |
| 6000 | | 100 | 300 | 500 | |
| Axial Load (lbs) | | Misalignment for each axial/ Radial Loads (lbs) radial load combination | | | |
| 2500 | | 100 | 300 | 500 | .0375 .01 |
| 6000 | | 100 | 300 | 500 | .0375 .01 |
| Axial Load (lbs) | | (Ball to pocket clearance of 100 mils) | | | |
| | | Misalignment angles(o) | | | |
| 500 | | .0375 | .0229 | .01439 | .01 |
| Axial Load (lbs) | | (Radial temp distribution in brg) | | | |
| | | Misalignment Angles | | | |
| 2500 | | .0375 | .0229 | .01439 | .01 |
| 6000 | | .0375 | .0229 | .01439 | .01 |

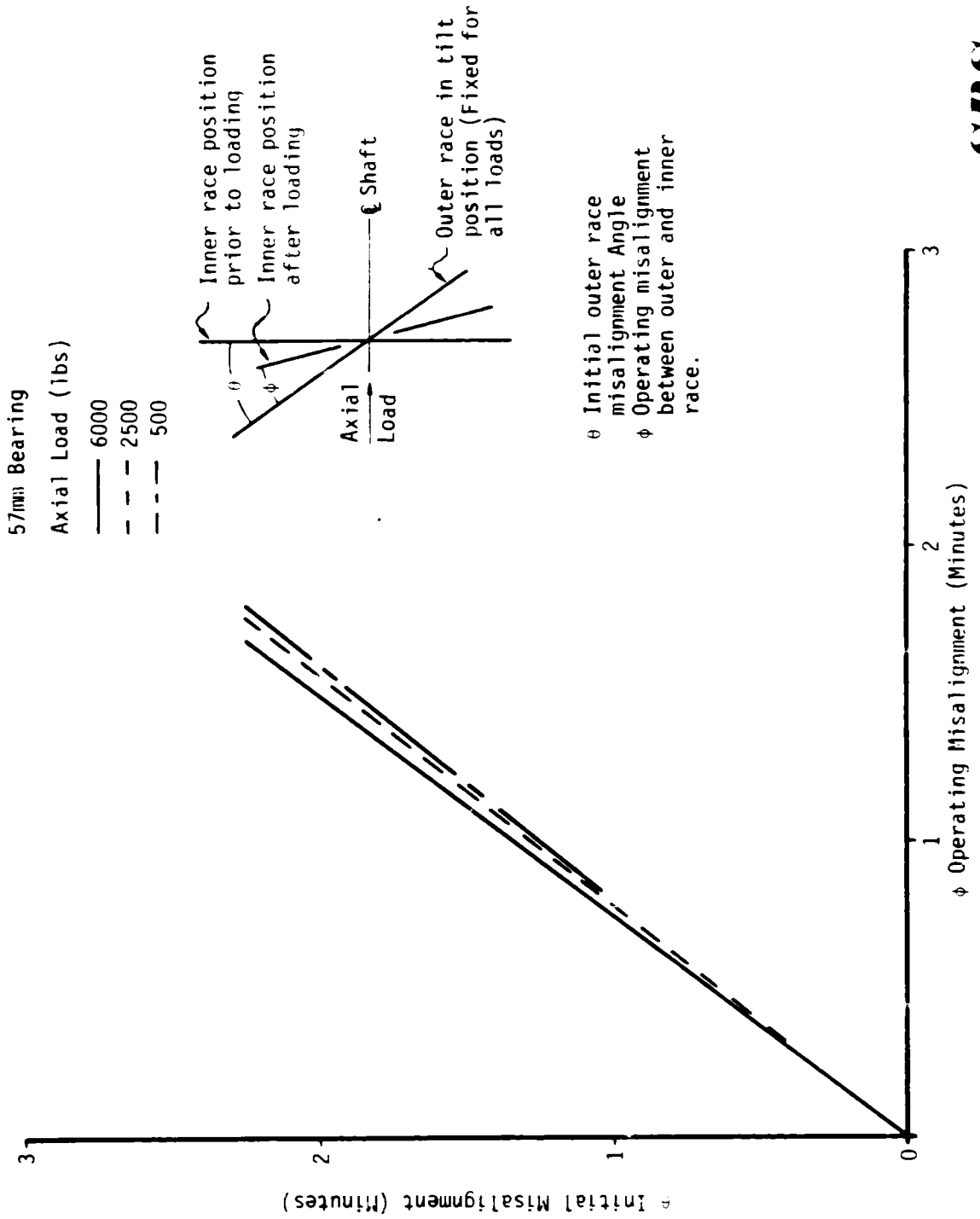
In reviewing the data, the most significant variations due to outer race misalignment is the ball orbital speed. This occurs for the 500 lb axial load condition. This is representative of tester bearings 1 and 4 with the normally accepted axial PA load of 2500 lbs. Comparisons of contact stresses, ball speed, and contact angles for the misaligned and normal conditions do not show significant variations in these parameters for the higher axial load cases. There is a maximum difference in ball orbiting speed of about 20 rad/sec for the 500 lb axial load condition. It is estimated that this causes + 8.5 mil movement of the ball relative to the ball pocket center. This should not cause a problem since there is 25 mils diametrical clearance between ball and ball pocket.

EFFECT OF AXIAL LOAD ON BEARING MISALIGNMENT

The effect of axial load on operating misalignment is shown in Figure 5.10.4. As the axial load is increased, the inner race is forced to rotate thus decreasing the angle between the inner and outer race. The degree of rotation is obviously dependent not only on bearing characteristics but also the stiffness of the shaft since the shaft exerts a clockwise movement on the bearing inner race as the race is forced to rotate counter-clockwise due to the outer race misalignment. Shaft and bearing characteristics were included in the bearing/shaft model.

ORIGINAL FACE IS
OF POOR QUALITY

FIGURE 5.10.4 OPERATING MISALIGNMENT VS INITIAL MISALIGNMENT AND AXIAL LOAD



SRS

spectra research systems

In summary, the analyses indicate no tester operational problems due to outer race misalignment with a carrier to housing clearance of 1.3 mils. Although the thermal analysis indicates a slight carrier to housing interference for steady state conditions, verification of this condition is necessary during early tester operation and should not be detrimental during the initial test phase in LN₂ when loads are relatively light. For higher loads and increased heat generation, further analysis is required to evaluate the adequacy of carrier to housing clearance. These analyses should use the thermal model "calibrated" by thermal data taken in the early BMT runs.

5.10.2 BEARING THERMAL ANALYSIS

Stability problems have been encountered with the bearing finite element thermal model. This has occurred because of the rapid change (with temperature) in the fluid heat transfer coefficient as the fluid changes phase. This coefficient increases to a peak value, as the bearing surface temperature exceeds the fluid saturation temperature, and decreases to a minimum value as the surface becomes very hot and vapor blanketed. This introduces an extremely nonlinear problem and numerical oscillations have occurred. This problem has been minimized by the application of dampening factors to the temperature calculated at each iteration. This condition has been most prevalent at the intermediate axial loads of 6000 lbs. Higher loads cause the components to be heated such that most surface temperatures are high enough to be in the vapor regime where the heat transfer coefficient does not change drastically with temperature. Although this has caused some delay in completing the definition of the operational envelope for the BMT, it is projected that this task can be completed (for LN₂) by the next reporting period.

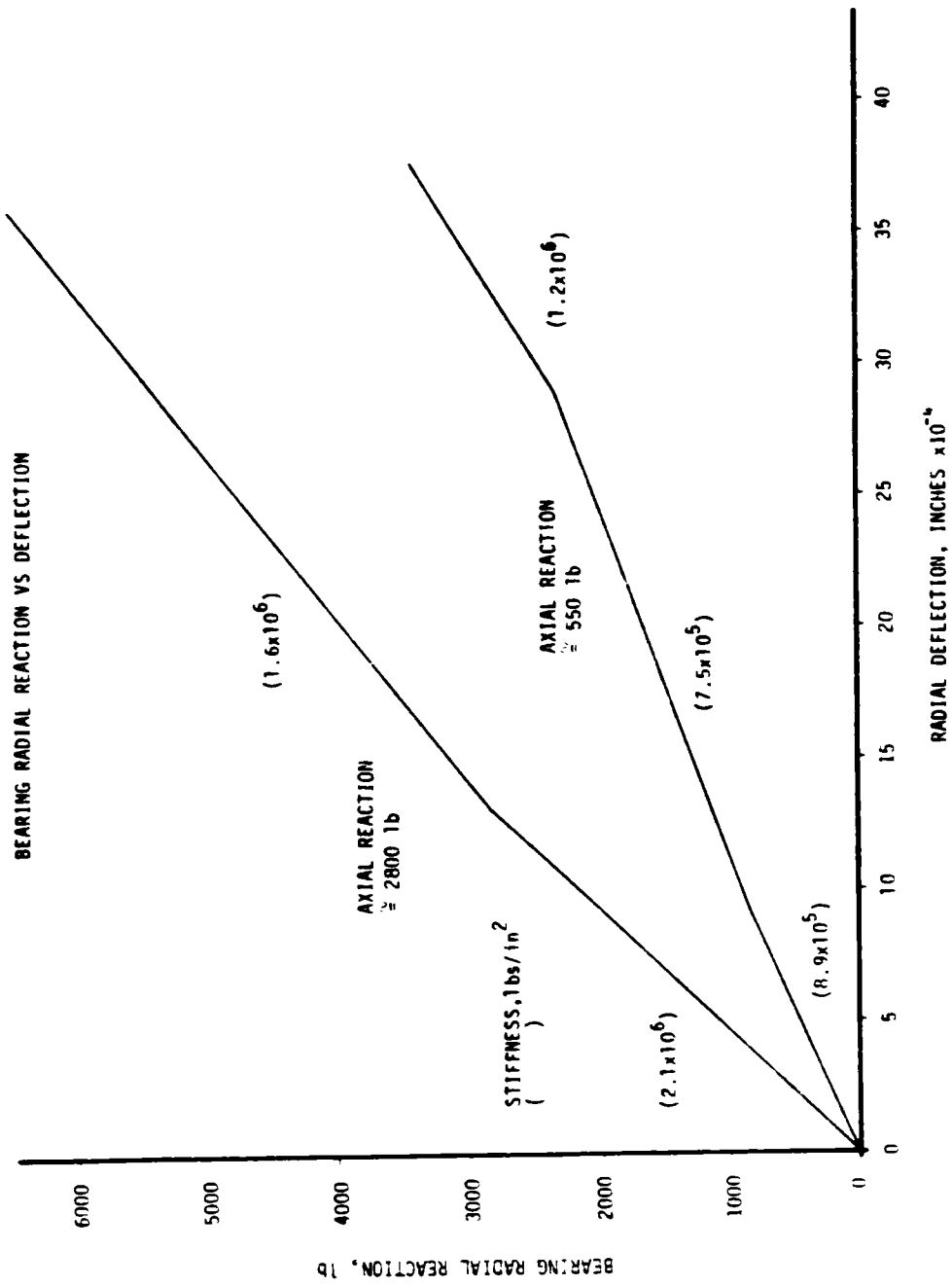
5.10.3 INVESTIGATION OF THE RADIAL STIFFNESS OF THE BMT 57mm BEARINGS

An analysis has been initiated to evaluate the effects on bearing operating characteristics (stresses, radial stiffness) caused by impressed radial loads. The purpose of this investigation is to identify these characteristics for input to test planning to determine the radial dynamic response of the bearing shaft system. The radial load range investigated was 500 to 6000 lbs. with axial loads of approximately 500 to 2800 lbs. Assuming an impressed axial load of approximately 2500 lbs due to the pressure differential across the bearing carriers, the two inboard bearings will be axially loaded to that value and the two outboard bearings will be unloaded. Preload is 1000 lbs to approximately 500 to 800 lbs. Since axial loads tend to stiffen an angular contact ball bearing in the radial direction, it was expected that the unloaded bearing would be the most distressed at high radial loads.

Shown in Figure 5.10.5 are the bearing deflections versus radial reactions. As expected, the bearing with the larger axial load exhibits the larger stiffness. There is also a stiffness change as the load increases. This is due to the increased radial deflections unloading balls, i.e., the total load is supported by fewer rolling elements. It is interesting to note that the unloaded bearing has three apparent stiffness values. The first change in slope (stiffness) occurs for the same reason as described above. The second change in stiffness is believed to be caused by the remaining load carrying balls being forced down on the inner race shoulder. Since at this location the inner contact angle is approaching zero, the only radial deflection possible is caused by compressing the balls (i.e., all ball movement is prevented). Shown in Figure 5.10.6 is the inner contact angle as a function of radial loads for the unloaded bearing. The bearing is reacting the radial load at an azimuth angle of zero. Notice that at this position, the inner contact angle drastically decreases as the load increases. As this happens, the ball is forced down to the shoulder of the inner race.

ORIGINAL VALUE OF
OF POOR QUALITY

FIGURE 5.10.5
BEARING RADIAL REACTION VS DEFLECTION



SRS

spectra research systems

Also observe, at an azimuth angle of 166°, the inner contact angle goes to zero for radial loads above about 1000 lbs. This indicates that the balls at this location have left the inner race and, due to centrifugal force, are following the outer race. At the higher radial loads only three balls are supporting the load. At the higher axial loads, this does not occur, and all balls are in contact with the inner race.

The influences of radial and axial loads on contact stresses are shown in Figure 5.10.7. The highest contact stress is produced in the unloaded bearing, and as shown, exceeds 500 ksi. This could cause permanent plastic deformation of the contact surfaces. An assessment of heat generated on bearing temperatures and the potential for thermal run away will require exercising the bearing thermal model for these conditions.

In summary, the current BMT design will produce several values of radial stiffness as the radial load is varied over a range of 4000 lbs. A radial load of 4000 lbs will probably plastically deform the contact surfaces of the unloaded bearing. If loads in this range are planned, a thermal analysis is recommended to evaluate the potential for thermal run away.

5.10.4 CUMULATIVE LOAD ASSESSMENT FOR BMT BEARING LIFE

A basic problem in fatigue analysis is the prediction of life for an element when time-dependent loading is applied. By progressively loading an element, damage accumulates within the material. Miner and Palmgren have postulated that failure resulting from multistage loading can be defined as:

$$(1) \sum \frac{n_i}{N_i} = 1 \quad \text{Miner's Rule}$$

Miner's Rule assesses the "damage" produced by a stress σ_i for n_i cycles as n_i/N_i and assumes the individual damages are additive and independent of sequence. [36]

If Miner's Rule is assumed to correctly predict the cumulative damage for the BMT, the following equation can be stated:

$$(2) \quad t_1/T_1 + t_2/T_2 + t_3/T_3 + \dots + t_n/T_n = 1$$

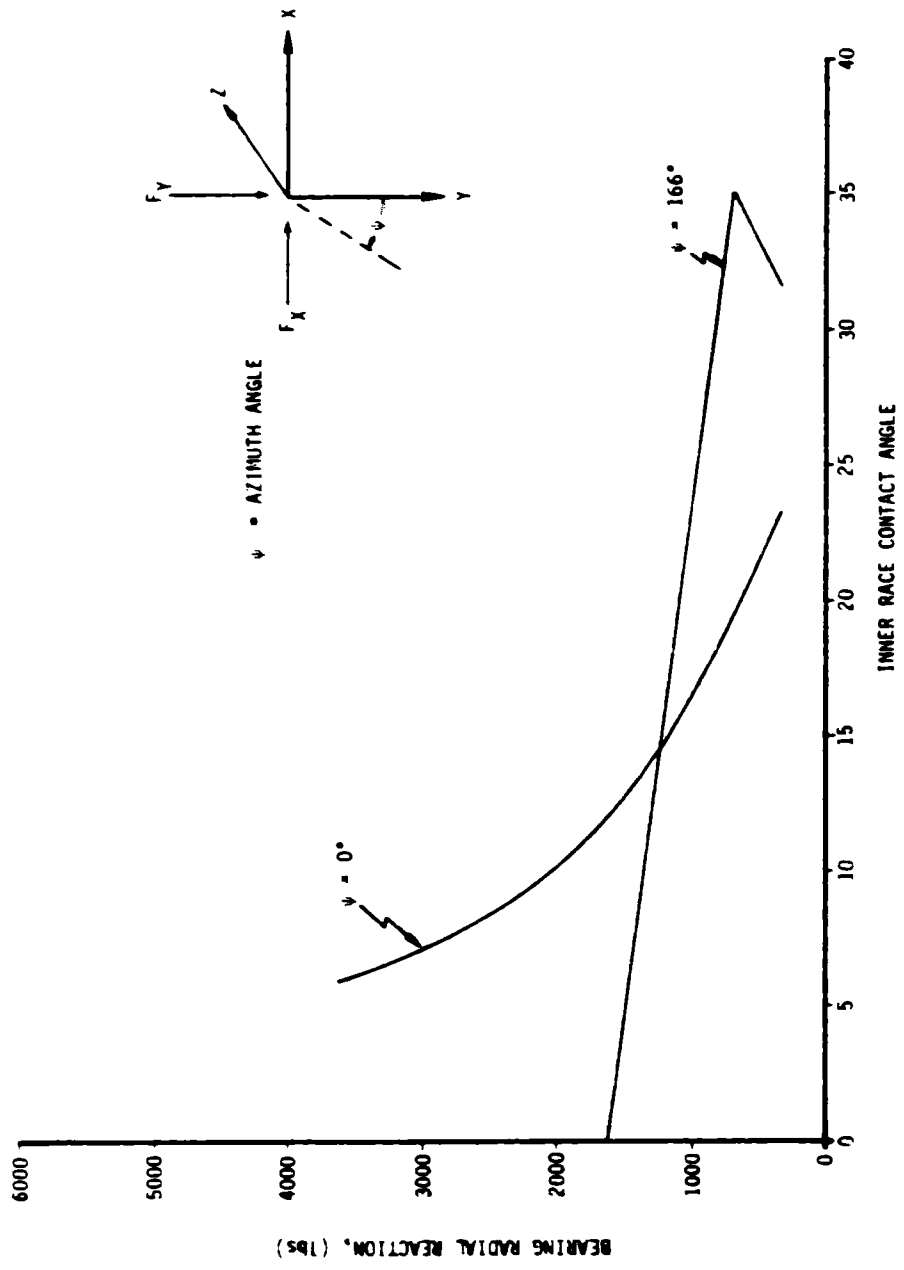
where t_n = time at load F_n
 T_n = Total time to failure at given stress level (S-N curve)

Since $T_n = L_n$, where L_n = life to failure predicted by an S-N curve, Equation (2) can be rewritten as

$$(3) \quad \frac{t_1}{L_1} + \frac{t_2}{L_2} + \frac{t_3}{L_3} + \dots + \frac{t_n}{L_n} = 1$$

or (4)
$$\sum_{i=1}^{i=n} \frac{t_i}{L_i} = 1$$

FIGURE 5.10.6
INNER RACE CONTACT ANGLE VS. RADIAL LOAD
AXIAL LOAD = 500 lbs/brg

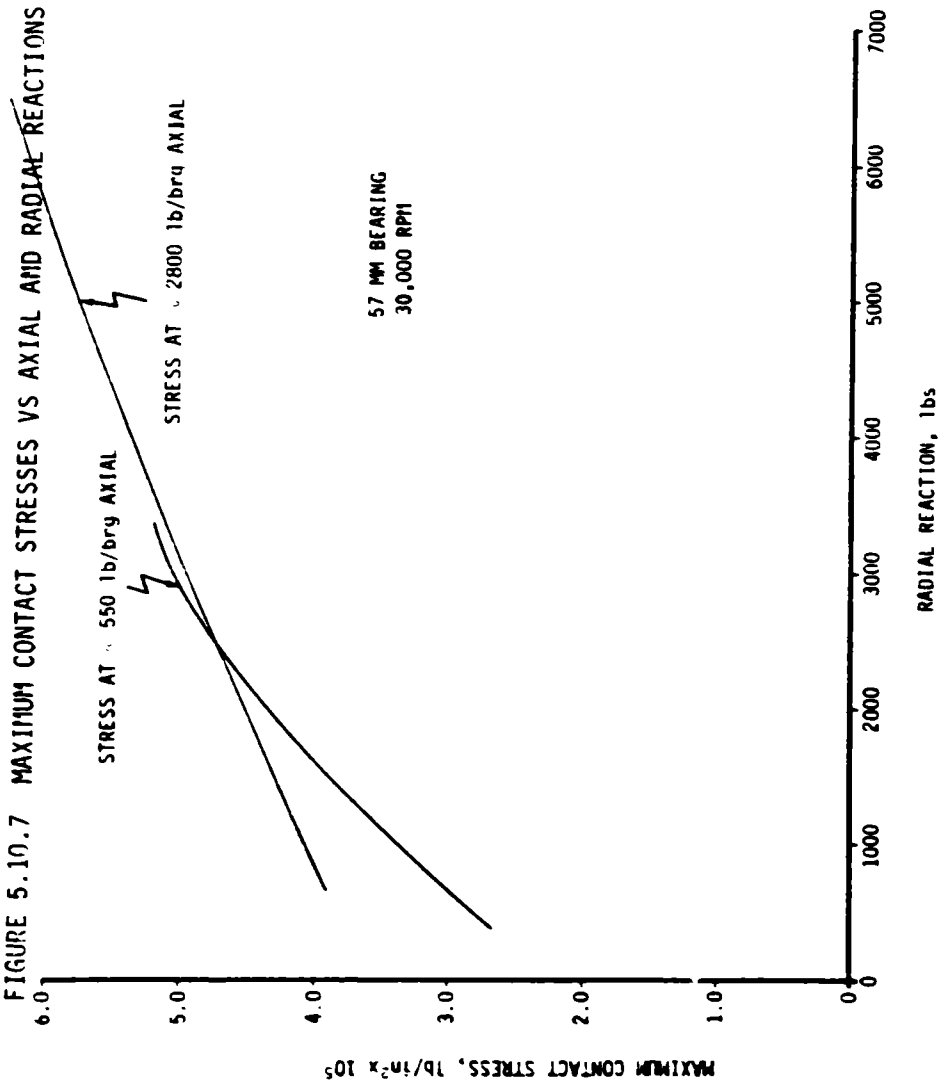


ORIGINAL FACE IS
OF POOR QUALITY

ORIGINAL FILED IN
OF POOR QUALITY

SRS

FIGURE 5.10.7 MAXIMUM CONTACT STRESSES VS AXIAL AND RADIAL REACTIONS



spectra research systems

Harris [1] defines a relationship based on the dynamic loading capacity as

$$(5) \quad L_i = \left(\frac{C}{F_i} \right)^P$$

where C = dynamic loading capacity
P = 3 for rolling bearings.

Defining a ratio such that

$$(6) \quad \frac{L_1}{L_2} = \left(\frac{F_2}{F_1} \right)^P$$

allows the life to be related to the applied axial reaction load and to failure at a given stress (force) level.

Defining Equation 6 in general terms gives

$$(7) \quad \frac{L_n}{L_{n+1}} = \left(\frac{F_{n+1}}{F_n} \right)^P$$

Substituting Equation (7) into (3) and assuming 3-stage loading gives

$$(8) \quad \frac{t_1}{L_2 \left(\frac{F_2}{F_1} \right)^P} + \frac{t_2}{L_2} + \frac{t_3}{L_2} = 1$$

A similar equation can be written for L_2 such that

$$(9) \quad \frac{t_1}{L_3 \left(\frac{F_3}{F_2} \right)^P \left(\frac{F_2}{F_1} \right)^P} + \frac{t_2}{L_3 \left(\frac{F_3}{F_2} \right)^P} + \frac{t_3}{L_3} = 1$$

or

$$(10) \quad L_3 = \frac{t_1}{\left(\frac{F_3}{F_1} \right)^P} + \frac{t_2}{\left(\frac{F_3}{F_2} \right)^P} + t_3$$

Equation (10) may be expanded to a general form:

$$(11) \quad L_n = \frac{t_1}{\left(\frac{F_n}{F_1} \right)^P} + \frac{t_2}{\left(\frac{F_n}{F_2} \right)^P} + \frac{t_3}{\left(\frac{F_n}{F_3} \right)^P} + \dots + \frac{t_{n-1}}{\left(\frac{F_n}{F_{n-1}} \right)^P} + t_n$$

or

$$(12) \quad L_n = t_n + \sum_{i=1}^{i=n-1} \frac{t_i}{\left(\frac{F_n}{F_i} \right)^P}$$

Recall that a summation can be represented by the integration of a function so that

$$L_n = t_n + \int_0^t \left(\frac{F_i}{F_n} \right)^P dt$$

Therefore,

$$\left(\frac{1}{F_n}\right)^D \int_0^t (F_i)^P dt$$

the integral term represents the area under a $(F_i)^P$ vs. Time curve. If a plot of $(F_i)^P$ vs time is given (See Figure 5.10.8), the life at a particular load can be graphically determined by calculating the area under the curve using the prescribed boundary conditions.

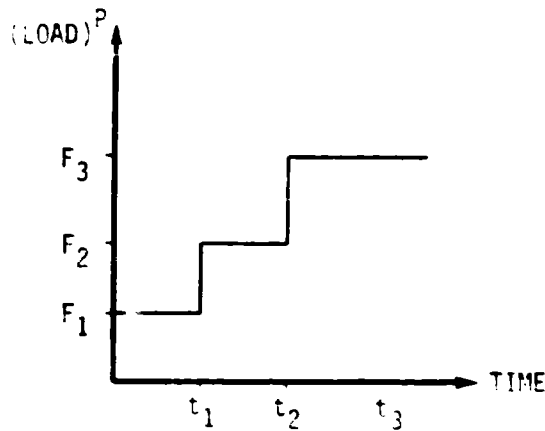


FIGURE 5.10.8 LOAD VS TIME

5.11 MAY, 1983

5.11.1 RADIAL STIFFNESS OF THE BMT 57mm BEARINGS AT 10,000 RPM

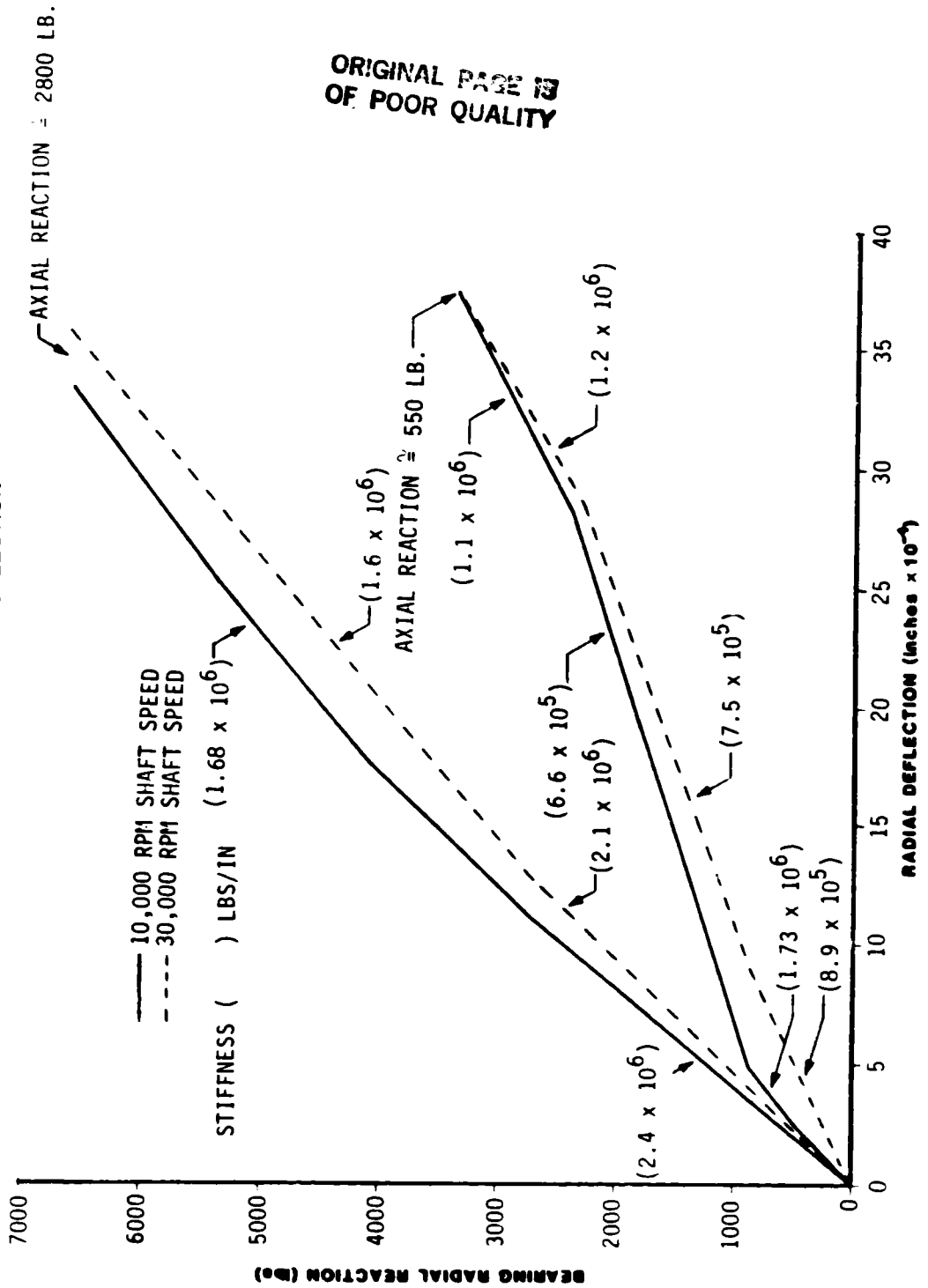
An analysis similar to the one reported in the April 1983 Progress Report, was conducted to evaluate the radial stiffness of the 57mm bearing at two levels of axial preload. The previous analysis was done for a shaft speed of 30,000 RPM while the current analysis is for 10,000 RPM. Results of the 10,000 RPM data are shown in Figure 5.11.1. The 30,000 RPM case reported in the reference is reproduced for convenient comparison. As shown, the greatest effect of speed on bearing deflection occurs for the low radial loads and low axial loads. At the lower speeds, centrifugal force is not as great and the inner contact angle is not decreased as much (compared to the higher speed case) thus improving the radial stiffness. This effect is more pronounced at the lower axial loads due to the reduced preload effect on radial stiffness. As the radial load increases, this effect overrides the centrifugal effects and the stiffness values become almost independent of speed. Shown in Figure 5.11.2 are the contact stresses for the loading conditions indicated. These stresses are very close to the values reported in the reference for 30,000 RPM.

5.11.2 STATUS AND RESULTS OF BEARING THERMAL ANALYSIS

Evaluation of the surface to fluid thermal conductors for the fluid boiling regimes is continuing. An improved nodal network for the ball has been generated and will be incorporated into the bearing thermal model. This change will improve

FIGURE 5.11.1

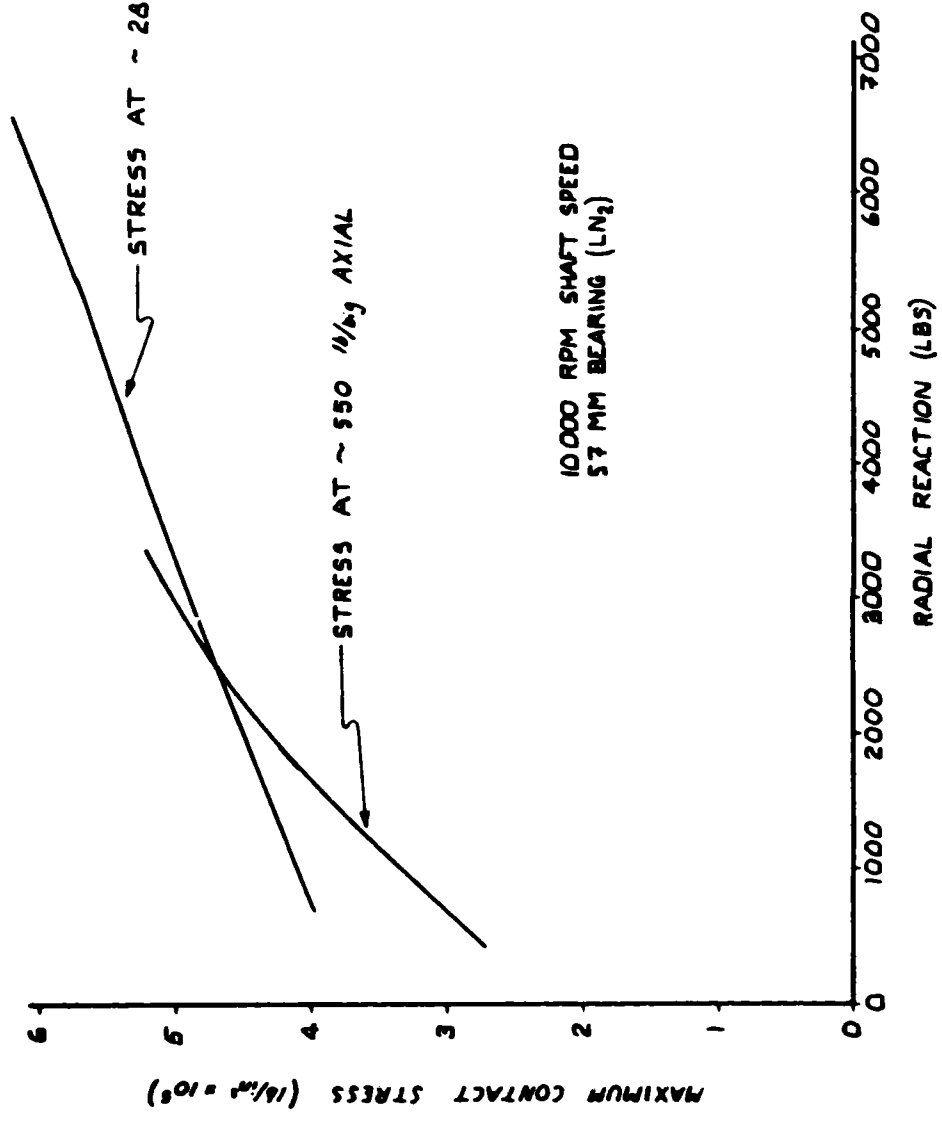
BEARING RADIAL REACTION vs DEFLECTION



ORIGINAL PAGE IS
 OF POOR QUALITY

ORIGINAL PAGE IS
OF POOR QUALITY

FIGURE 5.11.2
MAXIMUM CONTACT STRESS VS AXIAL AND RADIAL REACTIONS



convergence of the numerical solution of the finite difference heat transfer equations. The ball is the most likely component to cause numerical convergence problems because friction heat is generated at two contact points (inner and outer races) and there is a relatively small surface area available to reject the heat. This causes large thermal gradients in the ball especially when part of the ball surface is in the film boiling regime (low film heat transfer coefficient) and another part is in the nucleate/convective boiling regime (high film heat transfer coefficient).

The dependence of bearing cooling on coolant flow, load, and coolant inlet temperature has been investigated. This analysis was done by modeling the bearing on Shaberth and evaluating the heat generated as functions of axial load and radial temperature gradient. Viscous work on the fluid was accounted for as described in the January 1983 progress report. Friction and viscous loads were used as input to the SINDA thermal model to calculate bearing temperatures. This procedure was continued until agreement between the two codes was reached.

These analysis indicate that the dependence of bearing cooling on coolant flow is complicated due to the dependence of bearing internal clearances on component temperature. As internal clearances are reduced due to thermal growth of the inner race, with respect to the outer race, the normal forces and stresses at the contact surfaces are increased resulting in further increases in frictional heat generation and increased temperatures. Therefore, the bearing is not necessarily a constant heat generator for fixed load, speed, and varying coolant flow.

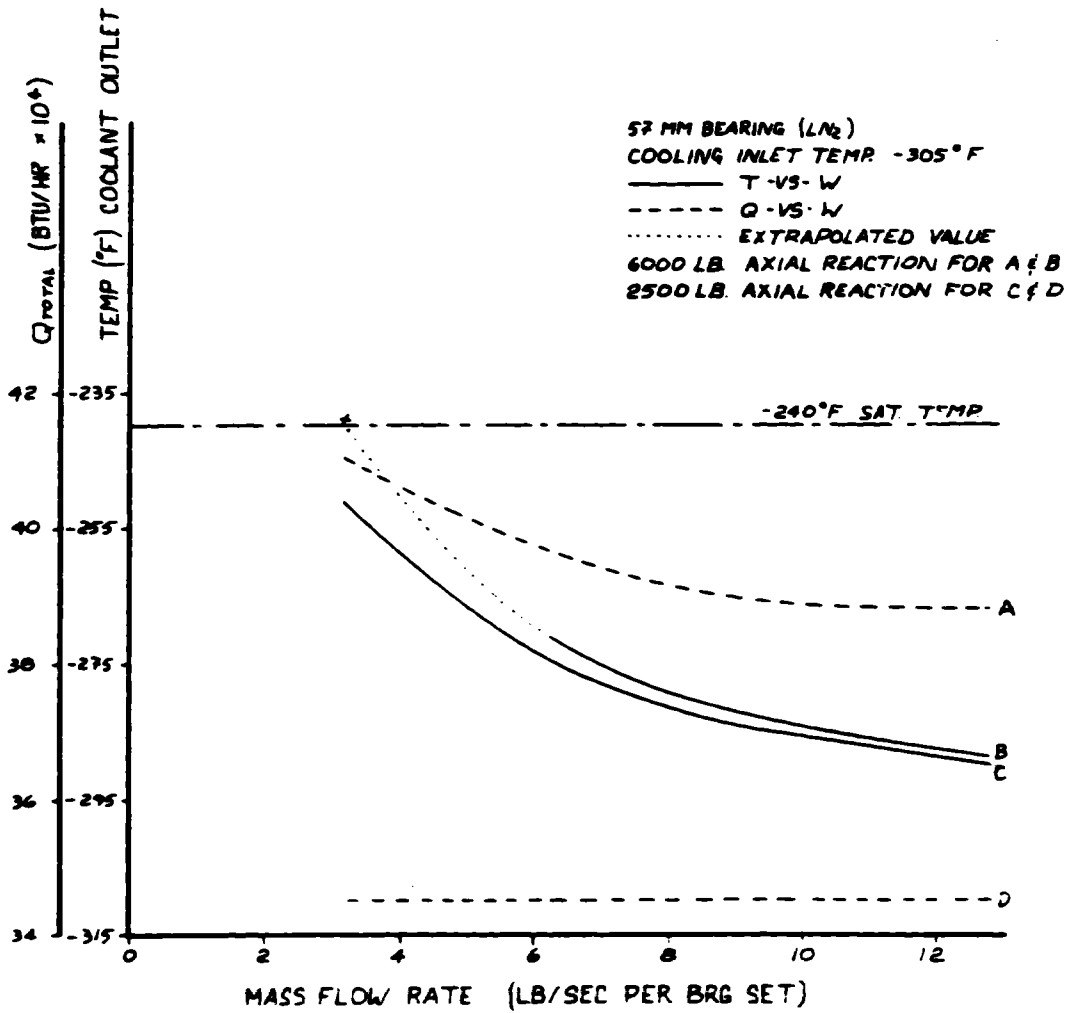
Figures 5.11.3 and 5.11.4 show analysis results that support the above discussions. Figure 5.11.3 illustrates the dependence of heat load, coolant outlet temperature, and coolant flow for the fixed conditions of load and coolant inlet temperature. The conditions shown are for a bearing set. The 6000 lb. axially loaded case shows an increase in heat load as the coolant flow is reduced below about 9 lbs/sec. As the coolant flow is further decreased, there are two factors causing an increase in coolant outlet temperature: increased heat load and flow reduction. If thermal equilibrium cannot be attained at a higher temperature compatible with bearing survival then failure occurs. The 2500 lb load case did not experience a heat load increase over the flow range investigated for this particular inlet coolant temperature (-305°F). Iteration between Shaberth and SINDA models did not produce a converging solution for the 6000 lb, 3.2 lb/sec case. Consequently, the coolant outlet temperature, for these conditions, could be at the saturation temperature or some where above saturation. The broken section of the curve in Figure 5.11.3 identifies this condition. As presently configured the thermal model is not capable of accounting for bulk vapor generation in the coolant. Local subcooled boiling is accounted for by using two phase boiling heat transfer correlations. This represents the physical system provided the outlet coolant temperature does not equal or exceed the coolant saturation temperature.

Figure 5.11.4 shows similar results for a coolant inlet temperature of -285°F. For these conditions, none of the 6000 lb load cases converged indicating a strong influence of coolant inlet temperature. As shown, the heat load begins to increase as the coolant flow is reduced below about 7 lb/sec indicating that the temperature gradient in the bearing has caused an adverse reduction in radial clearances resulting in increased heat generation.

Although quantitative values of these results should be considered preliminary at this time, the trends are believed to be correct. Further work currently in progress will provide improved confidence in the quantitative results especially in the convergence of the computer thermal code. Test data from the planned BMT tests are critical

ORIGINAL PAGE IS
OF POOR QUALITY

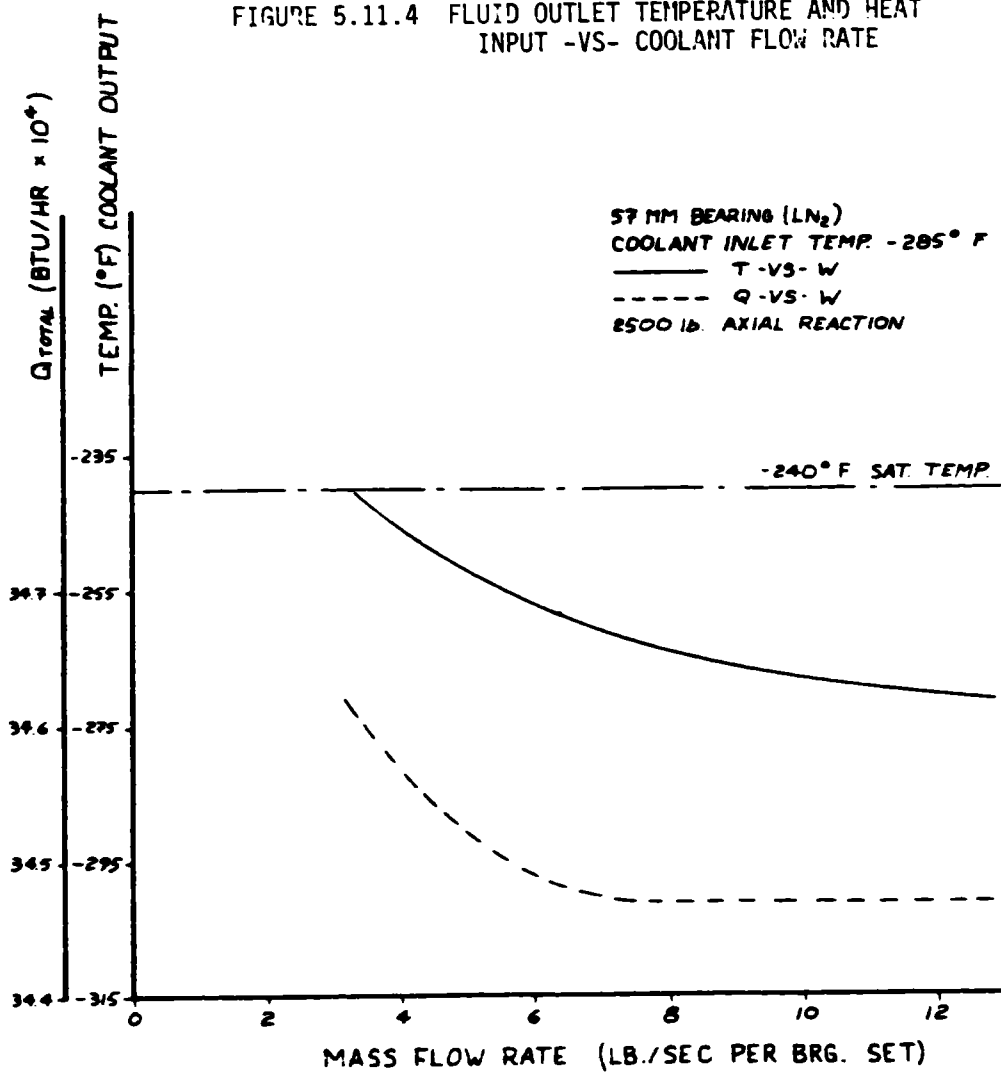
FIGURE 5.11.3 FLUID OUTLET TEMPERATURE AND
HEAT INPUT -VS- COOLANT FLOW RATE



SRS

ORIGINAL PAGE IS
OF POOR QUALITY

FIGURE 5.11.4 FLUID OUTLET TEMPERATURE AND HEAT
INPUT -VS- COOLANT FLOW RATE



SRS

spectra research systems

to guide and verify the analysis effort. This program is providing considerable insight into the thermo-mechanical interactions of the bearings which will, when verified, provide extremely valuable information for improving the design and life of flight hardware.

5.11.3 APPLICATION OF THE DOUBLE LINEAR DAMAGE RULE TO BEARING LIFE PREDICTIONS

Although Miner's Rule has been used to analyze cumulative damage, it does not account for the effects of load sequencing. Miner's Rule assumes that when the summation of cycle ratios (n/N) equals one, failure occurs. However, the cycle ratios can sum to be less than or greater than one when high-low or low-high load sequencing, respectively, is followed.

In the BMT, bearings will experience various load sequences and it is necessary to account for these associated effects to correctly predict bearing life. The application of the Double Linear Damage Rule (DLDR) to bearing life predictions is being evaluated. Most of the work by Halford at the Lewis Research Center has been with 0.25 inch diameter specimens. Discussions have been held with Dr. Halford concerning the feasibility of applying the DLDR to bearings, and early indications are that it can be applied.

5.12 JUNE, 1983

5.12.1 UPDATE OF BEARING THERMAL MODEL SURFACE-TO-FLUID HEAT TRANSFER COEFFICIENTS

The initial evaluation of heat transfer coefficients for the Bearing Thermal Model was provided in the November 1982 Progress Report. Continuing review of the literature and evaluation of the meager cryogenic boiling heat transfer data has resulted in revisions of the heat transfer correlations selected earlier and updating of the method for determining the various regimes of heat transfer. Test data or published correlations for heat transfer coefficients for subcooled, high pressure, high flow, boiling cryogenic systems have not been found in the literature. There appears to be no test data that matches the thermal and flow conditions in the bearing tester. Therefore, available information must be extrapolated to the bearing tester conditions and later verified by data from the tester.

The following describes the rationale for extrapolating existing data/correlation to represent the thermal and flow conditions in the bearing tester. Although similar techniques will be used for liquid oxygen, the results of the following development are for LN_2 .

The forced convection subcooled boiling process can be separated into four phases:

- 1) Forced convection to single liquid phase.
- 2) A combination of forced convection and nucleate boiling until a maximum heat flux is reached. This maximum heat flux is commonly referred to as the "burnout" heat flux.
- 3) Partial film boiling.
- 4) Stable film boiling.

The forced convection phase occurs without vapor generation and this phase of the heat transfer process is fairly well represented with published correlations and test data.

spectra research systems

Nucleate boiling is characterized by a very high heat transfer rate for small temperature differences. There are two subregimes in nucleate boiling: local boiling and bulk boiling. Local boiling is nucleate boiling in a subcooled liquid which is characteristic of the conditions in the bearing tester. Bulk boiling is nucleate boiling in a saturated liquid which will not occur in the tester unless the outlet fluid temperature reaches the saturated value. As will be discussed later, the effects of local nucleate boiling are significantly influenced by flow velocity and subcooling. When the population of bubbles becomes too high the bubbles leaving the surface restrict the flow of liquid to the surface and insulate it thus causing a rapid rise in surface temperature. This is defined as the "burnout" heat flux. It is important to define this point because in general the heat transfer mechanism changes from nucleate boiling to stable film boiling with a significant increase in surface temperature. Stable operation in the partial film boiling regime generally does not occur. Generally when the peak flux or "burnout" point has been passed the system moves to the stable film boiling regime.

In order to account for these various heat transfer mechanisms in the bearing thermal model, criteria was established for the changing modes of heat transfer as functions of the surface temperature of the specific nodal network. For example, as the inner race or ball surface node temperature increase from the subcooled liquid temperature to temperatures considerably in excess of the fluid saturation temperature, all the above modes of heat transfer will have been encountered. Consequently, the node surface temperature range for each mode of heat transfer must be established and the appropriate heat transfer correlation determined.

FORCED CONVECTION HEAT TRANSFER

As long as the surface temperature is below the local fluid saturation temperature, forced convection is the heat transfer mechanism. The appropriate heat transfer correlation for these conditions is the Dittus - Boelter equation for the inner and outer race surfaces and other surfaces in the flow stream with the exception of the ball. The heat transfer correlation for the ball was taken from reference 40 which correlates a wide range of heat transfer data for spheres.

The Dittus - Boelter equation is as follows:*

$$1) \frac{h_c D_e}{k} = .023 N_{re}^{.8} N_{pr}^{.4}$$

And Katsnellson's equation for spheres (Ref 41) is:

$$2) \frac{h_c D}{k} = 2 + 0.03 N_{pr}^{0.33} N_{re}^{0.54} + 0.35 N_{pr}^{0.356} N_{re}^{0.58}$$

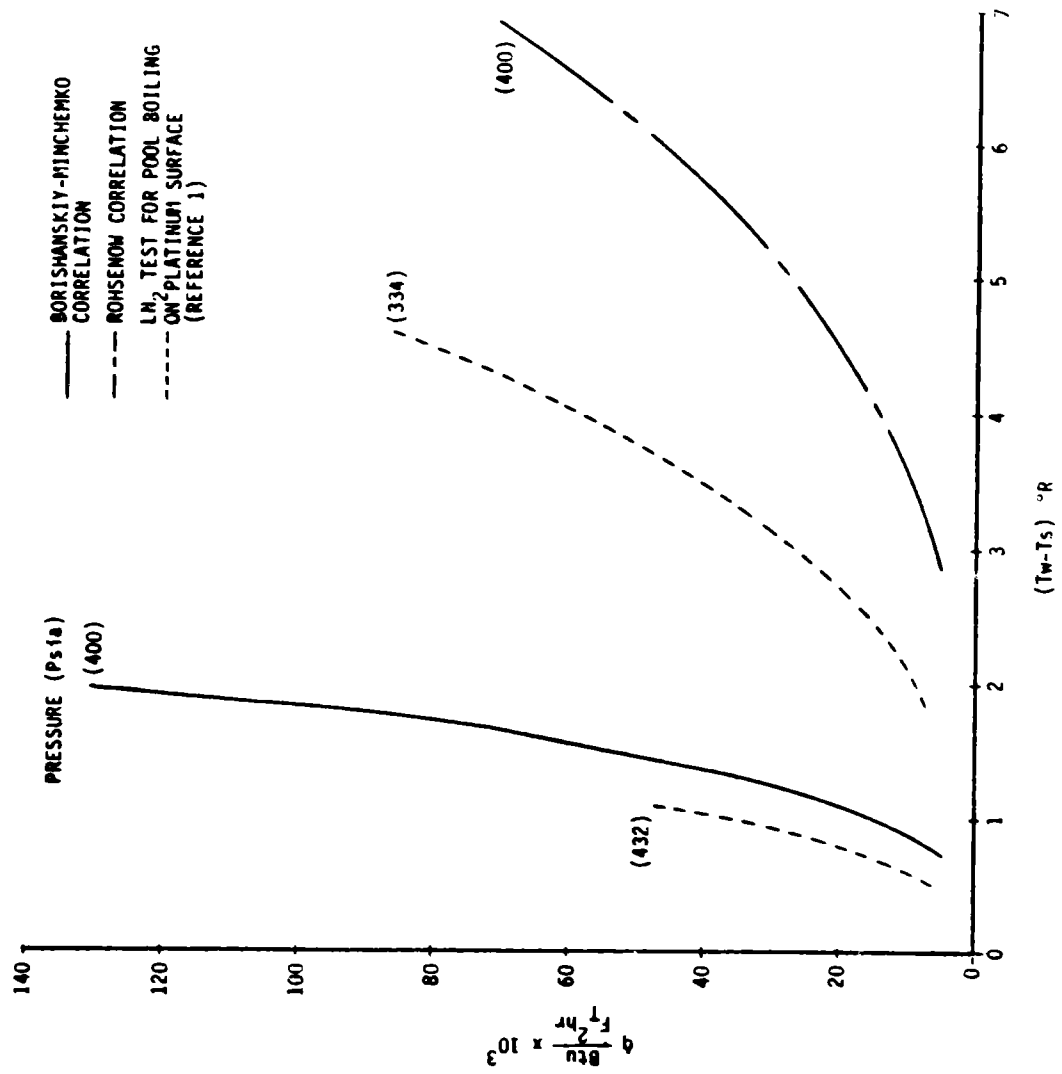
FORCED CONVECTION NUCLEATE BOILING

In this heat transfer regime, both forced convection and subcooled boiling occur simultaneously and no generalized correlations, for subcooled cryogenics, have been found. The first step in developing an approach for extrapolation of available information to these conditions is to select a pool boiling correlation that matches test data for high pressure LN₂. There are several pool boiling correlations available to select from. Examples are: Rohsenow, Forster - Zuber, Borishanskiy - Minchenko, Kutateladze and others. Reference 38 compares these correlations with nucleate boiling test data for several cryogens including LN₂. Figure 5.12.1 shows a sample of those

* Refer to nomenclature on page 5-162 for definition of terms.

ORIGINAL PAGE IS
OF POOR QUALITY

FIGURE 5.12.1 COMPARISON OF NUCLEATE BOILING CORRELATIONS



spectra research systems

comparisons. As shown, there is a considerable pressure effect on the boiling heat flux at a given value of ΔT . Also shown is the superior correlation with test data of the Russian equation compared to Rohsenow's expression. Based on these results, the Borishanskiy - Minchenko correlation was selected as the best representation of pool boiling LN_2 data. This equation can be expressed as follows:

$$3) \quad T_w - T_s = f(P) q_b^{0.3}$$

The next step in defining the heat transfer regimes is to determine the node surface temperature at the peak heat flux or "burnout" point. An expression, developed by Kutateladze, was selected based on the comparison with pool boiling burnout flux for LN_2 provided in Reference 38. This expression is as follows:

$$4) \quad \dot{q}_{bm} = 0.16 f(P)$$

Since the bearing tester operates in subcooled liquid, the effects of subcooling on heat flux should be accounted for. Reference 39, page 6-44 provides the following expression for correcting saturated pool boiling heat flux for subcooling.

$$5) \quad \frac{q_{sb}}{q_b} = 1 + \theta [T_s - T_L]$$

The above boiling data correlations are for static boiling systems, wherein the flow velocity is small or non existent. The procedure for extrapolating these correlations to a high flow subcooled boiling cryogenic system is as follows.

- 1) Estimate the surface temperature at which nucleate boiling initiates in the flow system.
- 2) Estimate the surface temperature at the burnout or maximum heat flux conditions.

After the above conditions are established it will be assumed that:

- 1) Forced convection is the dominant mode of heat transfer prior to the surface temperature reaching the incipient nucleate boiling temperature.
- 2) When the surface temperature is between the incipient boiling and the temperature corresponding to peak boiling, a combination of forced convection and nucleate boiling occurs.
- 3) When the surface temperature exceeds the temperature corresponding to the peak flux condition, stable film boiling occurs and this condition can be represented by the forced convection relationships using vapor properties.

ESTIMATION OF SURFACE TEMPERATURE FOR BOILING INITIATION

It is assumed that nucleate boiling will begin when the boiling heat flux as represented by equation 3 equals the heat that can be removed by forced convection. For example:

$$6) \quad \dot{q}_c = h_c (t_w - T_L)$$

Then from equation 3:

$$7) T_w - T_s = f(P) [h_c(T_w - T_L)]^{0.3}$$

In the above equation T_w is the surface temperature required to initiate nucleate boiling.

ESTIMATION OF SURFACE TEMPERATURE AT MAXIMUM HEATING CONDITIONS

The pool boiling "burnout" heat flux is estimated from equation 4 and corrected for the appropriate subcooling by equation 5. For the high flow system both boiling and forced convection occur throughout the nucleate boiling regime. Therefore, at burnout the total heat flux is assumed to be a combination of these mechanisms. The following expression can be written assuming that the nucleate boiling relationship still holds.

$$8) T_w - T_s = f(P) [h_c(T_w - T_L) + q_{sb}]^{0.3}$$

T_w in this case is the wall temperature at "burnout" and when this temperature is exceeded stable film boiling is assumed to occur.

The above technique has been programmed for computer evaluation of the thermal conductors required in the SINDA bearing thermal model. In general, it was found that forced convection heat transfer dominated in the high velocity regions. Heat transfer from the high-speed components, inner races, balls, etc, is effected very little by nucleate boiling. The major effect is at the point where the surface is estimated to be vapor blanketed (i.e., the point of "burnout").

The magnitude of the "burnout" heat flux can also be significantly affected by surface conditions such as roughness, coatings, etc. The maximum heat flux condition can be reached prematurely if flow instabilities or oscillation occurs. These rapid changes in flow can lower the local pressure increasing the local superheat near the wall and cause rapidly increased boiling. These added uncertainties along with the lack of experimental data relative to the thermodynamic conditions in the bearing tester emphasizes the importance of experimental data from the tester. By comparing measured and calculated temperature data the validity of the thermal model can be assessed.

5.12.2 SENSITIVITY OF BEARING COMPONENT TEMPERATURES TO TRANSITION TO FILM BOILING

Temperature measurements can serve as a guide in evaluating the transition point from forced convection nucleate boiling (burnout flux) to film boiling. An example of the importance in evaluating this parameter is shown in Figure 5.12.2. The average bearing component temperatures are shown as a function of the maximum wall superheat $(T_w - T_s)_{MAX}$ for forced convection nucleate boiling. As the maximum superheat is increased, considerably more surface area of the bearing components remain in the nucleate boiling regime. Therefore, these areas do not become vapor blanketed and the surface-to-fluid heat transfer remains relatively high resulting in lower temperatures. As $(T_w - T_s)_{MAX}$ is increased to the point that all surfaces remain in the nucleate boiling regime, the component temperatures become independent of the transition from nucleate to film boiling. In other words, for a given heat load, the transition point can be increased such that the surface temperature does not reach the transition point and film boiling does not occur. In Figure 5.12.2 this is represented by the higher ΔT_{MAX} values where the bearing component temperatures become independent of ΔT_{MAX} .

ORIGINAL PAGE IS
OF POOR QUALITY

FIGURE 5.12.2

Component Temperature As a Function
of Wall Superheat at Max Flux Conditions

Brg 2
Axial Load = 2500 lb
Flow Rate = 6.3 lb/s
 $T_{in} = -305^{\circ}F$
LN2

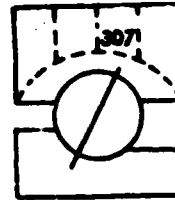
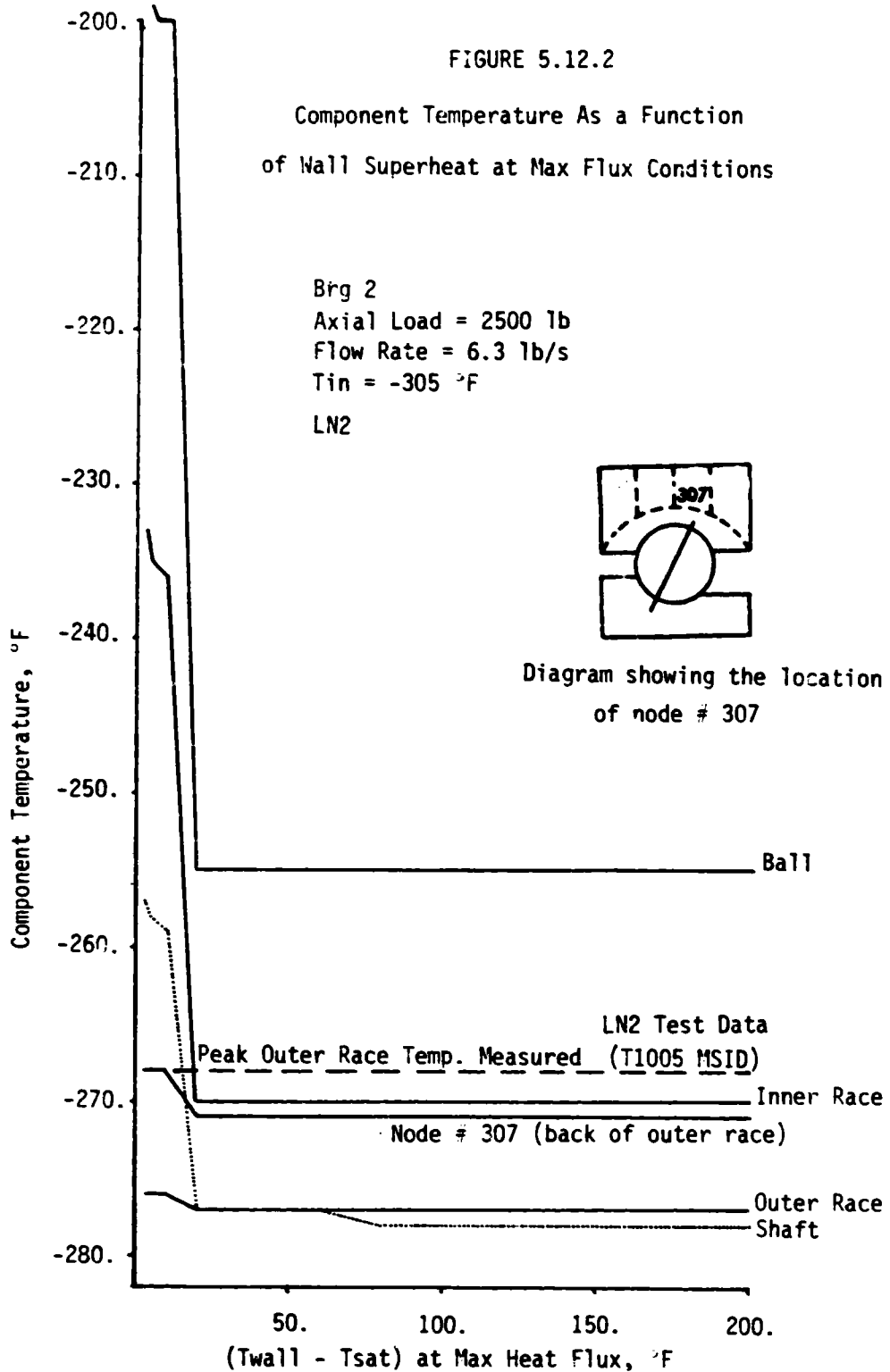


Diagram showing the location
of node # 307



SRS

spectra research systems

NOMENCLATURE FOR SECTION 5.12

| | |
|----------|---------------------------|
| C_p | Specific Heat |
| D | Diameter |
| g | Acceleration of Gravity |
| g_c | Conversion Factor |
| h_c | Heat Transfer Coefficient |
| H | Enthalpy |
| k | Thermal Conductivity |
| P | Pressure |
| q | Heat Flux |
| T | Temperature |
| σ | Surface Tension |
| ρ | Density |
| α | Thermal Diffusivity |
| N_{re} | Reynolds Number |
| N_{pr} | Pandel Number |

$$f(P) = \frac{\sqrt{\frac{\sigma}{\rho_L - \rho_g}}}{8.7 \times 10^{-4} k \left[\frac{1}{\alpha \rho_g H_{LG} \sqrt{\rho_L - \rho_g}} \right]^{.7} \left[\frac{P}{\sigma \sqrt{\rho_L - \rho_g}} \right]^{.7}}$$

$$F(P) = H_{LG} \rho_g \left[\frac{g g_c \sigma (\rho_L - \rho_g)}{\rho_g^2} \right]^{1/4}$$

$$\theta = \frac{0.1}{\rho_g^{1/3} L_g} \left(\frac{\rho_g}{\rho_L} \right)^{1/4} CPL \rho_L$$

| | |
|------|----------------------|
| | Subscripts |
| b | Boiling |
| bm | Maximum Boiling |
| C | Convection |
| e | Equivalent |
| g | Vapor |
| L | Liquid |
| Lg | Saturated Liquid/Gas |
| sb | Subcooled Boiling |
| s | Saturated |
| w | Wall |

The analysis described herein predicts that the peak flux will be reached at surface temperatures between 2.6 and 3.3°R, above saturation, depending on the magnitude of the forced convection heat transfer coefficient. Also shown is a temperature measurement for the number 2 bearing outer race. This measurement is in reasonable agreement with the calculated outer race temperature at the estimated ΔT_{MAX} point.

REPRESENTATIVE BEARING TEMPERATURE AND MODEL UPDATE

Prior convergence problems with the bearing thermal model have been solved. The model now achieves a system heat balance and meets convergence criteria concerning the allowable temperature change between iterations. Representative bearing component temperatures are shown in Figures 5.12.3, 5.12.4, 5.12.5, and 5.12.6 for the conditions noted. As shown, the gradients in the track area are significant for the higher loading conditions. Track surface temperatures, for the high loads, are of concern due to the possibility of high temperature breakdown of the solid film lubricant. Since the track temperatures are critical to lubricant performance, additional work is proceeding to enhance the nodal description in the track areas to allow a heat rate distribution to be applied in the contact area. This update should be completed during the next reporting period. Although this may affect the magnitude of track temperatures, the data shown in Figures 5.12.3, 5.12.4, and 5.12.5 should be representative of the expected trends.

5.12.3 BEARING LIFE MODELING

A NASTRAN model of the bearing inner race is being developed to determine the stress field in the contact area. Normal load distributions will be considered initially with tangential forces (friction) and thermal effects to be added later. Initial computer runs are planned for the next reporting period. This effort has been undertaken to gain an understanding of the friction and thermal effects on bearing life.

5.13 JULY, 1983

5.13.1 FLUID FILM THICKNESS ESTIMATES FOR MATERIAL FATIGUE TESTER

The minimum lubricant film thickness was estimated for a material fatigue tester to investigate possible degradation of fatigue life due to loss of lubrication. The tester configuration and design characteristics are shown in Figure 5.13.1. The lubricant is MIL-L-7808G. The lubricant properties are also provided in Figure 5.13.1. The results indicate that the film thickness to roughness ratio (h/σ) is not large enough to provide full EHD boundary lubrication.

There are several correlations available in the literature for the estimation of lubricant film thickness. Dawson (1) developed the following formula to calculate minimum film thickness in a rolling contact.

$$1) \quad \frac{h}{R_x} = 1.58 (\rho E')^{0.6} \left(\frac{\rho_0 U}{E R_x} \right)^{0.7}$$

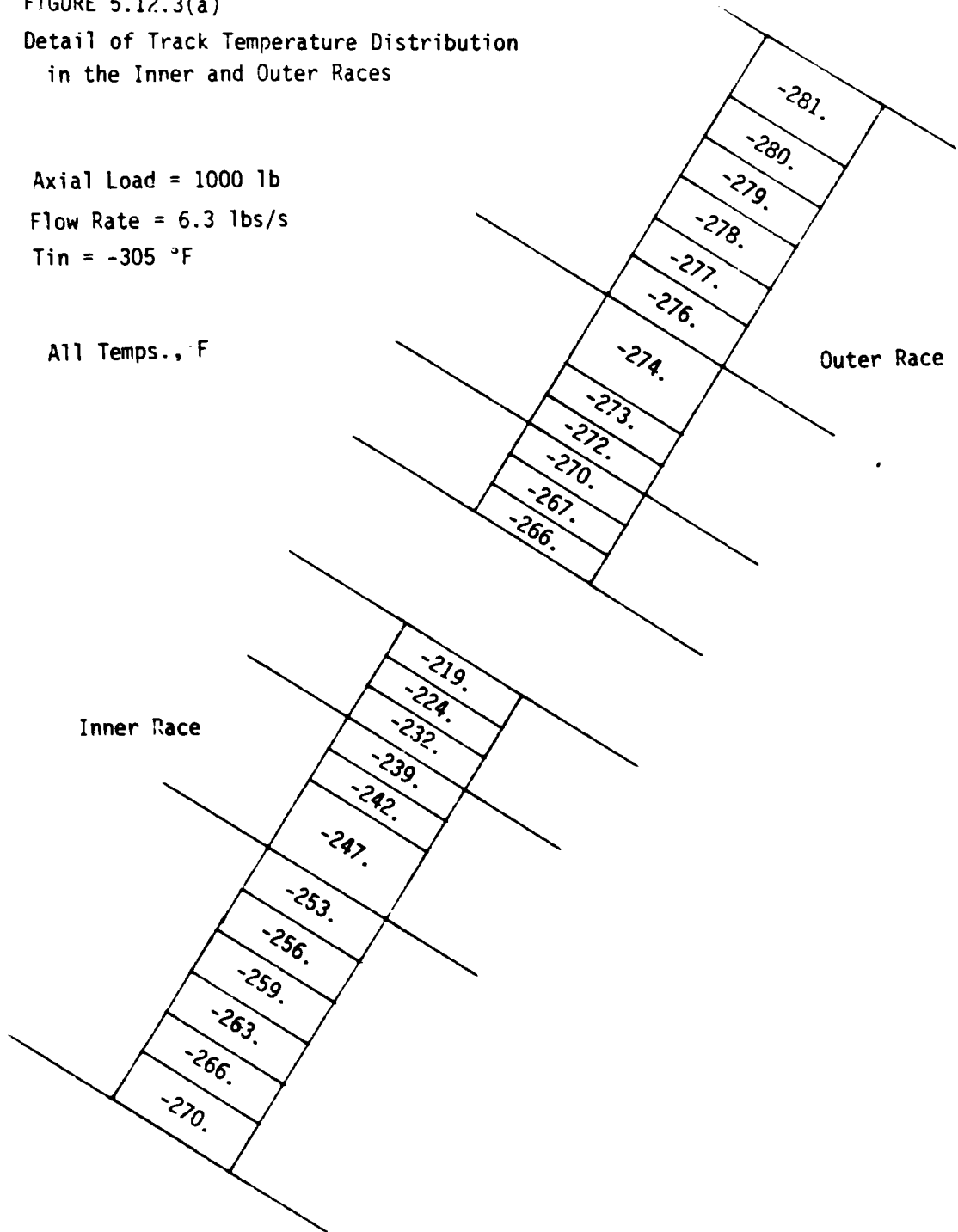
Grubin developed a similar formula:

$$2) \quad \frac{h}{R_x} = 1.87 \left[\left(\frac{\rho_0 U}{E R_x} \right)^{.7} \right] / \left[\left(\frac{w}{E R_x} \right)^{.091} \right]$$

FIGURE 5.12.3(a)
Detail of Track Temperature Distribution
in the Inner and Outer Races

Axial Load = 1000 lb
Flow Rate = 6.3 lbs/s
 $T_{in} = -305 \text{ } ^\circ\text{F}$

All Temps., $^\circ\text{F}$



ORIGINAL MADE IS
OF POOR QUALITY

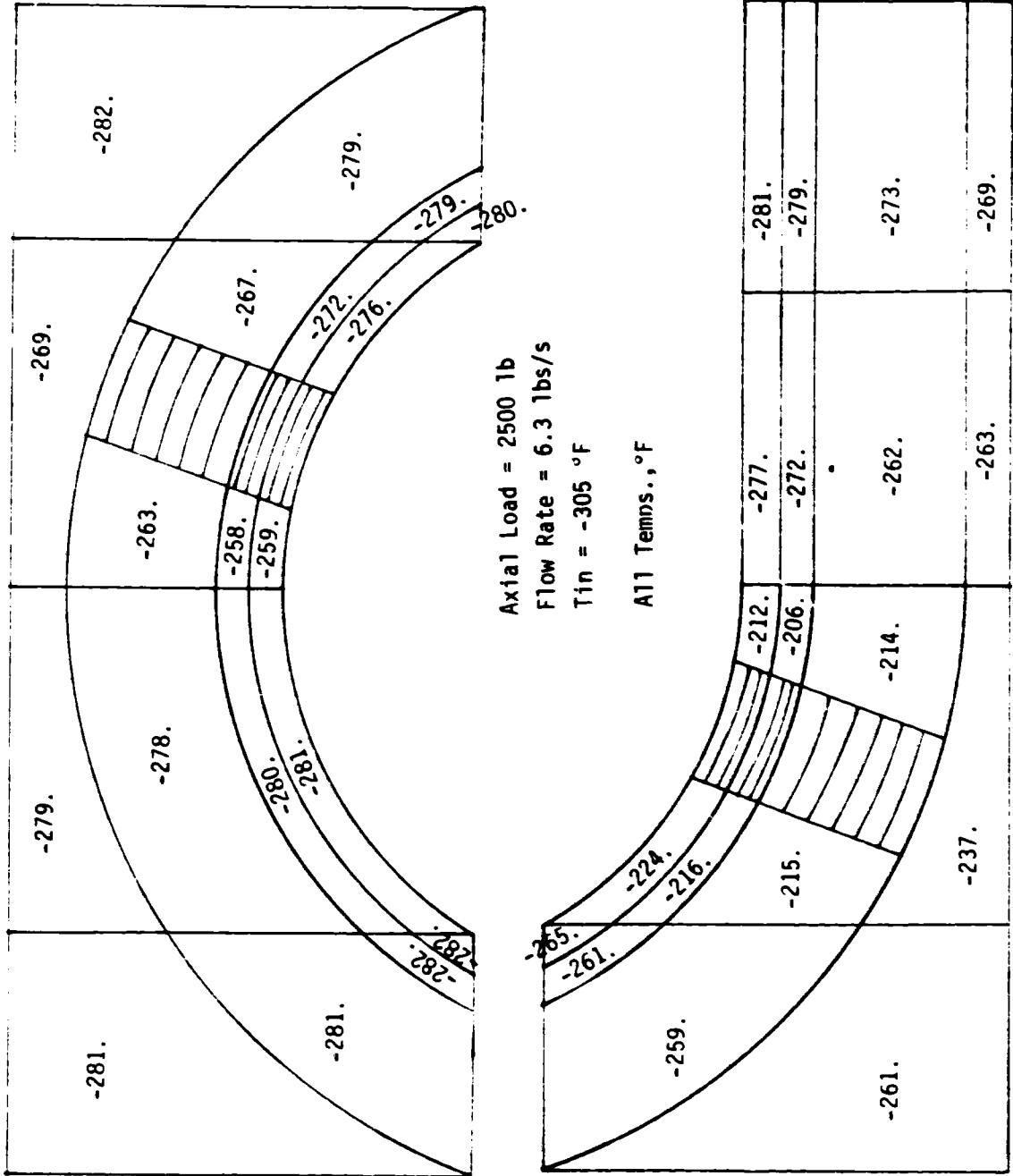


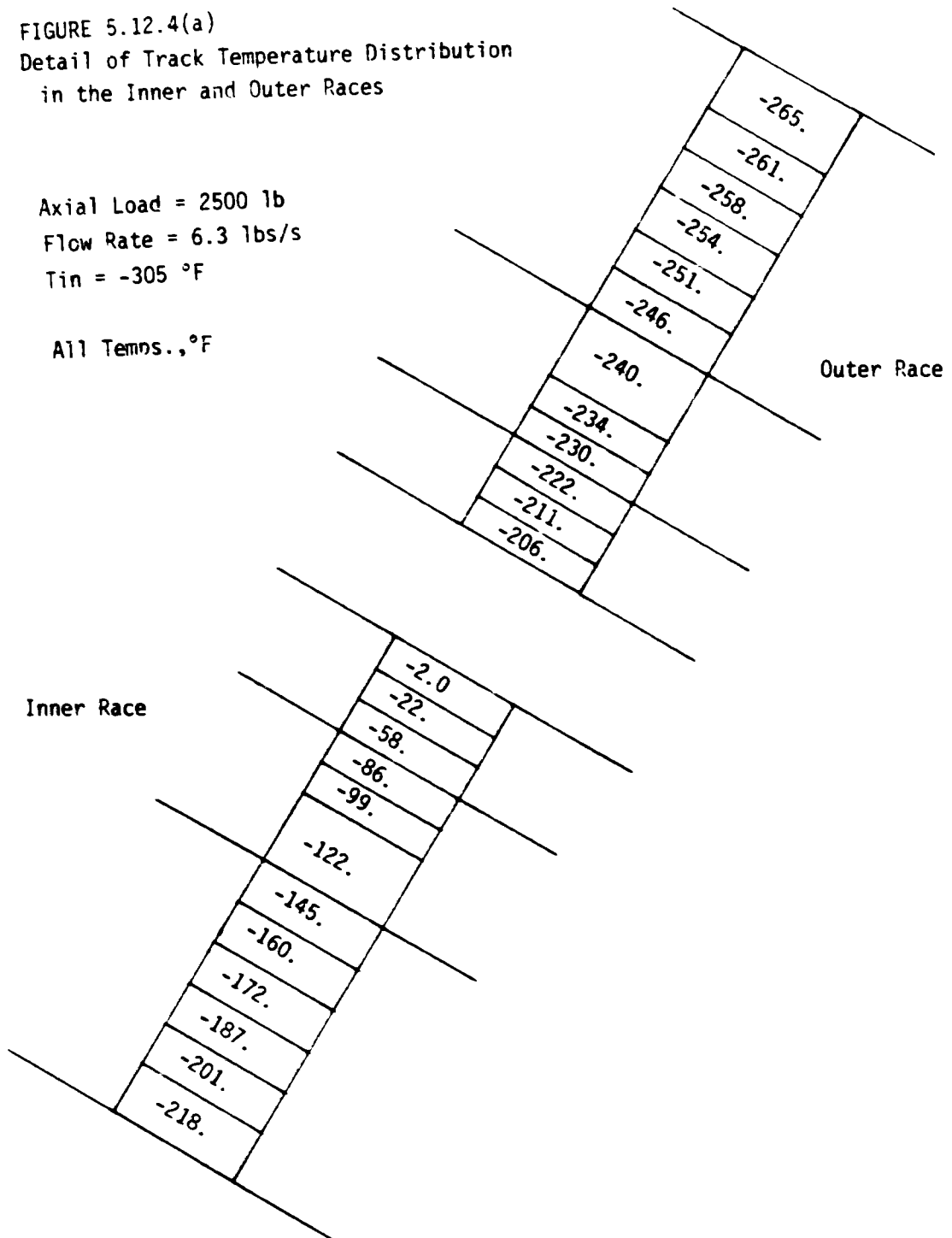
FIGURE 5.12.4 Temperature Distribution in the Inner and Outer Races

SRS

FIGURE 5.12.4(a)
Detail of Track Temperature Distribution
in the Inner and Outer Races

Axial Load = 2500 lb
Flow Rate = 6.3 lbs/s
 $T_{in} = -305\text{ }^{\circ}\text{F}$

All Temps., $^{\circ}\text{F}$



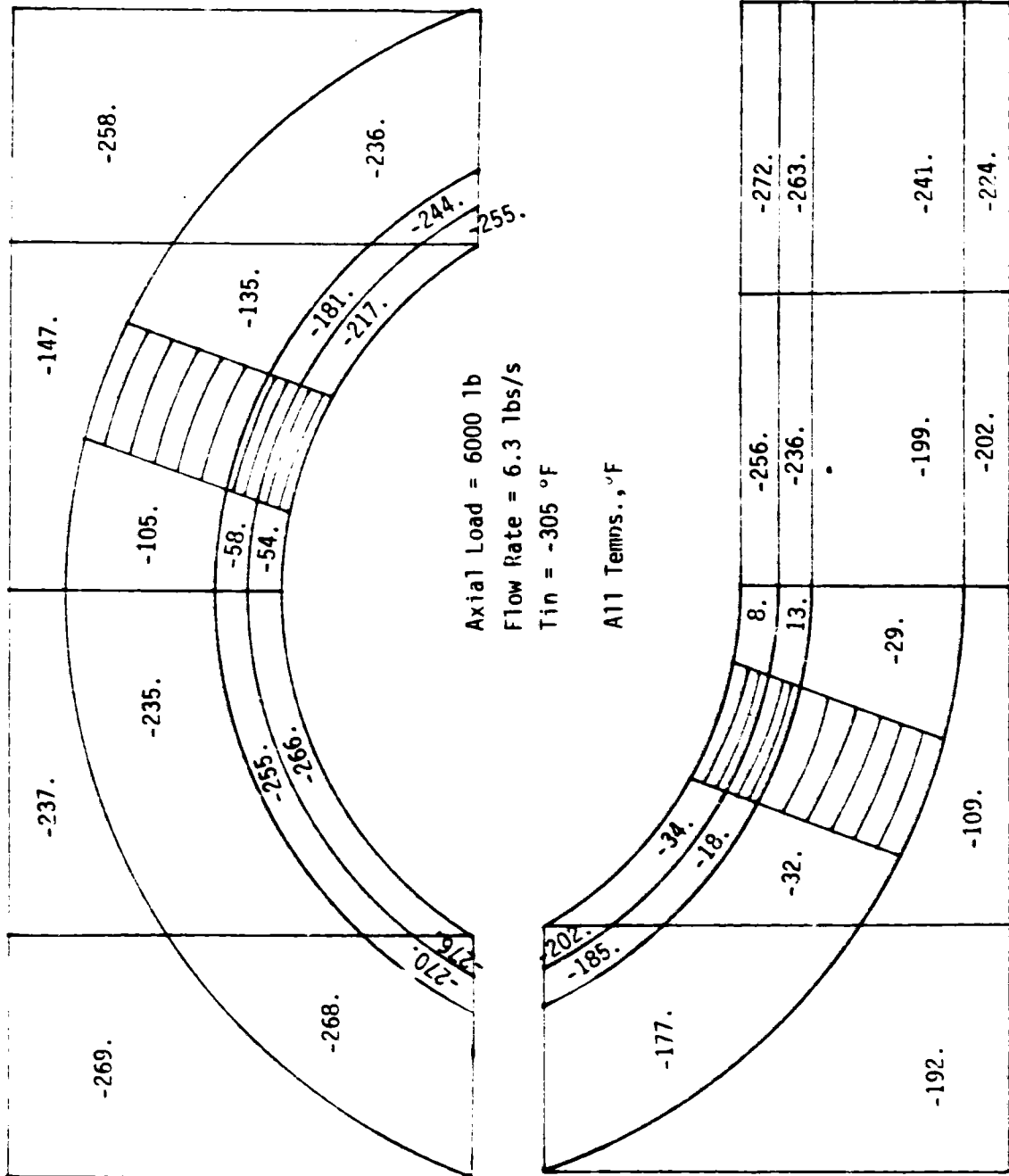


FIGURE 5.12.5 Temperature Distribution in the Inner and Outer Races

SRS

FIGURE 5.12.5(a)
Detail of Track Temperature Distribution
in the Inner and Outer Races

Axial Load = 6000 lb
Flow Rate = 6.3 lbs/s
 $T_{in} = -305\text{ }^{\circ}\text{F}$
All Temps., $^{\circ}\text{F}$

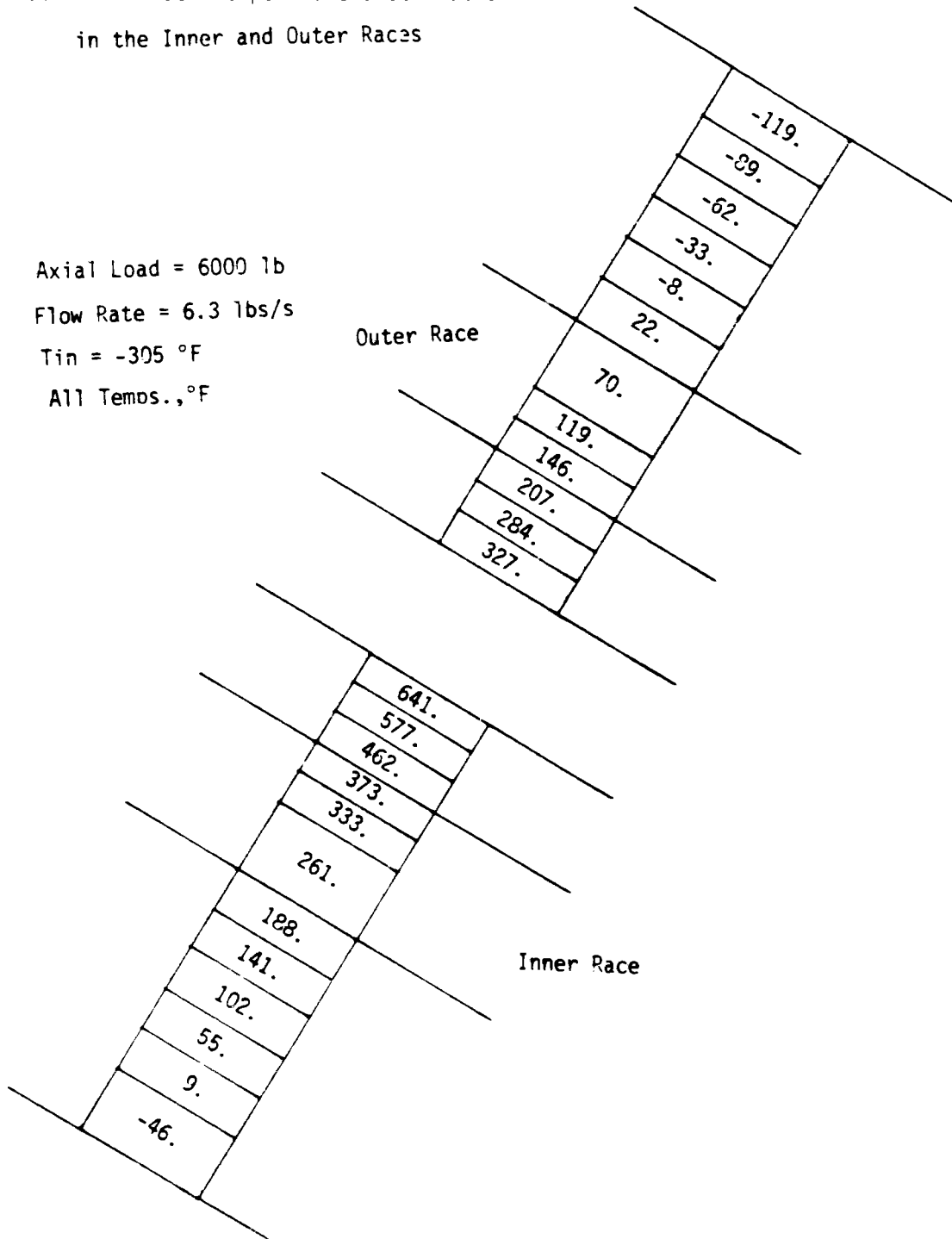
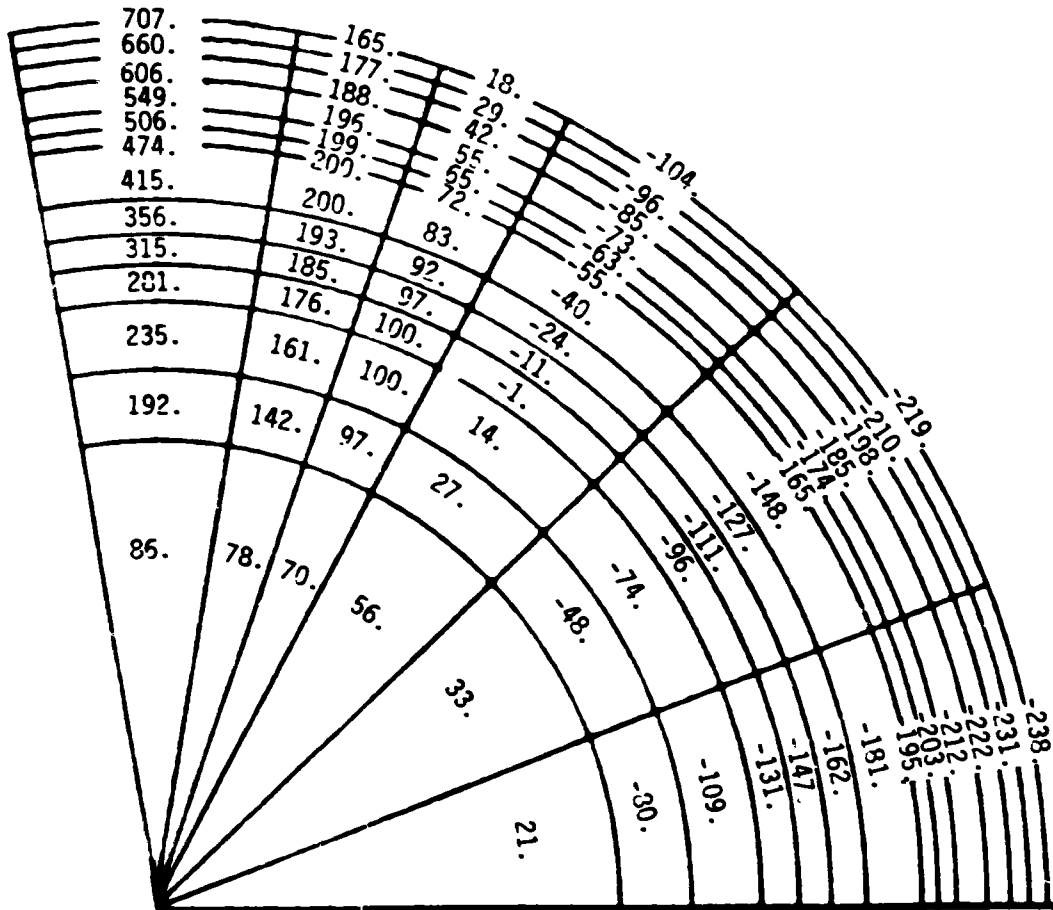


FIGURE 5.12.5(b) Rolling Element Temperature Distribution

Axial Load = 6000 lb
Tin = -305 °F
Flow Rate = 6.3 lbs/s

Track Node

All Temps., °F



SRS

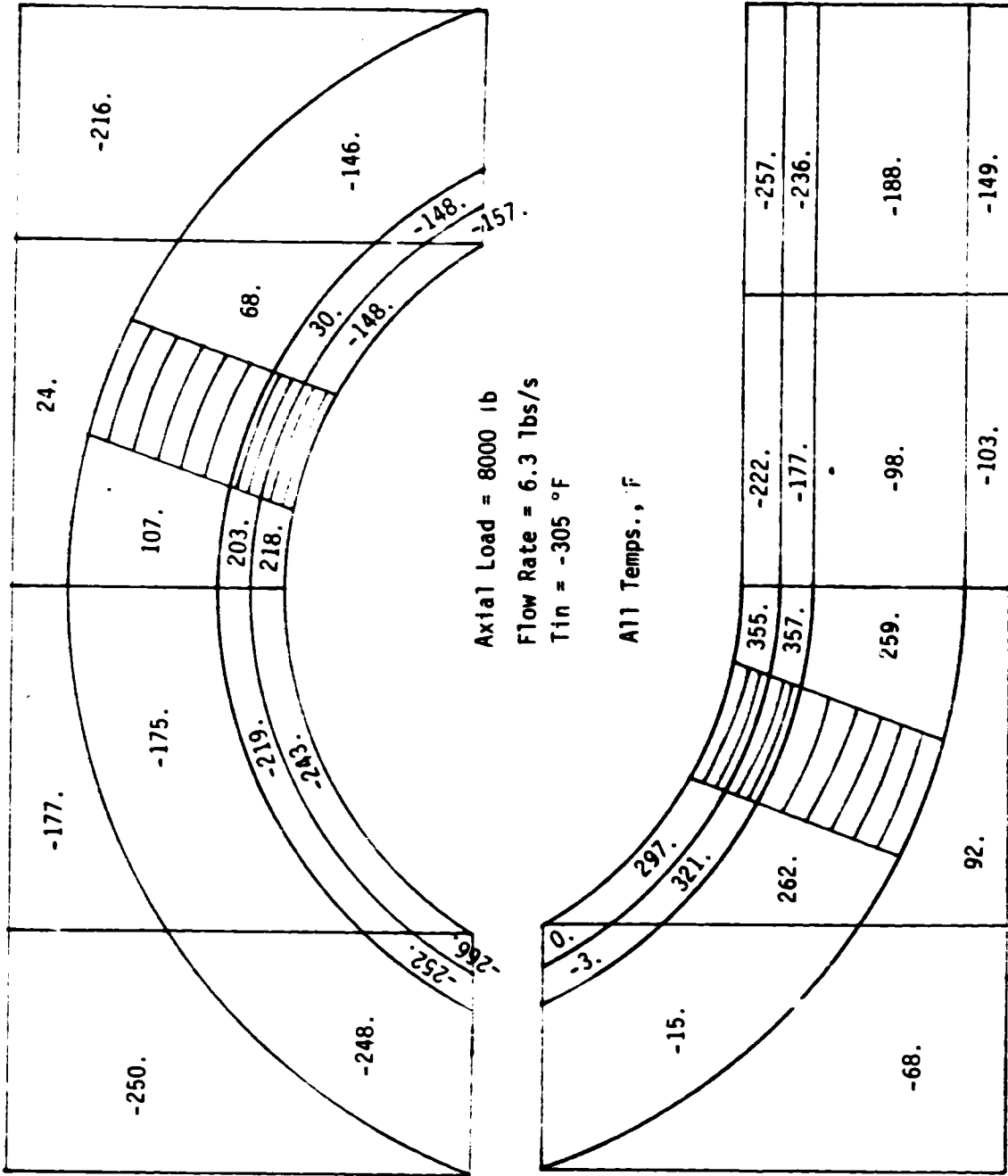


FIGURE 5 12.6 Temperature Distribution in the Inner and Outer Races

SRS

FIGURE 5.12.6(a)

Detail of Track Temperature Distribution
in the Inner and Outer Races

Axial Load = 8000 lb
Flow Rate = 6.3 lbs/s
 $T_{in} = -305^{\circ}F$

All Temps., $^{\circ}F$

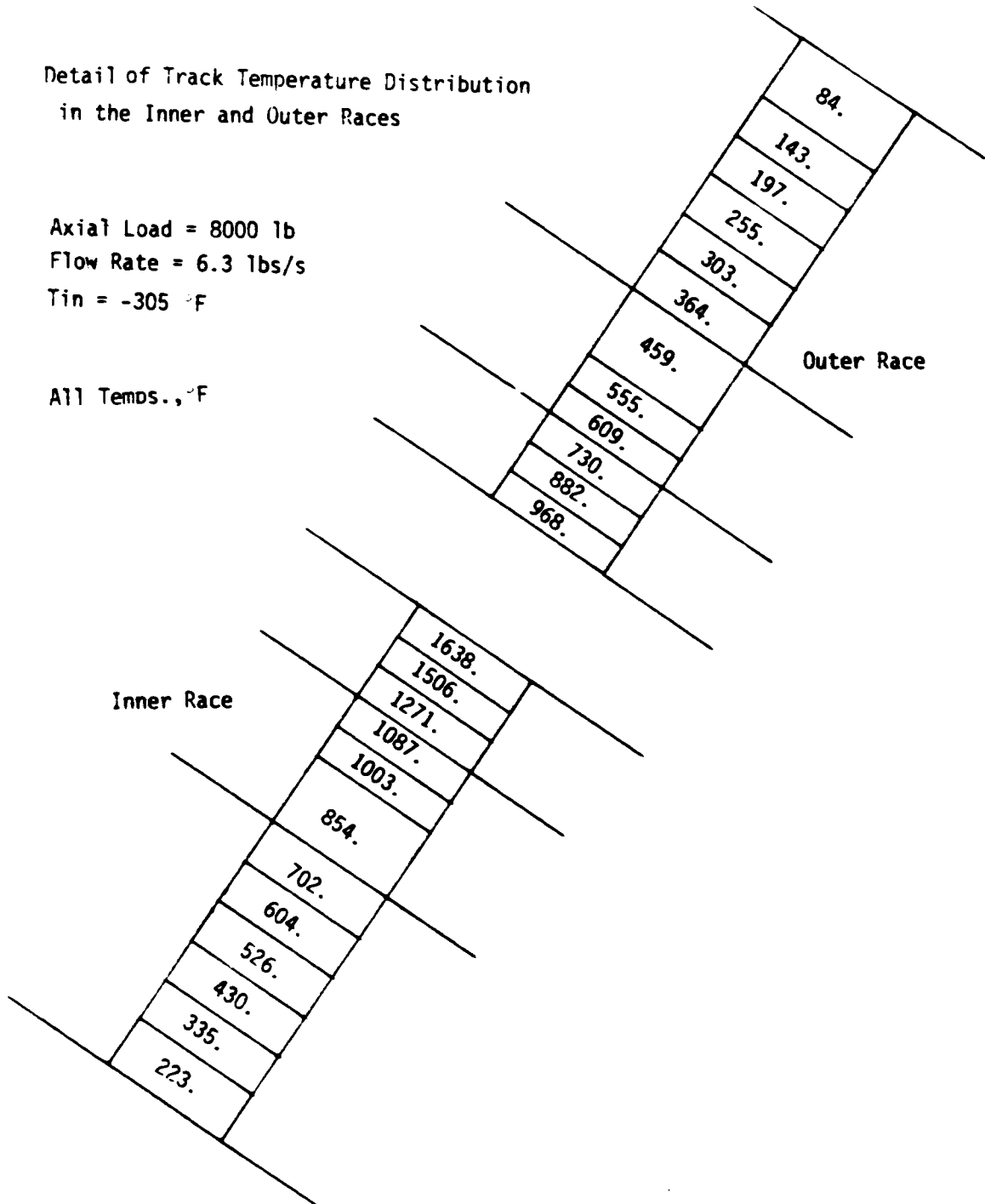


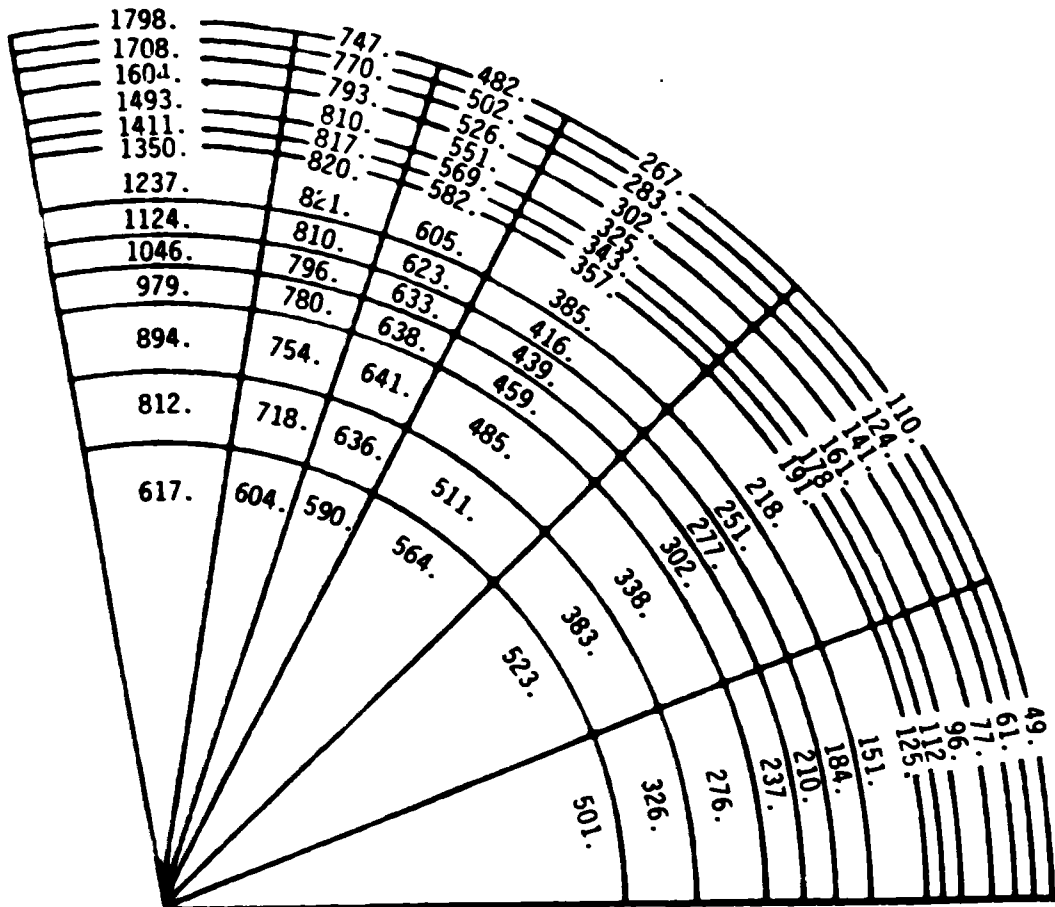
FIGURE 5.12.6(b) Rolling Element Temperature Distribution

ORIGINAL PAGE IS
OF POOR QUALITY

Axial Load = 8000 lb
Flow Rate = 6.3 lbs/s
Tin = -305 °F

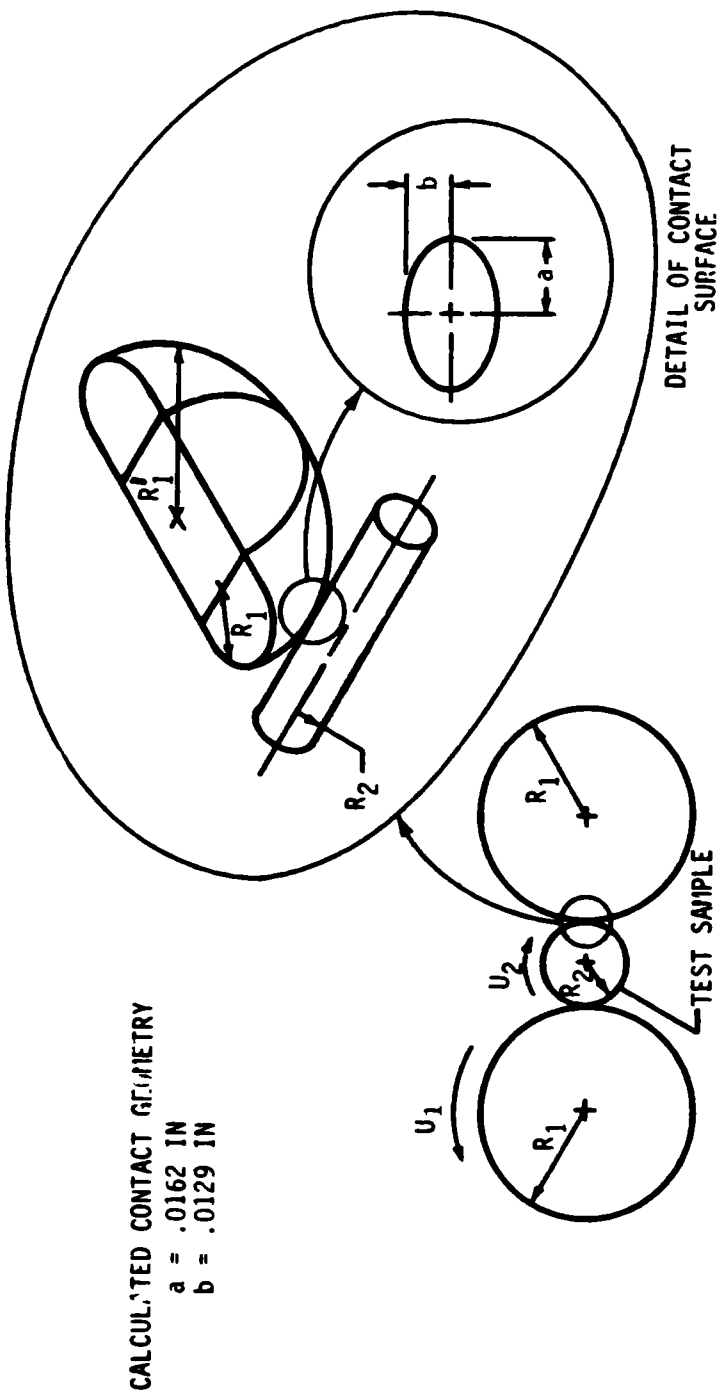
Track Node

All Temps., °F



SRS

FIGURE 5.13.1 TESTER CONFIGURATION AND LUBRICANT PROPERTIES



CALCULATED CONTACT GEOMETRY

$a = .0162 \text{ IN}$

$b = .0129 \text{ IN}$

SPEED 10,000 RPM
LOAD 326 lbs
ESTIMATED CONTACT STRESS (MAX) = 737,000 psi

| | | | | | | | |
|----------------|-------------|-----------------------------------|-----------------------|---|-------|---|--------------------|
| LUBRICANT TYPE | MIL-L-7808G | VISCOSITY LBS-SEC/IN ² | 1.77x10 ⁻⁶ | THERMAL CONDUCTIVITY LBS/SEC ² R | .0189 | PRESSURE VISCOSITY EXPONENT* (IN ⁻² /LB) | 1x10 ⁻⁴ |
|----------------|-------------|-----------------------------------|-----------------------|---|-------|---|--------------------|

* DATA FOR MIL-L-7808G NOT AVAILABLE - ESTIMATED BY COMPARISON WITH LUBRICANTS OF SIMILAR VISCOSITY

SRS

spectra research systems

$$R'_x = \frac{1}{R_1} + \frac{1}{R_2}$$

λ = Viscosity pressure coefficient (in²/lb)

μ = Ambient viscosity $\left(\frac{\text{lbs} \cdot \text{sec}}{\text{in}^2}\right)$

U = Entrainment velocity = $\frac{U_1 + U_2}{2}$ (in/sec)

$W = \frac{W_T}{4/3a}$ = Load per unit length (lbs/in)

W_T = Contact surface load (lbs)

a = Semi major axis of contact ellipse (in)

$E' = \frac{2E}{1-\nu^2}$ Assumes properties of wheel and roller to be equal

E = Modulus of elasticity (lbs/in²)

ν = Poisson's ratio

The above relationships are for isothermal conditions. H. S. Cheng (42) developed a Grubin type inlet film thickness analysis including the thermal effects. The results of this work yields correction factors to the isothermal film thickness estimates as follows:

$$3) \quad h_{\min} = \theta_T \cdot \theta_S \cdot h_{\min} \text{ (isothermal)}$$

θ_T is a reduction factor to account for the thermal effects on the lubricant and θ_S is a factor to account for side leakage in the contacts. Based on the lubricant properties, contact geometry, and entrainment velocity, these factors were estimated as follows:

$$\theta_T = 0.87$$

$$\theta_S = 0.9$$

Dawson's film thickness formula can be adjusted to account for thermal and side leakage as follows:

$$4) \quad \frac{h_{\min}}{R'_x} = 1.237 (\lambda E')^{.6} \left[\frac{U}{E' R'_x} \right]^{0.7} \left[\frac{W}{E' R'_x} \right]^{.13}$$

A similar adjustment can be made to Gurbin's formula. The minimum film thickness estimated from equation 4 is 3.5 μ inches. Gurbin's formula, including the reduction factors, provides a minimum film thickness of 6.2 μ inches. The difference is due primarily to the differences in exponents assigned to the load terms in the two equations.

To further investigate the validity of these estimates, data from reference (43) were compared with the above film thickness estimates. Table 5.13.1 gives the

TABLE 5.13.1 LUBRICANT PROPERTIES*

| MEAN PARAMETER | MIL-L-7808G | TYPE II ESTER | FLUOROCARBON | POLYPHENYLETHER | SYNTHETIC PARAFFINIC |
|---|-------------------------|-----------------------|-----------------------|-----------------------|-------------------------|
| k_j^* | ? | 10.7 | 30.6 | 3950 | 43.8 |
| \hat{n}_j | ? | 0.6 | 0.61 | 0.83 | 0.66 |
| PROPERTIES | | | | | |
| VISCOSITY C.S. | 12.8 | 29 | 298 | 358 | 443 |
| DENSITY ($\frac{gm}{cm^3}$) | .9526 | .85 | 1.59 | 1.05 | .74 |
| VISCOSITY ($\frac{lbs-sec}{in^2}$) | 1.7686×10^{-6} | 3.57×10^{-6} | 6.87×10^{-5} | 5.45×10^{-5} | 4.75×10^{-5} |

* ALL PROPERTIES EXCEPT FOR MIL-L-7808G TAKEN FROM REF. 43

SRS

spectra research systems

lubricants tested and experimental correlation factors determined from the tests. As shown, the type II Ester has viscosity values closest to the MIL-L-7808G lubricant.

The film thickness data from reference 43 was correlated with the following formula.

$$5) \quad \frac{h}{\sigma} = \left[\frac{U}{\rho_s} \right]^{0.5} s$$

ρ_s is a reduction factor for high stress conditions. These test data did not include stress conditions greater than 350ksi. Since the test fixture is stressed to 700ksi, a value of ρ_s could not be obtained directly from the test data. An optimistic value would be 0.5 which corresponds to a Hertz stress of 350ksi.

Using the correlation factors for type II Ester and the MIL-L-7808G fluid properties, the estimated film thickness from equation 5 is, 1.375 μ inches.

The surface roughness for the sample and wheels were given as:

TEST SAMPLE 4 μ TO 8 μ INCHES
WHEEL 6 μ INCHES

The combined RMS surface roughness is therefore:

$$= \sqrt{(8.)^2 + (6.)^2} = 10. \text{ inch}$$

The results of the previous analysis are summarized below:

| CORRELATION | MINIMUM FILM THICKNESS μ INCHES | FILM THICKNESS TO ROUGHNESS RATIO h/σ |
|-------------|-------------------------------------|--|
| Dawson | 3.5 | .35 |
| Gurbin's | 6.2 | .62 |
| Eq 5 | 1.4 | .14 |

According to reference (42), if $h/\sigma > 4$, thick EHD film exists and the lubrication should be satisfactory. If $1 > h/\sigma < 4$, partial EHD film exists and lubrication is most likely satisfactory but may deteriorate when h/σ approaches unity. If $h/\sigma < 1$, lubrication is marginal and operation in this region is in general not recommended without boundary lubrication additives. Pitting, scoring and progressive wear are likely to occur.

5.13.2 FLUID HEAT TRANSFER REGIMES AND FILM COEFFICIENTS FOR LOX COOLANT

Techniques developed and reported in Section 5.12 were used to evaluate the surface temperature for the incipient nucleate boiling range for LOX. The heat transfer regimes as a function of wall superheat ($T_w - T_s$) are shown in Figure 5.13.2. As shown, nucleate boiling for the forced convection⁵ LOX flow begins for a wall superheat of 12.8°R and the "burnout" heat flux occurs at a wall superheat of 13.8°R. This indicates that typical bearing surfaces will become vapor blanketed when the surface temperature exceeds the LOX saturation temperature by about 13°R. This compares with a value of about 3°R for LN₂ coolant as shown in Figure 5.13.3.

Figure 5.13.2 HEAT TRANSFER REGIMES FOR LOX

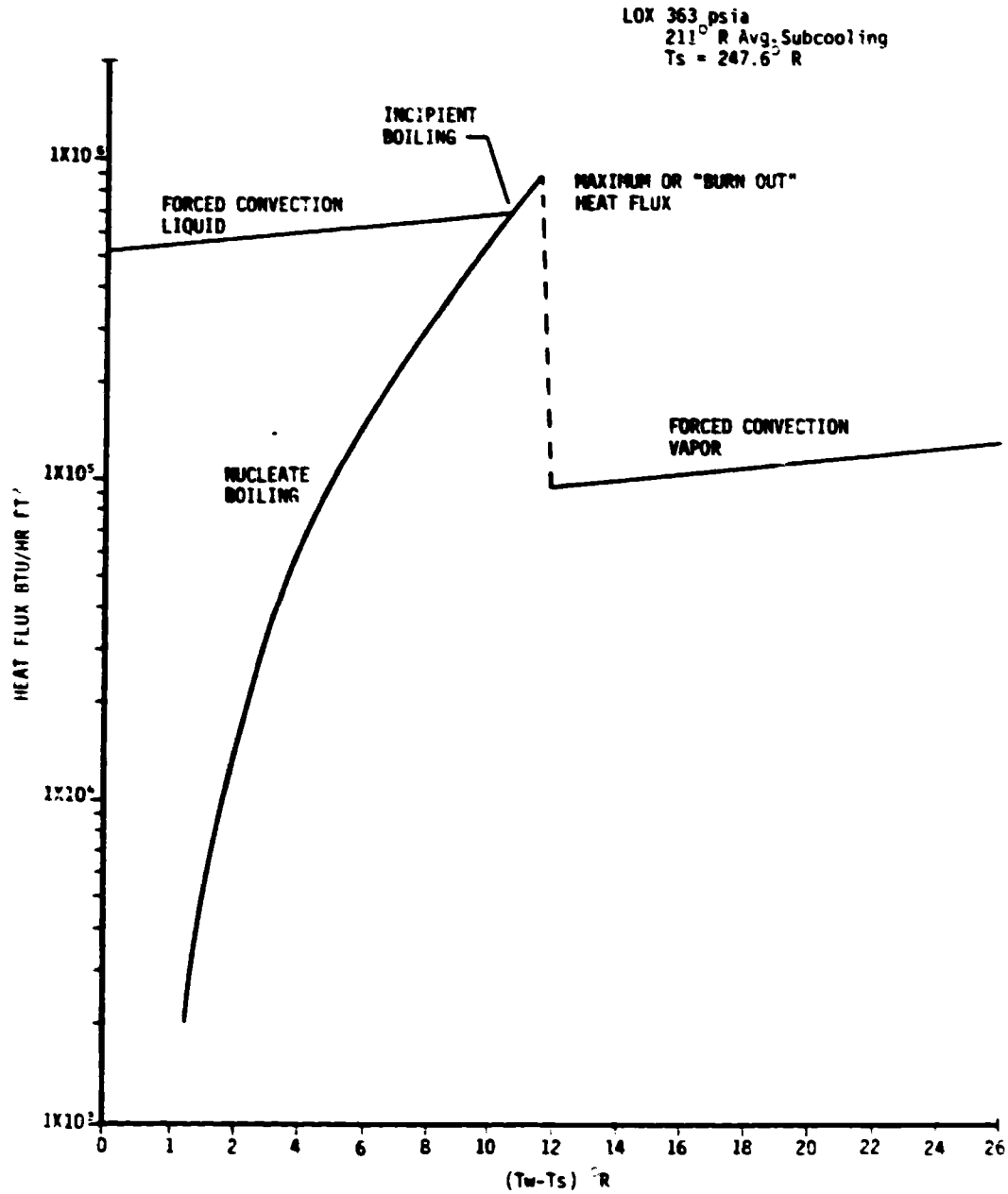
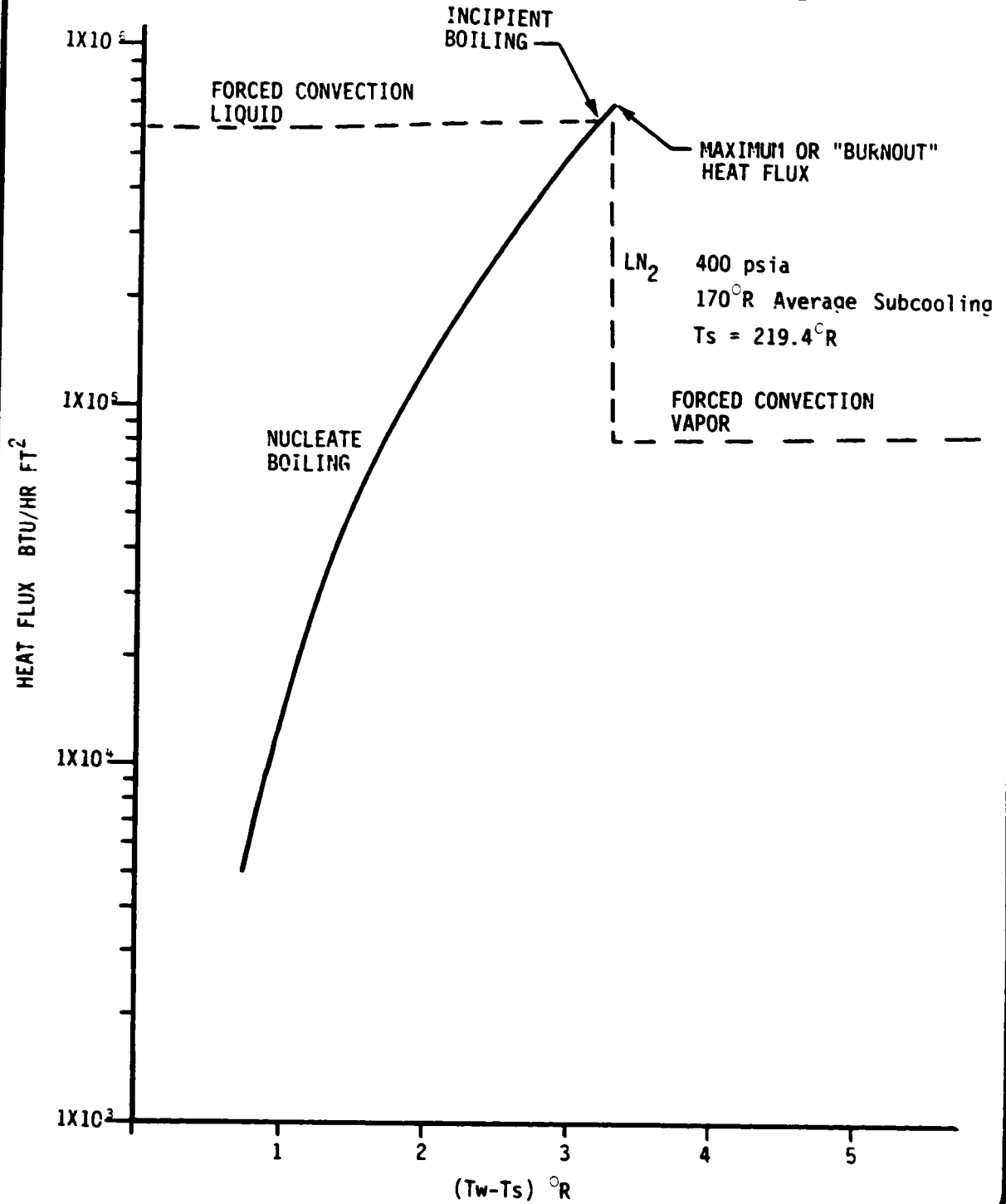


Figure 5.13.3 HEAT TRANSFER REGIMES FOR LN₂



SRS

5.13.3 STATUS OF THERMAL MODEL

An updated thermal model with the reconfigured (node network) inner and outer race is in the process of being checked out. This model will have the capability of allowing the frictional heat generated in the rolling element/race contact to be distributed along the major axis of the contact ellipse. The SHABERTH bearing analysis code provides the frictional heat generated in the bearing contacts. The calculation technique used by the code solves for the friction force and slip velocity at finite increments in the contact ellipse. The sum of the product of these parameters is the friction heat generated in the contact. By providing write statements at the appropriate locations within the SHABERTH code, the heat generation rate distribution along the major axis of the contact ellipse can be obtained. Examples of these distributions are shown in Figures 5.13.4 and 5.13.5 for the inner and outer races respectively. It is of interest to observe that the maximum normal force does not coincide with the location of maximum heat generation. The most heavily stressed area of the contact is therefore not at the highest contact temperature. This is a fortunate condition for those cases where material properties become marginal due to high temperatures.

5.13.4 ANTICIPATED WORK FOR AUGUST 1983

The following activities are planned during the next reporting period.

- 1) Finalize the nodal network for the thermal model and initiate analyses to verify, with the correct model configuration and two phase heat transfer coefficients, previous analyses of sensitivity of bearing operation to coolant flow, subcooling and load.
- 2) Continue development of the finite element stress model of the bearing contact.

ORIGINAL PAGE IS
OF POOR QUALITY

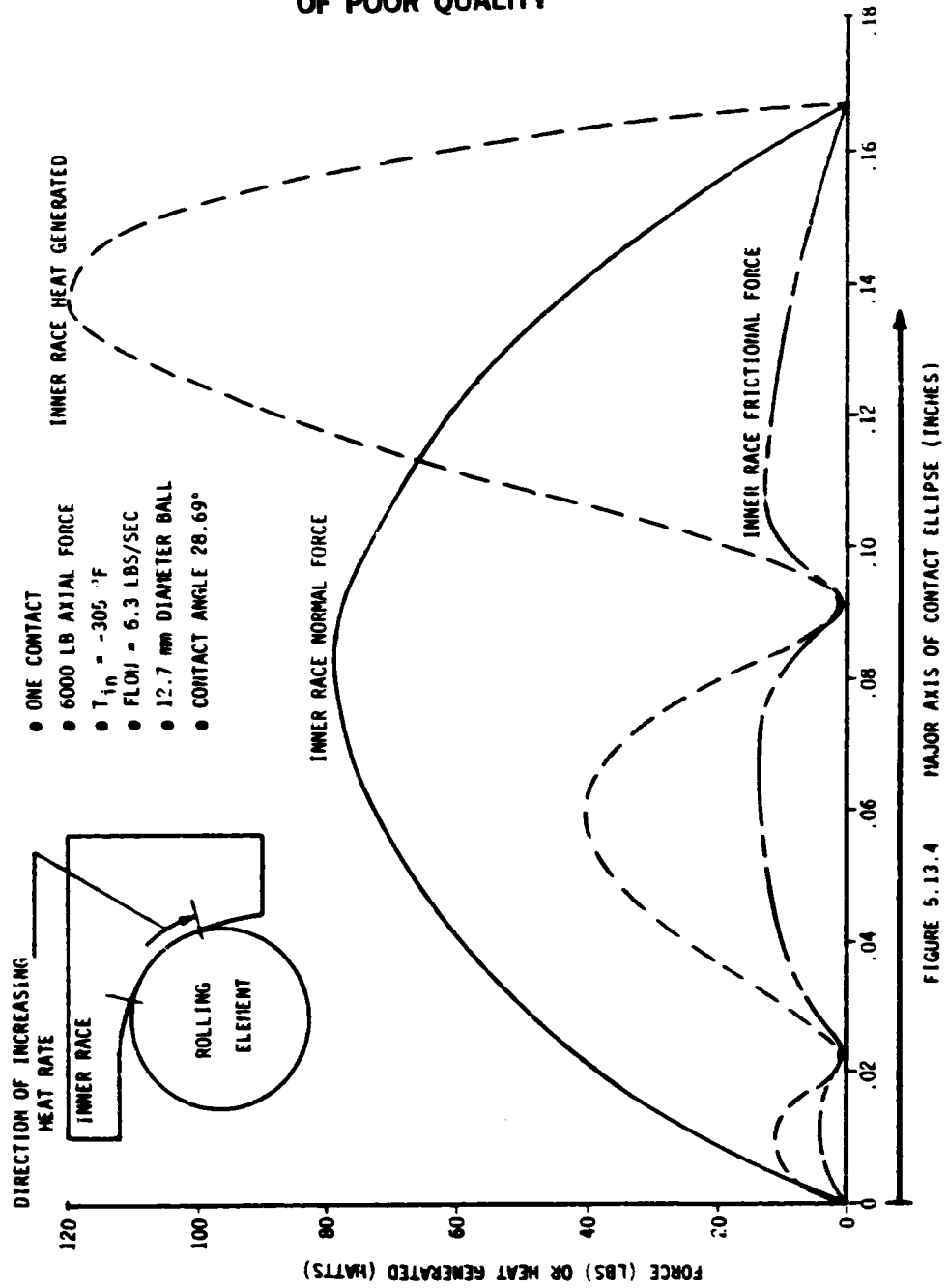


FIGURE 5.13.4 MAJOR AXIS OF CONTACT ELLIPSE (INCHES)

SRS

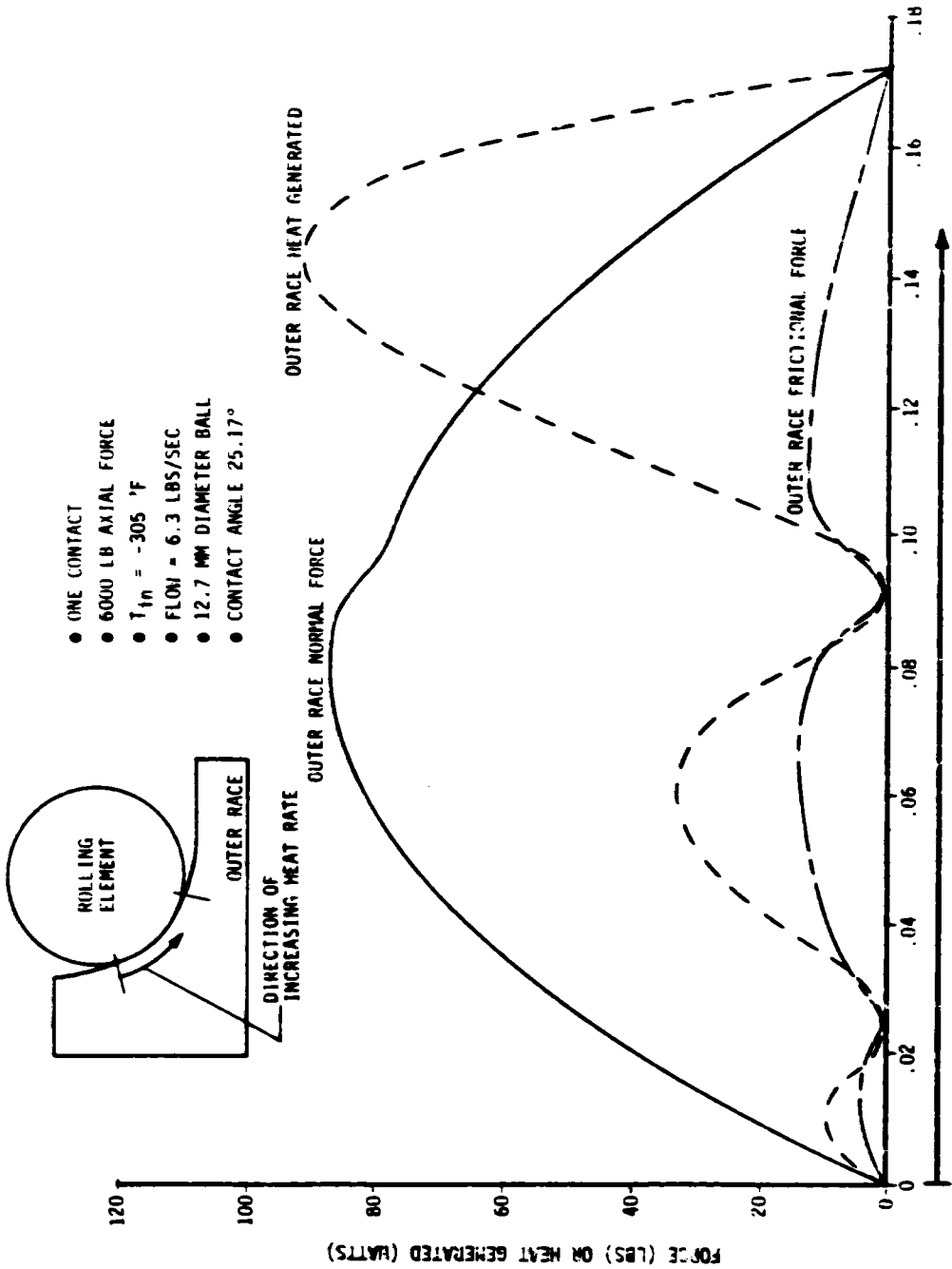


FIGURE 5.13.5 MAJOR AXIS OF CONTACT ELLIPSE (INCHES)

6.0 REFERENCES

- 1) "Rolling Bearing Analysis" by T. A. Harris, John Wiley & Sons, 1966.
- 2) NASA Report No. 793, "Experiments on Drag of Revolving Disks, Cylinders, and Streamline Rods at High Speeds", by T. Theodorsen and A. Regier.
- 3) Tallian, T. E., "On Competing Failure Modes in Rolling Contact", ASLE Transactions, 413-439, 1967.
- 4) Lundberg, G. and Palmgren, A., "Dynamic Capacity of Rolling Bearings" Acta Polytechnica, Mechanical Engineering Series 1, R.S.A.E.E., 403,7 (1947).
- 5) Tallian, T. E., "Weibull Distribution of Rolling Contact Fatigue Life and Deviations Therefrom". ASLE Transactions 5, 183-196, 1962.
- 6) Bamberger, E. N., Harris, T. A., "Life Adjustment Factors for Ball and Roller Bearings". ASME United Engineering Center, 345 East 47th Street, New York, NY 1971.
- 7) Weibull, W., "A Statistical Distribution Function of Wide Applicability", J. Applied Mechanics 18:293.
- 8) Chiu, Y. P., Tallian, T. E. and McCool, J. I., "An Engineering Model of Spalling Fatigue Failure in Rolling Contact", the Subsurface Model, Wear, 17(1971) 433-446.
- 9) Tallian, T. E., "An Engineering Model of Spalling Fatigue Failure in Rolling Contact", Engineering Discussion and Illustrative Examples, Wear 17(1971) 463-480.
- 10) Tallian, T. E., "The Theory of Partial Elastohydrodynamic Contacts", Wear 21(1972).
- 11) Tallian, T. E., and McCool, J. I., "An Engineering Model of Spalling Fatigue Failure in Rolling Contact" the Subsurface Model Wear 17(1971) 447-461.
- 12) Liu, J. Y., Tallian, T. E., and McCool, J. I., "Dependence of Bearing Fatigue Life on Film Thickness to Surface Roughness Ratio", ASLE Preprint 74 am - 7B-1, Presented May 1974.
- 13) Soda, N. and Yamamoto, T., "Effects of Tangential Traction and Surface Roughness on Mating Roller of CR-MO Steel on Rolling Fatigue Life of 0.45% Carbon Steel.
- 14) Lieblein, J. and Zelen, M., Statistical Investigation of the Fatigue Life of Deep-Groove Ball Bearings, Journal of Research of the National Bureau of Standards, Volume 57, No. 5, November 1956.
- 15) Hady, W. F., Allen, G. P., Johnson, R. L., "Boundary Lubrication Characteristics of a Typical Bearing Steel in Liquid Oxygen" NASTAN D-1580.
- 16) Barron, R. F.: Film Boiling of Liquid Nitrogen on a Sphere in an Enclosure. Adv. in Cryogenic Engng. 23, 305-213 (1978).
- 17) Berenson, P. J.: Film-Boiling Heat Transfer from a Horizontal Surface, ASME Trans., Journal of Heat Transfer, 83, Series C. No. 3, 351-358 (1961).

spectra research systems

- 18) Bergles, A. E., et. al.: Two Phase Flow and Heat Transfer in the Power and Process Industries, Hemisphere Publ. Comp., (1981).
- 19) Burton, R. A., Staph, He. E.: Thermally Activated Seizure of Angular Contact Bearings, ASLE Trans. 10, 408-417 (1967).
- 20) Ellerbrock, H., Liningood, J. N. B., Straight, D. M.: Fluid Flow and Heat-Transfer Problems in Nuclear Rockets - NASA SP-20, pp 27-57.
- 21) Frost, Walter (ed.): Heat Transfer at Low Temperatures. Plenum Press, N.Y., N.Y., (1975).
- 22) Giarratano, P. J.; Smith, R. V.: Comparative Study of Forced Convection Boiling Heat Transfer Correlations for Cryogenic Fluids., Adv. in Cryogenic Engng. 11, 492-506 (1966).
- 23) Hendricks, R. C.; Graham, R. W.; Hsu, Y. Y.; Friedman, R.: Experimental Heat Transfer and Pressure Drop of Liquid Hydrogen Flowing Through a Heated Tube, NASA TN D-765.
- 24) Hendricks, R. C.; Graham, R. W.; Hsu, Y. Y.; Friedman, R.: Experimental Heat Transfer Results for Cryogenic Hydrogen Flowing in Tubes...; NASA TN D-3095.
- 25) Hendricks, R. C.; Papell, S. S.: Estimating Surface Temperature in Forced Convection Nucleate Boiling - A Simplified Method., Adv. in Cryogenic Engng 23, 301-304 (1978).
- 26) Hetsroni, Gad (ed): Handbook of Multiphase Systems, Hemisphere Publ. Corp., (1982).
- 27) Hsu, Y. Y.: A Review of Film Boiling at Cryogenic Temperatures, Adv. in Cryogenic Engng. 17, 361-381 (1972).
- 28) Hsu, Y. Y.; Cowgill, G. R.; Hendricks, R. C.: Mist-Flow Heat Transfer Using Single-Phase Variable-Property Approach, NASA TN D-4149.
- 29) Kosky, Philip G.: Studies in Boiling Heat Transfer to Cryogenic Liquids., University of California, Berkeley, Ph.D. (1966).
- 30) Kutateladze, S. S.: Fundamentals of Heat Transfer, Academic Press, Inc., N.Y., N.Y. (1963).
- 31) Osizik, M. N.: Basic heat Transfer, McGraw-Hill, (1977).
- 32) vonGlahn, U. H.: A Correlation of Film-Boiling Heat Transfer Coefficients Obtained with Hydrogen, Nitrogen, and Freon 113 on Forced Flow, NASA TN-2294.
- 33) VonBerg, R. L.; Williamson, K. D.; Edeskuty, F. J.: Forced-Convection Heat Transfer to Nitrogen in the Vicinity of the Critical Point. Advances in Cryogenic Engng., 15, 238-247 (1970).
- 34) Evaluation of Axial Lockup of Space Shuttle Main Engine Bearings from High Pressure Oxygen Turbopump (Contract No. NAS8-33576 - Task No. 105) Nov. 24, 1980. Final Report.

**ORIGINAL PAGE IS
OF POOR QUALITY**

spectra research systems

- 35) NBS Technical Note 648, "Thermophysical Properties of Nitrogen from the Fusion Line to 3500°R for Pressures to 150,000 psia", December 1973.
- 36) Hashin, Z. and Rotem, A. "A Cumulative Damage Theory of Fatigue Failure". Materials Science and Engineering, 34, 1978.
- 37) Stresses Due to Tangential & Normal Loads on an Elastic Solid with Applications to Some Contact Stress Problems, J. O. Smith and Chang Keng Liu.
- 38) Studies in Boiling Heat Transfer to Cryogenic Liquids, Kosky, Philip George, University of California, Berkley, Ph.D., 1966.
- 39) Handbook of Multi Phase Systems, Gad Hetsroni, McGraw-Hill Book Company.
- 40) Fundamentals of Heat Transfer, Samson Semenovich Kutateladze, Academic Press Inc., New York, NY
- 41) SHABERTH Computer Program Operation Manual Technical Report AFAPL-TR-76-90 October 1976.
- 42) Calculation of Elastohydrodynamic Film Thickness in High Speed Rolling and Sliding Contacts; H.S. Cheng, Mechanical Technology Inc. Report (MTI-67TR24)
- 43) Correlation of Elastohydrodynamic Film Thickness Measurements for Fluorocarbon, Type II Ester, and Ployphenyl Ether Lubricants. NASA TN D-7825.

END

DATE

FILMED

NOV 15 1983

END

DATE

FILMED

NOV 15 1983